Les modelés du Quaternaire récent au front des Alpes : évolution du relief et du climat

Thibaut Cardinal

UNIVERSITÉ CÔTE D'AZUR

ÉCOLE DOCTORALE
SCIENCES FONDAMENTALES ET APPLIQUÉES

THÈSE DE DOCTORAT

Les modelés du Quaternaire récent au front des Alpes : évolution du relief et du climat

Thibaut Cardinal

Géoazur

Présentée en vue de l'obtention
du grade de docteur en **Sciences de la Terre**
de l'**Université Côte d'Azur**
Dirigée par : **Carole Petit / Laurence Audin**
Soutenue le : **31/03/2023**

Devant le jury, composé de :
Romain Delunel, CR, Environnement Ville Société
Vincent Godard, Pr, CEREGE
Laure Guérit, CR, Géosciences Rennes
Sébastien Migeon, Pr, Sorbonne Université
Marianne Saillard, CR, Géoazur
Yannick Thiery, CR, BRGM
Invités :
Yann Rolland, MC, Edytem
Pierre G. Valla, CR, ISTerre

RgF RÉFÉRENTIEL GÉOLOGIQUE DE LA FRANCE

Géosciences pour une Terre durable brgm

INITIATIVE D'EXCELLENCE

UCA J.E.D.I. UNIVERSITÉ CÔTE D'AZUR

Thèse de Doctorat

Les modelés du Quaternaire récent au front des Alpes : évolution du relief et du climat

Thibaut Cardinal

Géoazur

Jury :

Rapporteurs :
Romain Delunel, chargé de recherche, Environnement Ville Société Lyon II
Laure Guérit, chargée de recherche, Géosciences Rennes

Examinateurs :
Vincent Godard, professeur, CEREGE
Sébastien Migeon, Professeur, Sorbonne Université
Marianne Saillard, chargée de recherche, Géoazur
Yannick Thiery, chargé de recherche, BRGM

Invités :
Yann Rolland, professeur associé, Edytem
Pierre G. Valla, chargé de recherche, ISTerre

Résumé

La réponse érosive aux déformations de la surface terrestre permet d'obtenir un enregistrement des variations isostatiques et des variations climatiques locales et globales. L'étude de l'érosion permet de mieux comprendre et de quantifier les processus de soulèvement dans des chaines de montagne et de mieux contraindre les variations climatiques qui s'y opèrent.

Les processus qui ont conduit à la formation des paysages sont souvent mal quantifiés lorsqu'il s'agit de marqueurs géomorphologiques verticaux. En effet, ces morphologies 3D enregistrent une combinaison de différents mécanismes d'érosion. Pour explorer ces difficultés, nous combinons la cartographie 3D haute résolution et la méthode de datation *Cosmic Ray Exposure* (CRE) dans la Clue de Barles. La distribution des âges CRE obtenus met en évidence deux domaines géomorphologiques distincts le long des parois verticales de la gorge : i) la section supérieure est caractérisée par des groupes d'âges CRE similaires, interprétés comme étant liés à des événements d'éboulement paraglaciaire ; ii) la section inférieure présente des âges CRE dégressif à mesure que l'on se rapproche du niveau actuel de la rivière, qui sont attribués à de l'incision fluviale.

A travers la régularité de processus en réponse à des forçages court-termes, les rivières ajustent irrévocablement leurs taux d'incision au forçage tectonique long-terme. Cependant, il reste difficile d'identifier le forçage dominant à court et long terme. Pour tenter de résoudre ce problème, nous avons mesuré les concentrations de ^{36}Cl le long de plusieurs parois de gorges polies par des rivières dans des calcaires jurassiques des Alpes du Sud-Ouest. Notre analyse montre que les gorges connectées à des glaciers subissent l'impact significatif des fluctuations climatiques, mise en évidence par des variations de taux d'incision de fortes amplitudes lors de périodes de déglaciation, masquant le signal tectonique long-terme. En revanche, les taux

d'incision quantifiés dans des gorges déconnectées sont similaires aux taux de dénudation et de soulèvement long-terme estimés précédemment dans la région. Sur la base de ces observations, nous proposons que l'incision des rivières du Quaternaire récent dans les Alpes du Sud-Ouest est un réajustement à la fois dû au forçage climatique court-terme et au forçage tectonique long-terme.

Dans les zones précédemment englacées, la discussion sur l'origine des gorges reste ouverte, et plus particulièrement à propos de l'échelle de temps nécessaire à leur formation et les processus concernées (fluviale vs. glaciaire). Pour apporter un nouveau regard sur ces questions, nous réexaminons des données de datation CRE obtenues dans des gorges de la vallée de la Tinée. Cela nous permet d'explorer les différents scénarios pouvant expliquer l'exposition des parois des gorges étudiées, pour enfin proposer une nouvelle interprétation sur la formation et l'évolution de ces gorges et des processus érosifs agissant dans les bassins versants alpins anciennement glaciaires. Nous proposons que les taux d'incision fluviale postglaciaire peuvent être surestimés, car la formation des gorges sous-glaciaires des Alpes pourrait être un processus à long terme qui se déroule sur plusieurs cycles interglaciaires-glaciaires plutôt que le résultat seul des dernières déglaciations.

Dans une autre tentative de réponse à la question de l'échelle temporelle à laquelle les gorges sont formées, nous avons choisi d'étudier les Hautes Gorges du Verdon, situées dans l'avant-pays des Alpes du Sud-Ouest. Nous y avons échantillonné les surfaces polies pour la datation CRE ^{36}Cl, ce qui nous a permis de contraindre un taux d'incision long-terme de 0.06-0.2 mm/yr entre 60 et 15 ka. Comparés au taux de soulèvement et de dénudation régional, ces taux mettent en évidence le rôle du soulèvement tectonique comme principal moteur de l'incision du Verdon au Quaternaire récent. Cette incision lente et long-terme, extrapolée sur toute la hauteur des gorges, semble indiqué que la formation des Hautes Gorges du Verdon a commencé entre 1,5 et 2 Ma.

Mots clés : Géomorphologie Quaternaire ; Incision fluviatile ; Datation

Abstract

The erosive response to land surface deformation provides a record of isostatic variations and local and global climate variations. The study of erosion allows a better understanding and quantification of tectonic uplift in mountain ranges and a better constraint of the climatic variations that affect them.

The processes that led to the formation of landscapes are often poorly quantified when it comes to vertical geomorphological markers. Indeed, these 3D morphologies record a combination of different erosion processes. To explore these difficulties, we combine high-resolution 3D topographic mapping and Cosmic Ray Exposure (CRE) dating in the "Clue de Barles". The distribution of CRE ages obtained highlights two distinct geomorphological domains along the vertical profile: i) the upper section is characterised by groups of similar CRE ages, interpreted as being related to paraglacial rock-fall events; ii) the lower section shows increasing CRE ages with height, which are attributed to fluvial incision.

Through the regularity of short-term processes, rivers irrevocably adjust their incision rates to the long-term tectonic forcing in order to reach an equilibrium state. However, it remains difficult to identify the dominant short and long term forcing. To address this issue, we measured ^{36}Cl concentrations along several river-polished gorge walls in Jurassic limestones of the Southwestern Alps. Our analysis shows that gorges connected to glaciers show a significant impact of climatic fluctuations, evidenced by variations in incision rates of high amplitudes hindering the long-term tectonic signal. In contrast, the incision rates quantified in disconnected gorges are similar to the rates of denudation and long-term uplift previously estimated for the region. Based on these observations, we propose that the incision of late Quaternary rivers in the Southwestern Alps is a readjustment to both short-term climatic and long-term tectonic forcing.

In previously glaciated areas, the debate on the origin of inner bedrock gorges is still inconclusive, and specifically regarding the time scale for their formation and the processes involved (fluvial vs. glacial). To shed new light on these questions, we re-examine CRE dating data obtained from gorges in the Tinée valley. This allows us to explore several different possibilities that could explain the exposure history of the sampled gorges walls and thus to propose a new interpretation of the formation and evolution of these gorges and the erosive processes acting in previously glaciated alpine catchments. We propose that postglacial fluvial incision rates may be overestimated, as it appears that the formation of the internal gorges of the Alps is a long-term process that unfolds over several interglacial-glacial cycles.

In another attempt at answering the question regarding the time scale at which gorges are formed, we chose to study the Hautes Gorges du Verdon, located in the foreland of the southwestern Alps. Here we sampled polished surfaces for CRE ^{36}Cl dating, which allowed us to constrain a long-term incision rate of 0.06-0.2 mm/yr between 60 and 15 ka. Compared to the regional uplift and denudation rates, these rates highlight the role of tectonic uplift as the main driver of the Verdon incision in the Late Quaternary. This slow and long-term incision, extrapolated over the entire height of the gorges, seems to indicate that the formation of the Hautes Gorges du Verdon started approximatively 1.5 to 2 Ma ago.

Keywords : Quaternary geomorphology ; Fluvial incision ; CRE dating

Remerciements

Lors de cette thèse j'ai eu le plaisir de travailler étroitement avec mes deux encadrantes de thèse, Carole Petit et Laurence Audin, ainsi que Yann Rolland. Ce travail n'aurait donc pas vu le jour sans leur confiance et leur aide. Je tiens donc à vous remercier du fond du cœur pour m'avoir donné cette opportunité et m'avoir soutenu tout le long de cette expérience.

J'ai également eu le plaisir de collaborer avec d'autres chercheurs que j'aimerai remercier dans ces lignes. Stéphane Schwartz, qui m'a encadré durant mon M1 et qui a continué à suivre de près mon travail depuis, notamment en m'aidant pour les missions sur le terrain. Je ne peux aborder le terrain sans mentionner encore une fois Yann, qui a donné de sa personne pour aller chercher mes échantillons à flanc de falaise. Swann Zerathe, qui m'a accompagné lors de mon introduction au monde des datations et m'a aidé à développer un esprit critique pour l'utilisation des méthodes. Pierre Valla, qui est arrivé plus tard dans ma thèse mais qui m'a grandement aidé pour les interprétations et a toujours apporté un regard extérieur précieux et bienveillant sur mon travail lors de relectures. Merci également à Jérôme Nomade, Julien Carcaillet et Thierry Dumont. Merci à Francis Coeur pour le broyage.

Lors de cette thèse j'ai collaboré avec Régis Braucher, Valery Guillou et ASTER Team au CEREGE pour la préparation de mes échantillons. Je les remercie pour leur aide et leur travail.

Je tiens à exprimer ma gratitude au BRGM et le programme RGF pour le financement de ma thèse. Je remercie Denis Thiéblemont pour son suivi et ses encouragements.

Je remercie Myette Guiomar de la Réserve naturelle nationale Géologique de Haute-Provence (RNGHP) pour les autorisations d'échantillonnage.

Je remercie le laboratoire Géoazur ainsi que l'Université Côte d'Azur. Merci à Véronique Large pour son aide précieuse à l'organisation de mes déplacements et sa gentillesse.

Je tiens à remercier Charlotte Fillon, Vincent Godard, Denis Thiéblemont et Pierre Valla pour avoir accepté de faire partie de mon comité de suivi de thèse.

Je tiens à remercier Romain Delunel, Vincent Godard, Laure Guérit, Sébastien Migeon, Yann Rolland, Marianne Saillard, Yannick Thiery et Pierre Valla pour avoir accepté de faire partie de mon jury de thèse.

Durant ces trois années et demi de thèse (et même en master), j'ai pu faire la connaissance et partager de nombreux moments avec des personnes formidables. Sans rentrer dans les détails de ce qui nous lie, je tiens à remercier Maxime, Hugo, Marco, Arianna, Giuseppe, Leoncio, Natalia (et Fuji), René, David, Mélina, Etty, Mathieu, Estelle, Guillaume, Daniel, Ahmed et Marion. Ce sont les moments passés en votre compagnie, allant d'une simple pause-café au labo à un bivouac à -15°C en passant par une sortie d'escalade et autres activités de montagne, qui m'ont donné l'énergie d'arriver au bout de cette expérience.

A la maison, merci à Adrien pour m'avoir permis de m'échapper une fois par an dans le Sud Finistère et Mathieu pour ses encouragements.

També vull donar les gràcies a la Júlia, que m'ha donat suport i acompanyat, més que ningú, durant aquesta tesi.

Enfin, merci à ma famille, chez qui j'ai toujours pu trouver un havre de quiétude nécessaire de temps en temps. Merci à mes parents pour leur soutien intemporel. Ce travail est également le vôtre.

Tables des matières

Chapitre 1 : Introduction

1. Contexte de l'étude

1.1. Contexte scientifique

La forme des paysages de montagne actuels témoigne d'une compétition permanente entre l'érosion, la sédimentation et le soulèvement (Hack, 1960 ; Willet, 1999 ; Whipple, 2001 ; Lavé et Avouac, 2001 ; Willet et al., 2002 ; Willet et Brandon, 2002). En d'autres termes, les reliefs sont le résultat combiné de l'érosion destructive qui les aplanit et de la tectonique motrice, qui les soulève. On peut donc considérer les reliefs comme « le bilan topographique de la compétition entre l'érosion et la surrection de la lithosphère » (Penck, 1924). La réponse érosive aux déformations de la surface terrestre, lorsque l'on peut la quantifier, peut permettre de déchiffrer l'effet des variations isostatiques (England et Molnar, 1990 ; Lavé et Avouac, 2001 ; Wobus et al., 2006 ; Kirby et Whipple, 2012) et des variations climatiques locales et globales (Bacon et al., 2009 ; Pan et al., 2003 ; Van der Woerd et al., 2002). Comprendre et quantifier comment l'érosion opère et varie spatialement et temporellement peut permettre, moyennant certaines hypothèses, de démêler l'interaction des processus de surface avec les forçages externes (tectonique et climat) et d'identifier le forçage dominant, moteur de l'évolution des reliefs (Montgommery et Brandon, 2002).

La vitesse à laquelle l'érosion façonne le paysage est très variable et est contrôlée par des processus opérant à différentes échelles temporelles et spatiales (Figure 1, Daniels, 2008). Ces processus interagissent les uns avec les autres, et l'étude des processus « court termes » peut permettre de mieux appréhender la dynamique l'implication des processus opérant à plus long terme. Par exemple, comme les variations climatiques (10^3-10^6 années, Figure 1) contrôlent les débits moyens d'eau dans les rivières (Lague et al., 2005), comprendre comment des inondations ponctuelles (10^{-5}-10^0 années, Figure 1) influencent les taux d'incision donne un aperçu de la sensibilité à long terme du paysage aux changements climatiques (Hartshorn et al., 2002). Grâce à la régularité des processus à court terme (~10^{-7}-10^4 années, Figure 1), les

paysages s'ajustent irrévocablement, à travers les variations des taux d'érosion qui les affectent, au forçage tectonique long terme (10^5-10^9 années, Figure 1) afin d'atteindre un état d'équilibre, dans lequel l'érosion est égale au soulèvement des roches (Whipple et Tucker, 1999 ; Wobus et al., 2006).

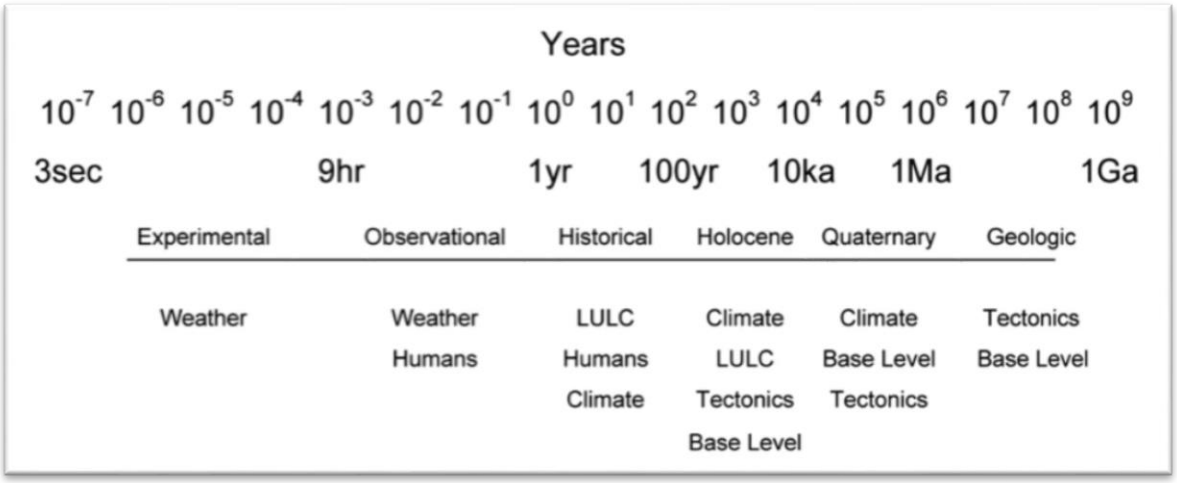

Figure 1-1 : De Daniels (2008) ; Conceptualisation de l'échelle temporelle à laquelle les différents forçages affectent l'érosion.

Ce travail de thèse s'inscrit dans la démarche de mieux préciser la chronologie et l'amplitude des phénomènes érosifs au cours du Quaternaire récent (depuis le LGM) dans les Alpes du Sud-Ouest. En particulier, nous souhaitons mieux quantifier l'incision fluviale associée aux bassins versants situés à l'extérieur et à l'intérieur de la zone d'influence glaciaire, ainsi que le moment de la déglaciation de cette dernière. Cette échelle nous permettra également de comparer la dynamique de l'incision du cœur de la chaîne aux zones extérieures, afin d'évaluer la contribution des mouvements verticaux et celle du climat.

1.2. Le moteur de l'évolution récente du relief dans les Alpes

Durant le dernier million d'années, le relief de la chaîne des Alpes a considérablement été affecté par les glaciations (e.g. Valla et al., 2011). Cependant, de récents résultats de modélisation indiquent que d'autres facteurs ont probablement contribué à l'accélération de l'érosion des Alpes depuis 1 Ma (Sternai et al., 2013). Ces auteurs mettent notamment en avant

une potentielle augmentation des taux de soulèvement, dont la cause (rebond isostatique ou soulèvement tectonique) est incertaine. Ainsi, l'identification du moteur dominant de l'érosion dans les Alpes est encore débattue.

De plus, contribuer à ces questionnements au moyen d'une approche géomorphologique, dans une chaîne de montagnes précédemment englacée, n'est pas tâche facile. En effet, la topographie et les marqueurs d'érosion formés au cours d'un cycle glaciaire-interglaciaire peuvent être rajeunis, voire effacés, lors du prochain cycle par l'érosion glaciaire et post-glaciaire.

1.2.1. Fluctuations climatiques

Les fluctuations du climat entraînent de fortes variations dans les modalités de l'érosion, en particulier en domaine de montagnes. L'augmentation de température en période inter-glaciaire entraîne le recul du permafrost, une réduction de la cryoclastie, un recul des glaciers, et une transition vers un régime dominé par le rôle de l'eau liquide : précipitation, dissolution, érosion des sols, augmentation du débit des rivières. Ces paramètres jouent un rôle clé pour l'érosion et l'amplification de l'incision. Les variations climatiques contrôlent ces paramètres et vont également induire de fortes variations spatiales et temporelles des taux d'érosion.

Au cours des changements climatiques répétés du Quaternaire, l'avancée et le recul des glaciers ont façonné le paysage alpin contemporain (Valla et al., 2011 ; Herman et al., 2013 ; Glotzbach et al., 2013). Les zones glaciaires accumulent un déséquilibre topographique pendant les glaciations (Norton et al., 2010), qui peut ne pas être entièrement compensé pendant les interglaciaires et peut donc s'accumuler sur plusieurs périodes glaciaires (Salcher et al., 2014). Après le retrait des glaciers, les vallées précédemment glaciaires subissent une érosion accélérée pour tenter de se réajuster aux perturbations induites par les glaciers (Norton et al., 2010 ; Fox et al., 2015). De plus, une période humide et très pluvieuse durant les interglaciaires favorisera l'érosion des versants et la remobilisation des dépôts glaciaires qui alimentent les

cours d'eau en charge solide grossière (Ballantyne, 2002 ; Meigs et al., 2006). Lors de périodes de fort débit liquide liées à un climat humide, la charge solide, et notamment la charge de fond grossière (Sklar et Dietrich, 1998) est transportée et contribue à l'érosion des berges et du lit des cours d'eau (Sklar and Dietrich, 1998 ; Whipple, 2001 ; Johnson and Whipple, 2007 ; Turowski et al., 2007 ; Whittaker et al., 2010).

Qui de l'érosion glaciaire ou interglaciaire a eu l'impact le plus conséquent sur les taux d'érosion est encore débattue. En effet, des analyses sédimentaires et géochimiques conduisent à proposer un plus fort pic d'érosion soit durant la période où les glaciers étaient actifs (Mariotti et al., 2021), soit durant la période de déglaciation (Hinderer, 2001). Néanmoins, plusieurs auteurs s'accordent pour dire que l'érosion actuelle des Alpes est une réponse au déséquilibre topographique engendré par les dernières glaciations (Schlunegger and Norton, 2013 ; Van den Berg et al., 2012).

1.2.2. Variations eustatiques

Les variations climatiques ont également un impact sur le niveau eustatique global. Pendant les périodes glaciaires, l'eau est retenue par les glaciers et les calottes polaires, et le niveau de la mer baisse. Cette baisse du niveau de la mer est ressentie par les cours d'eau et entraîne une incision accrue des rivières, qui vont tenter de rattraper la baisse du niveau de base (Kirby et Whipple, 2012).

Bien que d'origine non climatique, les impacts de la crise de salinité messinienne sur l'activité érosive des rivières bordant la mer Méditerranée illustrent les processus érosifs associés à une baisse forte du niveau de base (Loget et Van Den Driessche, 2009). En effet, durant la période allant de 5,96 Ma à 5,332 Ma (Gautier et al., 1994 ; Krijgsman et al., 1999 ; Lourens et al., 2004), la mer Méditerranée a vu son niveau baisser d'environ 1500 m (Clauzon et al., 1996). Les rivières périphériques, notamment le Rhône et la Durance, ont alors profondément incisé le substratum du pourtour méditerranéen (Clauzon, 1979, 1982).

1.2.3. Tectonique et réponse isostatique

Le mouvement vertical de la lithosphère dû à sa réponse isostatique (à la charge ou à la décharge de la surface ou à un changement de densité du manteau) peut entraîner des changements dans l'élévation de la surface terrestre. Localement, la surface peut subir un soulèvement ou un affaissement. Pour des échelles de temps correspondant aux cycles glaciaires ($<10^5$ ans), la fonte et la disparition des glaciers produit un soulèvement par un phénomène de rebond isostatique (Gudmundsson, 1994 ; Bishop et al., 2005 ; Vernant et al., 2013). En effet, en réponse à la perte de charge imposée par une masse de glace en cours de fonte, la lithosphère, qui possède des propriétés élastiques, s'élève à une vitesse imposée par l'écoulement du manteau visqueux sous-jacent (Walcott, 1973 ; Peltier et Fairbanks, 2006). La perte de matériel sédimentaire par érosion et transport peut également provoquer ce type de soulèvement (Molnar et England, 1990 ; Montgomery, 1994 ; Small et Anderson, 1995 ; Champagnac et al., 2007). Sur des échelles de temps plus grandes ($>10^6$ ans), les mouvements horizontaux à l'échelle des plaques lithosphériques peuvent provoquer des déplacements verticaux significatifs dont (par exemple) le plissement de la couverture sédimentaire et/ou la remontée tectonique des unités du socle cristallin. L'épaississement crustal qui en résulte est compensé isostatiquement par un soulèvement de la topographie qui va à son tour amplifier l'érosion (e.g. Schwartz et al., 2017). Ces phénomènes conduisent au soulèvement de la surface terrestre, ce qui perturbe le profil d'équilibre des rivières (Kirby et Whipple, 2012). En effet, en réponse à un gradient topographique accentué, l'augmentation des contraintes de cisaillement du cours d'eau sur le substratum rocheux va augmenter le taux d'érosion et stimuler l'incision des rivières pour équilibrer le soulèvement (Burbank, 2002).

Dans le massif cristallin externe (MCE) de l'Argentera-Mercantour, les taux de refroidissement estimés par thermochronologie à basse température (trace de fission de l'apatite et datation U-Th/He de l'apatite), sont en accord avec des taux d'exhumation de 0,8-1,4 mm/an

au cours des 10 derniers Ma (Bogdanoff et al., 2000 ; Bigot-Cormier et al., 2006 ; Sanchez et al., 2011). Dans le domaine frontal des Alpes, des datations à l'apatite (U-Th/He) sur des sédiments de bassin avaient montré un reset induit par la nappe de charriage de Digne (Figure 1B) et permettent d'estimer des taux d'exhumation moyens de l'ordre de 0,7 mm/an depuis 5 Ma (Schwartz et al., 2017). À l'est de la ville de Nice, Bigot-Cormier et al. (2004) ont analysé les profils de sismique-réflexion pour déduire des taux de soulèvement de 0,3-0,5 mm/an de la marge nord-ligure depuis 5 Ma. En ce qui concerne le soulèvement actuel, plusieurs études utilisant des données GPS dans les Alpes (Serpelloni et al., 2013 ; Nocquet et al., 2016 ; Walpersdorf et al., 2018 ; Sternai et al., 2019 ; Piña-Valdés et al., 2022) mettent en évidence des déplacements verticaux allant de ~1mm/an dans la partie centrale des Alpes de l'Ouest, à <0,5 mm/an dans les Alpes du Sud-Ouest.

La cause du soulèvement actuel des Alpes est débattue. Sternai et al. (2019) ont testé, par modélisation, le rôle de la fonte des glaciers, de l'érosion et des processus affectant le manteau. Les résultats indiquent que le soulèvement observé est causé pour moitié par un ajustement lithosphérique aux déglaciations et à l'érosion. L'origine du soulèvement est donc encore incertaine, et les mesures contemporaines montrent des taux trop faibles pour représenter, en prenant en compte leurs incertitudes, des résultats fiables.

1.3. Les marqueurs de l'érosion et leur intérêt pour comprendre la dynamique des paysages

L'étude de l'érosion peut permettre de mieux comprendre les processus qui contrôlent l'évolution du relief dans les chaînes de montagnes (Lavé et Avouac, 2001 ; Wobus et al., 2006 ; Kirby et Whipple, 2012) et d'estimer la réponse de ces dernières aux variations climatiques ou tectoniques.

1.3.1. Les principaux agents et processus d'érosion

L'eau, sous forme liquide ou solide, participe de manière significative au réajustement des reliefs par le mécanisme d'équilibrage « érosion-surrection ». En l'absence de glaciers, ce sont les rivières qui sont les agents d'érosion et d'évacuation des particules les plus efficaces (Hay, 1998 ; Hovius, 2000). Les glaciers et les rivières fixent le niveau de base local des versants adjacents, ils ont donc un grand impact sur la dénudation des vallées et l'évolution globale du relief (Willett, 1999). En effet, le recul des glaciers est connu pour être suivi d'une période de décompression des versants à l'origine des glissements de terrain (Meigs, 1998 ; Cossard et al., 2008 ; Ballantyne et al., 2014). De même, les rivières, en incisant le talweg des vallées, régissent la pente des versants (Burbank, 2002). Si l'incision s'accentue, la pente des versants augmente et ces derniers se trouvent alors plus sensibles à la dénudation par glissement de terrain, l'altération ou encore la cryoclastie. En se réajustant aussi à l'incision fluviatile ou à l'absence de pression par les glaciers, les versants s'érodent et le produit de cette érosion va s'accumuler par gravité au pied des versants jusque dans les cours d'eau. Cette charge solide est alors transportée par les rivières, ou déposée si l'énergie du cours d'eau n'est pas suffisante pour le transport.

L'efficacité de l'incision est contrôlée par des caractéristiques locales telles que la lithologie du substrat rocheux et la morphologie du chenal. En effet, la résistance et le degré de fracturation et d'altération de la lithologie du substrat influencent les taux d'incision (Whipple et al., 2000) et dictent le processus dominant du mécanisme d'érosion et son efficacité : l'abrasion et le détachement sont généralement dominants dans les roches peu fracturées et fracturées, respectivement (Sklar et Dietrich, 2001 ; Hartshorn et al., 2002 ; Cowie et al., 2008 ; Cook et al., 2013). De plus, la morphologie du chenal (largeur, courbure, rugosité du lit, pente) contrôle la distribution de la contrainte de cisaillement le long du chenal de la rivière, et a donc

un impact sur la capacité de transport des particules (Johnson et al., 2010), qui à son tour détermine l'efficacité de l'incision (Jansen et al., 2011 ; Cook et al., 2013).

1.3.2. Les marqueurs d'érosion fluviatile

1.3.2.1.Knickpoints

Le profil longitudinal « idéal » est lisse et concave, mais ce profil est assez rare pour des cours d'eau de type *bedrock streams* (qui coulent directement sur un substrat rocheux), qui sont souvent marqués par des irrégularités localement convexes (Phillips et Lutz, 2008). Ces convexités sont appelées *knickpoint*s ou *knickzones*, et forment une rupture de pente dans le profil en long d'un cours d'eau (Figure 2A, B ; Gardner, 1983 ; Bishop *et al.*, 2005) qui souligne un déséquilibre local dans le profil d'équilibre de la rivière. Les *knickpoint*s traduisent un état transitoire dans le profil de la rivière en réponse à une perturbation ou une caractéristique lithologique particulière. Ce sont des marqueurs de l'incision des cours d'eau (Phillips et Lutz, 2008), et ils peuvent être engendrés par des facteurs extérieurs ou par des caractéristiques lithologiques et/ou tectoniques locales (Gardner, 1983). De manière générale, la formation des *knickpoint*s est associée à l'intensification de l'érosion fluviatile (Phillips and Lutz, 2008).

La présence d'un *knickpoint* entraîne un changement du régime hydrologique. A l'approche de la lèvre (*lip*) du knickpoint, la largeur du cours d'eau diminue et l'érosion du lit s'accélère. Les *knickpoint*s évoluent donc rapidement après leur formation. Différents types d'évolutions peuvent affecter ces formes (Gardner, 1983) :

- L'évolution par aplanissement : implique une augmentation de la pente du *drawdown* (partie en amont de la lèvre du *knickpoint*) et une diminution de la pente du front du *knickpoint* (*knickpoint face*). Le *knickpoint* subit donc une érosion progressive et est ainsi amené à s'effacer. L'évolution par aplanissement se produit surtout dans le cas d'une lithologie de résistance homogène.

- L'évolution par replacement : si l'érosion fluviale s'accélère, ou dans le cas d'un mouvement tectonique (exemple : séisme), une fracture ou un joint situé en amont d'un premier *knickpoint* peut se transformer à son tour en un deuxième *knickpoint*. Suite à cette soudaine discontinuité dans le profil longitudinal, le premier *knickpoint* (aval) va se détruire plus rapidement, au profit de la formation du second (amont). Ainsi, de fracture/joint en fracture/joint, les *knickpoint*s peuvent migrer vers l'amont.

- L'évolution par recul parallèle (*headward retreat*) : implique une érosion continue de la partie sub-verticale du knickpoint (Figure 2C). Seul le front du *knickpoint* est concerné et migre vers l'amont. L'érosion qui conduit à cette migration est différente selon les caractéristiques lithologiques du substrat. Dans le cas d'une hétérogénéité lithologique, avec une couche sous-jacente moins résistante, le recul se fait par sapement de la base du front du *knickpoint*. Des blocs de la couche supérieure compétente sont alors mis en surplomb et se décrochent ou basculent par appel au vide. Dans le cas d'une homogénéité lithologique, le recul du *knickpoint* se fait par dégradation de la roche et déstabilisation rocheuse. Ce type de recul est qualifié de parallèle car toute la largeur de la lèvre du *knickpoint* est soumis au même taux de recul.

Les comportements d'évolution décrits concernent les knickpoints transitoires qui se forment en réponse à un déséquilibre le long du profil de la rivière. D'autres knickpoints peuvent se former en raison d'une résistance différentielle du substrat à l'érosion fluviale. Ainsi, lorsque les cours d'eau rencontrent une couche de roche plus compétente que les couches voisines, l'incision est ralentie et conduit à la formation d'une discontinuité dans le profil longitudinal. Ces points d'accroche lithologiques, s'ils sont formés dans une couche de roche compétente suffisamment épaisse, sont statiques et ne migrent pas vers l'amont (Jansen et al., 2010).

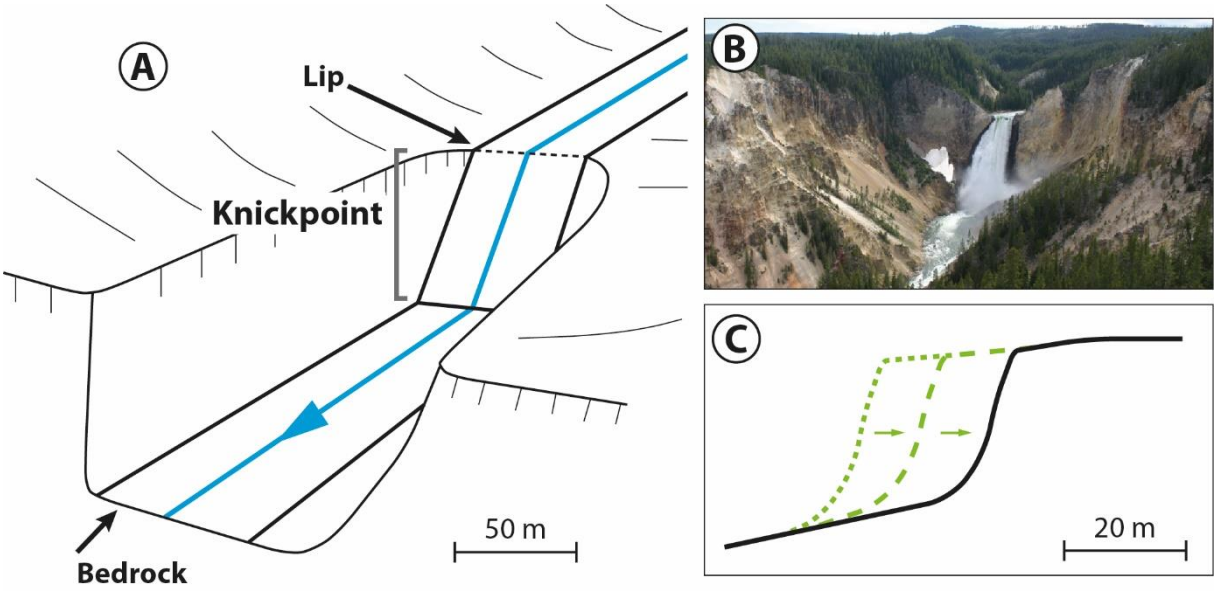

Figure 1-2 : A, morphologie d'un knickpoint (modifié de Hayakawa and Matsukura, 2003, d'après Gardner, 1993 ; Bishop et al., 2005) ; B, Photo d'un knickpoint (Yellowstone, USA) ; C, représentation schématique d'un recul de knickpoint.

L'analyse de l'évolution d'un knickpoint, et notamment la détermination de sa vitesse de recul, permet de quantifier l'incision d'un cours d'eau (Hayakawa et Matsukura, 2003 ; 2009). En effet, lors d'une chute du niveau de base, le réajustement du profil du cours d'eau par incision va commencer à l'embouchure pour progressivement remonter vers l'amont. On parle ici d'érosion régressive ou encore de « vague d'incision » qui se manifeste par le recul parallèle progressif du knickpoint (Weissel et Seidl, 1998 ; Whipple et Tucker, 1999).

1.3.2.2.Terrasses

Les terrasses alluviales sont des formes planes d'érosion (sans dépôts corrélatifs) ou d'accumulation (nappe alluviales). Il s'agit de fragments résiduels d'anciennes surfaces d'alluvionnement plus ou moins intactes et mises en relief lors de l'incision progressive de la rivière dans le substrat rocheux (Leland et al., 1998). Les terrasses alluviales se trouvent donc sur les versants de vallées incisées, perchées au-dessus du lit majeur actuel. Un fort débit liquide capable de transporter la charge sédimentaire favorise l'incision de la plaine alluviale et l'abandon des terrasses. A l'inverse, un fort apport sédimentaire et un faible débit favorisent la formation de surfaces d'alluvionnement (Schildgen et al., 2002).

Il existe deux types de terrasses alluviales (Merritts et al., 1994) :

- Les terrasses de comblement (*fill-terraces*) : surfaces de dépôt sédimentaire formées durant l'ensevelissement d'un fond de vallée lors d'une période d'aggradation. Les surfaces de dépôt sont abandonnées lorsqu'une nouvelle phase d'incision commence.

- Les terrasses rocheuses (*strath-terraces*) : surfaces rocheuses érodées et nivelées par un cours d'eau. Elles sont fréquemment recouvertes de dépôts alluviaux peu épais, voir érodées si elles sont assez basses pour être atteintes par les crues du cours d'eau. Si une période d'aggradation succède à un nivellement, les terrasses rocheuses deviennent des terrasses de comblement à fond plat.

Les terrasses se forment par rétrécissement de la plaine alluviale. Le régime du cours d'eau change et il s'en suit une incision. Lors de l'enfoncement du cours d'eau, la bande de divagation rétrécit, abandonnant ainsi une partie de la plaine alluviale en hauteur (Figure 3).

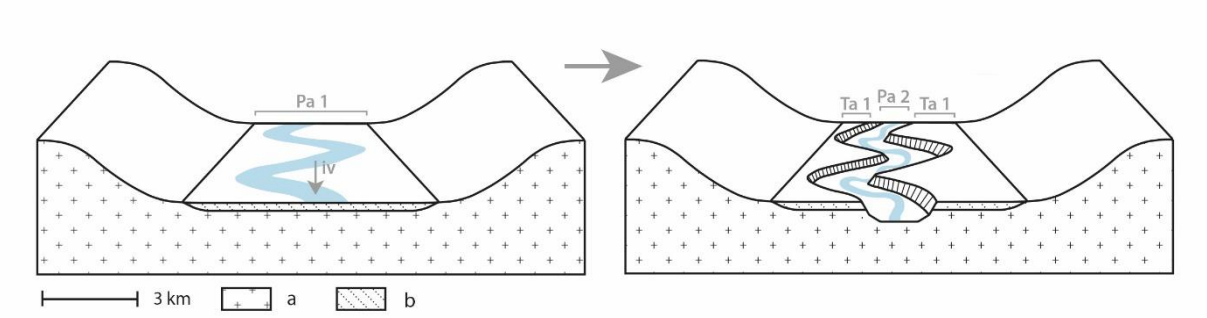

Figure 1-3 : Formation de terrasses alluviales (Pa : plaine alluviale ; Ta: terrasses alluviales ; iv : incision verticale ; a : substrat rocheux b: dépôts alluviaux ; modifié d'après Brocard, 2003).

A l'inverse, l'élargissement de la bande de divagation se produit en période froide, lors d'une augmentation de la charge sédimentaire et une diminution du débit (Gautier, 1992 ; Bloom, 1998). Les cours d'eau sont alimentés en sédiments par les versants, qui sont plus exposés à l'érosion en période froide. En effet, la réduction de la couverture végétale (Chapron, 1999) et l'imperméabilisation des sols à cause de la formation d'un permafrost (Bloom, 1998) favorisent le ruissèlement de surface. De plus, les contrastes thermiques impliquent la formation

de gélifracts et cryoclastes et entraînent des mouvements de terrains divers (cryoturbation, gélifluction, solifluction ; Bloom, 1998).

Les terrasses sont généralement synchrones, c'est-à-dire que l'on retrouve deux terrasses, formées au même moment, de chaque côté de la vallée. Cependant, il existe aussi des terrasses impaires (sans correspondance de l'autre côté du versant), qui se forment aléatoirement au gré de la divagation du cours d'eau pendant l'incision. Cependant, l'emplacement de terrasses alluviales peut être très difficilement lisibles dans le paysage. En effet, les terrasses qui se sont formées dans des terrains peu compétents (ex : marnes), ou encore les terrasses de comblement, sont très sensibles aux glissements de terrain ou aux effondrements. Les indices de l'incision peuvent donc être détruits au cours du temps, ou glisser le long des versants et atteindre une altitude ne correspondant plus au paléo-niveau auquel elles appartiennent.

La détermination de la concentration en ^{10}Be dans des galets riches en quartz à la surface de la terrasse permet de dater l'abandon de la terrasse, si l'on considère que l'âge d'abandon de la terrasse est contemporain de l'âge du dépôt de la couche la plus élevée de la terrasse (Carcaillet et al., 2009). Ensuite, connaissant la position de la terrasse par rapport au lit actuel de la rivière et l'âge d'abandon de cette terrasse, on peut estimer une vitesse moyenne d'incision (moyenne, car ne prend pas en compte les variations de vitesses d'incision dans le temps).

1.3.2.3.Gorges

Une gorge témoigne d'un fort et rapide épisode d'incision focalisée (Valla et al., 2010 ; Rolland et al., 2017). De surcroît, elles sont particulièrement propices à la conservation de marqueurs d'érosion du substrat rocheux. En effet, les parois verticales rocheuses sont recouvertes de cicatrices de l'incision et de traces des paléo-niveaux du cours d'eau à l'origine de la formation de la clue.

On y trouve notamment des marmites (ou *pot holes* ; Figure 4A). Ces cavités sont créées par la turbulence dans des cours d'eau de type torrentiel. Il s'agit de dépressions dans le lit d'un cours d'eau qui ont été élargies et creusées par l'action mécanique érosive de galets au fond de ses dernières. En effet, les galets pris au piège dans ces trous, au départ peu profonds, sont mis en mouvement par la turbulence qui les fait tourner et ainsi contribuent à émousser les bords de la marmite. Lorsque le cours d'eau s'encaisse, des traces de ces marmites peuvent être conservées sur les parois, et prennent la forme de légers renfoncements concaves. On retrouve également à l'intérieur de la gorge des surfaces polies (Figure 4B) et des replats (Figure 4C). Il faut toutefois faire attention à ne pas confondre ces traces d'érosion avec des niches d'arrachement créées par des déstabilisations rocheuses, très fréquentes dans les parois rocheuses verticales et dont les limites peuvent être effacées avec le temps (Valla et al., 2010).

En quantifiant la concentration de nucléides cosmogoniques dans ces surfaces affectées par l'érosion fluviatile, il est possible de dater leur exposition. La détermination de ces concentrations en plusieurs endroits le long d'un profil vertical permet de quantifier un taux d'incision, en comparant l'âge d'exposition avec la hauteur de la surface échantillonnée. Cette méthode est plus amplement décrite dans le Chapitre 2.

Figure 1-4 : Marqueurs de l'incision au sein des parois d'une gorge (a : marmite ; b : surface polie ; c : replat).

2. Présentation de la zone d'étude

Située dans les Alpes françaises du Sud-Ouest, la zone étudiée ici est située à la frontière entre l'avant-pays alpin relativement stable et la chaîne de montagne encore en cours de soulèvement, et également à la limite de l'étendue de la dernière glaciation. En effet, de nombreux bassins versants se situent au-delà du domaine précédemment englacé pendant les dernières périodes glaciaires, ce qui les rend appropriés pour quantifier la dynamique de l'incision fluviale dans un environnement non-glaciaire. Par conséquent, les Alpes du Sud-Ouest sont une zone d'étude majeure pour déchiffrer l'implication des forçages tectoniques et climatiques dans l'incision fluviale.

2.1. Présentation générale des Alpes du Sud-Ouest

La zone d'étude correspond au Sud-Ouest des Alpes Européennes, et plus précisément le Sud-Est des Alpes Françaises. Elle englobe globalement une région qui va de la ville de Digne-les-Bains jusqu'au Massif du Mercantour, et s'étend au sud-est jusqu'à la frontière Italienne (Figure 5A). Elle comprend tout ou partie des bassins versant de la Durance, du Var, de la Roya, ainsi que du Paillon.

2.2. Contexte géologique et tectonique

Dans les Alpes du Sud-Ouest (Figure 5A), la formation des montagnes résulte d'un processus de collision qui s'est produit pendant les phases tectoniques pyrénéenne (Crétacé supérieur à Éocène) et alpine (Néogène). L'avant-pays alpin correspond au front de déformation externe qui a commencé à se propager vers l'ouest et le sud pendant la collision alpine (34-32 Ma ; Ford et al., 2006). Le domaine de l'avant-pays correspond à une zone caractérisée par des plis et des chevauchements affectant la couverture sédimentaire de la plaque européenne. Les déformations chevauchantes de l'avant-pays s'enracinent dans le socle du massif cristallin externe de l'Argentera (ECM, Jourdon et al. 2014). Ce domaine du socle cristallin européen a été soulevé au cours du Mio-Pliocène (Lickorish & Ford, 1998 ; Sanchez et al., 2011) (Figure 5B). La nappe de charriage de Digne correspond à la limite occidentale de l'avant-pays alpin. Elle contient une séquence sédimentaire du Trias à l'Éocène de ≈5 km d'épaisseur (Gidon, 1997 ; Schwartz et al., 2017). La nappe de Digne chevauche des séries mésozoïques autochtones recouvertes par des bassins sédimentaires d'avant-pays cénozoïques (Figure 5B).

Du fait de son histoire structurale, les Alpes du Sud-Ouest sont caractérisées par de forts contrastes lithologiques. En effet, le plissement de la couverture sédimentaire produit à la surface une alternance entre barres de roches compétentes, correspondant principalement au calcaire Tithonien (Jurassique sup.), et autres lithologies moins compétentes, correspondant principalement aux marnes « Terres Noires » (Jurassique moy. à sup.) ou aux alternances marno-calcaires du Crétacé (Figure 5C).

Des études ont montré que la partie interne des Alpes est soumise à une déformation en extension depuis 3 Ma, alors que les Alpes externes subissent une compression (Sue et al., 2007 ; Bilau et al., 2020), comme le montrent la géodésie (Walpersdorf et al., 2018) et la sismicité (Mathey et al., 2021). Ce schéma de déformation est caractérisé par un taux de raccourcissement NW-SE à N-S ≤1 mm/an (Nocquet et Calais, 2004).

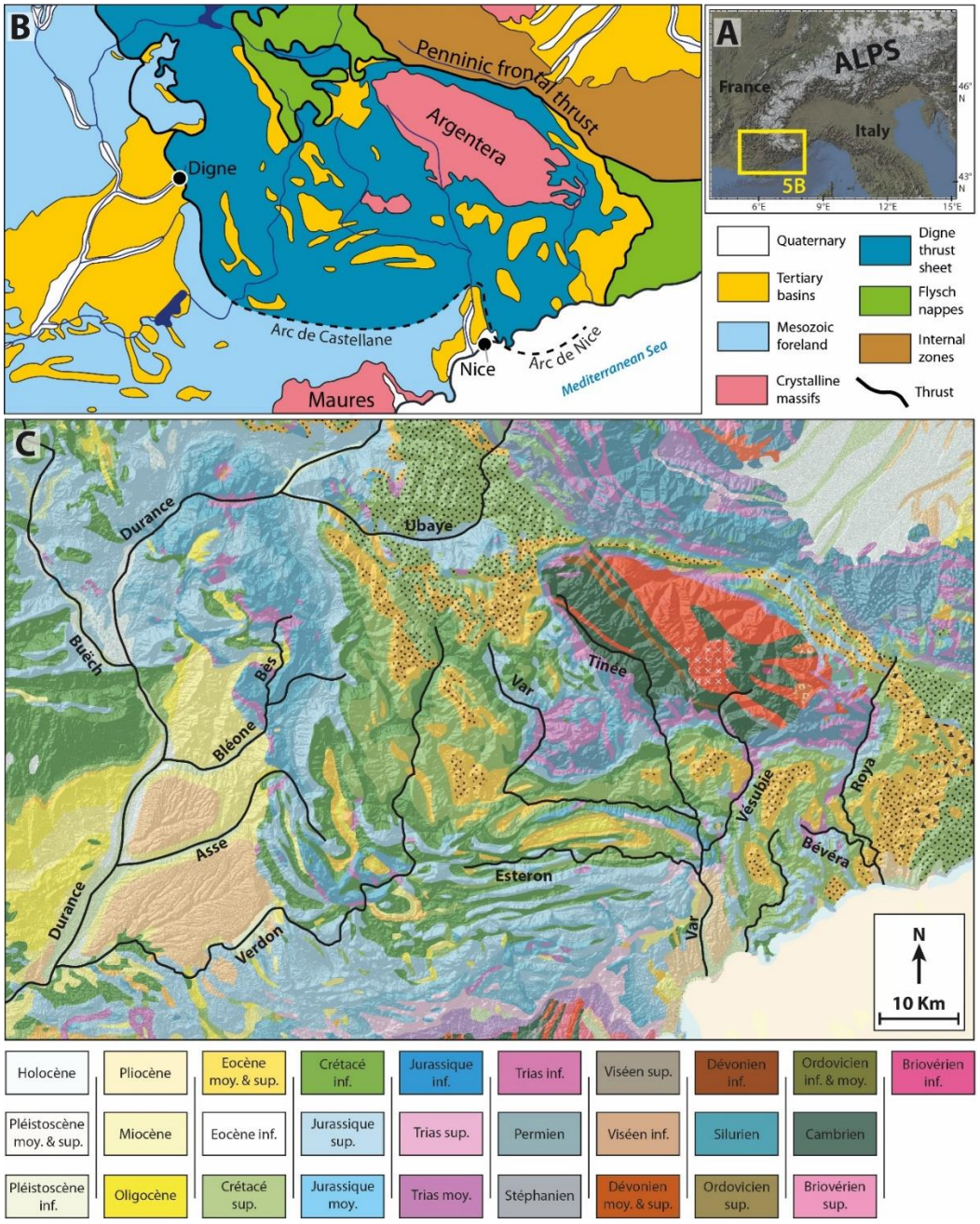

Figure 1-5 : A, Localisation de la zone d'étude dans les Alpes Européennes. B, contexte tectonique général des Alpes du Sud-Ouest (modifié après Schwartz et al., 2017). C, Carte géologique de la zone d'étude et localisation des principales rivières.

2.3.Variations climatiques du Quaternaire récent dans les Alpes

Le Dernier Maximum Glaciaire (LGM) correspond à la période où les glaciers ont atteint leur extension maximale, vers 19-26.5 ka (Clark et al., 2009). Le LGM a eu un impact considérable sur le relief alpin en accélérant et en concentrant l'érosion (Darnault et al., 2012). Avec une extension hétérogène dans les Alpes, le LGM est daté à 21,5 ka dans les Alpes du Sud-Ouest (Jorda et al., 2000). Dans cette région, les glaciers descendaient jusqu'à 600 m

d'altitude, avec une épaisseur variant de 600 à 1000 m (Cossart et al., 2008). Le LGM est suivi d'une période de fonte et de retrait des glaciers à partir de 18-19 ka, au cours de laquelle les glaciers ont perdu jusqu'à 80% de leur volume (Figure 6 ; Ivy-Ochs et al., 2006). La déglaciation n'a pas été continue. En effet, de nombreux événements climatiques ont marqué le processus de déglaciation pendant la période tardiglaciaire, de 18 à 11 ka (Ivy-Ochs et al. 2008).

Trois stades tardiglaciaires ont été datés dans les Alpes du Sud-Ouest. Sur le versant italien (NE) du massif de l'Argentera-Mercantour (Figure 1A), Federici et al. (2016) ont daté un ensemble préservé de moraines frontales dans la vallée du Gesso. La moraine la plus basse, à 750 m.a.s.l., permet d'estimer le début de la déglaciation LGM à 21-24 ka, et est suivie par le dépôt de deux autres moraines, situées à ≈850 m.a.s.l. et 1800 m.a.s.l., que les auteurs ont reliées aux stades de Bühl et d'Egesen, respectivement.

A partir de 11,7 ka, la planète entre dans l'Holocène (Figure 6 ; Ivy-Ochs et al., 2008 ; Heiri et al., 2014). Cette période de climat plus chaud et plus humide (Wanner et al., 2011, 2015) a également connu une période de ré-avancement mineur des glaciers (Ivy-Ochs et al., 2006 ; Darnault et al., 201 ; Schimmelpfennig et al., 2012 ; Federici et al., 2016). Warner et al. (2011) ont proposé une division de l'interglaciaire actuel en trois périodes climatiques : (1) une phase de déglaciation suivant immédiatement la fin de la phase froide du Dryas récent et caractérisée par une importante fonte des glaces ; (2) l' " Optimum thermique holocène " entre 11 et 5 ka (Wanner et al, 2008, Renssen et al., 2009, 2012), caractérisé par un climat plus chaud et plus stable, et (3) une période "néoglaciaire", avec des conditions plus froides et des taux de précipitations plus élevés à la fin de l'Holocène (Davis et al., 2003).

Les fluctuations du volume de glace des glaciers et la chronologie des retraits/avancées glaciaires sont moins bien marqués sur le versant français des Alpes du Sud-Ouest du fait d’une exposition majoritairement Sud des versants (Rolland et al., 2019). Cette exposition conduit à une déglaciation principale précoce après le LGM. Les marqueurs de la glaciation quaternaire,

tels que les moraines frontales, sont rares dans les basses vallées de la Tinée, de la Vésubie et du Var. En effet, la taille, l'altitude et la proximité de la mer Méditerranée font du bassin versant du Var un bassin très réactif, où les sédiments sont rapidement transportés et entraînés vers la mer (Bonneau et al., 2017 ; Mariotti et al., 2021).

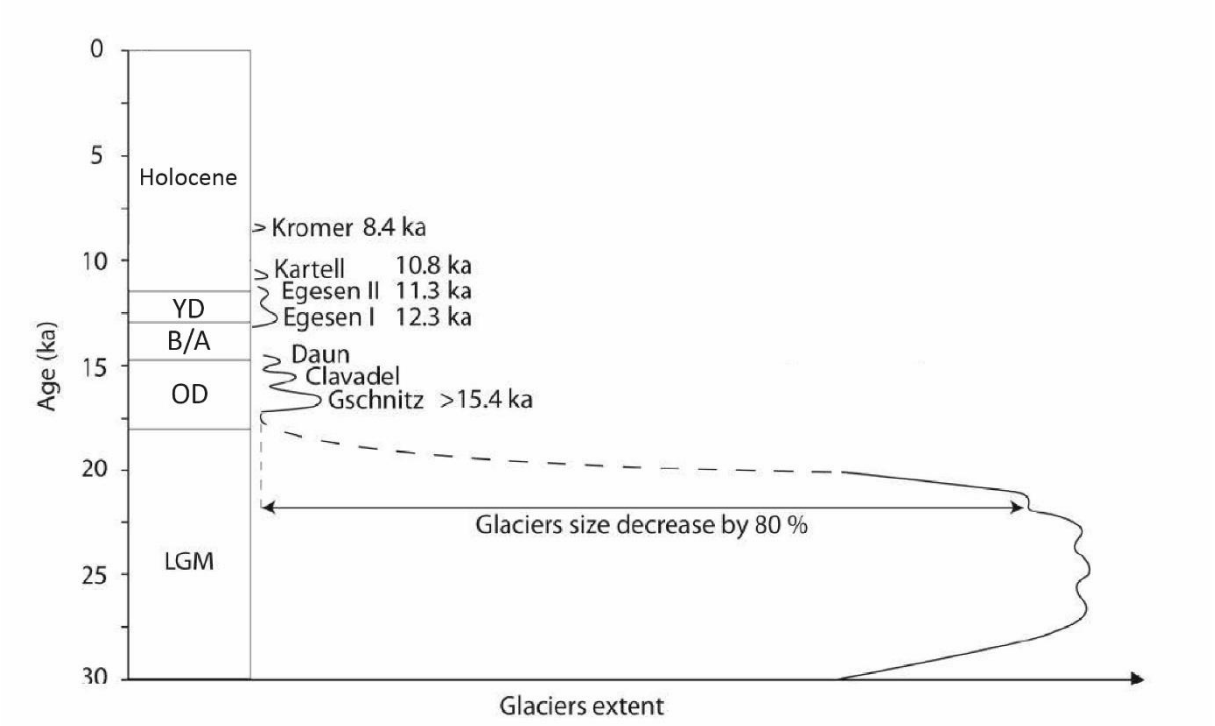

Figure 1-6 : Evolution théorique de l'étendue des glaciers Alpins au cours du dernier cycle glaciaire (modifié de Ivy-Ochs et al., 2006, d'après Bonneau, 2014 et références incluses).

3. Objectifs de la thèse

Les approches à l'échelle du bassin versant ont été couramment utilisées pour estimer les taux d'érosion moyens (i.e. Bierman et Steig, 1996), à l'aide de datations de surfaces d'érosion (i.e. Godard et al., 2020), d'analyses morphométriques des réseaux hydrographiques (i.e. Cyr et al., 2010), de la datation de terrasses alluviales (i.e. Brocard et al., 2013) ou encore de la datation des systèmes karstiques (i.e. Genuite et al., 2022). Différentes études ont été réalisées afin de quantifier des taux d'incision fluviale à partir de parois rocheuses verticales utilisant les nucléides cosmogéniques en Himalaya (Pratt et al., 2002), à Taiwan (Schaller at al., 2005) ou localement sur différents bassins versants des Alpes françaises du Sud-Ouest (i.e. Saillard et

al., 2014 ; Rolland et al., 2017 ; Petit et al ; 2019). Ces études ont démontré une forte relation entre l'accélération de l'incision fluviale et le retrait glaciaire post-LGM (Last Glacial Maximum, ~20 ka), pointant vers la transition climatique de conditions glaciaires à interglaciaires comme le principal facteur de contrôle de l'incision postglaciaire et de l'évolution de ces vallées. Les taux d'incision résultant de ces études montrent donc le potentiel de ces résultats comme proxy pour quantifier l'impact des variations climatiques sur l'érosion et contraindre la chronologie de ces variations.

L'utilisation de taux d'incision peut-elle pallier au manque de marqueurs géomorphologiques liés à l'avancée et au recul des glaciers dans les Alpes du Sud-Ouest ? Le premier objectif de cette thèse sera de tester le potentiel de cette approche et tenter d'affiner la chronologie des dernières glaciations et leurs impacts érosifs dans les Alpes du Sud-Ouest à partir de l'études des gorges.

Aucune de ces études régionales (i.e. Saillard et al., 2014 ; Rolland et al., 2017 ; Petit et al ; 2019) n'a pu démêler quantitativement la contribution respective du forçage climatique et du soulèvement tectonique à long terme dans le signal d'incision fluviale. En effet, isoler les contributions respectives de la tectonique et du climat à l'érosion des montagnes est un défi (Herman et al., 2013), surtout dans le contexte où les rivières étudiées sont encore possiblement en déséquilibre, celui-ci étant imposé par l'empreinte glaciaire récente sur la topographie (Norton et al., 2010). Le deuxième objectif va être de tester l'utilisation des taux d'incision provenant de gorges comme un proxy pour la quantification de taux de soulèvement tectonique et tenter de contraindre des vitesses de soulèvement dans les Alpes du Sud.

Les objectifs de cette thèse sont donc multiples, puisqu'ils sont d'ordre :

- Régional, en contribuant à l'avancée des connaissances sur les forçages climatiques et tectonique à l'œuvre dans les Alpes du Sud-Ouest ;

- Méthodologique, avec l'application d'une méthode de datation connue, la datation par les nucléides cosmogéniques, dans un contexte encore en développement, les surfaces verticales de gorges ;
- Fondamental, car cette étude constitue une avancée de la connaissance sur les processus érosifs affectant une chaîne de montagne et les facteurs externes les contrôlant.

En complétant les données d'incision déjà existantes dans les Alpes du Sud-Ouest, en échantillonnant d'autres gorges, nous allons essayer de répondre à la question principale :

- Quel est le moteur de l'incision dans les Alpes du Sud après le Dernier Maximum Glaciaire ?

Mais également tenter de répondre aux questions secondaires suivantes :

- Dans quelle mesure l'application de la datation par les nucléides cosmogéniques dans les gorges permet de quantifier des taux d'incision ?

- Quels processus contrôlent la formation des gorges et affectent leur évolution ?

4. Structure de la thèse

La thèse s'articule autour de 7 chapitres (dont l'introduction), qui seront ici brièvement présentés.

Le chapitre 2 présente les méthodes utilisées, décrit l'étendue du travail d'échantillonnage effectué sur le terrain durant cette thèse et synthétise les données de datation obtenues.

Les chapitres suivants (chapitres 3 à 6) constituent le cœur de cette thèse et présentent les principaux résultats sous la forme de manuscrits de journaux publiés ou en préparation. Par conséquent, certaines informations peuvent être dupliquées entre ces chapitres. De plus, étant publiés ou destinés à une prochaine publication, ces chapitres sont écrits en anglais mais précédés de résumés en français.

Le chapitre 3 est le manuscrit d'un article publié dans le journal Geomorphology en mai 2021. Le manuscrit s'intitule « *Interplay of fluvial incision and rockfalls in shaping periglacial mountain gorges* ». Ce travail a commencé lors de mon Master 2 et a abouti lors de ma première année de thèse. A travers la quantification de l'incision dans une gorge et la datation de sa formation, nous nous sommes attachés à identifier les différents processus qui contrôlent l'évolution morphologique d'une gorge périglaciaire.

Le chapitre 4 est le manuscrit d'un article publié dans le journal Geomorphology en décembre 2022. Le manuscrit s'intitule « *Fluvial bedrock gorges as markers for Late-Quaternary tectonic and climatic forcing in the Southwestern Alps* ». Sur la base de la quantification du taux d'incision fluviatile obtenus dans des gorges des Alpes du Sud-Ouest, nous proposons que l'incision des rivières des Alpes du Sud-Ouest au Quaternaire récent est liée à un réajustement à la fois dû au forçage climatique court-terme et au forçage tectonique long-terme.

Le chapitre 5 est présenté dans un format d'article adapté à une publication scientifique et est intitulé « *Re-evaluating the use of inner bedrock gorges as proxy for deglaciation and incision rate quantification* ». A travers la réinterprétation de données de datation par les nucléides cosmogéniques obtenues dans des gorges sous-glaciaires de la vallée de la Tinée, nous proposons que les taux d'incision fluviale postglaciaire peuvent être surestimés, car il semble que la formation de ces gorges soit un processus à long terme qui se déroule sur plusieurs cycles interglaciaires-glaciaires.

Le chapitre 6 est le manuscrit d'un article accepté pour publication dans le numéro spécial en hommage à Jean Aubouin de la revue Comptes Rendu Géologique. L'article est intitulé «*The interplay of geology, climate and tectonics on river incision: the example of the High Verdon Gorges, Southwestern French Alps*». Les taux d'incision obtenues dans les Hautes Gorges du

Verdon mettent en évidence le rôle du soulèvement tectonique comme principal moteur de l'incision du Verdon au Quaternaire récent.

Le chapitre 7 est une conclusion qui résume les principaux résultats de cette thèse en apportant des réponses aux questions présentées dans l'introduction (Chapitre 1). De plus, les résultats des quatre chapitres scientifiques sont discutés dans leur ensemble, fournissant de nouvelles perspectives sur les processus d'érosion et forçages affectant les Alpes du Sud-Ouest. Enfin, les perspectives de cette thèse sont données.

Chapitre 2 : Méthodes, terrain et données de datation

1. Méthode de datation

1.1. Datation par les nucléides cosmogéniques

Le terme « nucléide cosmogénique » (NC) désigne l'ensemble des éléments, ou nucléides, produits dans l'environnement terrestre (atmosphère ou lithosphère) lors de réactions nucléaires induites par une interaction avec des particules issues du rayonnement cosmique (Gosse et Phillips, 2001). Le mécanisme de production de NC à la surface des roches a pour origine l'interaction entre des rayons cosmiques de haute énergie, générés lors de l'entrée dans l'atmosphère de la radiation cosmique, et les atomes constituant les minéraux des roches (Lal, 1991 ; Gosse et Phillips, 2001 ; Granger et Riebe, 2007). La quantité de NC produits et accumulés dans les roches en contact (ou proche du contact) avec l'atmosphère est théoriquement proportionnelle à la durée d'exposition avec les rayons cosmiques. Cette production diminue exponentiellement avec la profondeur (environ 95% du rayonnement cosmique est absorbé dans les premiers 1,8 m ; Lal, 1991 ; Walker, 2005) et ne concerne donc que les 20 premiers mètres sous la surface (Lal, 1988 ; 1991 ; Braucher et al., 2011 ; Figure 1).

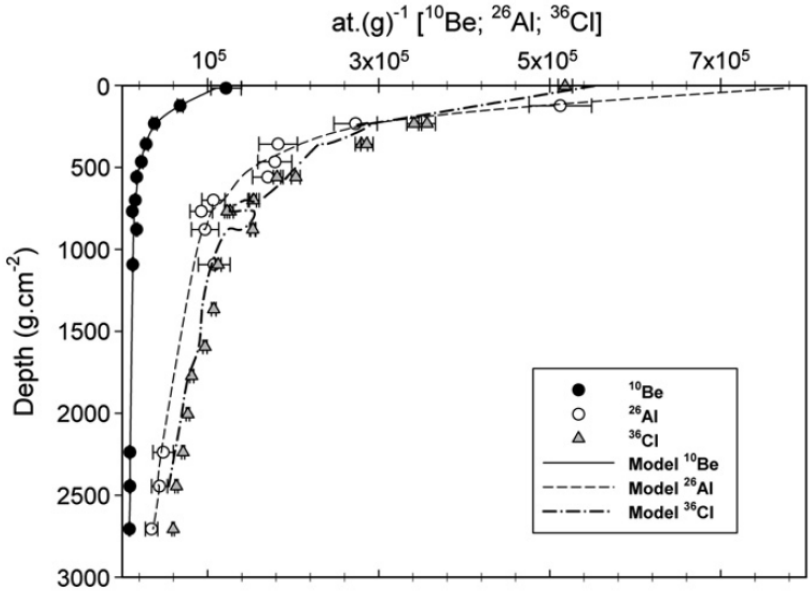

Figure 2-1 : Évolution de la concentration du ^{10}Be, ^{26}Al et ^{36}Cl en fonction de la profondeur massique (Les courbes pleines et pointillées représentent la modélisation de concentration ; Braucher et al., 2011). La profondeur, qui correspond ici à la longueur d'atténuation, est généralement exprimée en grammes par cm², et non en distance, de manière à être indépendante de la densité des roches considérées (Dunne et al., 1999 ; Braucher et al., 2009).

En déterminant la concentration de nucléides cosmogéniques d'une surface et connaissant le taux de production, on peut donc estimer un âge d'exposition nous renseignant sur la durée d'exposition de la surface. La méthode de datation par les nucléides cosmogéniques sera mentionnée par son nom anglophone dans le reste de ce manuscrit : Cosmic Ray Exposure (CRE) method.

1.2. Production de nucléides cosmogéniques

La concentration de NC à la surface d'une roche dépend principalement de la durée d'exposition aux rayonnements cosmiques. Cependant, d'autres facteurs influencent le taux de production et sont à prendre en compte (Dunne et al., 1999) :

- La latitude de la zone échantillonnée : le champ magnétique terrestre agit sur l'intensité des rayons cosmiques incidents. La force de ce champ n'est pas spatialement homogène, et se renforce à mesure que l'on se rapproche de l'Équateur. Ainsi, seuls les rayons de grande énergie atteignent la surface au latitude proche de l'Équateur, contrairement aux hautes latitudes, où on retrouve des concentrations de NC plus importantes (Lal, 1991 ; Dunai, 2000 ; Granger et Muzikar, 2001 ; Norton et Vanaker, 2009).

- L'altitude de la surface échantillonnée : l'altitude détermine l'épaisseur de la couche d'atmosphère présente au-dessus d'un point. La variation de cette épaisseur implique des variations de pression atmosphérique et d'accélération due à la gravité (Desilets et Zreda, 2003 ; Dunai, 2000 ; Stone, 2000). De plus, moins l'épaisseur d'atmosphère est grande, moins les rayons cosmiques subissent d'atténuation avant d'atteindre la surface de la Terre (Figure 2A ; Gosse et Phillips, 2001). De fait, la production de NC augmente avec l'altitude (Lal, 1991).

- L'écrantage topographique (ou masque) : la topographie environnante fait obstacle et empêche une partie des rayons cosmiques d'atteindre une surface (Figure 2A ; Dunne et al., 1999 ; Gosse et Phillips, 2001 ; Codilean, 2006).

- L'angle d'incidence des rayons : l'atmosphère terrestre joue également un rôle dans l'atténuation de l'énergie des rayons cosmiques (Dunne et al., 1999). Ainsi, un rayon ayant une trajectoire normale à une surface horizontale verra son énergie moins atténuée, car il aura traversé une épaisseur d'atmosphère inférieure, que le rayon ayant un angle d'incidence plus aigüe (Figure 2B ; Norton et Vanaker, 2009).

- La pente de la surface échantillonnée : la pente accroit l'écrantage (Gosse et Phillips, 2001), influence l'angle d'incidence des rayons cosmiques (Dunne et al., 1999) et l'impact des processus de dénudation. Ce dernier point sera abordé plus en détail par la suite.

- La chimie de l'échantillon : la composition chimique des surfaces échantillonnées, et notamment la concentration des éléments qui produisent les NC ciblés, impacte fortement la production de NC, en particulier pour le ^{36}Cl (Braucher et al., 2011 ; Marrero et al., 2016a). Une analyse chimique est donc indispensable (Zerathe et al., 2013) pour quantifier la part d'éléments majeurs (SiO_2, Al_2O_3, Fe_2O_3, MnO, MgO, CaO, Na_2O, K_2O, TiO_2, P_2O_5), et des éléments traces (U, Th, etc.). La chimie est également importante pour déterminer la part de chlore naturel (^{35}Cl), qui produit naturellement du ^{36}Cl et conditionne donc grandement l'incertitude relatif aux âges calculés (Gosse et Phillips, 2001 ; Alfimov et Ivy-Ochs, 2009).

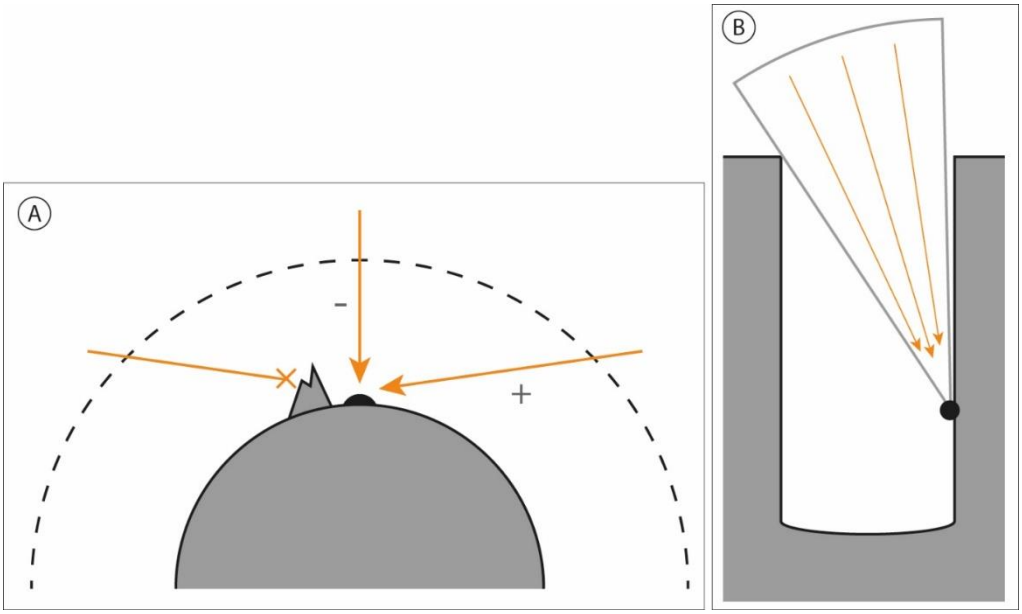

Figure 2-2 : A, Rayonnement cosmique et facteurs d'atténuation du rayonnement (en pointillés : atmosphère ; x : rayon bloqué par le relief ; - : épaisseur atmosphérique réduite dans le cas d'un rayon à incidence normale ; + : épaisseur atmosphérique plus importante). B, Représentation du flux très limité de rayons cosmiques reçu par une surface le long de la paroi verticale d'une gorge étroite du fait du fort angle d'incidence.t

D'autres facteurs peuvent également influencer la production de NC, tels que l'accumulation épisodique de sédiments ou de neige qui isole momentanément la surface du rayonnement cosmique (Gosse et Phillips, 2001) ou encore les variations du niveau de l'eau qui peut remonter suite à la création d'embâcle (Pratt et al., 2002). De plus, l'intensité du rayonnement cosmique peut varier temporellement à cause de modulations solaires (Nishiizumi et al., 1996 ; Potgieter, 2013) ou de fluctuations d'intensité du champ magnétique (Bucha, 1970 ; Dunai, 2000). Une surface peut aussi voir son altitude varier au cours du temps, à cause du rebond isostatique notamment (Jones et al., 2019).

1.3. Détermination de la concentration de NC

L'évolution dans le temps t (an) de la concentration N (at/g) du nucléide à une profondeur Z (m) est donnée par (Lal, 1991) :

$$N(Z,t) = N(Z,0) * e^{-\lambda.t} + \frac{P_n(0) * e^{-\frac{Z}{\Lambda_n}}}{\lambda + \frac{\varepsilon * \rho}{\Lambda_n}} * (1 - e^{-t*\left(\lambda + \frac{\varepsilon+\rho}{\Lambda_n}\right)})$$

Où N(Z,0) est la part de concentration héritée à t=0, λ est la constante de désintégration du radionucléide considéré, P_n (0) est le taux de production (at/g/an ; qui est fonction de la latitude, l'altitude et l'écrantage topographique et géométrie de la surface échantillonnée), Λ_n représente les longueurs d'atténuation (g/cm²) des particules considérées (neutrons, muons (lents, rapides)), ε est le taux de dénudation (cm/an) et ρ est la densité (g/cm²) de la roche échantillonnée.

Cette équation permet de mettre en évidence une information cruciale pour l'interprétation des âges : la concentration de NC dans une roche croît à partir du début de l'exposition de la surface jusqu'à atteindre un état d'équilibre, ou « steady state ». Cet état d'équilibre commence à partir du moment où la production de NC est compensée par la dénudation de la surface et/ou la désintégration du radionucléide considéré. La concentration de NC va alors connaître autant de gain (production) que de perte (dénudation et désintégration), et va donc stagner au niveau de saturation.

Par conséquent, pour contraindre la concentration de NC d'un échantillon, il est crucial de prendre en compte :

- La dénudation : L'érosion post-exposition des surfaces a pour effet de les rajeunir, en supprimant une partie des NC accumulés depuis l'exposition. La dénudation (érosion mécanique + altération chimique) peut se faire par des chutes de bloc, le ruissellement et/ou des phénomènes de météorisation des roches, tel que la dissolution des parois calcaires (Sadier et al., 2012).

- La concentration héritée : une certaine quantité de NC peut s'accumuler dans les roches proches de la surface avant leur exposition ou encore lors de leur transport/dépôt, dans le cas de roches sédimentaires (Sadier et al., 2012).

- L'épaisseur de l'échantillon : la production de NC diminuant exponentiellement avec la profondeur, la concentration de NC décroît sur toute l'épaisseur de l'échantillon, de son sommet (surface) à sa base.

1.4. Quantification de l'incision dans les gorges

Afin de quantifier l'incision fluviatile, la méthode de datation par les NC peut être appliquée sur des marqueurs géomorphologiques, horizontaux ou verticaux : tels que les terrasses alluviales (Burbank et al., 1996), les parois des gorges (Schaller et al., 2005 ; Ouimet et al., 2008), ou encore dans le lit rocheux des cours d'eau pour déterminer les vitesses d'incision actuelles (Seidl et al., 1997 ; Weissel et Seidl, 1998 ; Valla et al., 2010). Les gorges sont propices à l'estimation des vitesses d'incision car les parois verticales sont théoriquement exposées au fur et à mesure de l'incision (Figure 3A).

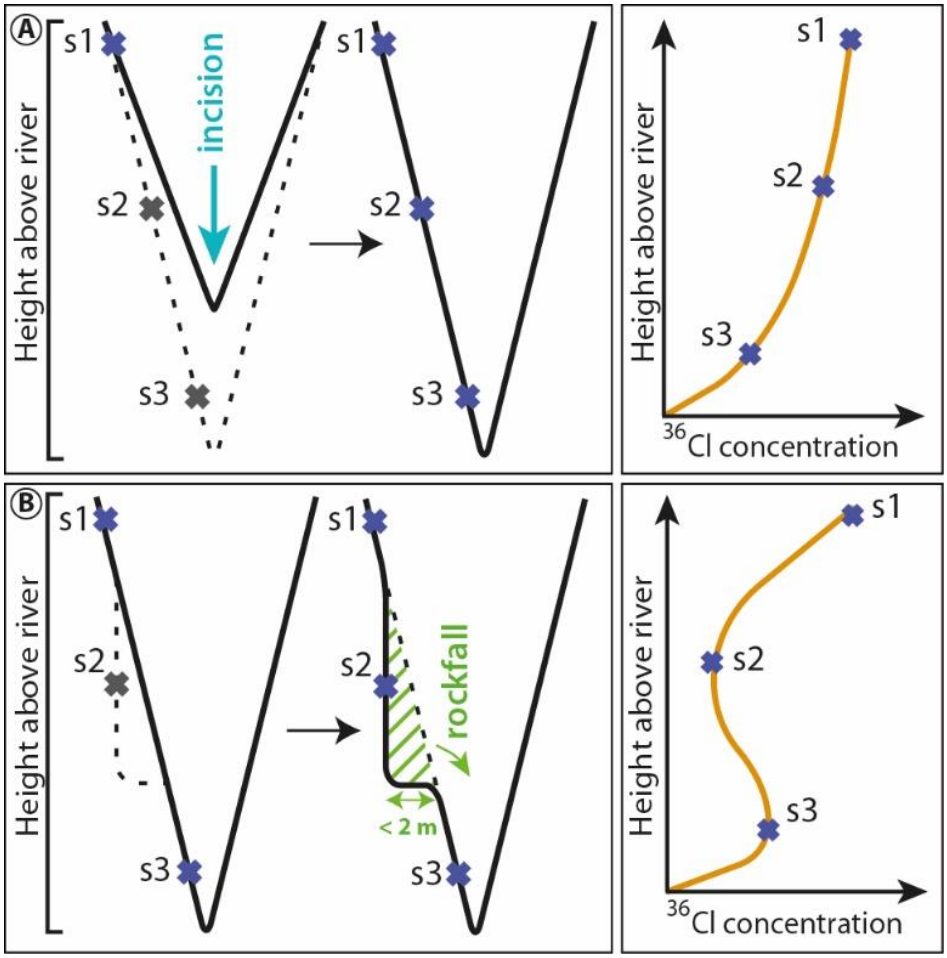

Figure 2-3 : A, Représentation théorique de l'exposition progressive de la paroi de la gorge calcaire pendant l'incision en cours et des concentrations attendues de ^{36}Cl en fonction de la hauteur des surfaces échantillonnées (s1, s2, s3). B, Représentation théorique de l'influence d'un événement gravitaire sur la concentration de ^{36}Cl en fonction de la hauteur de la surface échantillonnée (s1, s2, s3). Notez le " rajeunissement " de la surface s2, car l'âge d'exposition n'est plus représentatif de l'incision, mais de l'occurrence de la chute de blocs. Comme ≈ 95% du rayonnement cosmique est absorbé dans les premiers 1,8 m sous la surface (Lal, 1991), le bloc rocheux impliqué dans la chute doit être plus épais que ~2m pour que la surface soit entièrement rajeunie.

Cependant, la datation par les NC (^{36}Cl ici) de l'incision des clues calcaires est encore en développement, notamment parce qu'elle requiert de prendre en considération différents paramètres propres à ces objets géomorphologiques verticaux, tels que :

- **Dénudation** : L'efficacité du processus de dénudation (érosion mécanique et chimique) est contrôlée en partie par la pente et la convexité des surfaces concernées (Godard et al., 2016 ; Thomas et al., 2017). Dans le cas d'une paroi verticale, il faut considérer les processus de déstabilisations rocheuses, mais également les variabilités spatiales de l'efficacité de la dissolution, en raison des nombreuses irrégularités morphologiques de la paroi (vires,

surplombs, renfoncement, fractures). Il est globalement admis que les surfaces verticales et sub-verticales subissent moins de dissolution que les surfaces légèrement pentues et horizontales, car l'eau n'y stagne pas (Sadier et al., 2012).

- Écrantage topographique et pente : pour une surface verticale « infinie », le taux de production est 50% moins important que pour une surface horizontale (Dunne et al., 1999). Cette diminution du taux de production est causée par l'angle d'incidence très aigu, voire parallèle aux parois, des rayons cosmiques et l'important masque topographique (Gosse et Phillips, 2001). Ce masque topographique est d'autant plus important dans le cas d'une gorge car il s'agit de deux parois qui se font face et non d'une seule paroi (Figure 2B). L'estimation de l'écrantage topographique se fait couramment sur le terrain durant l'échantillonnage des surfaces et consiste à mesurer à l'aide d'une boussole des valeurs d'élévation de la topographie à 360° (la ligne d'horizon) autour de la surface échantillonnée (Gosse et Phillips, 2001). Ces valeurs permettent par la suite de calculer un facteur d'écrantage propre à chaque site échantilonné (Dunne et al., 1999). Ces mesures se font sur le terrain et peuvent se révéler délicates et incertaines (Li, 2013), notamment dans le cas d'une gorge où l'échantillonnage se fait sur corde (Figure 4).

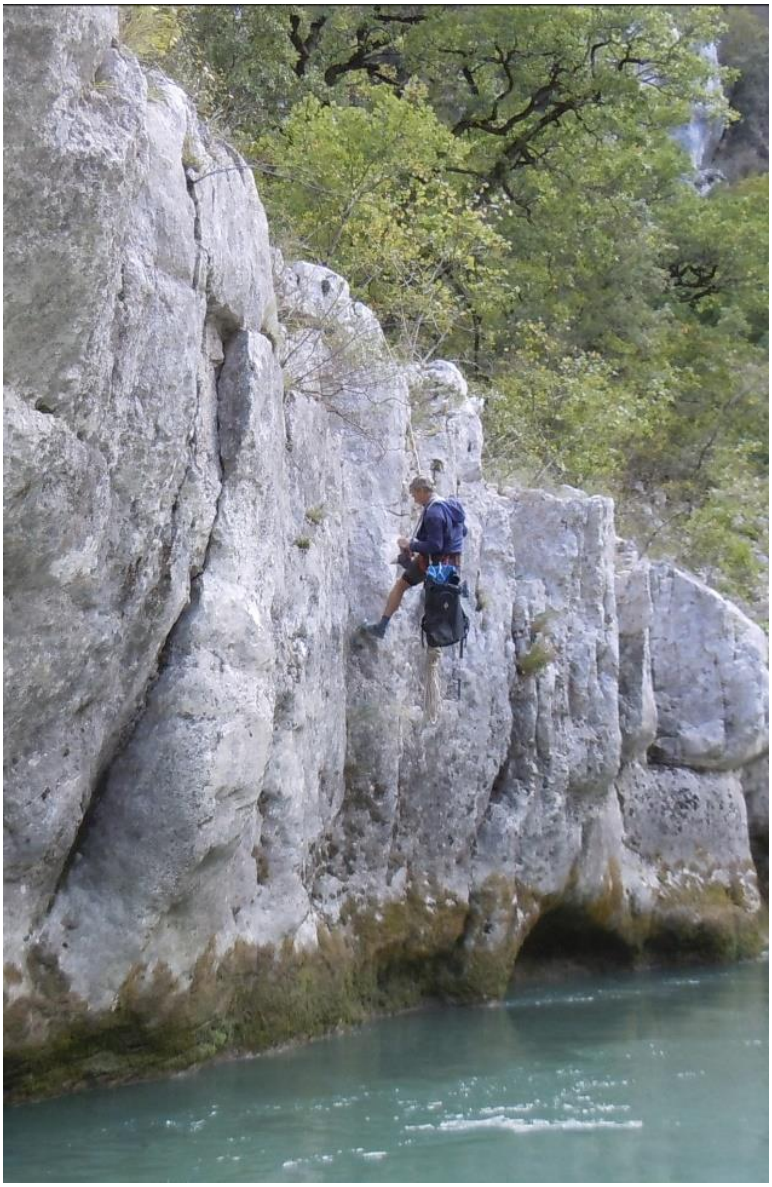

Figure 2-4 : Echantillonnage sur corde le long d'une paroi verticale, effectué par Yann Rolland (Site La Mescla, Verdon, octobre 2020).

Il existe des méthodes numériques d'estimation de l'écrantage topographique (Codilean, 2006 ; Balco et al., 2008) adaptées à des outils de cartographie SIG (Li, 2013), et couramment utilisées pour l'application du ^{10}Be détritique in-situ à l'échelle de bassins versant (Mudd et al., 2016). Cependant, ces outils sont davantage destinés aux études de grande dimension spatiale (<100 km²) à partir de MNT de faible résolution (maximum 5m ; Norton et Vanaker, 2009). Nous avons voulu explorer la possibilité de transférer cette approche numérique à notre cas d'étude de type « vertical » pour tenter d'affiner notre estimation de l'écrantage topographique.

En effet, dans le cas d'une clue, l'approche SIG classique (2,5D) se confronte à la verticalité des parois, où les échantillons, même si espacés en termes d'altitude (z), sont concentrés dans un espace 2D (x, y) de faible emprise (Figure 5). La détermination du masque topographique dans la clue à partir des méthodes numériques existantes requiert donc l'élaboration de MNT de très haute résolution, à travers notamment la méthode de photogrammétrie « *Structure-from-Motion* » (SfM) (voir Annexe 1).

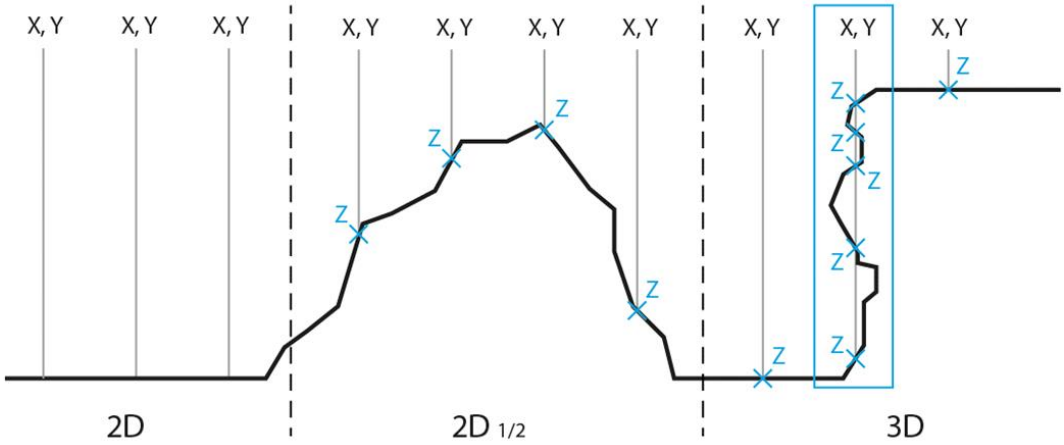

Figure 2-5 : Différence d'approche méthodologique selon la topographie (d'après Jaboyedoff et al., 2010)

1.5. Traitement analytique des échantillons

Nous avons préparé les échantillons de calcaire au 'Laboratoire National des Nucléides Cosmogéniques' (LN2C ; CEREGE, Aix-en-Provence) en suivant la procédure présentée par Schimmelpfennig et al. (2009). Les concentrations de ^{36}Cl ont été déterminées par spectrométrie de masse par accélérateur (SMA) réalisée à ASTER, la structure AMS nationale française (CEREGE, Aix-en-Provence) (Arnold et al., 2010). Toutes les mesures ont été calibrées par rapport à l'étalon interne CEREGE SM-CL-12 (Merchel et al., 2011). Les incertitudes totales tiennent compte des statistiques de comptage, de l'évolution de l'étalon pendant les mesures, de l'incertitude standard et des incertitudes externes de 2,74 %, 2,13 % et 1,62 % pour les rapports $^{36}Cl/^{35}Cl$, $^{36}Cl/^{37}Cl$ et $^{35}Cl/^{37}Cl$, respectivement (Braucher et al., 2018). Un taux de production de ^{36}Cl au niveau de la mer et aux hautes latitudes pour la spallation du calcium de 42,2±3,4

atomes de ^{36}Cl g-1 a-1 (Schimmelpfennig et al., 2009 ; Braucher et al., 2011) a été utilisé et mis à l'échelle selon Stone (2000) et corrigé en fonction du masque topographique (*topographic shielding*, TS) du site. Les âges ^{36}Cl ont été déterminés selon l'approche de Schimmelpfennig et al. (2009) en utilisant une densité de calcaire de 2,6 g. cm^{-3}.

1.6. Quantification de taux d'incision

Nous avons utilisé le code développé par Glotzbach et al. (2011), initialement conçu pour les données de thermochronologie, afin de déterminer les variations du taux d'incision avec le temps à partir de nos données et des données de la littérature. Le code définit les segments de courbe de régression les mieux ajustés aux points de données. Nous avons apporté quelques modifications au code pour le rendre plus adapté aux données d'âges CRE. Comme dans Glotzbach et al. (2011), nous avons utilisé une approche de Monte-Carlo pour diviser aléatoirement les données en 1, 2 ou 3 intervalles de temps successifs afin de définir des segments de courbe par régression linéaire pondérée, et de sélectionner les mieux ajustés en fonction de leur valeur R^2. Nous avons appliqué les critères suivants : aucun taux d'incision négatif n'est autorisé, donc les solutions contenant des segments avec des taux d'incision négatifs sont rejetées ; les segments de ligne contraints par moins de 3 points de données sont rejetés ; l'intersection entre deux segments de courbe doit correspondre à l'intersection entre les deux groupes de données qui ont été utilisés pour les calculer.

2. Sites étudiés et synthèse des données

Dans cette étude, nous présentons de nouvelles données acquises dans six gorges situées dans les Alpes françaises du Sud-Ouest, en complément des données similaires disponibles dans la région (Figure 6). Tous les bassins versants étudiés présentent de forts contrastes lithologiques qui, combinés à l'important plissement des couches de roches sédimentaires de la région, créent d'importantes convexités et ruptures de pente dans le profil longitudinal des rivières. Toutes les gorges mentionnées ci-dessus sont incisées dans des calcaires tithoniens

(Jurassique Sup.), que l'on retrouve à plusieurs reprises dans l'avant-pays alpin (Figure 1, Chapitre introduction).

De plus, nous distinguons trois caractéristiques de gorges en fonction de leur localisation géographique et au regard de l'extension glaciaire au cours du LGM (Figure 6) :

- Couvert : site directement couvert par un glacier pendant le LGM ;

- Connecté : site se trouvant le long d'un cours d'eau qui prend sa source dans la partie du bassin versant précédemment couverte par la glace pendant le LGM ;

- Indirectement connecté : site se trouvant le long d'un affluent d'un cours d'eau connecté ;

- Déconnecté : site se trouvant dans un bassin versant dépourvu de tout glacier et le long d'un cours d'eau n'ayant aucune connexion, directe ou indirecte, avec des zones couvertes de glace.

Nous présenterons dans ce chapitre chacun des sites étudiés avec 1) une description géomorphologique, 3) une localisation des échantillons, 4) une description détaillée des échantillons, 5) des notes sur les difficultés rencontrées et l'adaptation de la stratégie d'échantillonnage sur le terrain. Les sites étudiés dans de précédentes études seront aussi brièvement présentés.

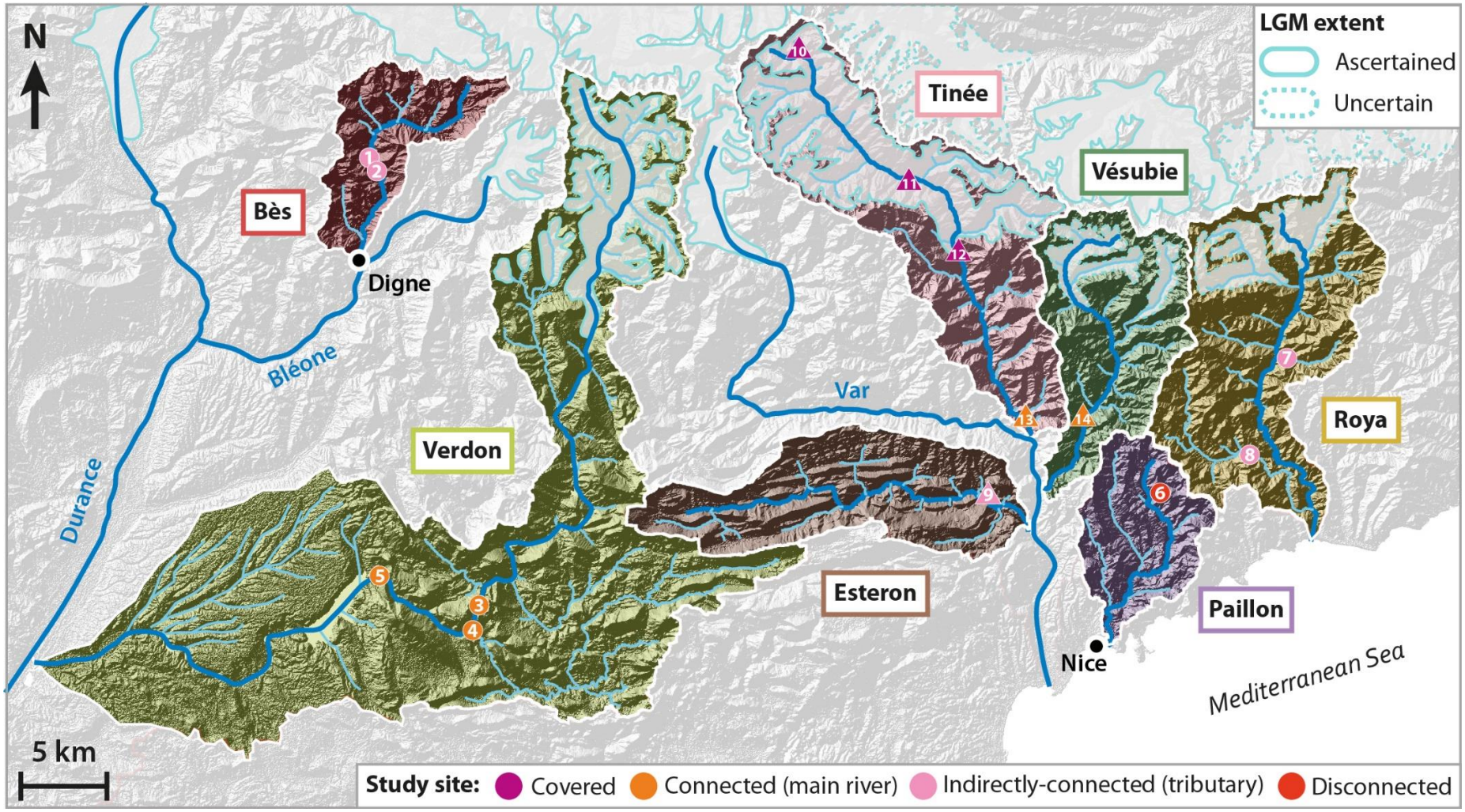

Figure 2-6 : Localisation des sites échantillonnés durant cette étude (ronds numérotés) : 1) Barles (Bès), 2) Pérouré (Bès), 3) Samson (Verdon), 4) Mescla (Verdon), 5) Galetas (Verdon), 6) Redebraus (Paillon), 7) Bendola (Roya), 8) Bévéra (Roya), et lors de précédentes études (triangles numérotés) : 9) Cerise (Esteron) (Petit et al., 2019), 10) Salso Moreno (Tinée), 11) Isola (Tinée), 12) Saint Sauveur (Tinée), 13) Courbaisse (Tinée) (Rolland et al., 2017), 14) Vésubie (Saillard et al. 2014). Les zones grises soulignées par un tracé bleu clair montre l'étendue des glaciers du LGM (modifié à partir de Brisset et al., 2015).

2.1. Les gorges du Var étudiées précédemment

Le bassin versant du Var est situé dans les Alpes du Sud-Ouest, sur le versant français du massif de l'Argentera-Mercantour (AM ; Figure 7A). Les sources du fleuve Var et de deux de ses principaux affluents (la Tinée et la Vésubie) sont situées dans le massif de l'AM et donc dans la zone précédemment englacée au cours du Dernier Maximum Glaciaire (*Last Glacial Maximum*, LGM ; Figure 1B). La topographie abrupte du massif peut atteindre 3200 m.a.s.l. et revêt encore, à des altitudes > ~2000 m, des morphologies typiques des érosions glaciaires. L'érosion glaciaire a créé des vallées typiques en U, qui se transforment en vallées fluviales profondément encaissées en V.

De précédents travaux se sont attachés à étudier l'incision dans des gorges le long de certains affluents du Var (Figure 7B) :

- La gorge de la Cerise (9), dans le bassin versant de l'Estéron (Petit et al., 2019) ;
- Salso Moreno (10), Isola (11) et Saint Sauveur (12), qui étaient précédemment recouvertes par les glaciers LGM de la Tinée (Rolland et al., 2017) ;
- Courbaisse (13), qui était hors d'atteinte des glaciers de la Tinée (Rolland et al., 2017) ;
- Une gorge de la Vésubie (14), hors d'atteinte des glaciers de la Vésubie (Saillard et al., 2014).

Pour de plus amples descriptions des sites, le lecteur est invité à se renseigner auprès des publications associées.

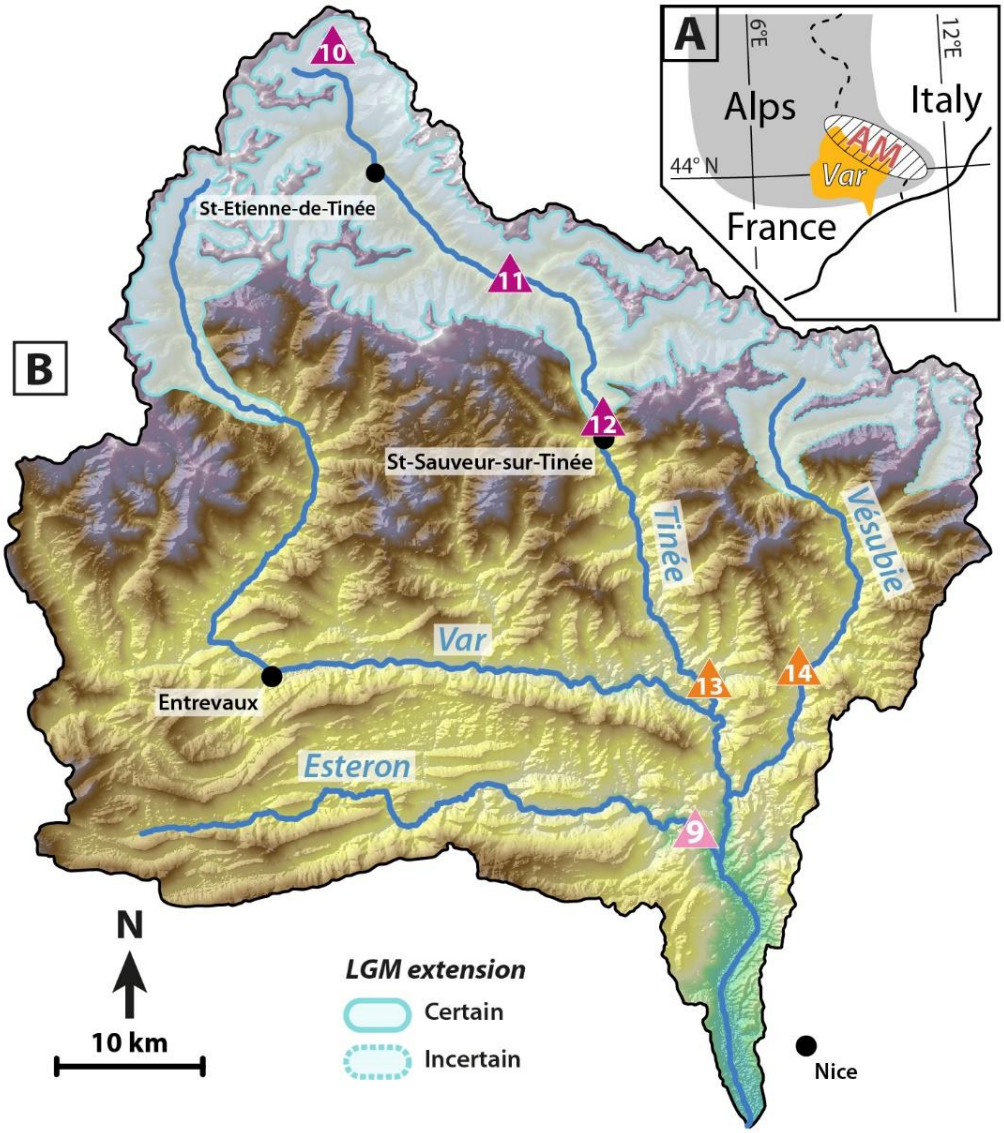

Figure 2-7 : Carte topographique du bassin versant du Var et localisation de : (9) La gorge de la Cerise (Petit et al., 2019) ; (10) Salso Moreno, (11) Isola, (12) Saint Sauveur, (13) Courbaisse (Rolland et al., 2017), (14) Vésubie (Saillard et al., 2014). Les zone grises soulignées par un tracé bleu clair montre l'étendue des glaciers du LGM (modifié à partir de Brisset et al., 2015).

2.2. Le Bès

La Clue de Barles et du Pérouré se trouvent dans la vallée du Bès, dont le bassin versant se situe dans le département des Alpes-de-Hautes-Provence (04) dans le Sud-Est de la France. D'une superficie de 233 km², ce bassin versant du Bès présente une forme allongée marquée par un changement de direction important (Figure 8A). Sa géométrie est contrainte par la présence de contrastes de lithologies marqués, qui avec les barres calcaires forment des clues comme celle de Barles ou du Pérouré (Figure 8B).

La vallée du Bès appartient à la « demi-fenêtre » tectonique de Barles : une fenêtre d'érosion creusée dans la nappe de charriage de Digne, qui met à jour la couverture sédimentaire dite « autochtone ». Cette fenêtre laisse apparaître une organisation plissée où les calcaires tithoniques dans lesquels sont incisées les gorges correspondent aux flancs d'anticlinaux (anticlinal du Pérouré et de la Grande Cloche). Les « Terres Noires » (marnes du Jurassique Sup.) constituent souvent le cœur des anticlinaux et des dépôts oligocènes discordants s'observent le plus souvent dans les synclinaux.

Les terrains traversés par le Bès, sur une longueur de 39 km, correspondent donc à une couverture sédimentaire mésozoïque déformée. La diversité de paysages dans la vallée du Bès s'explique par les variations de lithologie au sein de cette couverture et leur érosion différentielle. Les larges vallées ouvertes se sont formées dans des roches marneuses appelées localement les « Terres Noires ». Les versants de ces combes ont une apparence de gradins, du fait de la présence de replats topographiques. Ces combes sont séparées par des barres calcaires tithoniques verticalisées. L'incision de ces barres par le Bès forme des clues étroites (≈ 10 m) et profondes (≈200 m). Le bassin versant du Bès a été épargné de l'érosion des glaciers quaternaires dont l'extension ne touchait pas cette région basse (Brisset et al., 2015). Cependant, le Bès est connecté à la Bléone qui était englacée pendant le LGM (Figure 8A).

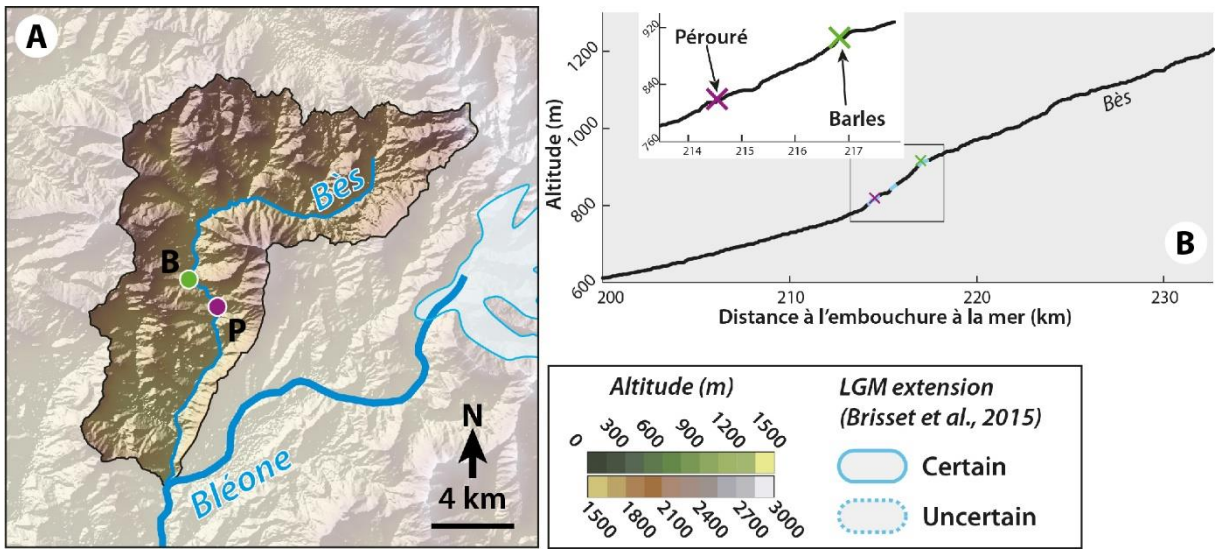

Figure 2-8 : A, Carte topographique du bassin versant du Bès et localisation des clues de Barles (B) et du Pérouré (P). B, Profil longitudinale du Bès et zoom sur les gorges.

2.2.1. La Clue de Barles

Un nombre de 18 échantillons de calcaires a été collecté le long d'un profil vertical dans la clue de Barles pour les mesures de ^{36}Cl et 4 échantillons ont été collectés sur le sommet horizontal plat oriental de la barre calcaire surplombant la gorge (Table 1). Le profil vertical s'étend de la rivière jusqu'à 80 m de hauteur sur deux strates calcaires verticales différentes, situées à l'extrémité sud de la gorge. Nous avons échantillonné des surfaces sans relief en surplomb (Figure 9), afin de maximiser l'exposition et de simplifier la détermination du facteur de masque topographique.

La clue de Barles est la seule gorge échantillonnée sur une hauteur aussi conséquente. Sa position dans la barre calcaire dans laquelle la clue est creusée permet d'y accéder en rappel par le haut. De plus, son profil majoritairement sub-vertical (légèrement en V) permet une exposition aux rayons cosmique satisfaisante. Les résultats de l'échantillonnage dans la clue de Barles ont influencé la stratégie d'échantillonnage adoptée durant le reste de l'étude. En effet, il s'est révélé que les parois des gorges sont fortement impactées par des déstabilisations gravitaires au-dessus de ~10 m de hauteur. Les âges d'exposition contraint à partir des

échantillons prélevés dans ces hautes surfaces ne correspondent donc pas à l'incision par la rivière, mais à des chutes de blocs. Pour le reste de l'étude, il a donc été décidé de restreindre l'échantillonnage aux 15 premiers mètres des gorges et présentant des signes indiscutables de polis de rivières (marmites).

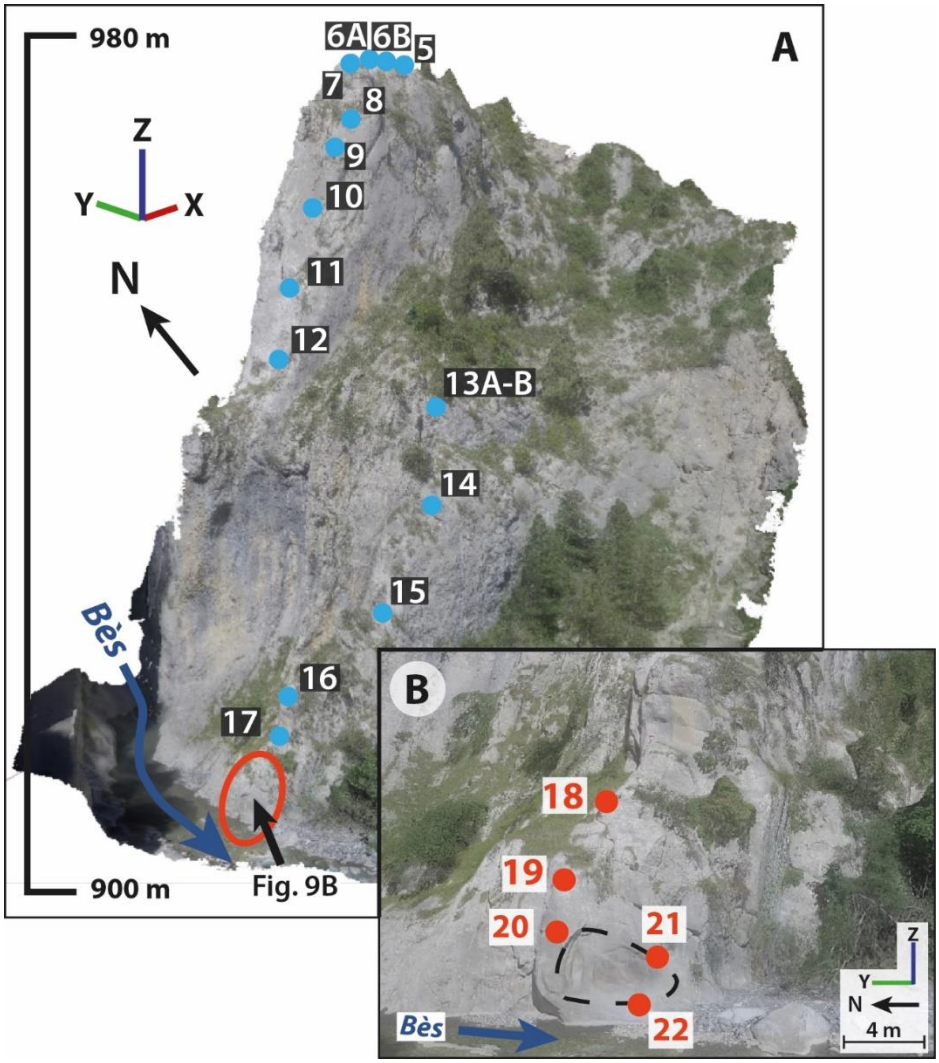

Figure 2-9 : Localisation des échantillons sur la paroi de la Clue de Barles (A) avec un zoom sur la partie basse de la paroi (B). Entouré en pointillé : figure d'incision fluviatile (marmite).

Barles (lat: 44.2345°; long: 6.2565°; elevation: 904 m.a.s.l.)										
Sample	Height above river (m)	Sample thickness (cm)	TS factor	Spall. scaling	^{35}Cl (ppm)	Ca (%)	Atoms ^{36}Cl (at/g)	Atoms ^{36}Cl ± (at/g)	CRE age (ka)	Denudation rate (mm/ka)
1	263.0	3	0.99	2.64	60.5	36.0	18885474	111338	-	32.83±1.94
2	253.6	3	0.99	2.64	48.5	39.0	2767824	155686	-	18.74±1.05
3	249.7	3	0.99	2.64	81.3	38.2	2844314	195423	-	22.91±1.57

4	252.9	3	0.99	2.64	38.0	31.9	1563115	84417	-	32.54±1.76
5	73.2	3	0.85	2.64	29.1	32.1	414312	21132	13.6± 0.7	-
6A	73.7	3	0.87	2.64	17.2	24.7	463710	20942	19.8± 0.9	-
6B	73.5	3	0.87	2.64	102.8	27.6	840309	279136	19.2± 6.4	-
7	73.1	3	0.87	2.64	20.6	38.9	518890	23489	15.3± 0.6	-
8	67.3	3	0.72	2.64	32.6	32.2	397913	24537	15.2± 0.6	-
9	64.8	3	0.76	2.64	17.5	38.2	451597	21698	15.8± 0.7	-
10	57.8	3	0.84	2.64	23.6	37.2	321967	15754	9.9±0 .5	-
11	48.7	3	0.80	2.64	23.5	38.6	310801	16034	9.8±0 .5	-
12	42.0	3	0.67	2.64	22.3	37.4	298013	15522	11.7± 0.6	-
13A	38.4	3	0.71	2.64	28.0	38.0	290021	15713	10.3± 0.5	-
13B	38.4	3	0.71	2.64	43.3	38.4	257546	22005	8.4±0 .7	-
14	28.9	3	0.65	2.64	29.8	37.3	467713	23683	19.2± 0.9	-
15	20.4	3	0.55	2.64	25.3	37.3	330443	16938	16.2± 0.8	-
16	13.4	3	0.47	2.64	27.3	31.8	341914	17288	22.3± 1.1	-
17	9.6	3	0.45	2.64	22.9	37.7	229307	13073	13.7± 0.8	-
18	6.2	3	0.43	2.64	29.0	38.0	396966	22406	25.8± 1.5	-
19	5.2	3	0.40	2.64	30.4	35.7	268197	14974	18.4± 1.0	-
20	3.4	3	0.41	2.64	28.8	33.2	98729	8562	6.6±0 .6	-
21	2.5	1	0.52	2.64	21.2	37.5	26219	3368	1.3±0 .2	-
22	1.6	1.5	0.53	2.64	22.6	37.4	17964	3489	0.8±0 .2	-

Tableau 2-1 : Caractéristiques des échantillons (^{36}Cl) et résultats géochronologiques du site Barles. Hauteur au-dessus du niveau de la rivière, facteur de masque topographique (TC), échelle de spallation (Spall. Scalling), teneur en chlore naturel (^{35}Cl), teneur en calcium (Ca), concentration en ^{36}Cl cosmogéniques et incertitude associée, âge d'exposition et taux de dénudation de la surface échantillonnée.

2.2.2. La Clue du Pérouré

Seulement 2 km en aval de la clue de Barles, l'entrée de la clue du Pérouré présente une grande surface polie et préservée, juste en contrebas d'un chemin forestier. Cette accessibilité

nous a donc permis de descendre en rappel et de prélever 9 échantillons (Table 2) le long de cette paroi de ~12 m de hauteur (Figure 10). L'inclinaison sub-verticale de la paroi et son orientation vers le NNO, c'est-à-dire vers une partie plus ouverte de la vallée car il s'agit d'une combe creusée dans les Terres Noires, suggère que l'exposition y est satisfaisante. Malheureusement, la force du courant lors de l'échantillonnage (novembre 2019) ne nous a pas permis de descendre au plus bas de la paroi. L'échantillon le plus bas a été prélevé à 1 m au-dessus du niveau actuel de la rivière.

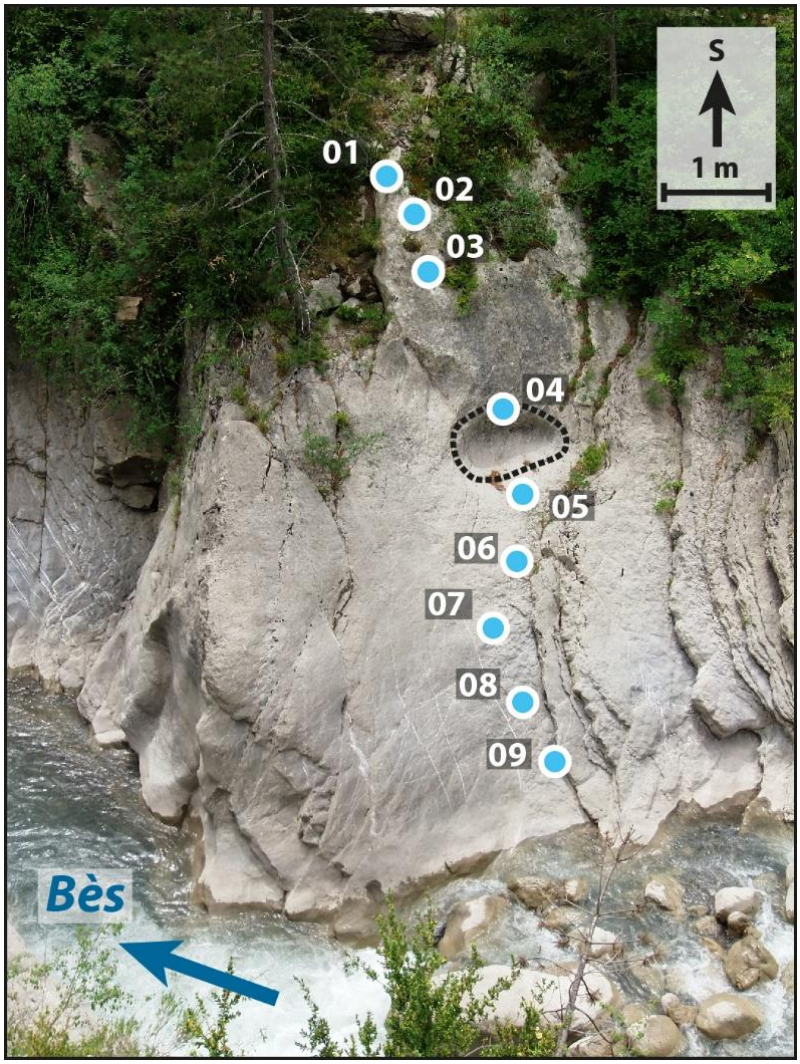

Figure 2-10 : Localisation des échantillons prélevés sur la paroi de la Clue du Pérouré.

Pérouré (lat: 44.2192°; long: 6.2734°; elevation: 814 m.a.s.l.)

Sample	Height above river (m)	Sample thickness (cm)	TS factor	Spall. scaling	^{35}Cl (ppm)	Ca (%)	Atoms ^{36}Cl (at/g)	Atoms ^{36}Cl ± (at/g)	CRE age (ka)
01	11.2	3	0.71	1.44	34.8	37.4	225855	14252	8.3±0.5
02	10.3	1	0.71	1.44	48.4	38.0	244501	18207	8.6±0.6
03	9.3	1	0.71	1.44	48.0	39.2	192883	13705	6.7±0.4
04	6.5	2	0.71	1.44	36.3	37.8	70483	5823	2.5±0.2
05	5.0	5	0.71	1.44	36.0	38.2	68158	7821	2.5±0.3
06	4.0	3	0.71	1.44	40.0	36.9	51295	11467	1.9±0.4
07	2.8	2.5	0.71	1.44	37.9	38.0	60377	8918	2.2±0.3
08	1.9	5	0.71	1.44	38.3	37.6	40900	6808	1.5±0.2
09	0.9	5	0.71	1.44	30.8	32.1	25038	3868	1.0±0.2

Tableau 2-2 : Caractéristiques des échantillons (^{36}Cl) et résultats géochronologiques du site Pérouré. Hauteur au-dessus du niveau de la rivière, facteur de masque topographique (TC), échelle de spallation (Spall. Scalling), teneur en chlore naturel (^{35}Cl), teneur en calcium (Ca), concentration en ^{36}Cl cosmogéniques et incertitude associée, âge d'exposition de la surface échantillonnée.

2.3. Les Hautes Gorges du Verdon

Prenant sa source à la bordure NW du massif du Mercantour, à environ 2500 m d'altitude, le Verdon rejoint la Durance à environ 255 m d'altitude. Avec une longueur de 166,54 km et un bassin versant de 2218 km², le Verdon est le principal affluent de la Durance. Le profil de la rivière reflète très bien les variations de lithologies que traverse le Verdon. On peut en effet y observer une convexité importante là où la rivière a creusé dans les calcaires massifs du Tithonien et formé les gorges, alors qu'en amont et en aval, le profil de la rivière est concave (Figure 11).

Compte tenu de l'envergure des Hautes Gorges du Verdon, il a semblé plus adéquat d'échantillonner plusieurs sites le long des gorges plutôt qu'un seul, comme cela avait été fait précédemment. Les principaux défis rencontrés dans la Hautes Gorges du Verdon sont l'étroitesse et la variation de la lithologie dans la gorge. En effet, les parties de la gorge constituées de calcaire plus massif, dans lesquelles nous nous attendons à trouver des surfaces polies de rivière bien préservées, sont les plus étroites avec la plus petite ouverture d'exposition aux rayons cosmiques. Inversement, des surfaces bien exposées sont trouvées dans certaines parties de la gorge qui sont très fracturées et très probablement affectées par des processus d'érosion post-incision (chutes de pierres principalement). Un compromis a donc été fait entre

la préservation et l'exposition. Cela nous a conduit à choisir des surfaces basses polies par la rivière situées dans (Figure 11 et 12) :

- La partie aval du couloir de Samson, à l'entrée amont de la gorge ;

- La Mescla, au milieu des gorges, à la jonction avec la rivière Artuby ;

- Galetas, à la sortie des gorges.

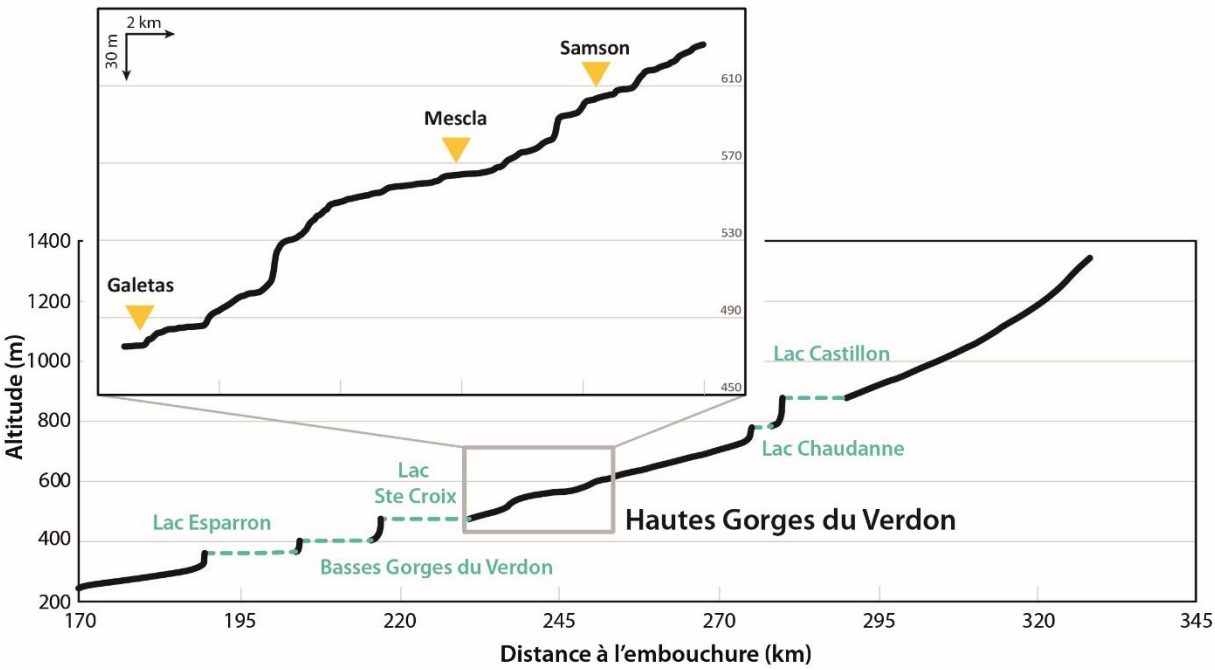

Figure 2-11 : Profile longitudinale du Verdon, localisation des sites échantillonnés et zoom sur les Hautes Gorges du Verdon. Le profil montre de nombreux lacs de barrages en amont et en aval des Gorges.

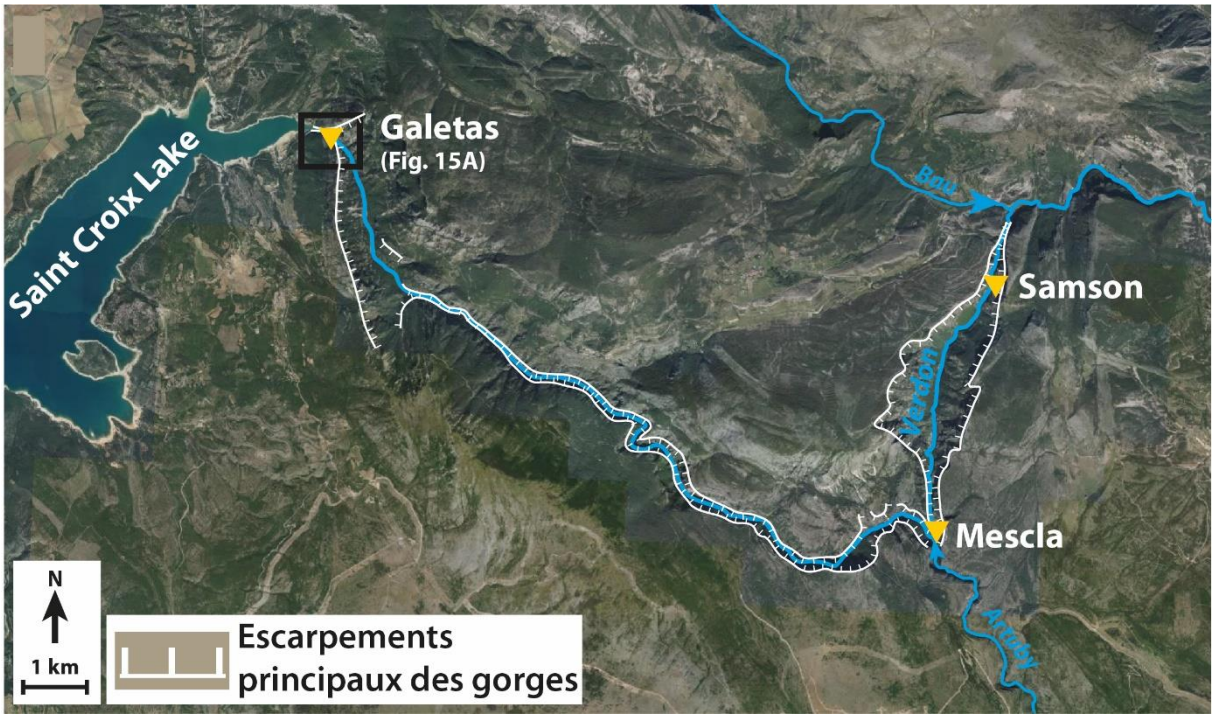

Figure 2-12 : Photo aérienne des Hautes Gorges du Verdon avec localisation du Verdon et de ses deux affluents (Baun et Artuby) et des sites échantillonnés.

2.3.1. Le Couloir Samson

Tout en étant très étroit mais bien préservé, le couloir Samson s'ouvre dans sa partie aval sur une section plus large de la gorge (Figure 12). Nous avons prélevé 11 échantillons (Table 3) une surface polie sub-verticale qui a montré de bons indices de préservation avec la présence de marmites dans la surface échantillonnée (Figure 13).

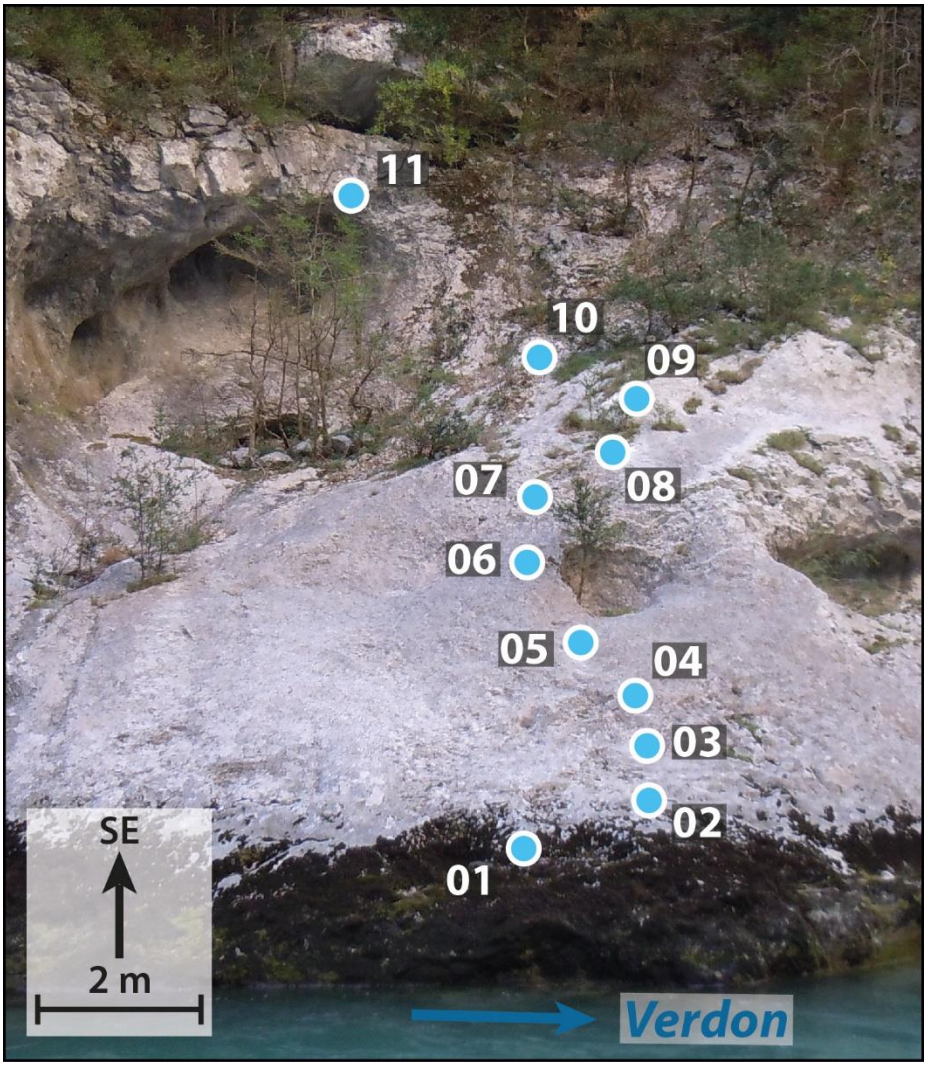

Figure 2-13 : Localisation des échantillons prélevés sur une paroi dans le couloir Samson.

Samson (lat: 43.7842°; long: 6.3936°; elevation: 606 m.a.s.l.)									
Sample	Height above river (m)	Sample thickness (cm)	TS factor	Spall. scaling	^{35}Cl (ppm)	Ca (%)	Atoms ^{36}Cl (at/g)	Atoms ^{36}Cl ± (at/g)	CRE age (ka)
11	11	1	0.16	1.67	24.5	40.4	110890	8575	21.6±1.7
10	8	1.5	0.16	1.67	33.1	40.6	190457	16417	37.3±3.2
09	7.7	1.5	0.16	1.67	23.4	40.7	205909	11192	40.9±2.2
08	7.1	1	0.16	1.67	28.6	40.8	205363	13024	40.4±2.6
07	6.8	1	0.16	1.67	28.1	40.8	187869	9775	36.9±1.9
06	5.8	2.5	0.16	1.67	32.0	41.7	188287	9862	36.0±1.9
05	4.6	1	0.16	1.67	31.5	40.6	136006	8988	26.4±1.7
04	3.7	1	0.16	1.67	35.0	40.7	118596	7068	22.7±1.4
03	3.3	1	0.16	1.67	32.5	40.8	91776	5730	17.5±1.1
02	2.4	1	0.16	1.67	29.9	40.7	89670	8452	17.2±1.6
01	2	1	0.16	1.67	37.3	40.7	83944	6349	15.9±1.2

Tableau 2-3 : Caractéristiques des échantillons (^{36}Cl) et résultats géochronologiques du site Samson. Hauteur au-dessus du niveau de la rivière, facteur de masque topographique (TC), échelle de spallation (Spall. Scalling), teneur en chlore naturel

(^{35}Cl), teneur en calcium (Ca), concentration en ^{36}Cl cosmogéniques et incertitude associée, âge d'exposition de la surface échantillonnée.

2.3.2. La Mescla

La Mescla, est caractérisée par un profond méandre du Verdon à la jonction avec la rivière Artuby (Figure 12). L'érosion fluviale concentrée sur le flanc sud par la forme prononcée du méandre a ouvert cette partie des gorges et créé un espace beaucoup plus exposé aux rayons cosmiques que dans les environs proches. Bien que cette partie des gorges soit caractérisée par des lits calcaires minces et fortement fracturés, certains éléments polis par la rivière sont visibles dans les strates plus épaisses. 8 échantillons ont été prélevés (Table 4) le long de deux surfaces polies remarquablement différentes (Figure 14). La première section présente un profil en surplomb, avec des marmites dans la partie basse (Figure 14), tandis que la seconde section présente un profil lisse et presque plat dans sa partie basse (Figure 14). Le site est également caractérisé par une aggradation considérable, créant un cordon de galets se développant vers la jonction avec la rivière Artuby.

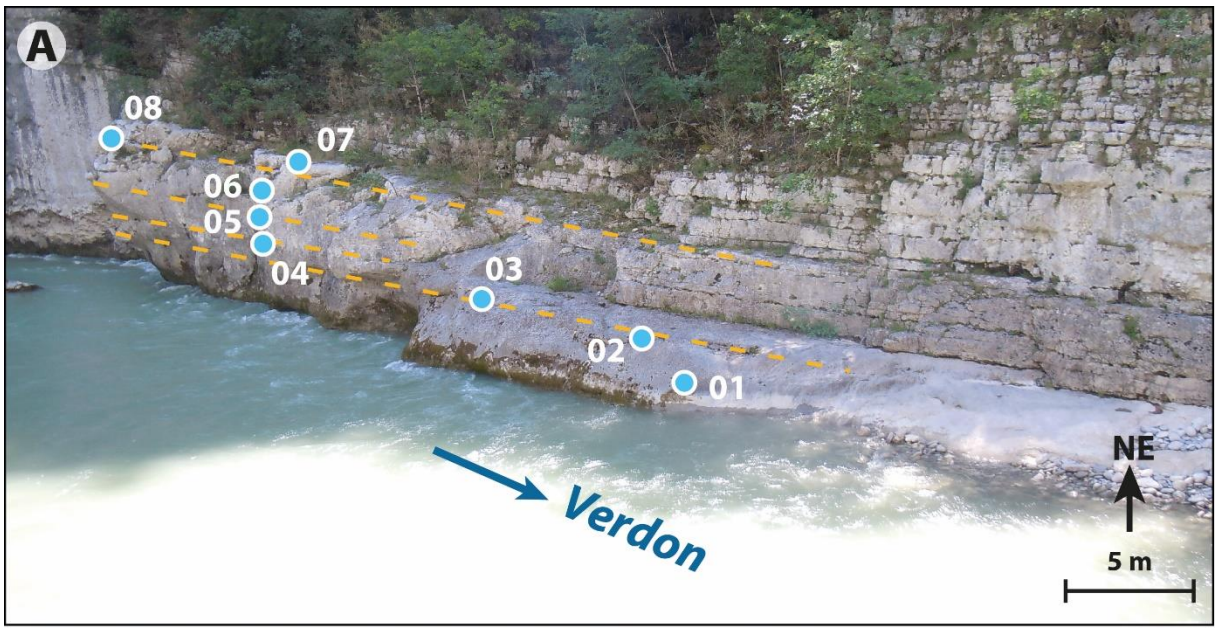

Figure 2-14 : Localisation des échantillons prélevés à la Mescla.

Mescla (lat: 43.7399°; long: 6.3794°; elevation: 564 m.a.s.l.)									
Sample	Height above river (m)	Sample thickness (cm)	TS factor	Spall. scaling	^{35}Cl (ppm)	Ca (%)	Atoms ^{36}Cl (at/g)	Atoms ^{36}Cl ± (at/g)	CRE age (ka)
01	1.1	1	0.39	1.61	43.1	40.5	388057	38470	32.5±3.2
02	2.0	1	0.39	1.61	47.3	40.5	568763	36811	48.2±3.1
03	2.8	1	0.39	1.61	33.5	40.6	677155	29949	59.0±2.6
04	3.9	1	0.39	1.61	36.5	40.5	386654	34273	32.6±2.9
05	4.7	3	0.39	1.61	37.8	41.1	184681	13407	15.0±1.1
06	5.6	2.5	0.39	1.61	43.7	41.1	198667	26792	16.1±2.2
07	6.3	2	0.39	1.61	43.0	40.7	669682	32058	57.4±2.7
08	6.2	1.5	0.39	1.61	49.3	40.6	651036	29465	55.4±2.5

Tableau 2-4 : Caractéristiques des échantillons (^{36}Cl) et résultats géochronologiques du site Mescla. Hauteur au-dessus du niveau de la rivière, facteur de masque topographique (TC), échelle de spallation (Spall. Scalling), teneur en chlore naturel (^{35}Cl), teneur en calcium (Ca), concentration en ^{36}Cl cosmogéniques et incertitude associée, âge d'exposition de la surface échantillonnée

2.3.3. Galetas

A Galetas, nous avons été confrontés à la limite de l'accessibilité, à la fois par le haut, en raison de la hauteur des murs, et par le bas, en raison de la profondeur de la rivière. Par conséquent, au lieu d'un profil vertical le long d'une seule paroi, nous avons choisi de faire un profil longitudinal en échantillonnant trois surfaces polies à 8-10 m au-dessus du lit de la rivière, le long du lit massif du Tithonien qui forme la sortie des gorges (Figure 15). Au total, 5 échantillons ont été prélevés (Table 5).

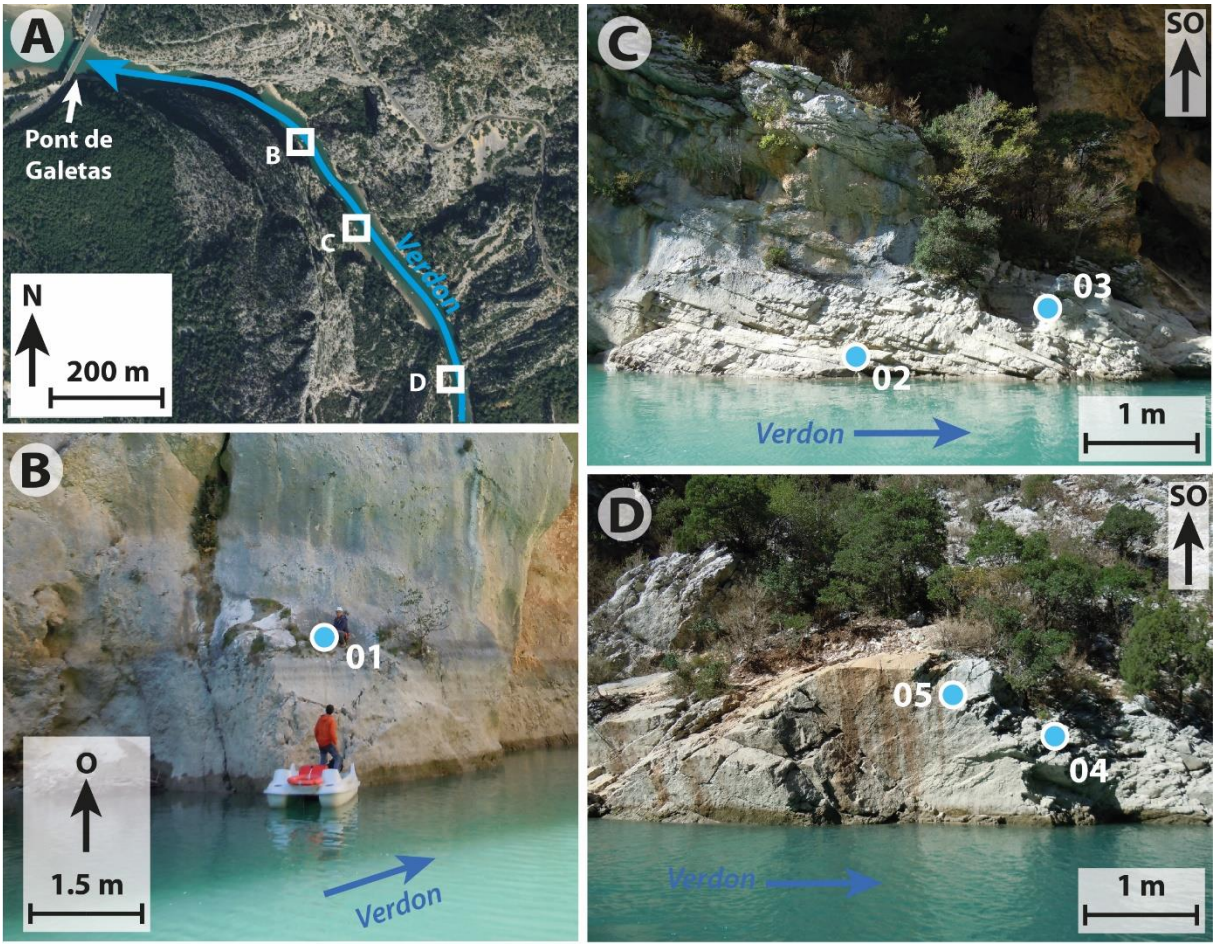

Figure 2-15 : A, Photo aérienne de la sortie des Hautes Gorges du Verdon et localisation des sites échantillonnés. B, C, D, Photographies des trois sites échantillonnés et localisation des échantillons.

Galetas (lat: 43.7972°; long: 6.2576°; elevation: 475 m.a.s.l.)									
Sample	Height above river (m)	Sample thickness (cm)	TS factor	Spall. scaling	^{35}Cl (ppm)	Ca (%)	Atoms ^{36}Cl (at/g)	Atoms ^{36}Cl ± (at/g)	CRE age (ka)
01	10	1	0.20	1.49	16.2	40.5	288596	13927	53.2±2.6
02	8.0	1	0.54	1.50	26.9	40.5	423770	18845	28.0±1.2
03	10.0	1	0.54	1.50	19.5	40.6	308352	15745	20.3±1.0
04	8.9	1	0.67	1.49	48.6	40.5	356756	18990	18.3±1.0
05	9.0	2.5	0.67	1.49	49.4	41.1	596356	29548	31.6±1.6

Tableau 2-5 : Caractéristiques des échantillons (^{36}Cl) et résultats géochronologiques du site Galetas. Hauteur au-dessus du niveau de la rivière, facteur de masque topographique (TC), échelle de spallation (Spall. Scalling), teneur en chlore naturel (^{35}Cl), teneur en calcium (Ca), concentration en ^{36}Cl cosmogéniques et incertitude associée, âge d'exposition de la surface échantillonnée.

2.4. Le Ravin de Redebraus (Paillon)

Le Paillon prend sa source à 1300 m d'altitude et se jette directement dans la Mer Méditerranée, 35,78 km en aval (Figure 16). Le bassin versant présente un fort gain d'élévation dans sa partie supérieure (>20 km de l'embouchure), souligné par la présence de profondes

gorges. Nous avons porté notre choix sur le Ravin de la Rébébraus, pour sa profonde incision dans le substrat calcaire et son aspect préservé. De plus, de par sa position très Sud, le Paillon est le seul bassin versant de notre étude qui est totalement (directement ou indirectement) déconnecté de l'extension des glaciers.

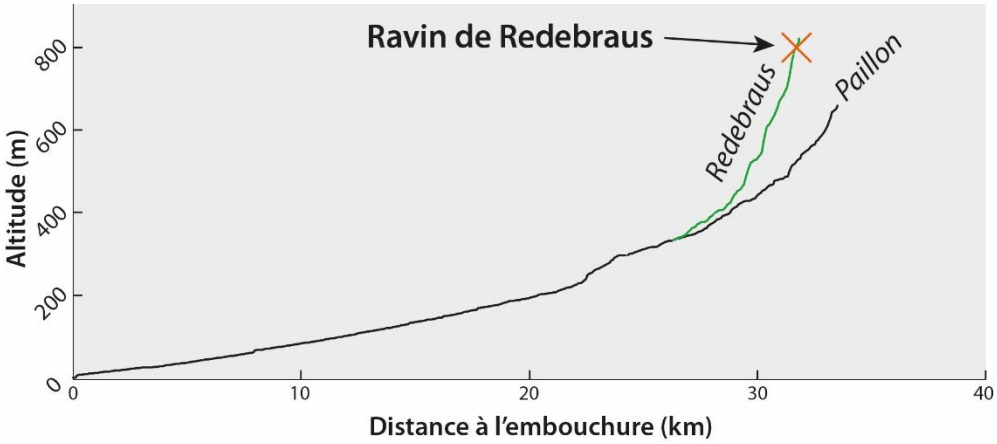

Figure 2-16 : Profil longitudinale du Paillon (noir) et de son affluent le Redebraus (vert) et localisation du site échantillonné (croix orange).

Le ravin de Redebraus présente une morphologie de gorge très contrastée avec l'apparition sporadique de parois très hautes et verticales, entrecoupées de rives à pente bien plus faible, voire plane avec la présence de terrasses, et grandement végétalisées. Le lit de la rivière est également très accidenté avec une succession de ressauts et de piscines creusées dans le substrat calcaire. Nous avons ici effectué deux profils d'échantillonnage, sur deux surfaces se faisant face (Figure 17A). La première étant une falaise verticale de 15 m de hauteur (Figure 17B) et la deuxième étant une surface polie de ~4 m avec une pente faible (Figure 17C). Le faible courant et hauteur d'eau nous ont permis ici d'échantillonner le lit du cours d'eau actuel (échantillon 12). La configuration du site nous a également permis d'échantillonner deux surfaces planes qui peuvent s'apparenter à des terrasses au sommet d'un knickpoint en amont des parois échantillonnées (Figure 17D). Le Ravin de Redebraus a donc fait l'objet d'un échantillonnage extensif et nous a permis de varier notre stratégie d'échantillonnage.

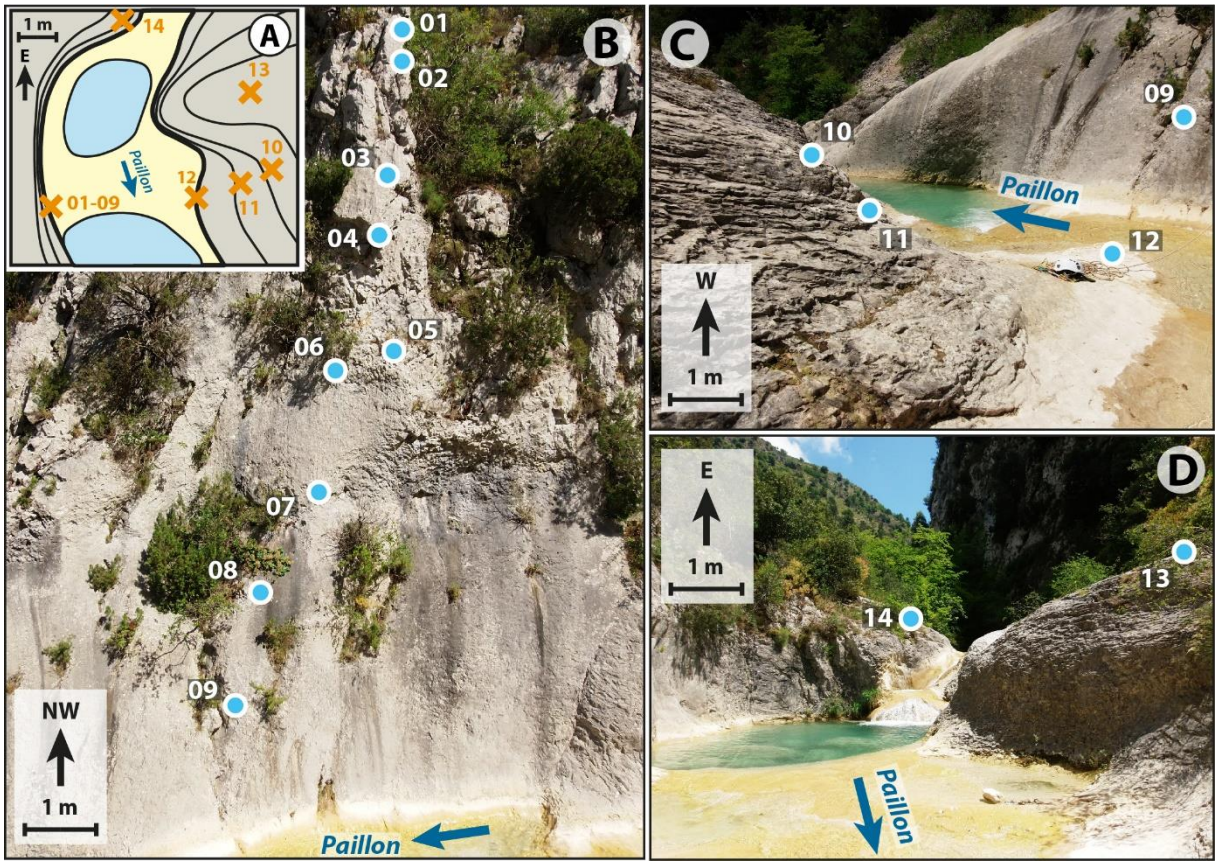

Figure 2-17 : A, Schéma de localisation des surfaces échantillonnées. B, C, D, différentes surfaces échantillonnées et localisation des échantillons.

Redebraus (lat: 43.8555°; long: 7.3772°; elevation: 527 m.a.s.l.)									
Sample	Height above river (m)	Sample thickness (cm)	TS factor	Spall. scaling	^{35}Cl (ppm)	Ca (%)	Atoms ^{36}Cl (at/g)	Atoms ^{36}Cl ± (at/g)	CRE age (ka)
01	14.0	2	0.42	1.58	18.86	40.1	946227	46163	83.5±4.1
02	13.2	3.5	0.42	1.58	19.22	41.3	778602	39778	65.5±3.3
03	10.5	5	0.42	1.58	14.97	39.1	559664	29727	18.9±1.0
04	8.5	1	0.42	1.58	15.10	39.0	568296	28656	49.7±2.5
05	7.1	2.5	0.42	1.58	19.14	40.1	280560	14695	23.1±1.2
06	6.3	0.5	0.42	1.58	20.16	40.3	416307	21504	34.5±1.8
07	4.8	0.5	0.30	1.58	19.78	41.5	444910	22703	51.3±2.6
08	3.2	2	0.30	1.58	18.82	41.	374066	19766	43.2±2.3
09	1.5	1	0.30	1.58	18.96	41.8	165956	11664	18.3±1.3
10	1.83	1	0.64	1.58	20.91	41.0	214946	14291	11.2±0.7
11	1.2	2	0.64	1.58	21.78	41.2	201575	15016	10.4±0.8
12	0.0	1	0.64	1.58	22.74	41.3	117198	12115	6.0±0.6
13	3.7	1	0.64	1.58	23.23	41.1	551920	28682	29.2±1.5
14	3.7	1	0.64	1.58	21.35	40.8	381736	20217	20.2±1.1

Tableau 2-6 : Caractéristiques des échantillons (^{36}Cl) et résultats géochronologiques du site Redebraus. Hauteur au-dessus du niveau de la rivière, facteur de masque topographique (TC), échelle de spallation (Spall. Scalling), teneur en chlore naturel (^{35}Cl), teneur en calcium (Ca), concentration en ^{36}Cl cosmogéniques et incertitude associée, âge d'exposition de la surface échantillonnée.

2.5. La Roya

Tout comme ce qui a été réalisé dans l'Esteron par Petit et al. (2017), nous avons décidé ici de focaliser notre attention sur les affluents non-englacés d'une rivière connectée aux glaciations LGM. En l'occurrence ici, les rivières étudiées sont la Bévéra et la Bendola, toutes deux affluents de la Roya (Figure 18).

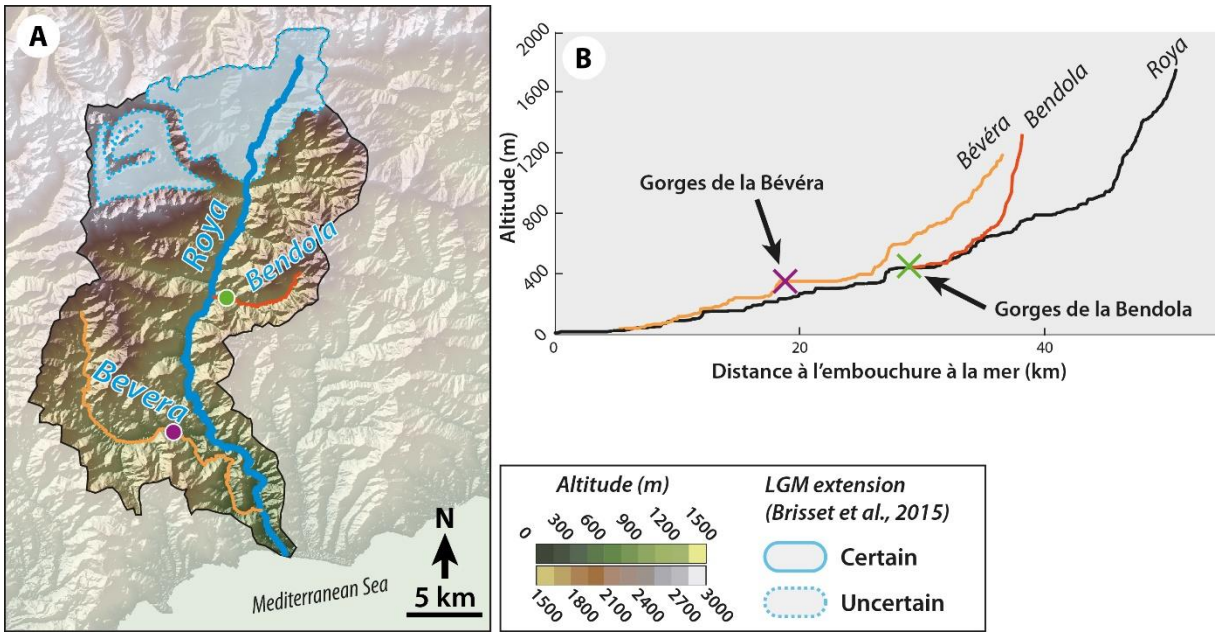

Figure 2-18 : A, Carte topographique du bassin versant de la Roya et localisation des affluents Bevera et Bendola le long desquels des gorges ont été échantillonnées. B, Profil longitudinal de la Roya et de ses affluents, Bévéra et Bendola et localisation des sites d'échantillonnage dans ces gorges.

2.5.1. Les Gorges de la Bendola

La Bendola présente de profondes gorges, localement appelées « Bains du Sémite », à proximité de la jonction avec la Roya. Cette gorge a été aménagée par l'homme. En effet, on y trouve un vieux pont de pierres permettant à l'époque d'accéder à la partie amont des gorges de la Bendola (Figure 19A). On peut voir que le pont n'a pas demandé de modification de la paroi naturelle, car construit à même la paroi sans besoin d'excavation des murs calcaires. Cette observation nous rassure donc sur le caractère préservé de la paroi échantillonnée. Nous y avons effectué un profil vertical de 15 m le long de cette paroi de ~20 m de haut. L'inaccessibilité par le haut nous a contraint à progresser vers le haut de la paroi en partant d'une vire (position de

Yann Rolland, Figure 19A) afin d'y équiper un rappel et échantillonner au fil de la descente depuis ce point. Nous avons encore une fois essayé d'échantillonner au plus près du lit de la rivière à partir d'une surface à pente faible en face de la paroi verticale (Figure 19B). Au total, 11 échantillons ont été prélevés sur ce site (Table 7).

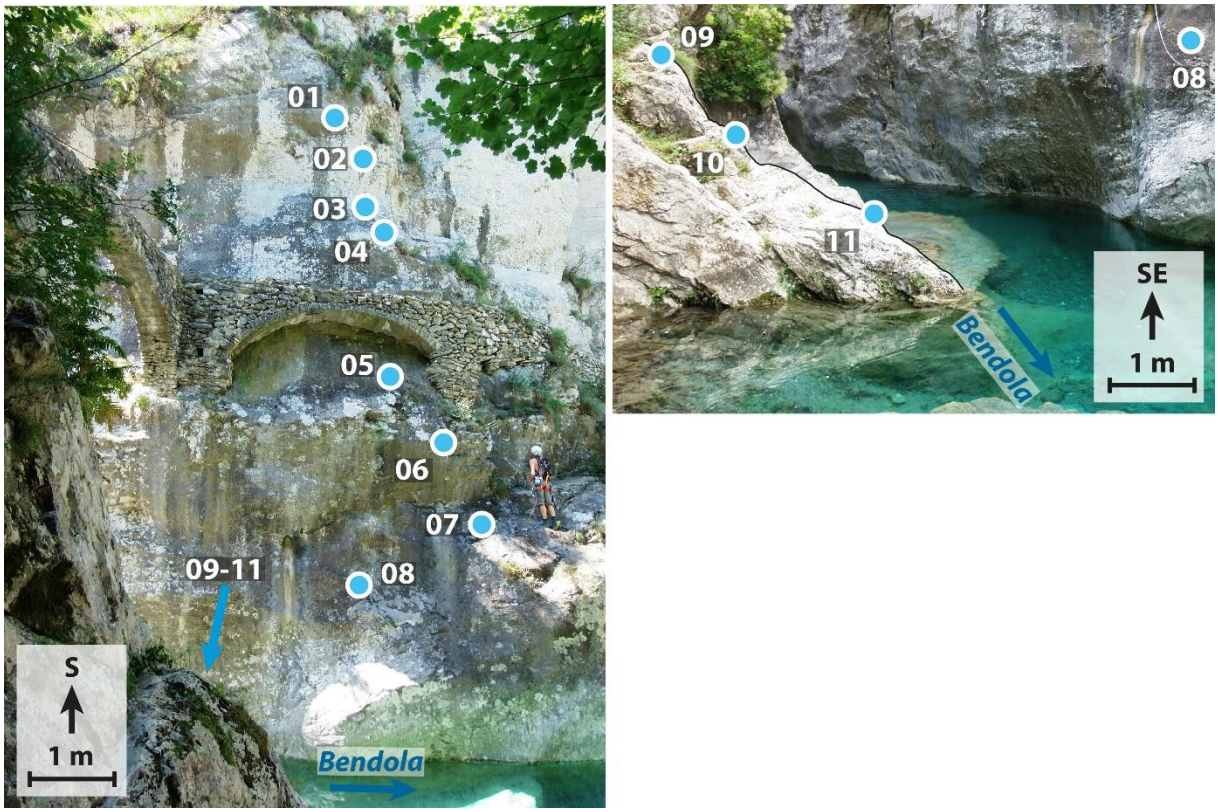

Figure 2-19 : A, Localisation des échantillons prélevés sur la première paroi. B, Localisation des échantillons prélevés sur la deuxième surface.

Bendola (lat: 43.9816°; long: 7.5470°; elevation: 357 m.a.s.l.)									
Sample	Height above river (m)	Sample thickness (cm)	TS factor	Spall. scaling	^{35}Cl (ppm)	Ca (%)	Atoms ^{36}Cl (at/g)	Atoms ^{36}Cl ± (at/g)	CRE age (ka)
01	14.2	3	0.32	1.35	40.9	40.3	284628	15689	35.1±1.9
02	13.0	2	0.32	1.35	42.8	40.3	262445	14997	32.2±1.8
03	11.6	1.5	0.32	1.35	34.1	41.0	303029	16727	37.2±2.1
04	10.5	2	0.32	1.35	29.3	40.9	346005	18060	43.1±2.2
05	7.2	1	0.32	1.35	62.4	41.4	254491	15799	29.8±1.8
06	5.6	0.5	0.62	1.35	17.4	40.9	117113	7733	7.3±0.5
07	3.8	1.5	0.62	1.35	51.4	41.1	243041	14049	14.7±0.8
08	2.1	2.5	0.62	1.35	39.0	41.0	101697	7463	6.2±0.5
09	2.1	2	0.62	1.35	41.5	40.5	75596	8545	4.6±0.5
10	1.8	3	0.62	1.35	45.9	40.5	66751	6722	4.0±0.4
11	0.7	3	0.62	1.35	67.8	41.0	51873	5002	3.0±0.3

Tableau 2-7 : Caractéristiques des échantillons (^{36}Cl) et résultats géochronologiques du site Bendola. Hauteur au-dessus du niveau de la rivière, facteur de masque topographique (TC), échelle de spallation (Spall. Scalling), teneur en chlore naturel (^{35}Cl), teneur en calcium (Ca), concentration en ^{36}Cl cosmogéniques et incertitude associée, âge d'exposition de la surface échantillonnée.

2.5.2. Les Gorges de la Bévéra

Les gorges de la Bévéra présentent un profil très différent des gorges étudiées au préalable. En effet, ici on accède directement au sommet de la strate de calcaire incisée. Ces gorges, peu profondes (<12 m) sont en revanche très étroites et tortueuses (Figure 20). On y voit des formes d'érosion fluviatile flagrantes, avec des marmites, latérales et dans le lit actuel, très profondes. La difficulté a donc été de trouver une surface polie continue, sans surplomb formé par le creusement d'une marmite afin de maximiser l'exposition. La grande facilité d'accès de cette gorge nous a également permis d'expérimenter l'échantillonnage de deux faces complètes de la gorge (Figure 20). 7 échantillons ont été prélevé sur chacune des deux parois se faisant face (Table 8).

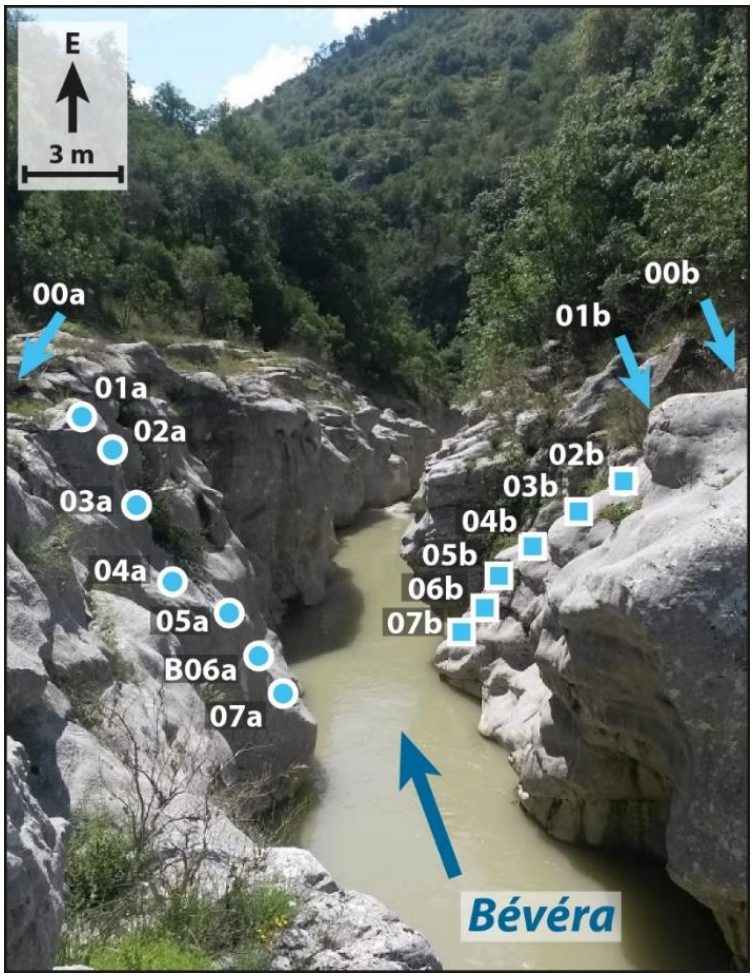

Figure 2-20 : Localisation des échantillons prélevés sur deux faces dans les gorges de la Bévéra.

Bévéra (lat: 43.8847°; long: 7.4961°; elevation: 281 m.a.s.l.)								
Sample	Height above river (m)	TS factor	Spall. scaling	^{35}Cl (ppm)	Ca (%)	Atoms ^{36}Cl (at/g)	Atoms ^{36}Cl ± (at/g)	CRE age (ka)
00a	12.5	0.89	1.27	11.3	37.8	380994	16676	19.0±0.8
01a	11.0	0.89	1.27	11.4	37.9	331854	15069	16.4±0.7
02a	10.3	0.80	1.27	18.9	37.9	243162	10644	13.1±0.6
03a	9.4	0.63	1.27	12.4	38.0	231557	10194	16.2±0.7
04a	7.9	0.56	1.27	12.4	37.9	134514	8034	10.5±0.6
05a	7.2	0.56	1.27	21.1	37.8	143352	7200	10.9±0.5
06a	6.2	0.66	1.27	17.1	37.8	111662	5721	7.3±0.4
07a	4.9	0.64	1.27	16.1	37.8	85610	4754	5.8±0.3
00b	13.5	0.81	1.27	15.4	38.0	351203	14916	18.9±0.8
01b	11.0	0.81	1.27	33.4	37.7	310241	13924	15.8±0.7
02b	9.3	0.75	1.27	12.9	37.9	190555	8637	11.1±0.5
03b	8.9	0.69	1.27	15.9	38.0	144324	7151	9.1±0.4
04b	8.4	0.62	1.27	16.0	37,9	136508	6619	9.5±0.5
05b	6.8	0.54	1.27	12.9	38.0	100400	5648	8.1±0.5
06b	5.7	0.48	1.27	17.2	38.0	78976	4716	7.0±0.4
07b	4.1	0.48	1.27	19.1	37.9	66429	4192	5.9±0.4

Tableau 2-8 : Caractéristiques des échantillons (^{36}Cl) et résultats géochronologiques du site Bévéra. Hauteur au-dessus du niveau de la rivière, facteur de masque topographique (TC), échelle de spallation (Spall. Scalling), teneur en chlore naturel (^{35}Cl), teneur en calcium (Ca), concentration en ^{36}Cl cosmogéniques et incertitude associée, âge d'exposition de la surface échantillonnée.

Chapitre 3 : Interplay of fluvial incision and rockfalls in shaping periglacial mountain gorges

Résumé

L'incision fluviale est la conséquence du réajustement du paysage à des processus tectoniques et climatiques combinés. Dans les Alpes du Sud-Ouest (Géoparc de Haute Provence), les gorges incisées par la rivière Bès témoignent de l'efficacité de processus d'érosion affectant le front des Alpes. Le bassin versant du Bès se trouve en périphérie des Alpes, hors du domaine englacé durant les dernières périodes glaciaires, ce qui le rend approprié pour quantifier l'incision fluviale et les processus d'érosion associés dans un environnement périglaciaire. Dans cet article, nous combinons la cartographie 3D haute résolution et la datation par les nucléides cosmogéniques d'une gorge (la "Clue de Barles"). Premièrement, la modélisation topographique 3D réalisé à partir de photos aériennes et acquises par drone permet de cartographier les marqueurs d'érosion sur les parois de la gorge et de déterminer avec précision le masque topographique pour la datation CRE. Deuxièmement, la distribution des âges CRE met en évidence deux domaines géomorphologiques distincts le long des parois de la gorge: i) la section supérieure est caractérisée par des groupes d'âges CRE similaires, interprétés comme étant liés à des événements d'éboulement paraglaciaire ; ii) la section inférieure présente des âges croissants avec la hauteur, qui sont attribués à une incision fluviale se produisant à un taux de 0,15 mm/an depuis 25ka, et de 2 mm/an depuis 2ka. Nos résultats pour la Clue de Barles, comparés à d'autres sites dans les Alpes françaises du Sud, soulignent que : i) la morphologie de la gorge est le résultat de la combinaison de l'incision fluviale verticale et des processus gravitationnels latéraux, ii) le taux moyen d'incision fluviale

quaternaire dans le bassin versant de la rivière Bès est au moins deux fois plus faible qu'à l'Est, dans les Alpes anciennement glaciaires.

Interplay of fluvial incision and rockfalls in shaping periglacial mountain gorges

Thibaut Cardinal[1], Laurence Audin[2], Yann Rolland[3], Stéphane Schwartz[2], Carole Petit[1], Swann Zerathe[2], Laurent Borgniet[4], Régis Braucher[5], Jérôme Nomade[2], Thierry Dumont[2], Valery Guillou[5], and ASTER team[5,*]

[1] Université Côte d'Azur, CNRS, Observatoire de la Côte d'Azur, IRD, Géoazur, F-06560 Valbonne, France, cardinal@geoazur-unice.fr, petit@geoazur-unice.fr

[2] Université Grenoble Alpes, Université Savoie Mont Blanc, CNRS, IRD, IFSTTAR, ISTerre, 38000 Grenoble, France, laurence.audin@ird.fr, thierry.dumont@univ-grenoble-alpes.fr, jerome.nomade@univ-grenoble-alpes.fr, stephane.schwartz@univ-grenoble-alpes.fr, swann.zerathe@ird.fr

[3] Université Savoie Mont Blanc, CNRS, Pôle Montagne, Edytem, F-73370 Le Bourget-du-Lac, France, yann.rolland@univ-smb.fr

[4] Université Grenoble Alpes, INRAE, LESSEM, F-38000, Grenoble, France laurent.borgniet@inrae.fr

[5] CEREGE, Aix-Marseille Univ., CNRS, IRD, Coll. de France, INRAE, Technopôle de l'Environnement Arbois-Méditerranée, BP80, 13545 Aix-en-Provence, France, braucher@cerege.fr, guillou@cerege.fr, bourles@cerege.fr

**ASTER Team: Georges Aumaître, Didier L. Bourlès, Karim Keddadouche*

Abstract

Fluvial incision is the consequence of landscape readjustment to combined tectonic and climatic processes. In the southwestern Alps (Haute Provence Geopark), deep gorges incised by the Bès River attest of efficient erosional processes at the front of the Alpine mountain range. This catchment stands in a peripheral Alpine position, out of the glaciated domain during the

last glacial periods, which makes it suitable to quantify fluvial incision and related erosional processes in a glacier-free environment. In this paper, we combine high resolution 3D topographic mapping and in situ produced cosmogenic ^{36}Cl dating of a mountain gorge (the "Clue de Barles" Gorge). First, the very high-resolution 3D topographic modeling from aerial and drone surveys permits to map the erosion markers on the gorge walls and to accurately determine the topographic shielding factor for CRE dating. Secondly, ^{36}Cl Cosmic Ray Exposure (CRE) age distribution highlights two distinct geomorphic domains along the vertical profile: i) the higher section is characterized by clusters of similar CRE ages, interpreted as related to paraglacial rockfall events; ii) the lower section shows increasing ages with height, which are ascribed to fluvial incision occurring at a rate of 0.15 mm/yr since 25ka, and of 2 mm/yr since 2ka. Our results for the Clue de Barles, compared to other sites in the South French Alps highlight that: i) the gorge morphology is the result of the combination of both vertical fluvial incision and lateral gravitational processes, ii) the mean Quaternary fluvial incision rate in the Bès River catchment is at least twice lower than further east in the formerly glaciated Alps.

Keywords: Fluvial incision; Mountain gorge; Rockfalls; CRE ^{36}Cl dating; High-resolution 3D mapping; Southwestern Alps

1. Introduction

The erosive response of landscapes through times provides a record of the interaction between lithospheric and atmospheric forcing. The lithospheric forcing comprises isostatic readjustment and tectonic motions (England and Molnar, 1990; Lavé and Avouac, 2001; Wobus et al., 2006), while the atmospheric forcing consists of local or global climate variations (Van der Woerd et al., 2002; Pan et al., 2003; Bacon et al., 2009). Fluvial, glacial and gravitational erosion processes play a significant role in the shaping of the landforms in an "erosion-uplift" self-balancing system (Adams, 1985). River dynamics therefore provide quantitative

information on landscape evolution because their morphology and erosive power are directly linked to processes that can affect landforms: tectonic, mass movements, climate change (Pratt et al., 2002; Kirby and Whipple, 2012).

The study of fluvial landscapes evolution relies on available Quaternary geomorphological markers like terraces and incised river gorges (Pazzaglia et al., 1998; Saillard et al., 2014; Rolland et al., 2017). However, processes that led to the formation of these geomorphological objects are often poorly quantified when it comes to vertical markers. Indeed, these 3D morphologies record a combination of different mechanisms such as fluvial incision, gravitational destabilization, like landslides or rockfalls, or glacier advances related to late glacial episodes (Whipple et al., 1999; Brocklehurst and Whipple, 2002; Montgomery, 2002; Brocard, 2003; Valla et al., 2011). Quaternary geomorphological shaping of the Alpine belt and the evolution of landforms are generally explained by the alternation of glacial and inter-glacial phases, which produce significant vertical uplift after each deglaciation (Champagnac et al., 2007, 2008; Valla et al., 2010) and lead to a strong bedrock incision by the river network. The formation of peculiar fluvial markers, like bedrock gorges (named in local French language “clues” when the river runs perpendicular to the bedding), marked by deeply incised rock walls have been variously interpreted as features typical of sub-glacial incisions (Korup and Schlunegger, 2007; Montgomery and Korup, 2010) or of fluvial incision of the Late Quaternary (Saillard et al., 2014; Rolland et al., 2017; Petit et al., 2017; 2019). In all these studies, the contribution of rockfall events has never been put forward as an efficient process for the long-term shaping of mountain gorges. These investigated catchments have headwaters located in high altitude massifs, under the influence of glaciers since the Late Glacial Maximum (LGM), which led to efficient fluvial incision during deglaciation. For all these investigated sites, the CRE data evidenced a strong relation between the onset of incision and the post-LGM deglaciation, which led these authors to propose that climatic variations are the major external

factor responsible for the incision through punctual but strong glacial outburst floods during interglacials (e.g. Petit et al., 2017; Rolland et al., 2017).

In this paper, we focus on the Clue de Barles (CdB) Gorge in southwestern Alps (Southern French Alps). The site is located at the front of the subalpine fold and thrust belt, in the Bès Valley (Figure 1A), which catchment has likely been disconnected from any significant glacial influence during the LGM (Brisset et al., 2015 and references therein). This valley is currently at the boundary between the stable Alpine foreland and the actively uplifting chain, as detected by vertical GPS measurements (>0.5 mm/yr; Serpelloni et al., 2013; Nocquet et al., 2016; Sternai et al., 2019). It thus appears as a key area to determine the response of a catchment unaffected by glaciers influence and undergoing a slow uplift.

In this paper, we aim to highlight the different erosive processes that lead to the gorge formation in a fluvial-dominated catchment, based on the acquisition of a high-resolution Digital Elevation Model (DEM) of the CdB Gorge and its related environment and a high-resolution CRE dating profile of the ~100 meters high, nearly vertical gorge walls. These new data allow us to assess the relative contribution of gravitational and fluvial incision processes in the shaping of gorges along an apparently smooth profile. Finally, we compare these data with previous studies available along different catchments in the Alpine foreland after the LGM.

2. Geological and geomorphological settings

2.1. Geological setting: The Barles erosional "half-window"

Our geomorphic target, the "Clue de Barles" (CdB Gorge), is located in the foreland of the southwestern Alps (Figure 1A). This fold-and-thrust belt has undergone tectonic shortening in Cenozoic times due to the Alpine collision (Dumont et al., 2012; Schwartz et al., 2017). The geological structure of the region comprises the Digne nappe, made of a thick Early Jurassic

limestone and marl series in the study area, which was thrust over onto the Cenozoic foreland molassic basin presently outcropping in an erosional half-window: the Barles “half-window” in the Digne Geopark (Figure 1B; Hippolyte and Dumont, 2000). At the present time, the region is still undergoing active but very slow deformation, under a compressive tectonic context (Sue et al., 2007), as shown by geodesy (Walpersdorf et al., 2018) and seismicity (Delacou et al., 2004).

In the study area, erosion due to the Bès River, a tributary of the Durance River, has participated to the formation of the erosional half-window (Figure 1B) revealing the folded and faulted sedimentary cover in the foreland beneath the Digne Nappe (Figure 1C). The formation of this erosional feature is related to tectonic uplift controlled by Pliocene crustal thickening (Schwartz et al., 2017). Thermochronological inversion modeling by Schwartz et al. (2017) showed that the onset of the half-window exhumation began at 6 Ma (with a denudation rate of ≈0.7 mm/yr). Since then, erosion, in response to the tectonic uplift (Figure 1C), has removed up to 4 km of the Digne nappe cover.

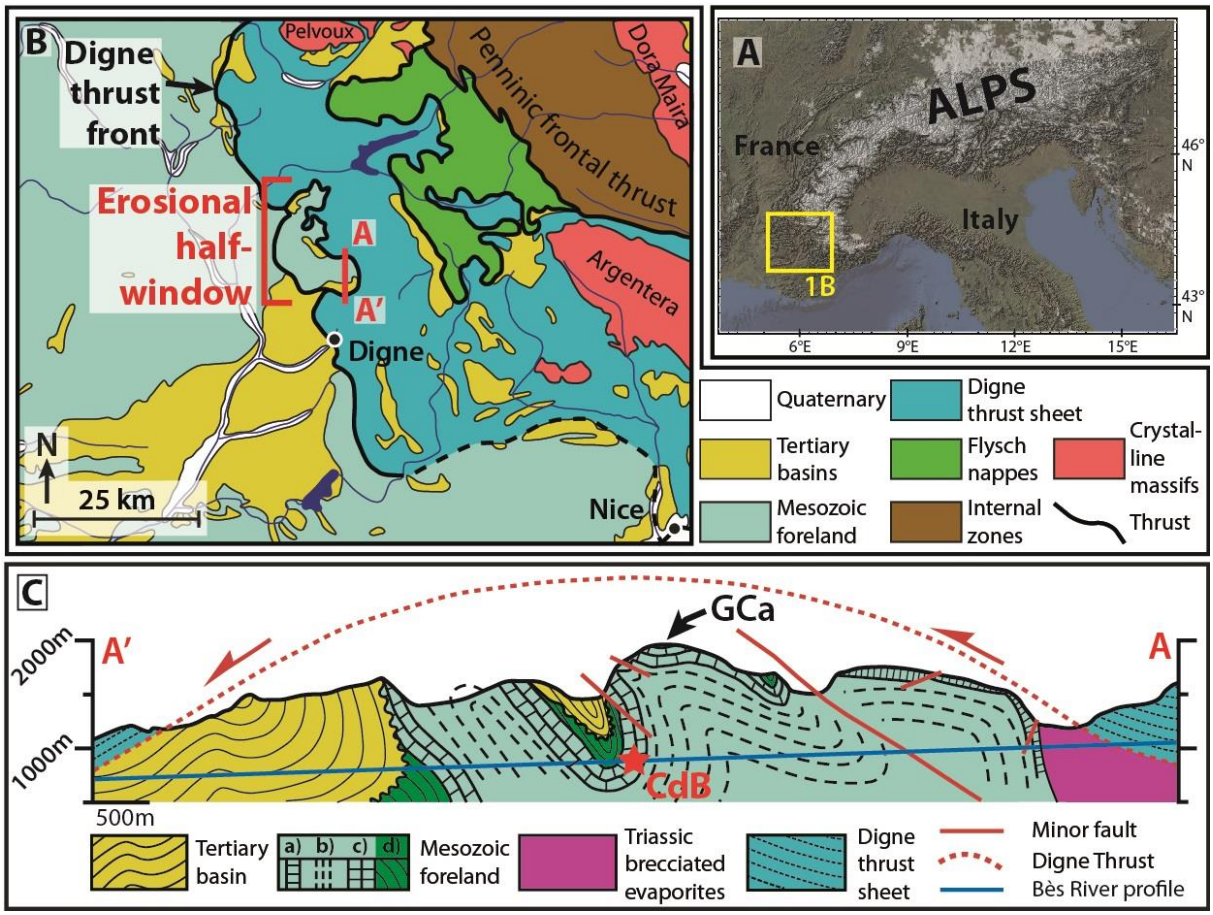

Figure 3-1 : A, Location of study area in the European Alps. B, Location of the Barles half-window in the Western Alps general tectonic framework (modified from Schwartz et al., 2017). C, Geological cross-section of the Barles erosional half-window along the Bès River profile. Mesozoic foreland a) massive Early Jurassic; b) Middle to Late Jurassic "Terres Noires"; c) Late Jurassic "Tithonian limestones"; d) Cretaceous. Note the folding of the Tithonian limestones that form the Grande Cloche anticline (GCa) in which the Clue de Barles Gorges (red star ; CdB) is dug by the Bès River.

2.2. Geomorphological setting

The diversity of landscape morphologies in the Bès Valley is partly explained by differential erosion due to the strong lithological variations between marly and carbonate rich formations. Indeed, wide, smooth and open valleys shaped by landslides and gully dynamics are observed in Middle Jurassic shales locally named the "Terres Noires formation" (Figure 2A). These low relief areas are delineated by adjacent strata of much more competent Late Jurassic limestones. The Terres Noires formation is exposed in the core of anticlines while the synclines preserve Cretaceous strata, as well as Oligocene to Miocene molassic deposits unconformably lying over the Mesozoic sequence (Figures 1C). The absence of any glacial geomorphological markers, such as moraines or U-shaped valleys, precludes any significant

glacial erosion in the Bès catchment during the LGM, as also documented by studies on the maximum glacial extension in the SW Alps (Brisset et al., 2015 and references therein). Recent incision of the Late Jurassic limestones (up to 250m thick) by the Bès River has shaped the CdB Gorge in the southern flank of the overturned "Grande Cloche" anticline (GCa; Figure 1C and 2A).

Figure 2 presents three different domains along the gorge perpendicular profile:

1) sub-horizontal surfaces above the gorge,

2) steep slopes of the two gorge walls facing each other that are widening as the altitude increases, reaching ≈ 150 m of width at ≈ 150 m high above the river level,

3) sub-vertical river polished walls that form a narrow incision canyon in the lowest part (≈ 10 m high) (figure 2B, C and D).

The V-shaped profile of the gorge suggests that at larger scale its morphology may not only be controlled by fluvial incision, but also by lateral erosional processes affecting the gorge walls as the Bès River incises vertically.

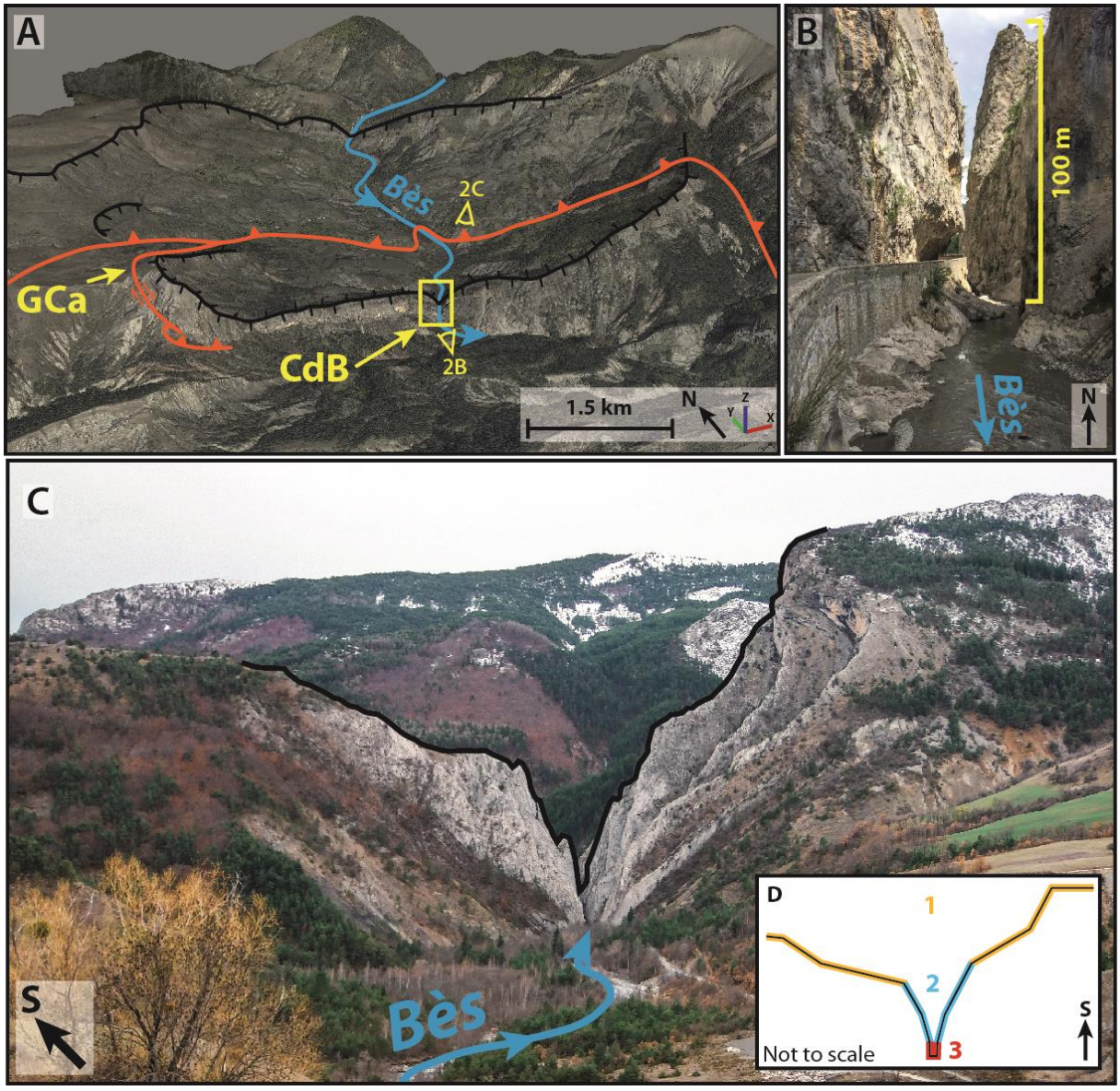

Figure 3-2 : A, Digital Elevation Model (DEM) based 3D view from the of the study area featuring the incised limestone bars (thick black lines) north and south of a large open valley. B, Terrestrial photographs of the Clue de Barles (CdB) Gorge. C, Panoramic view of the CdB Gorge towards the South featuring the vertical Tithonian limestone strata. Note the V shaped lateral profile of the gorge, highlighted on the photographs (black thick line). D, schematic interpretation of the V shaped profile of the gorge showing the 3 different domains: 1) sub-horizontal surfaces above the gorge, 2) steep slopes of the two gorge walls facing each other that are widening as the altitude increases, reaching ≈ 150 m of width at ≈ 150 m high above the river level, 3) sub-vertical river polished walls that form a narrow incision in the lowest part (≈ 10 m high).

3. Methods

3.1. Strategy and sampling

Gorge walls are theoretically gradually exposed during the incision process (Schaller et al., 2005; Ouimet et al., 2008). Therefore, cosmogenic radionuclide exposure (CRE) dating of the gorge wall should reveal a systematic rejuvenation of the CRE ages towards the current riverbed

level trough a correlation between the altitude of the samples and their CRE age. However, gravitational processes, like rockfall events, may also cause the rejuvenation of a gorge wall surface. If the wall compartment involved in a rockfall event is thicker than ≈ 2m, the resulting exposed surface should not retain any cosmogenic inheritance prior to the gravitational event, as ≈ 95% of the cosmic radiation is absorbed in the first 1.8 m below the surface (Lal, 1991). Hence its concentration in cosmogenic nuclides should be null at the time of the rockfall, and subsequently, the CRE age should correspond to that of the gravitational event. Therefore, cosmogenic radionuclide concentration measurement is a well suited dating method to obtain chronological information of both gravitational and fluviatile processes, and thus allows dating rockfall events and quantifying incision rate on the same spot.

Sampled surfaces were chosen for incision rate estimation, based on the following morphological indices: i) a surface with evidence of induration varnish or with low apparent superficial dissolution, indicating little erosion since exposure or ii) vicinity to peculiar concave erosional surfaces ("pot holes") preserved in the gorge walls that points to the last stalling point before the incision phase. The identification of such markers and the necessity to avoid samples with a too large topographic shielding led to the choice of a ≈10 m high, well-preserved wall located at the southern (i.e., downstream) extremity of the gorge (Figure 3). The dissolution, weathering patina and superficial smoothing of the limestone surface of the gorge prevented us from confidently identifying a priori gravitational markers from the wall morphology through field and DEM based observations, by any rockfall scars characterized by edged surface and distinct coloration due to the lack of patina. We then chose to sample regularly the ≈ 70 m high wall rising above the preserved surface along a sub-vertical profile (Figure 3A and 3C).

Along this profile, twenty limestone samples were collected, using a drill, hammer and chisel. The sampled surfaces include the lower and preserved river-polished surface and the upper slightly widening part of the gorge wall. In total, the gorge profile extends from the river

up to 80 m high on two parallel vertical limestone strata (Figure 3C). We sampled surfaces with no overhanging relief to minimize the topographic shielding and to simplify the topographic shielding factor determination.

In parallel, four samples were collected on the eastern sub-horizontal top of the limestone bar overlooking the gorge to constrain the local denudation rate in this part of the catchment (Figure 2C and 3A)

3.2. Analytical protocol

Samples were prepared at the Laboratoire National des Nucléides Cosmogéniques (LN2C; CEREGE, Aix-en-Provence) following the procedure presented by Schimmelpfennig et al. (2009). ^{36}Cl concentrations were determined by accelerator mass spectrometry (AMS) performed on ASTER, the French national AMS facility (CEREGE, Aix en Provence) (Arnold et al., 2010). All measurements were calibrated against in-House CEREGE SM-CL-12 standard (Merchel et al. 2011). Total uncertainties account for counting statistics, standard evolution during measurements, standard uncertainty and external uncertainties of 2.74%, 2.13% and 1.62 % for ^{36}Cl/^{35}Cl, ^{36}Cl/37Cl and ^{35}Cl/^{37}Cl ratios, respectively (Braucher et al., 2018). The full chemical compositions of the two sampled Tithonian limestone strata were analyzed at CRPG (Nancy) in order to take into account for the various ^{36}Cl production pathways (Schimmelpfennig et al., 2009). A sea level and high latitude ^{36}Cl production rate for calcium spallation of 42.2±3.4 atoms ^{36}Cl g^{-1} yr^{-1} (Schimmelpfennig et al., 2009; Braucher et al., 2011) has been used and scaled after Stone (2000) and corrected for topographic shielding (see next paragraph). ^{36}Cl ages have been determined using the approach of Schimmelpfennig et al. (2009) using a limestone density of 2.6 g.cm^{-3}. CRE data are displayed in Table 1.

Topographic shielding was first determined from field data. Furthermore, we chose to use a high resolution DEM, built from a drone survey of the gorge and its surroundings, in order to be able to precisely recalculate the shielding parameters on each sampled surface.

3.3. Topographic shielding estimation in a narrow gorge

The estimation of topographic shielding (TS) allows the calibration of the sampled surfaces exposure ages by evaluating how much cosmic rays were obstructed by the surrounding topography, which decreases the cosmogenic nuclides production rate (Dunne et al., 1999). The TS factor is defined as the ratio of the received cosmic flux at a given point over the maximum flux at this point assuming an unshielded exposure (Dunne et al. 1999; Gosse and Phillips 2001). It is commonly calculated using the following equation from Dunne et al. (1999):

$$C_T = 1 - \frac{1}{2\pi}\sum_{i=1}^{n} \Delta\emptyset_i \, sin^{m+1}(\theta_i)$$

Where C_T is the TS factor, n is the number of topographic obstructions that are measured around a sampled surface, each obstruction being represented by a pair of azimuth $\emptyset_i$ and elevation angles θ_i, m is a constant which commonly cited value is 2.3 (Gosse and Phillips 2001). This factor is commonly estimated in the field during surface sampling by measuring, using a compass, the horizon elevation at 360° around the sampled surface (Gosse and Phillips, 2001). However, such protocol is difficult to implement in gorges while sampling the vertical wall, and is complexified by the 3D geometry of the gorge.

Numerical methods exist to estimate TS from Digital Elevation Models (DEM), which have been demonstrated on basin-averaged denudation rate studies (e.g. Codilean, 2006; Balco et al., 2008). In this paper, we used the tools developed by Li (2013), for the GIS software ArcGis, using high-resolution DEMs of the CdB Gorge and its surrounding. The DEM used are built from the Structure-from-Motion method, using aerial photographs acquired by plane, for the surrounding gorge topography, and UAV, for the mapping of the vertical parts (gorges walls), following an adaptation of the methodology presented in Vasquez-Tarrio et al. (2017).

The resulting data set has a resolution of 50 cm (precision RMSE of 2.6m), for the model

surroundings used for the TS factor determination, and 7cm with a precision of 16.8 cm (RMSE) for the DEM used for the mapping of the incision markers in the gorge. Such precision has been achieved in a vertical environment, such as the CdB Gorge without GPS signal, with the use of a total station (Leica TS02) for the acquisition of Ground Control Point (GCP). The code by Li (2018) allows us to calculate the maximum elevation for each azimuth value (horizontal angle from 0° to 360° by 5° increment) around the sampled surface.

In a previous study, Norton and Vanacker (2009) mentioned that the use of a DEM with resolution lower than 5 m (5 m being the optimal resolution) can cause an overestimation of the TS factor, because of the ability of cosmic rays to pass through small obstructions without any significant interaction (Norton and Vanacker, 2009). However, in gorges, the use of a higher resolution DEM is required for the numerical determination of the TS factor, as the samples were all gathered in a narrow horizontal (XY) space, even if they lie at a larger distance from each other in the vertical Z dimension. Furthermore, the only obstructions in the gorge are the ≈200 m thick limestone walls. A precise estimate of TS is very important in the CdB Gorge, as it has a large impact on the calculated CRE ages.

3.4. Denudation rates

Denudation, which includes mechanical and chemical erosion, is an important process in the shaping of carbonate landscapes (Ryb et al., 2014a; 2014b). The efficiency of the denudation process is controlled in part by the slope and convexity of the surfaces that are involved (Godard et al., 2016; Thomas et al., 2017). Gravitational processes must be considered, but also the spatial variability of the carbonate dissolution efficiency, which results from numerous slope morphological irregularities (overhangs, recesses, fractures). Because the radionuclide concentration at the surface results from a constant competition between surface denudation and production by exposure to cosmic rays, the denudation rate is an important factor that needs to be determined in order to calculate the CRE ages. In the SW Alps, a regional

denudation rate of ≈30 mm/kyr has been estimated in the literature (e.g. Godard et al., 2016; 2020; Thomas et al., 2017), and this parameter has also been constrained locally for our site by using steady-state radionuclide concentrations. For this purpose, four sub-horizontal surfaces have been sampled on the top of the limestone bar in which the gorge was incised (≈ 250 m above riverbed) (Figure 2C and 3A). The denudation rates are calculated assuming a steady-state between radionuclide production and denudation, after the procedure described Schimmelpfennig et al. (2009).

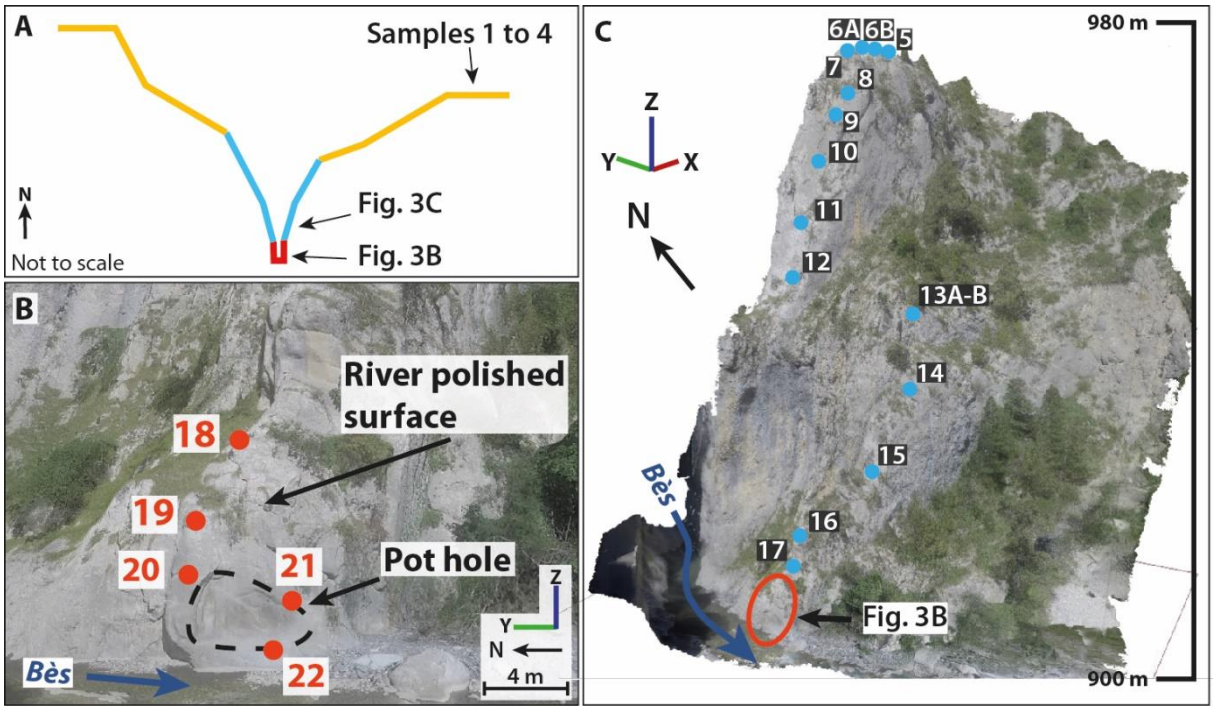

Figure 3-3 : A, schematic interpretation of the gorge V shaped profile and location of the sample gathered for CRE dating. B, Digital Elevation Model (DEM) based 3D view of the lower part of the sampling profile and location of the corresponding samples (18 to 20). Note the presence of a "pot hole" that indicates the preserved nature of the river polished sampled surface. Above sample 18, the preservation of the fluvial polished surface on the gorge wall is not sure and might have suffer post-incision erosion processes (dissolution and/or gravitational processes). C, All samples located on the high-resolution 3D DEM of the 80 m high CdB Gorge wall.

4. Results

4.1. Flat upper surface: steady-state denudation rates

Measured radionuclide concentrations (samples 1 to 4, Figure 2C and 3A, ≈250m above river) for the horizontal high hanging paleo surfaces of the limestone bar range from 1.56 to 18.88×10^6 ^{36}Cl at/g (Table 1). Assuming these samples at steady state (i.e. their exposure time

is long enough to ensure that concentrations have reach a plateau), yields to steady-state denudation rates ranging between 18.74 ± 1.05 and 32.83 ± 1.94 mm/ka for these top samples. These values are in agreement with previous estimates (e.g. Godard et al., 2016; 2020; Thomas et al., 2017, Siame et al., 2004; Zerathe et al., 2013), for the SW Alps.

4.2. Gorge steep slope / middle part: rockfall markers

4.2.1. Fracturation

The CdB Gorge walls are heavily fractured and prone to rock mass movements, as observed by our field structural analysis: two major fracture families have been measured on the gorge walls, both trending N30°E (i.e., parallel to the gorge strike), the first one dipping ~70°W and the second one dipping 40-50°E, while the bedding is ~EW and vertical (Figure 4).

4.2.2. CRE age

Denudation rates obtained on horizontal surfaces do not reflect the true denudation that has affected the vertical walls of the gorge. Indeed, it is generally considered that vertical and sub-vertical surfaces undergo less dissolution than gently dipping or horizontal surfaces, as they receive much less water runoff, and water does not stagnate or percolate (Sadier et al., 2012). Compiling denudations rates determined from our data and those from literature, we have decided to consider a denudation rate of 10 mm/ka for vertical or sub-vertical surfaces, following Sadier et al. (2012). CRE ages determined from the ^{36}Cl concentrations are reported in the age-elevation plots (Figure 5A). The profile displays ages between 22 and 8 ka We can observe two ages clusters, one at ≈17 ka (samples 5 to 9) and the other one at ≈10 ka (samples 10 to 13A), respectively.

As shown on Figure 5A, the CRE ages distribution does not correlate with the altitude of the samples and especially, we do not see any systematic rejuvenation of the CRE ages towards the base of the gorge at the current riverbed level, as it would be expected for a gorge slope affected by post-incision erosion processes (such as rockfall or dissolution). The interpretation

of these ages therefore requires a more detailed analysis taking into account the 3D morphology of the gorge walls, and the processes that may have affected the history of their exposure to cosmic rays.

4.3. River polished vertical surface / lower part: fluvial incision

CRE ages determined from the ^{36}Cl concentrations in the gorge lower part are reported in the age-elevation plots (Figure 5B). The five samples (18 to 22) display ages between 26 ka and 800 a (Table 1). From these ages, we can compute two distinct incision rates: 0.15 mm/yr from 25 ka to 2 ka and 1.97 mm/yr from 2 ka to present day, assuming a y-intercept equal to zero.

Sample	Altitude above sea level (m)	Height above river (m)	Lat	Long	Spall. scaling	35Cl (ppm)	Ca (%)	Atoms ^{36}Cl (at/g)	Atoms ^{36}Cl uncertainty (at/g)	CRE age (yr)	Denudation rate (mm/ka)	TS factor	Surface strike and dip
1	1165.0	263.0	44.23	6.26	2.64	60.5	36.0	18885474	111338	-	32.83 ± 1.94	0.99	Sub-horizontal
2	1155.6	253.6	44.23	6.26	2.62	48.5	39.0	2767824	155686	-	18.74 ± 1.05	0.99	Sub-horizontal
3	1151.7	249.7	44.23	6.26	2.61	81.3	38.2	2844314	195423	-	22.91 ± 1.57	0.99	Sub-horizontal
4	1154.9	252.9	44.23	6.26	2.62	38.0	31.9	1563115	84417	-	32.54 ± 1.76	0.99	Sub-horizontal
5	975.2	73.2	44.23	6.26	2.27	29.1	32.1	414312	21132	13598 ± 694	-	0.85	N118E23
6A	975.7	73.7	44.23	6.26	2.27	17.2	24.7	463710	20942	19805 ± 894	-	0.87	N22E4
6B	975.5	73.5	44.23	6.26	2.27	102.8	27.6	840309	279136	19240 ± 6391	-	0.87	N21W12
7	975.1	73.1	44.23	6.26	2.27	20.6	38.9	518890	23489	15334 ± 694	-	0.87	N171W33
8	969.3	67.3	44.23	6.26	2.26	32.6	32.2	397913	24537	15229 ± 639	-	0.72	N151W37
9	966.8	64.8	44.23	6.26	2.25	17.5	38.2	451597	21698	15810 ± 760	-	0.76	N170W68
10	959.8	57.8	44.23	6.26	2.24	23.6	37.2	321967	15754	9877 ± 483	-	0.84	N145W72
11	950.7	48.7	44.23	6.26	2.22	23.5	38.6	310801	16034	9791 ± 505	-	0.80	N77W72
12	944.0	42.0	44.23	6.26	2.21	22.3	37.4	298013	15522	11668 ± 608	-	0.67	N14W72
13A	940.4	38.4	44.23	6.26	2.21	28.0	38.0	290021	15713	10276 ± 556	-	0.71	N106W87
13B	940.4	38.4	44.23	6.26	2.21	43.3	38.4	257546	22005	8397 ± 717	-	0.71	N106W87
14	930.9	28.9	44.23	6.26	2.19	29.8	37.3	467713	23683	19233 ± 974	-	0.65	N140E89
15	922.4	20.4	44.23	6.26	2.17	25.3	37.3	330443	16938	16245 ± 833	-	0.55	N4E84
16	915.4	13.4	44.23	6.26	2.16	27.3	31.8	341914	17288	22348 ± 1130	-	0.47	N162W26
17	911.6	9.6	44.23	6.26	2.16	22.9	37.7	229307	13073	13660 ± 779	-	0.45	N13W71
18	908.2	6.2	44.23	6.26	2.15	29.0	38.0	396966	22406	25803 ± 1456	-	0.43	N140W80
19	907.2	5.2	44.23	6.26	2.15	30.4	35.7	268197	14974	18429 ± 1029	-	0.40	N179W61
20	905.4	3.4	44.23	6.26	2.14	28.8	33.2	98729	8562	6581 ± 572	-	0.41	N0E84
21	904.5	2.5	44.23	6.26	1.49	21.2	37.5	26219	3368	1267 ± 163	-	0.52	N155E83
22	903.6	1.6	44.23	6.26	1.49	22.6	37.4	17964	3489	830 ± 161	-	0.53	N150E56

Tableau 3-1 : ^{36}Cl CRE sample characteristics and geochronological data. Sample field information, natural chlorine, calcium, and cosmogenic ^{36}Cl contents in the limestone samples and resulting ^{36}Cl CRE ages and denudation rates, TS factor and strike and dip of the sampled surfaces are indicated.

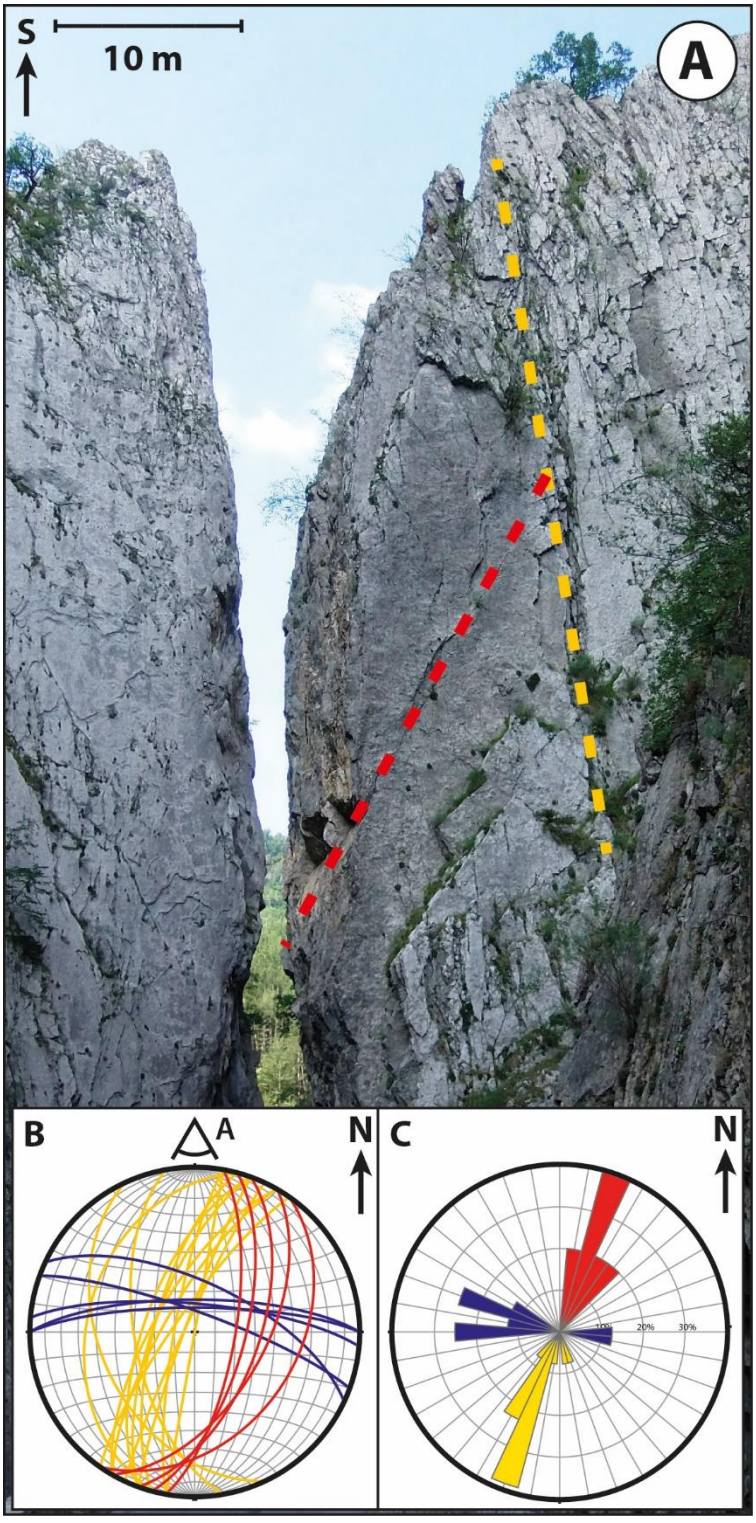

Figure 3-4 : A, West flank of CdB Gorge viewed towards the south with the two major representative fracture planes highlighted by red and yellow dashed lines. B, Projection of bedding plane (in blue), major fracture planes visible in A (red and yellow), Wulff projection, lower hemisphere. C, Rose diagram of bedding and fracture planes (same colors).

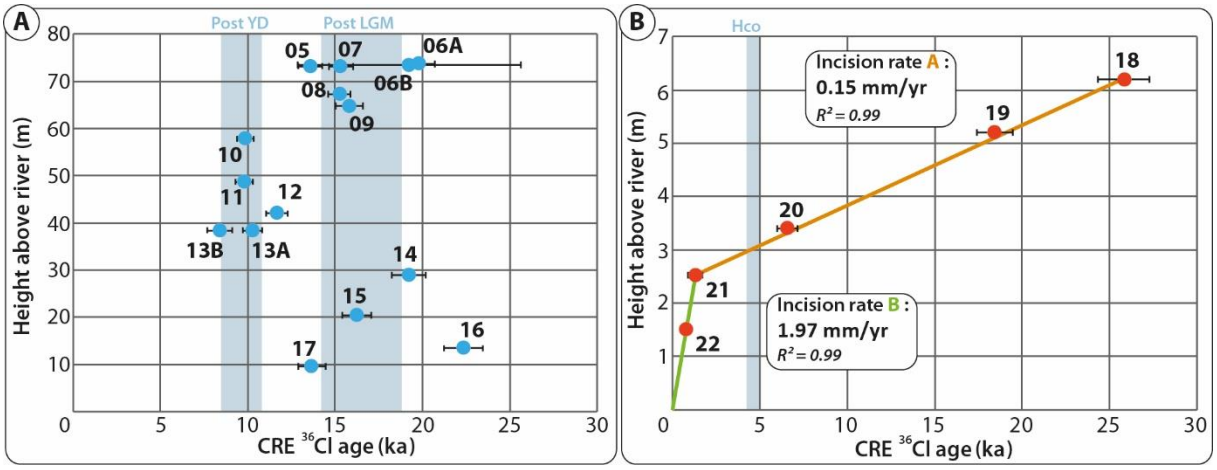

Figure 3-5 : Height above river bed versus exposure age, determined by ^{36}Cl concentration, for the 18 dated samples collected in the middle (A) and lower part (B) of the CdB Gorge. The dot colors are in reference to the Figure 3: the red dots refer to the river polished lower part, and the blue dots refer to the middle part of profile. With the five CRE ages ascribed to the fluvial incision process (B), we are able to compute incision rates ranging from 0.15 mm/yr to 1.97 mm/yr, which might suggest an acceleration of incision after 2 ka. Known deglaciation periods are chronologically represented by light blue columns: post LGM (Last Glacial Maximum): ≈ 19-14 ka; Post YD (Post Younger Dryas): ≈ 11-8 ka. Hco (Holocene climatic optimum): ≈ 5-4 ka.

5. Discussion

5.1. Geomorphological interpretation of the CRE ages

Field and DEM observations evidence that the CdB Gorge walls have been rejuvenated several times in the middle part of the sampling profile (samples 5 to 17).

Detailed field structural investigations of the gorge (Figure 4) and DEM-based morphological analysis of the sampled wall (Figure 6A, B, C) attest of such gravitational processes in the CdB Gorge. All the planes (fractures and bedding) described in previous section 4.2. (Figure 4) can play a role in the occurrence of rockfall events by isolating polygonal blocks susceptible to fall from the rock scarp. Furthermore, differential erosion between the various vertical limestone strata of different thickness, ranging from ≈ 20m to > 1m, destabilizes the vertical walls and thus leads more competent strata to be in an unstable overhanging position. These observations highlight the predisposing factors and vulnerability of the gorge to rockfall hazard. The combination of vertical incision and lateral gravitational processes can therefore explain the peculiar V-profile of the CdB Gorge.

The main fracture orientations (yellow; Figure 4 and 6A, B, C), are parallel to the surface

of the profile in its middle part (from samples 07 to 12; Figure 6C) suggesting that this surface may result from rockfall events. The fracture pattern and the morphology of the wall suggest the toppling of a large vertical column (≈ 20 m high; Figure 6D), prepared by joints opened within the vertical limestone beds. Following this observation and the CRE ages, it appears that the column was toppled by two distinct events, involving first the upper part of the column (samples 7 to 9) and then its lower part (samples 10 to 12) at ≈17 ka and ≈10 ka respectively (Figure 5). Other sampled surfaces, from samples 5 to 6B and 13A to 17, show an age distribution with three clusters ranging from 14.5 to 22 ka, from 10 to 30m above riverbed. The age versus height distribution does not show any clear trend, which suggests that these surfaces were later rejuvenated by gravitational processes.

Finally, in the lower part of the profile, the linear decrease of CRE ages towards the riverbed is suggestive of fluvial incision, which can be separated into two phases: i) from sample 18 to 21 (0.15 mm/yr), and ii) from sample 21 to riverbed (2.15 mm/yr). However, the latter incision rate only concerns the foot of the gorge wall (>2.5m high) which can be rejuvenated by punctual and recent flood events, and is constrained by only two points (three of we take into account the (0,0) point corresponding to the river bed). Hence, the estimated incision rate of 2.15 mm/yr is not representative of the long-term fluviatile incision process that is responsible for the formation of the CdB Gorge.

5.2. Climatic control on gravitational events

Major rockfall events can be interpreted as the result of changing climate conditions, as these processes are well known to be sensitive to permafrost degradation during warming phases (e.g. Ravanel et al., 2010; Hilger et al., 2021). Based on our case example, these gravitational processes appear to be an important factor of the gorge erosion process. We obtained two age clusters which we interpret as two instantaneous rockfall events having occurred at ≈17 and ≈10 ka respectively. These ages correspond to the two last major

deglaciation phases: post LGM (≈ 19-14 ka; Clark et al., 2009) and post Younger Dryas (≈ 11-8 ka; Darnault et al., 2012) (Figure 5). Although reconstructions of permafrost are still lacking for this period of time, we suggest that this relatively high-altitude area could have been under permafrost influence, due to its elevation above the equilibrium line altitude for glaciers during the LGM and Younger Dryas, and its proximity to the glacier front (Brisset et al., 2015 and references therein). Therefore, these gravitational events could have been caused by permafrost degradation, adding to a potential increased of freezing and thawing cycles during glacial phases (Sanchez et al., 2010; Lebrouc et al., 2013; Hilger et al., 2021). These observations therefore suggest that the CdB Gorge results from a vertical fluvial incision process, and is later widened by glacial and postglacial processes related to climate phases.

5.3. Regional comparison of river incision rates in SW Alps and possible controlling factors: climate, fluvial regime and surface uplift

Several studies based on CRE dating have been carried out on gorges and valleys of the SW Alps (Saillard et al., 2014; Rolland et al., 2017; Petit et al., 2019; Figure 7). The comparison of fluvial incision at the scale of SW Alps from gorges formed in valleys with or without glacial influence shows the dominance of high and variable incision rates in formerly glaciated catchments, while catchments devoid of glacial influence have lower incision rates since the LGM. Indeed, glaciated areas accumulate topographic disequilibrium during glaciation (Brocard and van der Beek, 2006). Readjustments after glacial perturbations imply enhanced erosion by fluvial and hillslopes processes, especially during deglaciation (Norton et al., 2010; Fox et al., 2015). In catchments dominated by glaciers during the LGM and Younger Dryas in their higher part, the above authors determined incision rates ranging from 1 mm/yr to ≈8 mm/yr (Figure 7B), which they attributed to efficient fluvial incision. The most extreme values are restricted to the catchments higher altitude (>900m) and can be attributed to transient incision of late glacial morphologies after the Younger Dryas (Rolland et al., 2017). In formerly

glaciated areas, the post-LGM incision might be controlled by climatic variations, through punctual post-glacial outbursts, and topographic readjustment through transient headward erosion. Therefore, these locally very high incision rates cannot be used to infer any long-term tendency.

Out of the influence of glaciers, the incision rates estimated for the Estéron River (Petit et al., 2019) and the Bès River (this study) are of ≈ 1.0 and 0.15 mm/yr respectively (Figure 7; Petit et al., 2019; this study). However, if we compare incision rates between the Vésubie, Estéron and Bès rivers after the last cold climatic event (i.e., the Younger Dryas), despite the fact that all three profiles are measured in a similar lithology and under comparable climatic settings, the mean incision rate of the Bès river (0.15 mm/yr) appears significantly lower than in the Vésubie (2.0 ± 0.1mm/yr), like for all catchments with glacial influence. In comparison to a catchment positioned in a similar glacier-free setting, the Esteron River (1.0 ± 0.1 mm/yr), the river incision rate value estimated for the Bès is still significantly lower.

Surface uplift, which is a combination of isostatic rebound, tectonic uplift and erosion, may also cause incision rate variability (e.g. Kirby and Whipple, 2012). Isostatic rebound, either induced by Quaternary erosion and LGM glacier retreat, has been shown to be insignificant in the SW Alps (Norton and Hampel, 2010; Champagnac et al., 2007; Sternai et al., 2019). Regarding the tectonic uplift component, cooling rates from Apatite Fission Track measurements in the external crystalline massif of the Argentera-Mercantour (Bogdanoff et al., 2000; Bigot-Cormier et al., 2006) lead to long-term exhumation rates of 1.1-1.4 mm/yr (rock uplift) over the last 10 Myr. Closer to our study area, Schwartz et al. (2017) demonstrated by low-temperature thermochronometry that the Barles erosional half-window area has been exhuming at a long-term rate of ≈ 0.7 mm/yr since 5 Ma. Recent studies using GPS monitoring in the Alps (Walpersdorf et al., 2018; Sternai et al., 2019) evidence a present-day surface uplift rate of 0.5 to 1 mm/yr in the highest parts of the Alpine massifs, while GPS stations closer to

our study area (La Javie and Moustiers-Sainte-Marie) have short-term uplift rates of 0.025+/-0.9 and -0.41+/-0.58 mm/yr, respectively (Sternai et al., 2019).

Hence, the relatively high incision rates recorded in the Var catchment and tributaries compared to the slow rates determined at the CdB gorge may reflect the east to west (i.e. massifs highest parts to Alpine foreland) regional variability of both long-term and short-term uplift rates. Nevertheless, in order to better discriminate the respective role of local catchment dynamics (glacial or not) and uplift rates variability on fluvial incision process, further constraints on incision rates are needed at the scale of SW Alps.

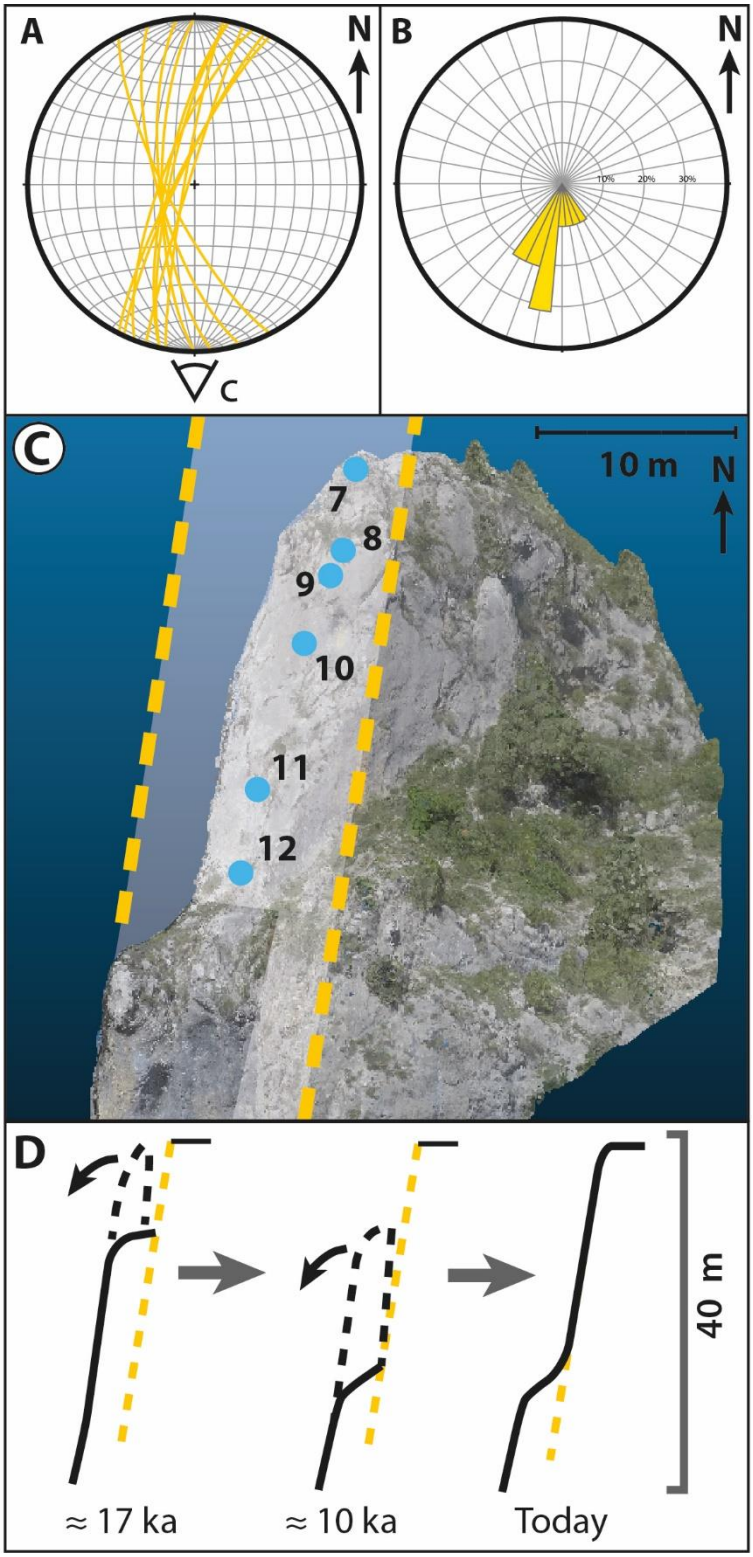

Figure 3-6 : Geometrical characteristics of the rockfall domain in the middle part of the CdB Gorge profile. A-B, Dip and strike measurements of the sample profile upper part (calculated from the DEM) in a Wulff stereographic projection, lower hemisphere (A) and in a Rose diagram (B). C, Mean plane deduced from the DEM calculated strike and dip of the upper sampled surface (yellow dashed framed rectangle) and location of the rejuvenated samples (samples 7 to 12; blue dots). D. Interpretation of the rockfall process by toppling that may have caused the rejuvenation of the sampled surface.

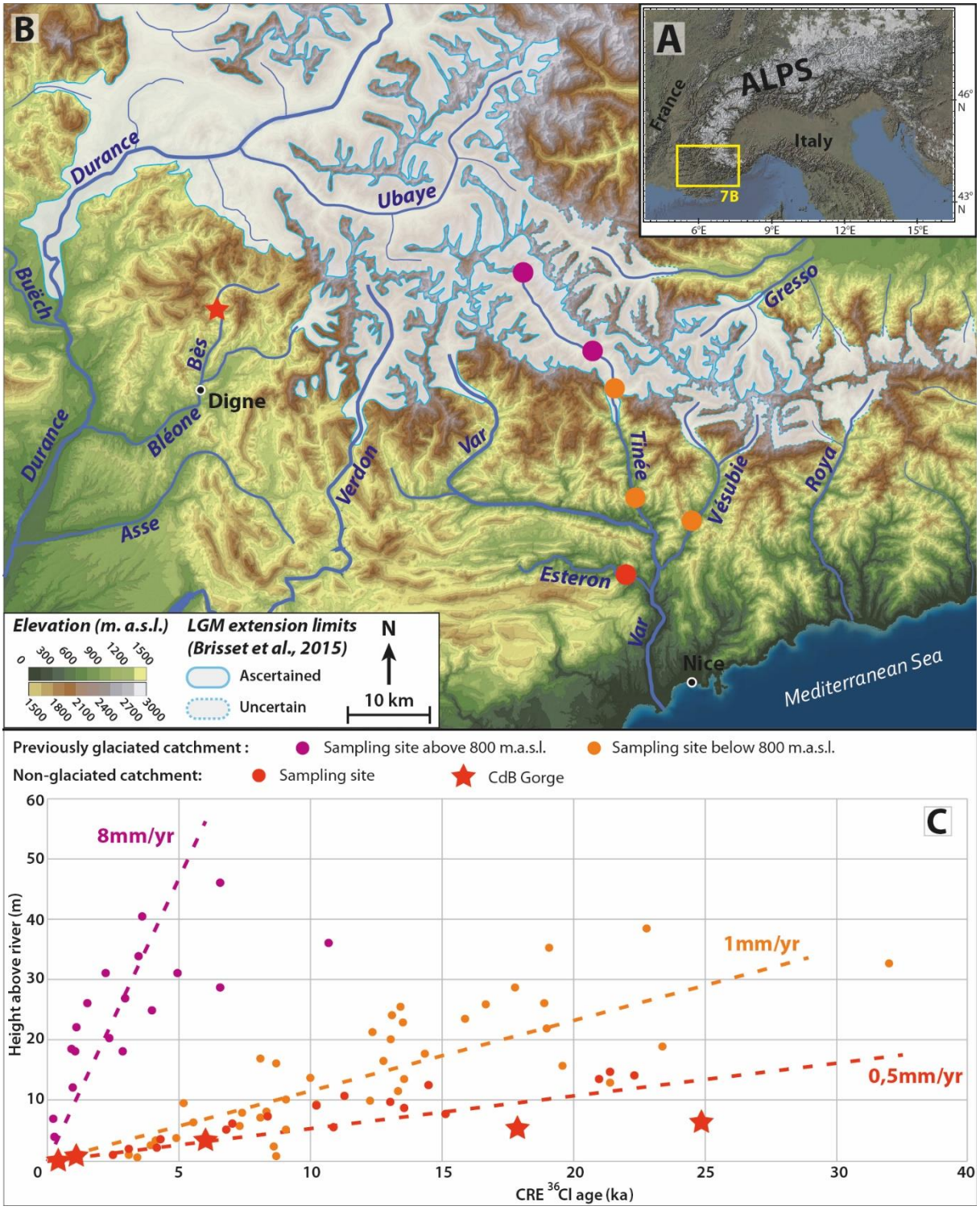

Figure 3-7 : A, Location of study area in the European Alps. B, Location of the CdB Gorge from this study and previous ones (Saillard et al., 2014; Rolland et al., 2017; Petit et al., 2019) in the SW Alps set against the Last Glacial Maximum (LGM) extension limits (modified from Brisset et al., 2015). Note that the glaciated/non-glaciated specification refers to the glaciation of the catchment during the LGM, and not the sampling site itself. C, Comparison of incision rate determined by CRE dating from this study (red stars) and previous ones (Saillard et al., 2014; Rolland et al., 2017; Petit et al., 2019). Note the increase of site specific incision rate according to their altitude and location in regard of the LGM extension limits.

6. Conclusion

We sampled and measured in situ-produced ^{36}Cl concentrations in twenty Jurassic limestone samples along an 80 m high sub-vertical and continuous profile of the V-shaped CdB Gorge (SW Alps) and in four samples collected at the top of the Jurassic limestone bar in which the CdB Gorge is incised. High-resolution DEM analysis and CRE ages show that the CdB Gorge was first dug by fluvial incision and subsequently widened by secondary gravitational processes. The top four samples are suggestive of a steady-state ^{36}Cl concentration that allows quantifying a denudation rate between 18 and 33 mm/kyr in the flatter upper, perfectly exposed surfaces on the shoulders of the gorge. CRE ages of the 10 m above riverbed profile allow quantifying a mean fluvial incision rate of 0.15 mm/yr over the last 25 ka, with an acceleration up to 2 mm/yr for the last 2 ka that can be linked to extreme flood events. The comparison of CRE dating results at the scale of SW Alps shows that the fluvial incision of Bès River is significantly lower than in other basins, which is ascribed to its frontal position in the Alps and glacier-free watershed during glacial phases. Moreover, CRE ages obtained in the middle part of the gorge are suggestive of two main rockfall events, which occurred ≈17 ka and ≈10 ka ago. These two events correspond to deglacial stages of the LGM and Younger Dryas, respectively, while their geometry suggests debuttressing along two recognized fracture families identified in the field. These data suggest the triggering of rockfalls in a warming climate during periglacial episodes. More sporadic rockfalls may explain age variability in the profile middle part. Based on this example, fluvial gorges in periglacial settings could be efficiently shaped by rockfalls during deglaciation periods, once fluvial incision has exposed the walls.

Acknowledgments

This study has been supported and funded by the French Geological Survey (Bureau de Recherches Géologiques et Minières; BRGM) through the national program “Référentiel Géologique de France” (RGF-Alpes), the AO7 OSUG@2020 (ANR10 LABX56) and by the

CNRS-INSU SYSTER Program. The ^{36}Cl measurements were performed at the ASTER AMS national facility (CEREGE, Aix en Provence) which is supported by the INSU/CNRS, the ANR through the "Projets thématiques d'excellence" program for the "Equipements d'excellence" ASTER-CEREGE action and IRD. Fruitful discussions with Ludovic Ravanel benefited the interpretation of the results. The authors are grateful to Myette Guiomar from the Réserve naturelle nationale Géologique de Haute-Provence. The authors warmly thank Francis Coeur (GeoThermoChronology Platform, ISTerre) for the technical support. Magali Bonnefoy is thanked for her help in the sample preparation. We are grateful to two anonymous reviewers and to Editor Markus Stoffel for their insightful comments.

References

Adams, J., 1985. Large-scale tectonic geomorphology of the Southern Alps, New Zealand. In: Morisawa M., Hack J.T., Eds., Tectonic Geomorphology. Allen and Unwin, Boston, 105-128.

Arnold, M., Merchel, S., Bourlès, D.L., Braucher, R., Benedetti, L., Finkel, R.C., Aumaître, G., Gottdang, A. and Klein, M., 2010. The French accelerator mass spectrometry facility ASTER: improved performance and developments. Nucl. Instrum. Methods Phys. Res., B 268, 1954–1959.

Bacon, S.N., McDonald, E.V., Caldwell, T.G. and Dalldorf, G.K., 2009. Timing and distribution of alluvial fan sedimentation in response to strengthening of late Holocene ENSO variability in the Sonoran Desert, southwestern Arizona, USA. Quaternary Res., 73, 425-438.

Balco, G., Stone, J.O., Lifton, N.A. and Dunai, T.J., 2008. A complete and easily accesible means of caltulating surfaces exposure ages or erosion rates from ^{10}Be and ^{26}Al measurements. Quat. Geochronol., 3, 174-195.

Bigot-Cormier, Sosson, M., Poupeau, G., Stéphan, J.-F. and Labrin, E., 2006. The denudation history of the Argentera Alpine External Crystalline Massif (Western Alps, France-Italy): an overview from the analysis of fision tracks in apatites and zircons. Geodinamica Acta, 19, 6, 455-473.

Bogdanoff, S., Michard, A., Mansour, M. and Poupeau, G., 2000. Apatite fission track analysis in the Argentera massif: evidence of contrasting denudation rates in the External Crystalline Massifs of the Western Alps. Terra Nova, 12, 117-125.

Braucher, R., Merchel, S., Borgomano, J. and Bourlès, D.L., 2011. Production of cosmogenic radionuclides at great depth : a multi element approach. Earth Planet. Sci. Lett., 309, 1-9.

Braucher, R., Keddadouche, K., Aumaître, G., Bourlès, D.L., Arnold, M., Pivot, S., Baroni, M., Scharf, A., Rugel, G. and Bard, E., 2018. Chlorine measurements at the 5 MV French AMS national facility ASTER: associated external uncertainties and comparability with the 6MV DREAMS facility. Nuclear Inst, and Methods in Physics Research, B 420, 40–45.

Brisset, E., Guiter, F., Miramont, C., Revel, M., Anthony, E.J. , Belhon, C., Arnaud, F., Malet, E. and de Beaulieu, J.-L., 2015. Lateglacial/Holocene environmental changes in the Mediterranean Alps inferred from lacustrine sediments. Quaternary Sci. Rev., 110, 49-71.

Brocard, G.Y., van der Beek, P., Bourlès, D., Siame, L. and Mugnier, J.-L., 2003. Long-term fluvial incision rate and postglacial river relaxation time in the French Western Alps from ^{10}Be dating of alluvial terraces with assessment of inheritance, soil developpement and wind ablations effects. Earth Planet. Sci. Lett., 209, 197-214

Brocard, G. and van der Beek, P., 2006. Influence of incision rate, rock strength, and bedload supply on bedrock river gradients and valley-flat widths: Field-based evidence and calibrations from western Alpine rivers (southeast France). Geol. Soc. Am. Bull., 398, 101-126.

Brocklehurst, S.H. and Whipple, K.X., 2002. Glacial erosion and relief production in the Eastern Sierra Nevada, California. Geomorphology, 42, 1-24.

Champagnac, J.D., Molnar, P., Andersion, R.S., Sue, C. and Delacou, B., 2007. Quaternary erosion-induced isostatic rebound in the western Alps. Geol. Soc. Am. Bull., 35, 3, 195-198.

Champagnac, J.D., van der Beek, P., Diraison, G. and Dauphin, S., 2008. Flexural isostatic response of the Alps to increased Quaternary erosion recorded by foreland basin remnants, SE France. Terra Nova, 20, 213-220.

Clark, P.U., Dyke, A.S., Shakum, J.D., Carlson, A.E., Clark, J., Wohlfarth, B., Mitrovica, J.X.,

Hostetler, S.W. and McCabe, A.M., 2009. The Last Glacial Maximum. Science, 325, 710-714.

Codilean, A.T., 2006. Calculation of the cosmogenic nuclide production topographic shielding sclaning factor for large areas using DEMs. Earth Surf. Proc. Land., 31, 6, 785-794.

Darnault, R., Rolland, R., Rolland, Y., Bourlès, D., Revel, M., Sanchez, G. and Bouissou, S., 2012. Timing of the last deglaciation revealed by receding glaciers at the Alpine-scale: impact on mountain geomorphology. Quaternary Sci. Rev., 3, 127-142.

Delacou, B., Sue, C., Champagnac, J.-D. and Burkhard, M., 2004. Present-say geodynamics in the bend of the western and central Alps as constrained by earthquake analysis. Geophys. J. Int., 158, 753-774.

Dumont, T., Schwartz, S., Guillot, S., Simon-Labric, T., Tricart, P. and Jourdan, S., 2012. Structural and sedimentary records of the Oligocene revolution in the Western Alpine arc. J. Geodyn., 56-57, 18-38.

Dunne, F., Elmore, D. and Muzikar, P., 1999. Scaling factors for the rates of production of cosmogenic nuclides for geometric shielding and attenuation at depth on sloped surfaces. Geomorphology, 27, 3-11.

England, P. and Molnar, P., 1990. Surface uplift, uplift of rocks, and exhumation of rocks. Geology, 18, 1173-1177.

Fox, M., Leith, K., Bodin, T., Balco, G. and Shuster, D.L., 2015. Rate of fluvial incision in the Central Alps constrained throught joint inversion of detrital ^{10}Be and thermochronometric data. Earth Planet. Sci. Lett., 411, 27-36.

Godard, V., Ollivier, V., Bellier, O., Miramont, C., Shabanian, E., Fleury, J., Benedetti, L., Guillou, V. and ASTER Team, 2016. Weathering-limited hillslope evolution in carbonate landscapes. Earth Planet. Sci. Lett., 446, 10-20.

Godard, V., Hippolyte, J.-C., Cushing, E., Espurt, N., Fleury, J., Bellier, O., Ollivier, V. and ASTER Team, 2020. Hillslope denudation and morphologic response across a rock uplift gradient. Earth Surf. Dynam., 8, 221–243.

Gosse, J. and Phillips, F., 2001. Terrestrial in situ cosmogenic nuclides: Theory and application. Quaternary Sci. Rev., 20, 1475-1560.

Hilger, P., Hermanns, R. L., Czekirda, J., Myhra, K. S., Gosse, J.C. and Etzelmüller, B., 2021. Permafrost as a first order control on long-term rock-slope deformation in (Sub-) Arctic Norway. Quaternary Science Reviews, 251, 106718.

Hippolyte, J.-C. and Dumont, T., 2000. Identification of Quaternary thrusts folds and faults in a low seismicity area: examples in the Southern Alps (France). Terra Nova, 12, 156-162.

Kirby, E. and Whipple, K.X., 2012. Expression of active tectonics in erosional landscapes. J. Struct. Geol., 44, 54-75.

Korup, O. and Schlunegger, F., 2007. Bedrock landsliding, river incision, and transience of geomorphic hillslope-channel coupling: Evidence from inner gorges in the Swiss Alps. J. Geophys. Res., 112, F03027.

Lal, D., 1991. Cosmic ray labeling of erosion surfaces: in situ nuclide production rates and erosion models. Earth Planet. Sci. Lett., 104, 424-439.

Lavé, J. and Avouac, J.P., 2001. Fluvial incision and tectonic uplift across the Himalayas of central Nepal. J. Geophys. Res., 106, B1, 25 561-25 593.

Lebrouc, V., Schwartz, S., Baillet, L., Jongmans, D. and Gamond, J.F., 2013. Permafrost extension modeling in a rock slope since the Last Glacial Maximum : application to the large Séchilienne landslide (French Alps). Geomorphology, 198, 189-200.

Li, Y.-K., 2013. Determining topographic shielding from digital elevation models for cosmogenic nuclide analysis : a GIS approach and field validation. J. Mt. Sci., 10, 3, 355-362.

Li, Y.-K., 2018. Determining topographic shielding from digital elevation models for cosmogenic nuclide analysis: a GIS model for discrete sample sites. J. Mt. Sci., 15, 5 939-947.

Merchel, S., Bremser, W., Alfimov, V., Arnold, M., Aumaître, G., Benedetti, L., Bourlès, D.L., Caffee, M., Fifield, L.K., Finkel, R.C., Freeman, S. P. H. T., Martschini, M., Matsushi, Y., Rood, D.H., Sasa, K., Steier, P.,Takahashi, T.,Tamari, M., Tims, S.G., Tosaki ,Y., Wilcken, K.M. and Xu, S., 2011. Ultra-trace analysis of ^{36}Cl by accelerator mass spectrometry: an interlaboratory study , Anal. Bioanal. Chem., 400, 3125-3132.

Montgomery, D.R., 2002. Valley formation by fluvial and glacial erosion. Geology, 30, 1047-1050.

Montgomery, D. R. and Korup, O., 2010. Preservation of inner gorges through repeated Alpine glaciations. Nat. Geosci., 4, 62-67.

Nocquet, J.-M., Sue, C., Walpersdorf, A., Tran, T., Lenôtre, N., Vernant, P., Cushing, M., Jouanne, F., Masson, F., Baize, S., Chéry, J. and van der Beek, P. A., 2016. Present-day uplift of the western Alps. Sci. Rep., 6, 28404.

Norton, K.P. and Vanacker, V., 2009. Effects of terrain smoothing on topographic shielding correction factors for cosmogenic nuclide-derived estimates of basin-averaged denudation rates. Earth Surf. Proc. Land., 34, 145-154.

Norton, K.P., Abbühl, L.M. and Schlunegger, F., 2010. Glacial conditioning as an erosional driving force in the Cenral Alps. Geology, 38, 7, 655-658.

Norton, K.P. and Hampel, A., 2010. Postglacial rebound promotes glacial re-advances – a case study from the European Alps. Terra Nova, 22, 297-302.

Ouimet, W.B., Whipple, K.X., Crosby, B.T., Johnson, J.P. and Schildgen, T.F., 2008. Epigenetic gorges in fluvial landscapes. Earth Surf. Proc. Land., 33, 13, 1993-2009.

Pan, B., Burbank, D.W., Wang, Y., Wu, G., Li, J. and Guan, Q., 2003. A 900 k.y. Record of strath terrace formation during glacial-interglacial transitions in northwest China. Geology, 31, 957-960.

Pazzaglia, F. J., Gardner, T. W. and Merritts, D. J., 1998. Bedrock fluvial incision and longitudinal profile development over geological time scales determined by fluvial terraces. In: Wohl, E., Tinkler, K. (Eds.), Bedrock Channels. American Geophysical Union. Geophysical Monograph Series 107, Washington, 207–235.

Petit, C., Rolland, Y., Braucher, R., Bourlès, D., Guillou, V. and Petitperrin, V., 2019. River incision and migration deduced from ^{36}Cl cosmic-ray exposure durations: The Clue de la Cerise gorge in southern French Alps. Geomorphology, 330, 81-88

Petit, C., Goren, L., Rolland, Y., Bourlès, D., Braucher, R., Saillard, M. and Cassol, D., 2017. Recent, climate-driven river incision rate fluctuations in the Mercantour crystalline massif, southern French Alps. Quaternary Sci. Rev., 165, 73-87.

Pratt, B., Burbank, D.W., Heimsath, A. and Ojha, T., 2002. Impulsive alluviation during early Holocene strengthened monsoons, central Nepal Himalaya. Geology, 30, 10, 911-914.

Ravanel, L., Allignol, F., Deline, P., Gruber, S. and Ravello, M., 2010. Rockfalls in the Mont Blanc Massif in 2007 and 2008. Landslides, 7, 4, 493-501.

Rolland, Y., Petit, C., Saillard, M., Braucher, R., Bourlès, D., Darnault, R., Cassol, D. and ASTER Team, 2017. Inner gorges incision history: A proxy for deglaciation ? Insights from Cosmic Ray Exposure dating (^{10}Be and ^{36}Cl) of river-polished surfaces (Tinée River, SW Alps, France). Earth Planet. Sci. Lett., 457, 271-281.

Ryb, U., Matmon, A., Erel, Y., Haviv, I., Katz, A., Starinsky, A., Angert, A. and ASTER Team, 2014a. Controls on denudation rates in tectonically stable Mediterranean carbonate terrain. The Geol. Soc. Am. Bull. Bulletin, 126, 553-568.

Ryb, U., Matmon, A., Erel, Y., Haviv, I., Benedetti, L. and Hidy, A.J., 2014b. Styles and rates of long-term denudation in carbonate terrains under a Mediterranean to hyper-arid climatic gradient. Earth Planet. Sci. Lett., 406, 142-152.

Sadier, B., Delannoy, J.-J., Benedetti, L., Bourlès, D.L., Jaillet, S., Geneste, J.-M., Lebatard, A.-E. and Arnold, M., 2012. Further constraints on the Chauvet cave artwork elaboration. PNAS, 109, 8002-8006.

Saillard, M., Petit, C., Rolland, Y., Braucher, R., Bourlès, D. L., Zerathe, S., Revel, M. and Jourdon, A., 2014. Late Quaternary incision rates in the Vésubie catchment area (Southern French Alps) from in situ-produced ^{36}CI cosmogenic nuclide dating: Tectonic and climatic implications. J. Geophys. Res. Earth Surface, 119, 1121-1135.

Sanchez, G., Rolland, Y., Corsini, M., Braucher, R., Bourlès, D., Arnold, M. and Aumaître, G., 2010. Relationships between tectonics, slope instability and climate change: Cosmic Ray exposure dating of active faults, landslides and glacial surfaces in the SW Alps. Geomorphology, 107, 1-2, 1-13.

Schaller, M., Hovius, N., Willett, S.D., Ivy-Ochs, S., Synal, H.-A. and Chen, M.-C., 2005. Fluvial bedrock incision in the active mountain belt of Taiwan from in situ-produced cosmogenic nuclides. Earth Surf. Proc. Land., 30, 955-971.

Schimmelpfennig, I., Benedetti, L., Finkel, R., Pik, R., Blard, P.-H., Bourlès, D.L., Burnard, P. and Williams, A., 2009. Source of in situ ^{36}Cl in basaltics rocks. Implication for calibration of production rates. Quat. Geochronol., 4, 441-461.

Schwartz, S., Gautheron, C., Audin, L., Dumont, T., Nomade, J., Barbarand, J., Pinna-Jamme,

R. and van der Beek, P., 2017. Foreland exhumation controlled by crustal thickening in the Western Alps. Geology, 45, 2, 139-142.

Serpelloni, E., Faccenna, C., Spada, G., Dong, D. and Williams, S. D. P., 2013. Vertical GPS ground motion rates in the Euro-Mediterranean region: New evidence of velocity gradients at different spatial scales along the Nubia-Eurasia plate boundary. J. Geophys. Res.: Solid Earth, 118, 6003-6024.

Sternai, P., Sue, C., Husson, L., Serpelloni, E., Becker, T.W., Willet, S.D., Faccenna, C., Giulio, A.D., Spada, G., Jolivet, L., Valla, P., Petit, C., Nocquet, J.-M., Walpersdorf, A. and Castelletort, S., 2019. Present-day uplift of the European Alps : Evaluating mechanisms and models of their relative contributions. Earth Science Reviews, 190, 589-604.

Stone, J.O., 2000. Air pressure and cosmogenic isotope production. J. Geophys. Res.: Solid Earth, 105, 23 753-23 759.

Sue, C., Delacou, B., Champagnac, J.-D., Allanic, C. and Burkhard, M., 2007. Aseismic deformation in the Alps: GPS vs. seismic strain quantification. Terra Nova, 1, 182-188.

Thomas, F., Godard, V., Bellier, O., Shabanian, E., Ollivier, V., Benedetti, L., Rizza, M., Espurt, N., Guillou, V., Hollender, F., Molliex, S. and ASTER Team, 2017. Morphological controls on the dynamics of carbonate landscapes under a mediterranean climate. Terra Nova, 29, 3, 173-182.

Valla, P.G., van der Beek, P.A. and Carcaillet, J., 2010. Dating bedrock gorge incision in the French Western Alps (Ecrin-Pelvoux massif) using cosmogenic ^{10}Be. Terra Nova, 22, 18-25.

Valla, P.G., Shuster, D.L. and van der Beek, P.A., 2011. Significant increase in relief of the European Alps during mid-Pleistocene glaciations. Nat. Geosci., 4, 688–692.

Van der Woerd, J., Tapponnier, P., Ryerson, F.J., Meriaux, A.-S., Meyer, B., Gaudemer, Y., Finkel, R.C., Caffee, M.W., Zhao, G. and Xu, Z., 2002. Uniform postglacial slip-rate along the central 600 km of the Kunlun Fault (Tibet), from ^{26}Al, ^{10}Be, and ^{14}C dating of riser offsets, and climatic origin of the regional morphology. Geophys. J. Int., 148, 356-388.

Vasquez-Tarrio, D., Borgniet, L., Liébault, F. and Recking, A., 2017. Using UAS optical imagery and SfM photogrammetry to characterize the surface grain size of gravel bars in a braided river (Vénéon River, French Alps). Geomorphology, 285, 94-105.

Walpersdorf, A., Pinget, L., Vernant, O., Sue, C., Deprez, A. and RENAG team, 2018. Does long-term GPS in the Western Alps finally confirm earthquake mechanisms? Tectonics, 37, 3721-3737.

Whipple, K.X., Kirby E. and Brocklehurst, S.H., 1999. Geomorphic limits to climate-induced increases in topographic relief. Nature, 401, 39-43.

Wobus, C., Whipple, K.X., Kirby, E., Snyder, N., Johnson, J., Spapolou, K., Crosby, B. and Sheehan, D., 2006. Tectonics from topography: procedures, promise, and pitfalls. In: Willett, S.D., Hovius, N., Brandon, M.T., Fisher, D.M., Eds., Tectonics, Climate, and Landscape Evolution. Geol. Soc. Am. Bull. Special Paper, 398, 55-74.

Zerathe, S., Lebourg, T., Braucher, R. and Bourlès, D., 2014. Mid-Holocene cluster of larger-scale landslides revealed in the Southwestern Alps by ^{36}Cl dating. Insight on an Alpine-Scale landslide activity. Quaternary Sci. Rev., 90, 106-127.

Chapitre 4 : Fluvial bedrock gorges as markers for Late-Quaternary tectonic and climatic forcing in the Southwestern Alps

Résumé

L'incision fluviale est l'un des principaux processus érosifs agissant à la surface de la Terre et est très sensible à la tectonique et aux variations isostatiques et climatiques. L'objectif de cette étude est de faire la distinction entre la contribution des fluctuations climatiques court terme et du forçage tectonique long terme à l'incision fluviale du Quaternaire récent, afin de mieux comprendre la chronologie et les mécanismes moteurs. Pour atteindre cet objectif, nous avons mesuré les concentrations de ^{36}Cl produits in situ le long de plusieurs parois de gorges formée dans des calcaires jurassiques des Alpes du Sud-Ouest. Nous avons ensuite comparé nos résultats avec ceux obtenues dans des gorges de bassins versants voisins précédemment datées. Ceci nous permet de mettre en évidence trois tendances de dynamiques d'incision distinctes, et de discuter de leurs relations avec le climat et la tectonique. La tendance 1 montre l'impact direct d'une crise paraglaciaire dans les rivières directement connectées aux glaciers. La tendance 2 suggère une vague d'incision se propageant le long des affluents non glaciaires en réponse à une incision accrue dans les cours d'eau principaux. La tendance 3 montre des taux d'incision constants et faibles dans les gorges déconnectées de toute réponse fluviale au retrait des glaciers. La tendance 3 semble également mettre en évidence le potentiel des lithologies résistantes à isoler des portions du réseau fluvial de la propagation de l'incision post-glaciaire. Notre analyse montre que les gorges connectées aux glaciers en amont présentent une réponse significative de l'incision fluviale aux fluctuations climatiques, mise en évidence par des

variations de taux d'incision de forte amplitude masquant le signal tectonique à long terme. En revanche, les taux d'incision déduits des gorges déconnectées sont en accord avec les taux de dénudation et de soulèvement rocheux long terme estimés précédemment dans la région. Sur la base de ces derniers, nous pouvons conclure que l'incision des rivières du Quaternaire supérieur dans les Alpes du Sud-Ouest se réajuste à la fois au forçage climatique court terme et au forçage tectonique long terme.

Fluvial bedrock gorges as markers for Late-Quaternary tectonic and climatic forcing in the Southwestern Alps

Thibaut Cardinal[1], Carole Petit[1], Yann Rolland[2-3], Laurence Audin[2], Stéphane Schwartz[2], Pierre G. Valla[2], Swann Zerathe[2], Régis Braucher[4], and ASTER team[4,*]

[1] Université Côte d'Azur, CNRS, Observatoire de la Côte d'Azur, IRD, Géoazur, 250 rue Albert Einstein, Sophia Antipolis 06560 Valbonne, France cardinal@geoazur-unice.fr

[2] Université Grenoble Alpes, Université Savoie Mont Blanc, CNRS, IRD, Université Gustave Eiffel, ISTerre, 38000 Grenoble, France

[3] Université Savoie Mont Blanc, CNRS, Pôle Montagne, Edytem, F-73370 Le Bourget-du-Lac, France

[4] Université Aix-Marseille, CNRS-IRD-Collège de France-INRAE, UM 34 CEREGE, Technopôle de l'Environnement Arbois-Méditerranée, BP80, 13545 Aix-en-Provence, France

**ASTER Team: Georges Aumaître, Didier L. Bourlès†, Karim Keddadouche*

Abstract

Fluvial incision is one of the major erosive processes acting at Earth's surface and is highly sensitive to tectonic, isostatic and climatic variations. The aim of this study is to distinguish between the short-term climatic fluctuations versus the long-term tectonic forcing contribution to Late-Quaternary fluvial incision, to better understand its timing and driving mechanism(s). To achieve this goal, we measured in situ-produced ^{36}Cl concentrations along several river-polished gorge walls in Jurassic limestones of the Southwestern Alps. We then compared our dating results to previously-dated river gorges from nearby catchments. This allows us to highlight three trends of distinct incision dynamics, and to discuss their relationships with climate and tectonics. Trend 1 shows the direct impact of a paraglacial crisis in the rivers directly connected to glaciated areas. Trend 2 suggests an incision wave

propagating along the non-glaciated tributaries following enhanced incision in the main streams. Trend 3 displays steady and low incision rates in gorges disconnected from any fluvial response to glacier retreat. Trend 3 also seems to highlight the potential of resistant lithologies to isolate portions of the river network from post-glacial incision propagation. Our analysis shows that gorges connected to upstream glaciers exhibit a significant response of fluvial incision to climatic fluctuations, evidenced by high-amplitudes incision rate variations hindering the long-term tectonic signal. In contrast, incision rates inferred from disconnected gorges are in agreement with previously-estimated long-term denudation and rock-uplift rates in the area. Based on the latter, we can conclude that Late-Quaternary river incision in the Southwestern Alps is readjusting to both short-term climatic forcing and long-term tectonic forcing.

Keywords: River gorges; Quaternary; Fluvial incision; ^{36}Cl dating; Southwestern Alps

1. Introduction

The morphology of mountainous landscapes is the result of a dynamic balance between erosion/sedimentation and uplift/subsidence (Penck, 1924; Hack, 1960; Willett, 1999; Whipple, 2001; Lavé and Avouac, 2001; Willett et al., 2002). As one of the major erosive processes acting at the Earth's surface, fluvial incision is highly sensitive to vertical motions linked to the isostatic response of the lithosphere or to tectonic forces (England and Molnar, 1990; Howard et al., 1994; Lavé and Avouac, 2001; Wobus et al., 2006), and to external forcing mainly represented by climatic fluctuations and associated base-level changes (Bacon et al., 2009; Pan et al., 2003; Van der Woerd et al., 2002; Ferrier et al., 2013).

Fluvial incision can be used as a first-order proxy for quantifying such dynamic processes over 10^4-10^5 yr timescales. Indeed, in a perfectly balanced system between uplift and erosion,

the quantification of fluvial incision allows direct estimate of the mean uplift (Royden and Perron, 2013). However, this can only be valid if rivers processes and longitudinal profiles have reached steady-state conditions (Molnar and England, 1990; Burbank et al., 1996; Whipple, 2001; Whipple and Tucker, 1999), which has only been demonstrated in few areas (e.g. Cyr and Granger, 2008; Lavé and Avouac, 2001).

Although this hypothesis may be valid over long time scales (10^5-10^6 yr), fluvial incision rates often fluctuate over shorter time scales (10^3-10^4 yr) as they respond to climatic fluctuations (Pratt et al., 2002; Saillard et al., 2014; Rolland et al., 2017). Indeed, the erosive potential of rivers is principally controlled by the amount of water runoff and transported sediments within the drainage network (Seild and Dietrich, 1992; Whipple et al., 2000; Lague et al., 2005; Stock et al., 2005; DiBiase and Whipple, 2011), which can be enhanced through extreme and punctuated events such as floods, landslides or glacial outbursts (Tucker and Whipple, 2002; Pratt et al., 2002; Holm et al., 2004; Korup and Schlunegger, 2007; Gran et al., 2013; Lebrouc et al., 2013). The occurrence of these events is directly linked to climatic variations, especially in mountainous areas like the European Alps, where the conditions had been wetter and warmer during interglacial periods (Brocard et al., 2003; Bigot-Cormier et al., 2005; Sanchez et al., 2010; Zerathe et al., 2014). In addition, and over longer time scales, Plio-Quaternary glaciations have shaped the Alpine valleys and topography through cyclic fluctuations between glacial and interglacial periods (van der Beek and Bourbon, 2008; Brocard et al., 2003; Norton et al., 2010; Valla et al., 2011; Fox et al., 2015) and have led to a drastic increase in erosion rates and sedimentation fluxes from the internal reliefs to the surrounding basins (Hinderer, 2001; Kuhlemann et al., 2002; Champagnac et al., 2007; Herman and Champagnac, 2016).

While catchment-scale approaches have commonly been used to estimate average erosion rates (e.g. Bierman and Steig, 1996), few studies have focused on more local features such as Alpine headwalls (Mair et al., 2019) or bedrock fluvial gorges (Schaller et al., 2005; Ouimet et

al., 2008). Some of these studies have been carried out to quantify local fluvial incision rates on different catchments from the Southwestern (SW) French Alps, where bedrock gorges walls have been dated by Cosmic Ray Exposure (CRE) dating methods (e.g. Saillard et al., 2014; Rolland et al., 2017; Petit et al., 2017; 2019). These studies demonstrated a strong relationship between the onset of fluvial incision and the post-LGM (Last Glacial Maximum, i.e. after ca. 20 ka) glacial retreat, pointing towards the climatic transition from glacial to interglacial conditions as the main factor for controlling the postglacial incision and evolution of these valleys. However, none of these studies was able to quantitatively disentangle the respective contribution of climatic forcing and long-term tectonic uplift in the fluvial incision signal.

Indeed, isolating the respective contributions from tectonics and climate to mountain erosion is challenging (Herman et al., 2013), especially in this context where studied rivers are still possibly in disequilibrium, triggered by the recent glacial imprint on the topography (Norton et al., 2010), thus obscuring any potential long-term tectonic signal.

Based on these observations and current knowledge gaps, the major questions addressed in this work are the following:

- What is the driving mechanism for bedrock gorge incision after the LGM in the SW Alps?
- What is the relative contribution of short-term climatic fluctuations vs. long-term tectonic forcing in the observed fluvial incision rates in the SW Alps?

In the following, we present new CRE dating from five bedrock gorges in the Bès, Verdon, Paillon and Roya rivers catchments, distributed from the western to the eastern sides of the SW Alpine foreland (Figure 1). These five sites where chosen to complement the previously-acquired CRE dating dataset in foreland catchments disconnected from LGM ice-extent (e.g. Petit et al., 2019; Cardinal et al., 2021), in order to document incision rates at the scale of the entire SW Alps. To quantify incision rates, we dated fluvially-polished limestone bedrock

gorges with in situ-produced ^{36}Cl. We then compared these new data with previously-published results with the aim to (1) discuss the timing and spatial variations in fluvial incision across the SW External Alps and (2) identify the major factors (climate vs. tectonics) that controlled fluvial incision dynamics over the last ca. 30 kyr.

2. Study area

2.1. Geological and tectonic settings

The studied area is located in the French Southwestern Alps (Figure 1A), where mountain building results from Cenozoic Alpine collision between European and African (Apulian) plates. The shortening of the European foreland has lead to the exhumation of the crystalline basement (External Crystalline Massif or ECM) by crustal-scale thrusting (Nouibat et al. 2022) and fold and thrust belt propagation in the sedimentary foreland (Jourdon et al., 2014). In the SW Alps, the sedimentary cover is decoupled from the basement and transported by the Digne thrust sheet prolonged in the SE by the Arc of Castellane (Figure 1B). This fold-and-thrust belt is undergoing uplift and erosion due to the late implication of basement in the shortening. In this context, the Argentera ECM has been uplifted since 20 Ma (Lickorish & Ford, 1998; Sanchez et al., 2011) (Figure 1B). At the front of the Digne thrust, the sedimentary cover has been carved by an erosional window since 5 Ma (Schwartz et al., 2017). The folding of the sedimentary cover produces at the surface alternation between resistant rock bars, corresponding to the Tithonian (Upper Jurassic) limestone, and low-resistance lithologies, corresponding to the middle-late Jurassic “Terres Noires” marls and Cretaceous limestone-marl alternations.

Regarding to the present-day tectonic setting of the Alps, studies have shown a slow and complex deformation pattern in a global strike-slip context related to the rotation of Apulian plate (Mathey et al., 2021; Piña-Valdés et al., 2022). In this context, the internal part of the Alps has been subjected to extensional deformation since 3 Ma, whereas its external part still

undergoes compression (Sue et al., 1999; Bilau et al., 2020), as shown by geodesy and seismicity (Walpersdorf et al., 2018; Mathey et al., 2021; Piña-Valdés et al., 2022). This deformation pattern is characterized by a shortening rate of ≤1 mm/yr (Nocquet et al., 2016) and vertical component culminating in the ECMs with rates > 1mm/yr (Serpelloni et al., 2013).

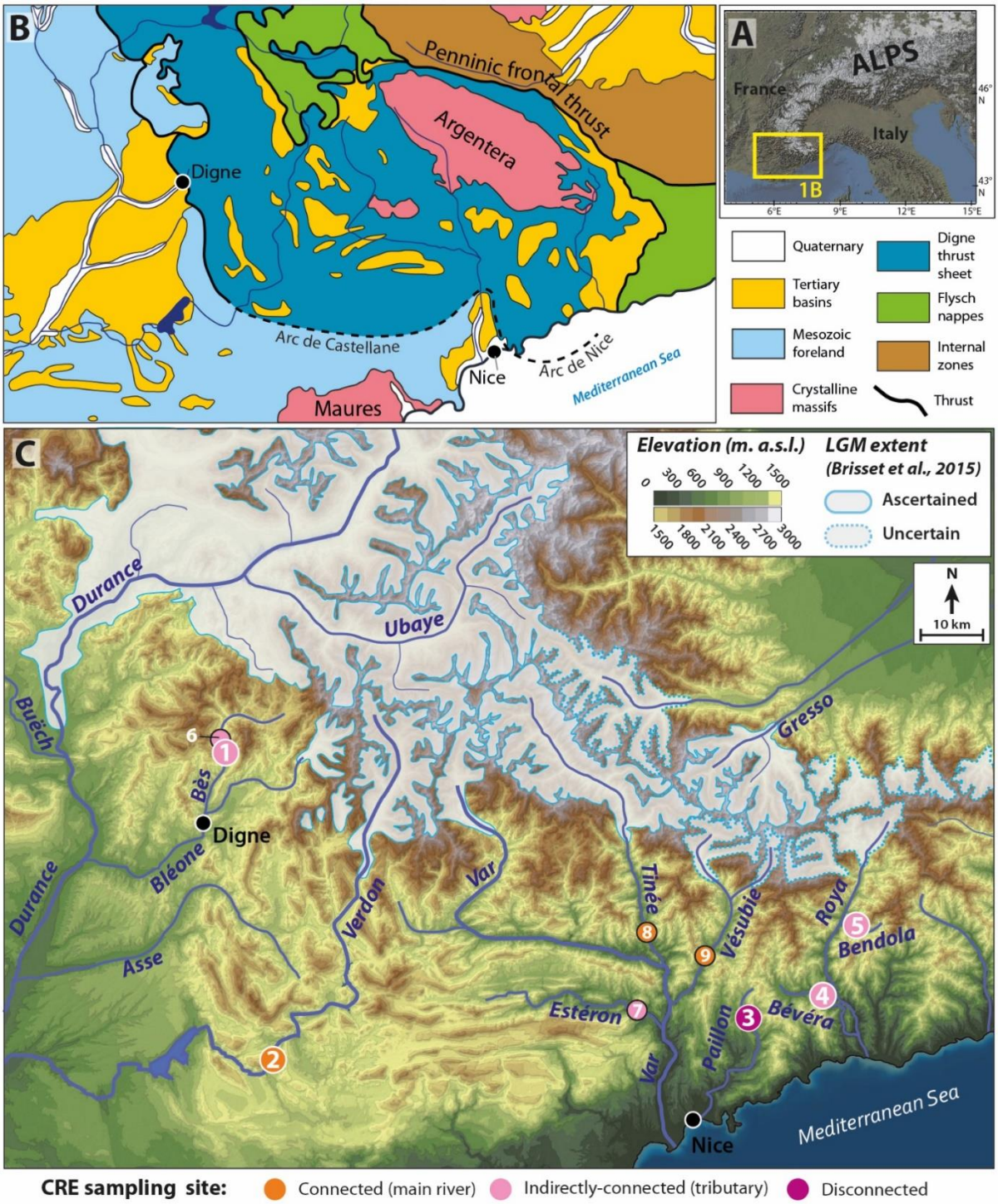

Figure 4-1 : A, Location of study area in the European Alps. B, Southwestern Alps general tectonic framework (modified after Schwartz et al., 2017). C, Location of the Pérouré (1), High Verdon (2), Redebraus (3), Bévéra (4) and the Bendola (5) gorges

from this study (white wider circles) and previously dated sites from literature (black circles): (6) Clue de Barles (Cardinal et al., 2021); (7) Estéron (Petit et al., 2019); (8) Courbaisse (Rolland et al., 2017); (9) Vésubie (Saillard et al., 2014). The grey area shows the Last Glacial Maximum (LGM) glacier extent (modified from Brisset et al., 2015).

2.2. Late-Quaternary Alpine climatic variations

The last major glaciation in the European Alps culminated during the Last Glacial Maximum (LGM; 26.5-19 ka; Clark et al., 2009). The LGM had a huge impact on the SW Alpine relief by enhancing and focusing erosion (Darnault et al., 2012). It was followed by a period of rapid glacial retreat (Clark et al., 2009), which is evidenced in the high-elevation areas of the Argentera massif by glacier thinning at 19-18 ka, followed by a major retreat of glaciers at elevations > 2500 m by ca. 14.5 ka (Darnault et al., 2012; Brisset et al., 2015; Rolland et al., 2019), similar to other observations at the scale of the European Alps (Ivy Ochs et al., 2008; Rea et al., 2020). Although Federici et al. (2012) dated moraines at 20 ka on the Italian side of the Southwestern Alps, the maximal glacial extent during the LGM is still not well constrained on the French side due to the lack of preservation of frontal moraines in the low-elevation valley floors (Figure 1C; Julian, 1980; Brisset et al. 2015). A later and spatially limited glacial re-advance occurred at ca. 12 ka during the Younger Dryas (Hinderer, 2001; Heiri et al., 2014), which rapidly receded at 11-10 ka (Federici et al., 2008; Darnault et al., 2012; Wanner et al., 2015).

The Holocene started at about 11.7 ka with a transition to warmer climatic conditions (Wanner et al., 2011, 2015). Climatic reconstructions during the Holocene can be problematic because both the timing and magnitude of the warming vary substantially between different regions (Renssen et al., 2009). However, Wanner et al. (2011) proposed a division of the present interglacial into three climatic periods: (1) a deglaciation phase immediately following the end of the Younger Dryas cold phase and characterized by important ice melting; (2) the ‘Holocene Thermal Optimum’ between 11 and 5 ka (Wanner at al., 2008, Renssen et al., 2009, 2012), characterized by a warmer and more stable climate, and (3) a ‘Neoglacial’ period, with colder

conditions and higher precipitations during the late-Holocene (Davis et al., 2003). These climatic variations can play a major role for the erosion processes including river incision in zones of high lithological contrasts (Petit et al., 2019).

2.3. Study sites

In this study, we present new data acquired from five gorges located in the French Southwestern Alps (Figure 1C). The Pérouré Gorge is located in the Bès catchment, a tributary of the Durance River. The High Verdon Gorge is formed by the Verdon River, which is also a tributary to the Durance River. The Redebraus Gorge is located in the Paillon catchment, which reaches the Mediterranean Sea in the city of Nice. The Bévéra and Bendola gorges are located along the eponym rivers, which are tributaries to the Roya River catchment located along the southern France-Italy border. All the studied catchments feature strong lithological contrasts which, combined with the widespread folding of the region, create significant convexities and slope breaks in the longitudinal river profiles. Indeed, all the above-mentioned gorges are incised in Tithonian limestones, which occur repeatedly in the Alpine Foreland and is surrounded by less resistant marls, and form strong lithological knickpoints along longitudinal river profiles (Figure 2).

Together with published data, this new dataset allows us to distinguish three gorge dynamics according to their geographical location and regarding the ice-covered domains during the LGM (Figure 1C):

- Connected: the gorge site is located on a main stream that takes its source in the previously LGM ice-covered part of the catchment;
- Indirectly-connected: the gorge is located along a tributary of a connected main stream;
- Disconnected: the gorge is located along a catchment that was devoid of any glacier and along a stream with no, direct nor indirect, connection to ice-covered areas.

The Verdon River is considered as ‘connected’, as its upper catchment belongs to the LGM

glaciated areas. The Bendola, Bévéra and the Bès Rivers are 'indirectly-connected' to glaciations, because they are tributaries of main rivers that have their sources in previously glaciated areas. The Paillon River on the other hand had no glaciers in its catchment, and can therefore be considered as totally "disconnected" from any significant glacial extension during the LGM (Figure 1C). In order to compare our data with previous results, we also selected previously-sampled limestone bedrock gorges "indirectly-connected" (Esteron Gorge, Petit et al., 2019; and Barles Gorge, Cardinal et al., 2021) and connected (Courbaisse Gorge, Rolland et al., 2017; Vésubie Gorge, Saillard et al., 2014) from the literature (Figure 1C).

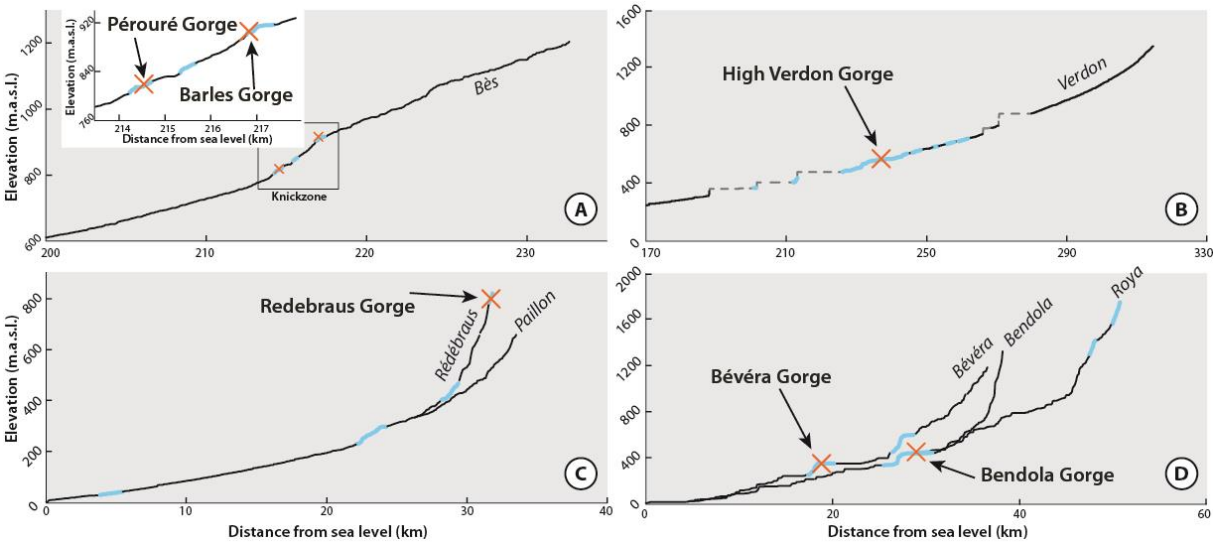

Figure 4-2 : Longitudinal profiles of the sampled rivers and their main stream. A: Bès River, with a blow-up on a knickzone and the location of two sampled gorges (Pérouré, this study, and Barles, Cardinal et al., 2021); B: Verdon River; C: Paillon Rive and the tributary Redebraus; D: Roya River and the tributaries Bévéra and Bendola. Sampling sites are indicated with a red cross; location of outcropping massive Tithonian limestones along the channels are indicated by a thick blue line. Dashed grey lines correspond to artificial lakes (dams) along the Verdon River. The distance from sea level correspond to the distance from the river mouth to the Mediterranean Sea.

3. Methods

3.1. ^{36}Cl CRE dating method

In this study, we used in situ-produced cosmogenic ^{36}Cl measurements to constrain exposure ages along the flanks of the five studied bedrock gorges incised into resistant limestone lithologies.

3.1.1. Sampling strategy and field work

We aim at quantifying gorge incision rates along steep (almost vertical) bedrock walls that were theoretically gradually exposed as the river incised (Schaller et al., 2005; Ouimet et al., 2008). We can therefore expect a distribution of younger to older CRE ages from the current riverbed level to the top of the bedrock gorge walls. Sampled surfaces were chosen based on the following morphological indices: i) evidence of preservation of an induration varnish or with low apparent superficial dissolution, indicating little weathering since exposure or ii) presence of smooth river-polished surfaces and "pot holes", representing polished and concave fluvial erosional surfaces preserved in the gorge walls (Figure 3 and 4) and iii) with no overhanging relief and located in the most opened part of their respective gorges, in order to maximize exposure to cosmic rays.

Our main goal was to find and sample a continuous wall of polished limestone bedrock. In addition, we sampled, when possible, two facing walls along the same gorge (Figure 3C, E and 4B) as well as abandoned flat erosional surfaces above to the sampled walls (Figure 3D). Although we strived to collect sample as close to the river bed as possible, as it has been done in the Redebraus and Bendola Gorges (Figure 3D, E and 4B), stream depth and strong currents have sometimes prevented us from reaching the lower part of the gorge. The selected profiles are also shorter than 15 m to avoid any influence of potential rock-falls, which may cause the rejuvenation of the gorge wall surface, as demonstrated by Cardinal et al. (2021). Samples were gathered using a drill, hammer and chisel. In total, a number of 61 limestone samples have been collected (Table 1).

3.1.2. Analytical protocol

We prepared the bulk limestone samples at the 'Laboratoire National des Nucléides Cosmogéniques' (LN2C; CEREGE, Aix-en-Provence) following the procedure presented in Schimmelpfennig et al. (2009). ^{36}Cl concentrations were determined by accelerator mass

spectrometry (AMS) performed on ASTER, the French national AMS facility (CEREGE, Aix-en-Provence) (Arnold et al., 2010). All measurements were calibrated against in-house CEREGE SM-CL-12 standard (Merchel et al., 2011). Total uncertainties account for counting statistics, standard evolution during measurements, standard uncertainty and external uncertainties of 2.74%, 2.13% and 1.62 % for $^{36}Cl/^{35}Cl$, $^{36}Cl/37Cl$ and $^{35}Cl/^{37}Cl$ ratios, respectively (Braucher et al., 2018). A sea-level and high-latitude ^{36}Cl production rate for calcium spallation of 42.2±3.4 atoms $^{36}Cl\ g^{-1}\ a^{-1}$ (Schimmelpfennig et al., 2009, Braucher et al., 2011) has been used and scaled following Stone (2000) and corrected for topographic shielding (TS), constrained from field measurement data. ^{36}Cl ages have been determined using the approach of Schimmelpfennig et al. (2009) using a limestone density of 2.6 g cm^{-3}.

3.2. Incision rate quantification

We used the code developed by Glotzbach et al. (2011) originally designed for thermochronology data, to define best-fitting line segments passing through the CRE data points, in order to determine incision rate variations with time from our data and literature data. We made some modifications to the code in order to make it more suitable for CRE age data. As in Glotzbach et al. (2011) we used a Monte-Carlo approach to randomly split the data into 1, 2 or 3 successive time intervals in order to define line segments by weighted linear regression, and select the best-fitting ones according to their R^2 value. We have implemented the following criteria: no negative incision rate is allowed, thus solutions containing segments with negative incision rates are discarded; line segments constrained by less than 3 data points are discarded; the intersection between two line segments must correspond to the intersection between the two groups of data that were used to compute them (so that there is no data point that is used to compute a line segment, but lies outside of its boundaries).

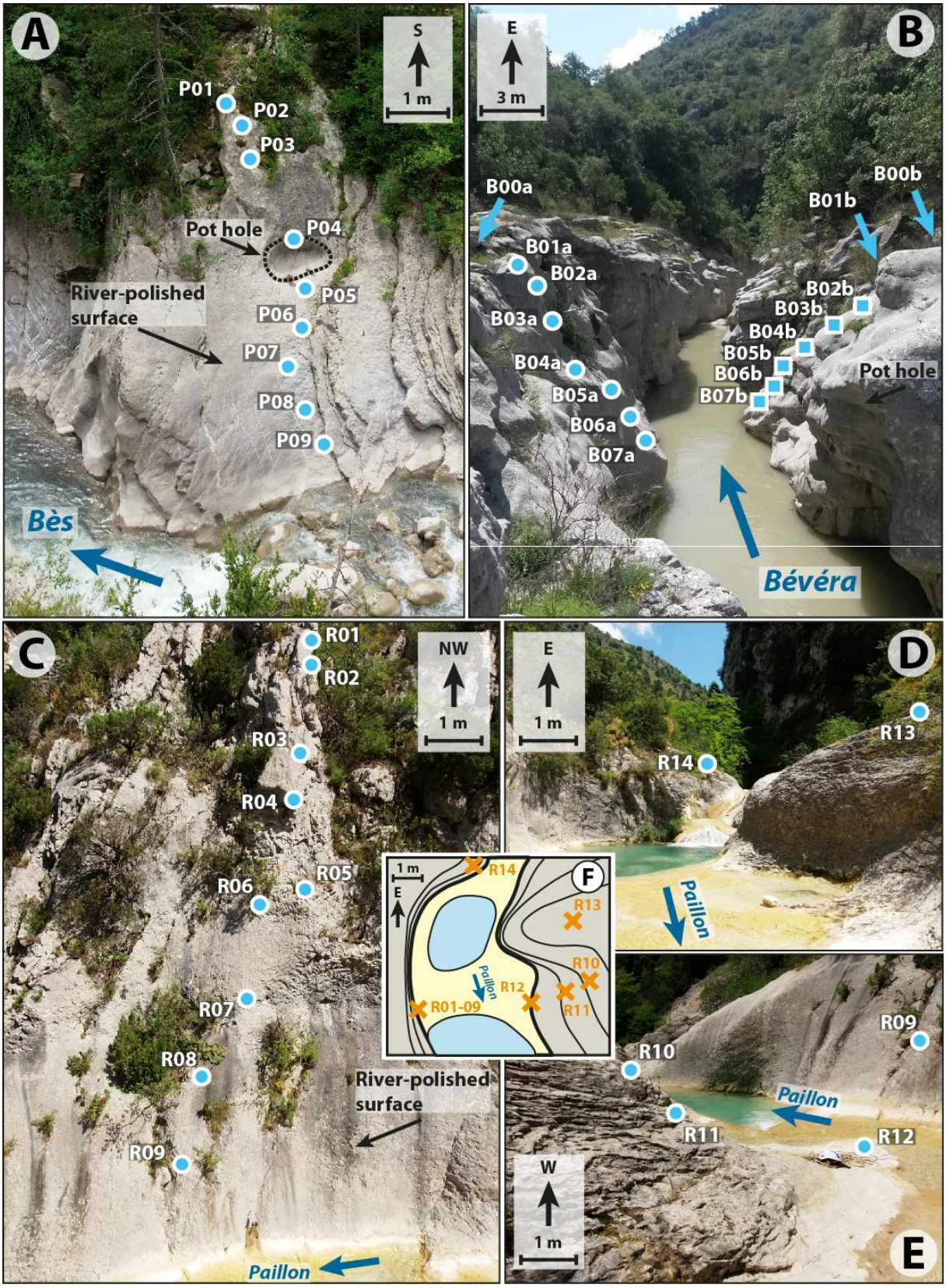

Figure 4-3 : Sampling sites in the (A) Pérouré Gorge, (B) northern (circles) and southern (squares) flanks of the Bévéra Gorge and (C, D and E) Redebraus Gorge. The inset (F) locates the different sampled surfaces in the Redebraus Gorge.

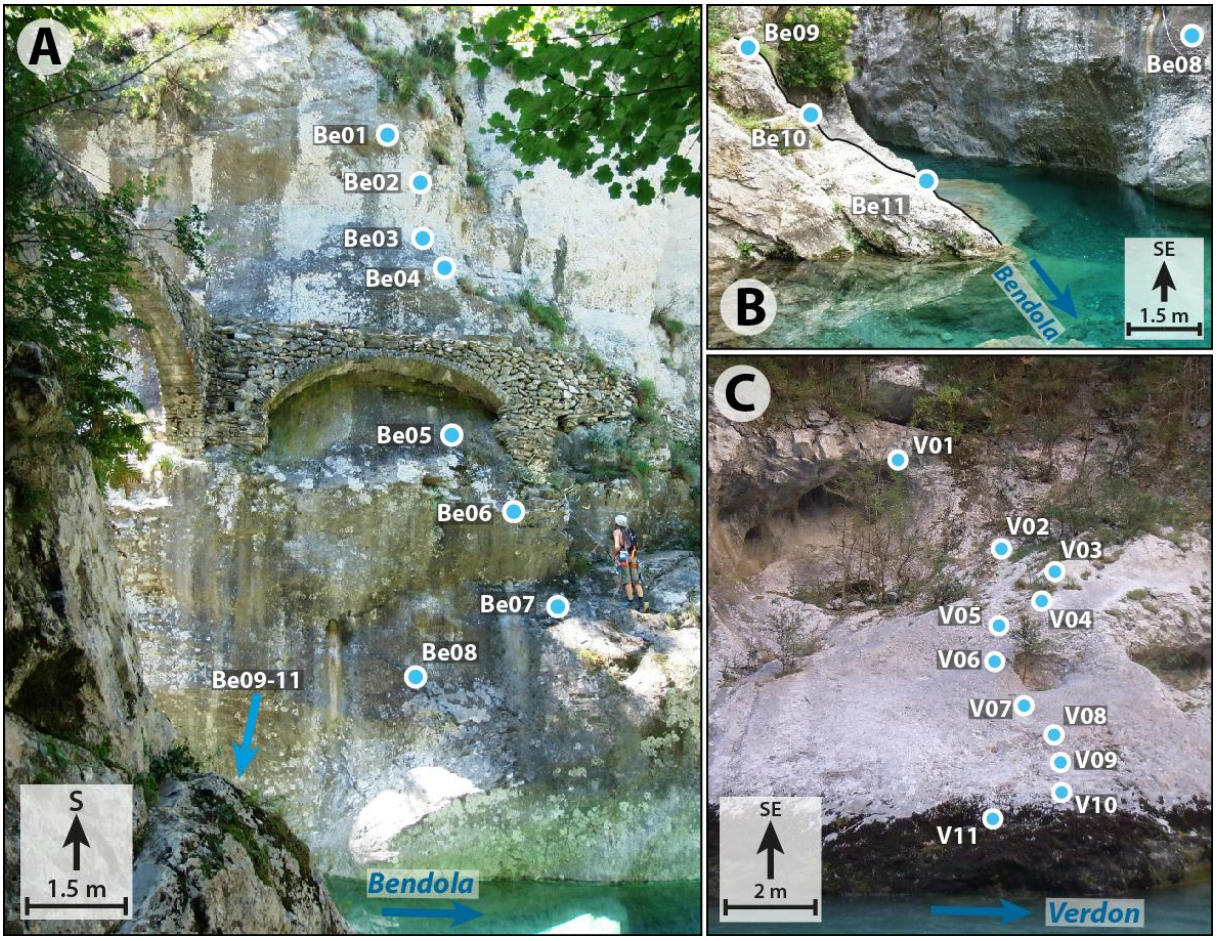

Figure 4-0-4 : Sampling sites and samples location in the Bendola Gorge (A, B) and the High Verdon Gorge (C).

4. ^{36}Cl CRE dating results

4.1. New ^{36}Cl CRE dating results in the SW French Alps

For the five studied gorges, CRE ages determined from ^{36}Cl concentrations are reported in the age-elevation plots (green circles; Figure 5), with the corresponding regression lines (black lines). From these data, we estimated the mean incision rate (blue lines), with the corresponding uncertainty envelope (grey envelopes), which are shown in the same plot for each site.

The nine limestone samples gathered from the Pérouré Gorge (Figure 3A) display ages ranging between ca. 1 and 9 ka (Table 1). From these ages, we can compute two mean incision rates: a first, poorly-constrained (regarding the R^2) incision rate of 0.76±0.11 mm/yr from 3 ka to 9 ka (from 11 to 6 meters above riverbed level), with a R^2 of 0.47, and a second, better constrained value of 3.34±0.88 mm/yr from 1 ka to 3 ka (from 1 to 6 meters above riverbed

level), with a R^2 of 0.73.

The eleven ^{36}Cl CRE ages obtained along a polished surface of the High Verdon Gorge range from 15 ka to 40 ka. From these ages, we can estimate a steady incision rate of 0.21±0.01 mm/yr, from 15 to 45 ka, with a R^2 of 0.97. Two samples (V01 and V02; Table 1) are discarded as it seems that their exposure ages are related to post-incision rejuvenation of the bedrock wall, which is most likely representative of rock-fall occurrences (Figure 4C).

Fourteen limestone samples were collected along a 15 m high vertical wall in the Redebraus Gorge. From the sample ^{36}Cl concentrations, we obtained CRE ages ranging between 6 and 84 ka, giving a steady mean incision rate of 0.21±0.03 mm/yr with a R^2 of 0.85. In this data set, two samples (R03 and R05; Table 1) are not taken into account for the incision-rate computation, as their exposure ages are probably related to a rock-fall event that occurred at ca. 20 ka (Figure 3C, D, E, F).

The sixteen samples gathered in the Bévéra Gorge display CRE ages between 19 and 5 ka (Table 1). From these ages, we can compute a mean incision rate increasing from 0.52±0.15 mm/yr, between 20 and 10 ka (with a R^2 of 0.68), to 0.84±0.51 mm/yr, from 10 to 5 ka , (with a R^2 of 0.73, Figure 3B).

In the Bendola Gorge, the CRE ages of eleven carbonate samples ranges between 5 and 44 ka. The mean incision rate is estimated at 0.28±0.04 mm/yr during this period, with a R^2 of 0.88. On this profile, two samples (Be01 et Be02; Table 1) are considered as outliers and therefore not taken into account for the incision rate computation. Indeed, their young exposure ages, compared to the ages of the surrounding samples, and their location, seems to indicate a post-incision rejuvenation of the bedrock walls (Figure 4A, B).

4.2. ^{36}Cl CRE dating results from literature

In order to interpret our data in a more regional framework, we propose here a compilation of CRE dating studies that have been previously carried out on bedrock gorges and valleys at

the scale of the SW Alps (Saillard et al., 2014; Rolland et al., 2017; Petit et al., 2019; Cardinal et al., 2021; Figure 1). In order to compare the results with our data, we re-computed the previously estimated incision rates with the same method as in this study (Figure 6). We chose to use only the CRE data considered by the authors as suitable for deriving fluvial incision rates. The data considered as outliers, for reasons such as rock-falls, are not presented in this study.

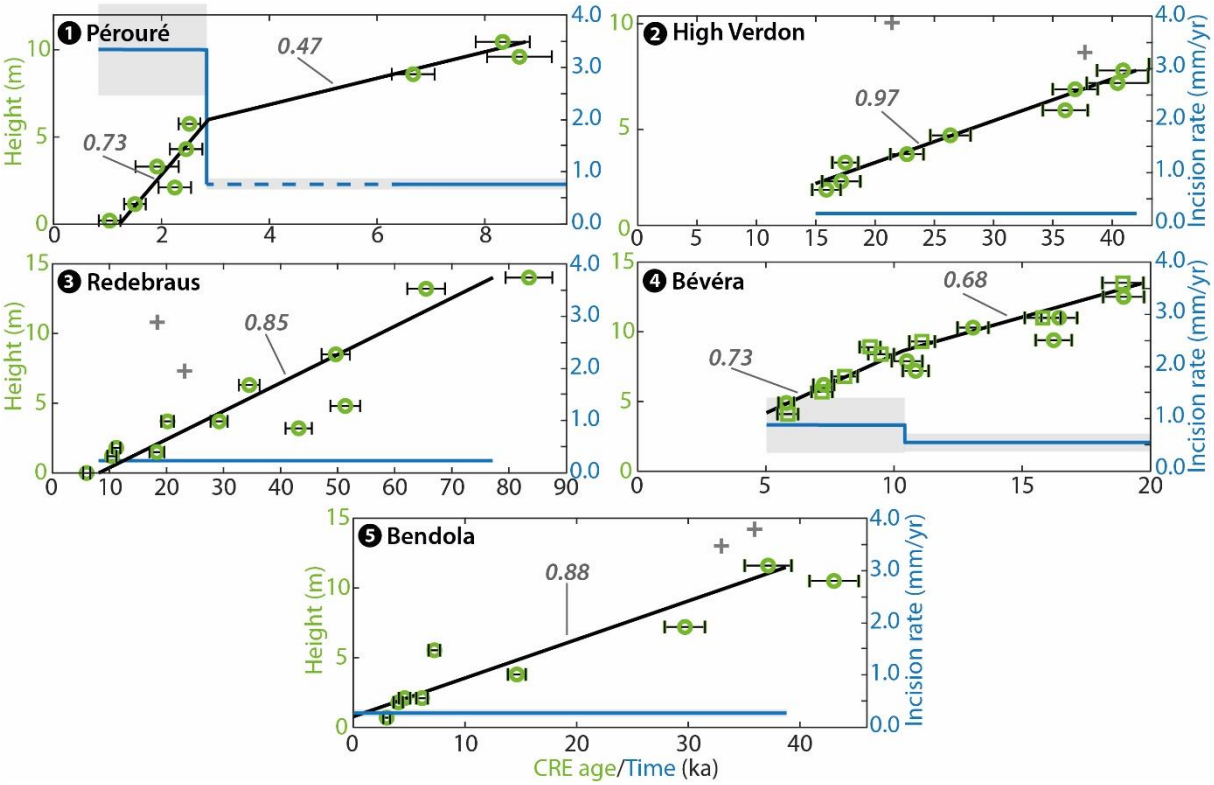

Figure 4-5 : CRE age vs height (green circles) and corresponding regression (black line, with R^2 value); mean incision rate (blue line) throughout time, with uncertainty (grey envelope), plot of the gorges (1) Pérouré; (2) High Verdon; (3) Redebraus; (4) Bévéra, and (5) Bendola, from this study. The blue dashed line for Pérouré (plot 1) corresponds to the temporal range where the estimate of incision rate is poorly constrained, due to a lack of data and low R^2. The number of each plot refers to the location of sites displayed in Figure 1C. The grey crosses are outliers considered as representing rejuvenation of the gorge walls following a rock-fall event and are therefore not representative of fluvial incision.

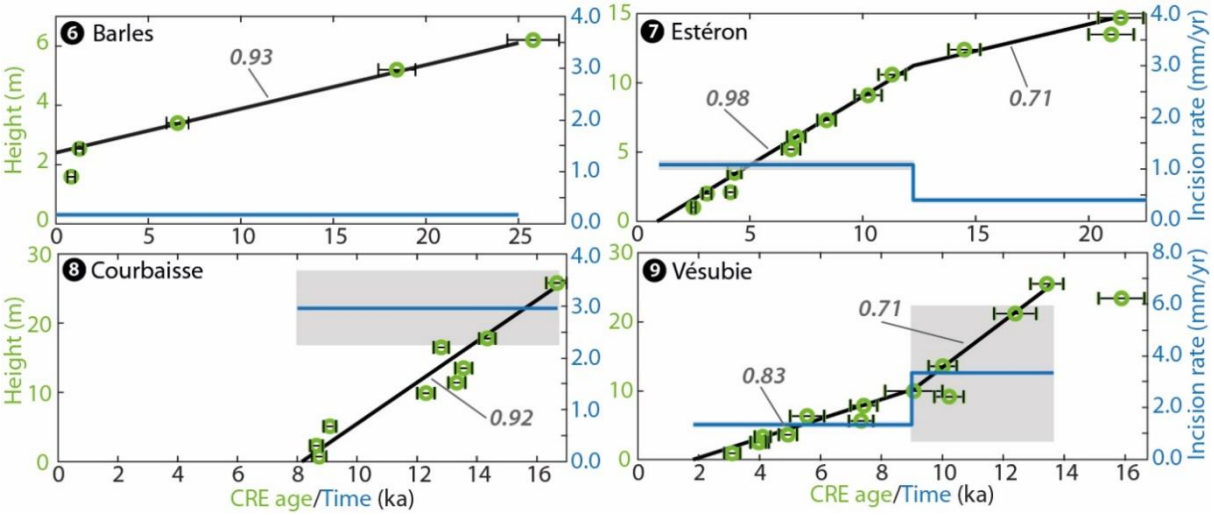

Figure 4-6 : CRE age vs height (green circles) and corresponding regression (black line, with R^2 value); mean incision rate (blue line) throughout time, with uncertainty (grey envelope), of the gorges from literature: (6) Clue de Barles (Cardinal et al., 2021); (7) Estéron (Petit et al., 2019); (8) Courbaisse (Rolland et al., 2017); (9) Vésubie (Saillard et al., 2014). Data have been selected based on the authors interpretation of the sampled surfaces as representative of exposure related to fluvial incision.

Sample	Height above river (m)	TS factor	Spall. scaling	^{35}Cl (ppm)	Ca (%)	Atoms ^{36}Cl (at/g)	Atoms ^{36}Cl ± (at/g)	CRE age (ka)
Pérouré Gorge (lat: 44.2°; long: 6.3°; elevation: 814 m.a.s.l.)								
P01	11.2	0.71	1.44	34.8	37.4	225855	14252	8.3±0.5
P02	10.3	0.71	1.44	48.4	38.0	244501	18207	8.6±0.6
P03	9.3	0.71	1.44	48.0	39.2	192883	13705	6.7±0.4
P04	6.5	0.71	1.44	36.3	37.8	70483	5823	2.5±0.2
P05	5.0	0.71	1.44	36.0	38.2	68158	7821	2.5±0.3
P06	4.0	0.71	1.44	40.0	36.9	51295	11467	1.9±0.4
P07	2.8	0.71	1.44	37.9	38.0	60377	8918	2.2±0.3
P08	1.9	0.71	1.44	38.3	37.6	40900	6808	1.5±0.2
P09	0.9	0.71	1.44	30.8	32.1	25038	3868	1.0±0.2
High Verdon Gorge (lat: 43.8°; long: 6.4°; elevation: 606 m.a.s.l.)								
V01	*11*	*0.16*	*1.67*	*24.5*	*40.4*	*110890*	*8575*	*21.6±1.7*
V02	*8*	*0.16*	*1.67*	*33.1*	*40.6*	*190457*	*16417*	*37.3±3.2*
V03	7.7	0.16	1.67	23.4	40.7	205909	11192	40.9±2.2
V04	7.1	0.16	1.67	28.6	40.8	205363	13024	40.4±2.6
V05	6.8	0.16	1.67	28.1	40.8	187869	9775	36.9±1.9
V06	5.8	0.16	1.67	32.0	41.7	188287	9862	36.0±1.9
V07	4.6	0.16	1.67	31.5	40.6	136006	8988	26.4±1.7
V08	3.7	0.16	1.67	35.0	40.7	118596	7068	22.7±1.4
V09	3.3	0.16	1.67	32.5	40.8	91776	5730	17.5±1.1
V10	2.4	0.16	1.67	29.9	40.7	89670	8452	17.2±1.6
V11	2	0.16	1.67	37.3	40.7	83944	6349	15.9±1.2

Redebraus Gorge (lat: 43.8°; long: 7.4°; elevation: 527 m.a.s.l.)								
R01	14.0	0.42	1.58	18.86	40.1	946227	46163	83.5±4.1
R02	13.2	0.42	1.58	19.22	41.3	778602	39778	65.5±3.3
R03	*10.5*	*0.42*	*1.58*	*14.97*	*39.1*	*559664*	*29727*	*18.9±1.0*
R04	8.5	0.42	1.58	15.10	39.0	568296	28656	49.7±2.5
R05	*7.1*	*0.42*	*1.58*	*19.14*	*40.1*	*280560*	*14695*	*23.1±1.2*
R06	6.3	0.42	1.58	20.16	40.3	416307	21504	34.5±1.8
R07	4.8	0.30	1.58	19.78	41.5	444910	22703	51.3±2.6
R08	3.2	0.30	1.58	18.82	41.	374066	19766	43.2±2.3
R09	1.5	0.30	1.58	18.96	41.8	165956	11664	18.3±1.3
R10	1.83	0.64	1.58	20.91	41.0	214946	14291	11.2±0.7
R11	1.2	0.64	1.58	21.78	41.2	201575	15016	10.4±0.8
R12	0.0	0.64	1.58	22.74	41.3	117198	12115	6.0±0.6
R13	3.7	0.64	1.58	23.23	41.1	551920	28682	29.2±1.5
R14	3.7	0.64	1.58	21.35	40.8	381736	20217	20.2±1.1
Bévéra Gorge (lat: 43.9°; long: 7.5°; elevation: 281 m.a.s.l.)								
B00a	12.5	0.89	1.27	11.3	37.8	380994	16676	19.0±0.8
B01a	11.0	0.89	1.27	11.4	37.9	331854	15069	16.4±0.7
B02a	10.3	0.80	1.27	18.9	37.9	243162	10644	13.1±0.6
B03a	9.4	0.63	1.27	12.4	38.0	231557	10194	16.2±0.7
B04a	7.9	0.56	1.27	12.4	37.9	134514	8034	10.5±0.6
B05a	7.2	0.56	1.27	21.1	37.8	143352	7200	10.9±0.5
B06a	6.2	0.66	1.27	17.1	37.8	111662	5721	7.3±0.4
B07a	4.9	0.64	1.27	16.1	37.8	85610	4754	5.8±0.3
B00b	13.5	0.81	1.27	15.4	38.0	351203	14916	18.9±0.8
B01b	11.0	0.81	1.27	33.4	37.7	310241	13924	15.8±0.7
B02b	9.3	0.75	1.27	12.9	37.9	190555	8637	11.1±0.5
B03b	8.9	0.69	1.27	15.9	38.0	144324	7151	9.1±0.4
B04b	8.4	0.62	1.27	16.0	37,9	136508	6619	9.5±0.5
B05b	6.8	0.54	1.27	12.9	38.0	100400	5648	8.1±0.5
B06b	5.7	0.48	1.27	17.2	38.0	78976	4716	7.0±0.4
B07b	4.1	0.48	1.27	19.1	37.9	66429	4192	5.9±0.4
Bendola Gorge (lat: 44.0°; long: 7.5°; elevation: 357 m.a.s.l.)								
Be01	*14.2*	*0.32*	*1.35*	*40.9*	*40.3*	*284628*	*15689*	*35.1±1.9*
Be02	*13.0*	*0.32*	*1.35*	*42.8*	*40.3*	*262445*	*14997*	*32.2±1.8*
Be03	11.6	0.32	1.35	34.1	41.0	303029	16727	37.2±2.1
Be04	10.5	0.32	1.35	29.3	40.9	346005	18060	43.1±2.2
Be05	7.2	0.32	1.35	62.4	41.4	254491	15799	29.8±1.8
Be06	5.6	0.62	1.35	17.4	40.9	117113	7733	7.3±0.5
Be07	3.8	0.62	1.35	51.4	41.1	243041	14049	14.7±0.8
Be08	2.1	0.62	1.35	39.0	41.0	101697	7463	6.2±0.5
Be09	2.1	0.62	1.35	41.5	40.5	75596	8545	4.6±0.5

Be10	1.8	0.62	1.35	45.9	40.5	66751	6722	4.0±0.4
Be11	0.7	0.62	1.35	67.8	41.0	51873	5002	3.0±0.3

Tableau 4-1 : ^{36}Cl CRE sample characteristics and geochronological results. Sample field information, natural chlorine, calcium, cosmogenic ^{36}Cl contents in the limestone samples, resulting ^{36}Cl CRE ages, and topographic shielding (TS) factor of the sampled surfaces, are indicated. Samples written in italics correspond to the CRE ages identified as outliers and discarded for incision rate computation.

5. Discussion

5.1. Synthesis of ^{36}Cl CRE dating results for bedrock gorges in the SW Alps

From the synthesis of CRE datings of gorges in the SW Alps, we are able to highlight different spatial and temporal patterns of bedrock gorge incision rates at a regional scale. Two orders of information emerged from the plot of incision rate variations through time (Figure 7A): (i) the differences in incision rate magnitude from one site to another, and (ii) the temporal variations of incision rates for each individual site. From these observations, we can distinguish three distinct trends (Figure 7A):

- The first trend (Trend 1, green lines) shows a high incision rate (~3 mm/yr) between 17 and 8 ka. The concerned gorges (Courbaisse #10 and Vésubie #12) are located along "Connected" rivers.
- The second trend (Trend 2, orange lines) shows initially lower (~0.5 mm/yr) incision rates that increase up to 1 mm/yr after 10 ka. The concerned gorges (Bévéra, Estéron and Pérouré) are located along "Indirectly-connected" tributaries.
- The third trend (Trend 3, blue lines) shows steady and lower incision rates at around 0.25 mm/yr, from 80 ka to the present day. The concerned gorges (Barles, High Verdon, Redebraus and Bendola) have mixed locations regarding the LGM extent.

Most of the studied gorges show significant change in incision rates around 10 ka, while four sites do not undergo any changes in their incision rate since up to 80 ka. Incision rate increase occurs before 10 ka for Trend 1 and later for Trend 2. These variations will be discussed in the following section.

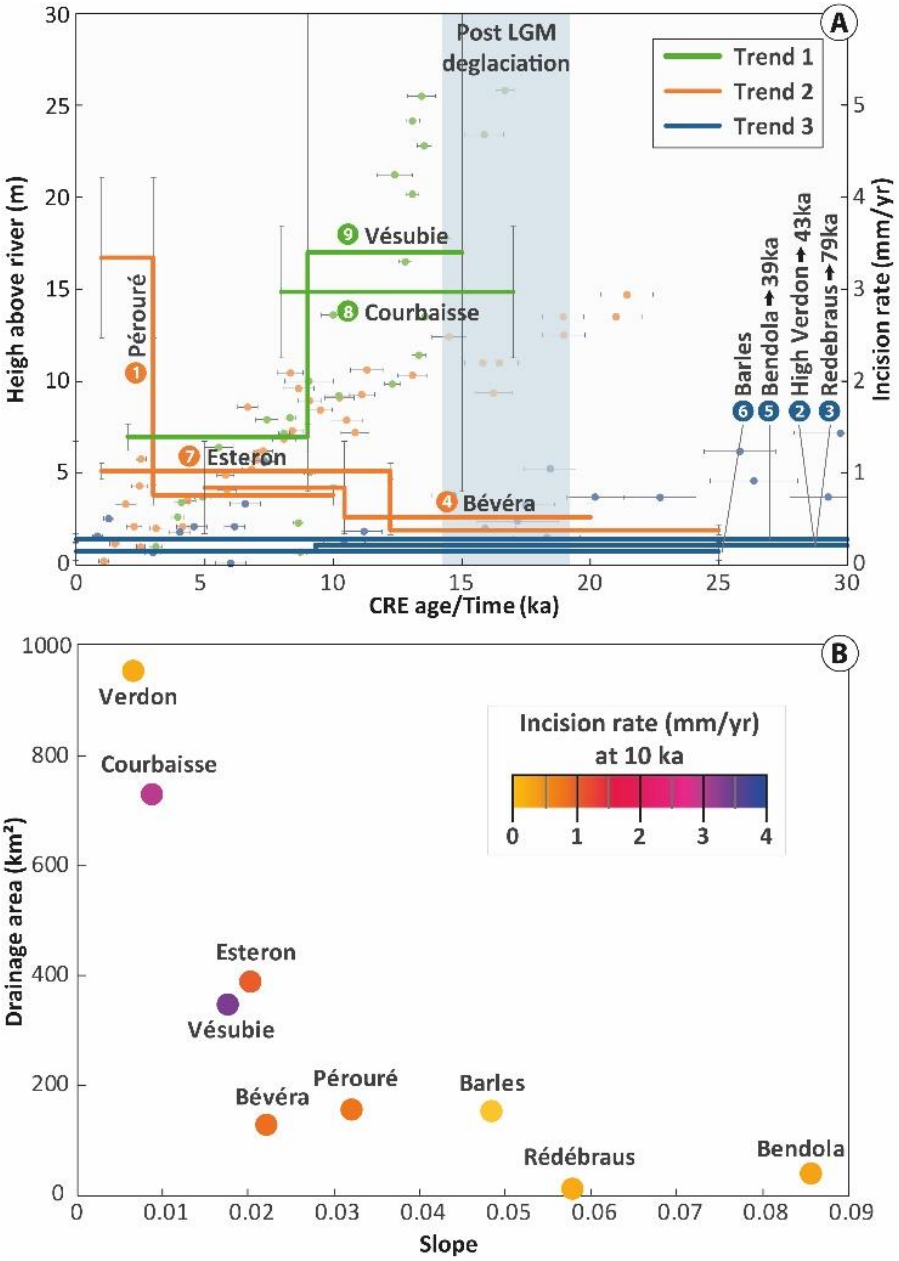

Figure 4-7 : A, Incision rate trends (Trend 1 to 3) in SW Alps gorges, constrained by ^{36}Cl exposure ages; individual dots correspond to dated samples (left vertical axis) and lines to the corresponding incision rate (right vertical axis). Note that the plot only displays data since 30 ka. Bendola, High Verdon and Redebraus gorges ages show a similar incision rate extending up to 39, 43 and 79 ka respectively, as indicated. B, Upstream drainage area versus local slope plot of sampled SW Alps bedrock gorges, with corresponding mean incision rates (color scale) estimated at 10 ka.

5.2. Regional pattern of river incision rates in SW Alps and their relationship to lithology, climate and uplift

Comparison of incision rates obtained from several catchments at the scale of the SW Alps is not straightforward, as fluvial incision is influenced by local factors like stream and catchment morphologies. Before addressing any regional interpretation of the obtained incision

patterns, it is crucial to take into account some local features, such as upstream drainage area, local slope and rock erodibility, which control the incision efficiency (e.g., Kirby and Whipple, 2012). We tested the hypothesis that variations in drainage area, which is considered as a proxy of river discharge and sediment flux (Bishop et al., 2005), and in local slope could explain the measured differences in incision rates from one gorge to another. Both variables are co-dependent to the position of a considered point along the river profile: the more upstream this point is, the higher the slope and the smaller the drainage area (e.g., Wobus et al., 2006). We choose incision rates at 10 ka in order to compare our incision data with present-day catchments metrics. Our analysis (Figure 7B) shows this expected decreasing exponential relationship between upstream drainage area and channel slope. As these two parameters control the incision, we would expect, when comparing incision rates from gorges with their respective catchment metrics, to find higher incision rates for both high slope and drainage area sector. However, although there is a group of high incision rates (Bévéra, Vésubie, Pérouré, Estéron) for intermediate slopes and drainage areas, no clear tendency emerges from this plot: both high and low incision rates are recorded either for large and small drainage areas and similarly for high and low local slopes. This analysis suggests that other factors could explain the different trends of incision rates highlighted in Figure 7A, which are discussed below.

5.2.1. Trend 1: direct deglaciation impact

Trend 1 (green lines, Figure 7A), which includes data from Courbaisse (Rolland et al., 2017) and Vésubie (Saillard et al., 2014) gorges, shows a mean incision rate of ~3 mm/yr between 17 and 8 ka, which decreases to 1.4 mm/yr for the Vésubie Gorge and appears to become null in Courbaisse Gorge after ca. 10 ka (Figure 7A). During this period, the SW Alps were under the influence of climatic fluctuations, with a transition period from full glacial (LGM) to interglacial (after 10 ka) conditions (e.g. Ivy Ochs et al., 2008). Direct erosion by glaciers is known to be very efficient in the shaping of the Alps (Champagnac et al., 2007; Valla et al.,

2011; Sternai et al., 2013). Indeed, during the LGM, the erosion rate in the Argentera ECM has been estimated at 1.8 mm/yr by Darnault et al. (2012). The sampled gorges of Vésubie and Courbaisse are located in formerly-glaciated catchments, downstream and outside of the LGM glacial extent. Furthermore, fluvial incision occurred in these gorges since at least the end of the LGM, when main glaciers were retreating. This time marks the beginning of the paraglacial period (Church and Ryder, 1972), which is characterized by enhanced fluvial processes, such as increased stream flow (Seidl and Dietrich, 1992; Tucker and Whipple, 2002) and increased sediment yield (Ballantyne, 2002; Meigs et al., 2006; Savi et al., 2014). Church and Ryder (1972) proposed a theoretical paraglacial model, in which the sediment yield peaks shortly after the onset of deglaciation and decreases until reaching a steady state, after paraglacial sediment supply exhaustion. Although additional processes (discussed below) may control the apparent stop of incision in the Courbaisse Gorge, the CRE dating data displayed by Trend 1 could fit with the theoretical paraglacial model (Church and Ryder, 1972; Ballantyne, 2002), which seems to illustrate the consequence of increased sediment yield from upstream Tinée and Vésubie catchments between the end of the LGM (ca. 19 ka) and the Younger Dryas/Holocene transition (ca. 10 ka).

While it is commonly assumed that sediment yield/discharge plays an important role in bedrock incision process (Seild and Dietrich, 1992; Whipple et al., 2000; Stock et al., 2005; DiBiase and Whipple, 2011), the direct relationship between incision and sediment supply is more complex (Sklar and Dietrich, 2001; Whipple and Tucker, 2002). Indeed, sediment transported by rivers can both provide the tools for bedrock incision, through abrasion or plucking process, and, if excessively profuse, can insulate and protect the underlying riverbed from erosion (Sklar et Dietrich, 2001). The apparent ceasing of incision in the Courbaisse Gorge, observed in the CRE data (Figure 6A) may be controlled by the cover effect. Indeed, the gorge is located in a much more opened part of the Tinée valley, where hillslope-derived

sediment seems to have filled the bottom of the valley, impeding the bedrock incision.

Our results suggest continuous incision during the Late glacial period (19-11ka), that we associated with increased sediment yield. Similarly, Van den Berg et al. (2012) quantified present-day incision rate of 1.3 mm/yr and proposed post-LGM incision rates of 2.1-2.8 mm/yr to explain the formation of inner-gorges in the Entlen Catchment (Switzerland), which suggests a similar pattern at the scale of the Alpine belt. It is worth noting that sediment yield in the Var basin (Bonneau et al., 2017) and denudation rates in the Argentera ECM (Mariotti et al., 2021) estimated from marine sediment records show two peaks since 30 ka: a major one at the end of the LGM and a secondary one at ca. 10 ka. Between these two periods, both studies of Bonneau et al. (2017) and Mariotti et al. (2021) reported a decrease in sediment yield and apparent denudation rates respectively. The discrepancy between these studies and ours might be the result of transient sediment storage, either on land, at the mouth of the Var River, or on the submarine slope (Petit et al., preprint).

5.2.2. Trend 2: indirect deglaciation impact

Trend 2 (orange lines, Figure 7A), which includes data from Esteron (Petit et al., 2019), Bévéra and Pérouré (this study) gorges, shows incision rates of ~ 0.5 mm/yr that increase up to ~ 1 mm/yr after 10 ka. While we see the influence of deglaciation in rivers that are directly connected to formely-glaciated areas, we can observe an acceleration of incision after 10 ka in rivers that are tributaries of these "Connected" rivers, and thus indirectly connected to glaciations (Figure 1C). This acceleration could be related to the propagation of an incision wave in tributaries, whose local base level at the outlet dropped, as the main river underwent a paraglacial crisis and associated profile re-equilibration (Figure 8, top). The possible control of a regional base level is not considered here because no significant drop of the Mediterranean Sea level has been observed since the end of LGM (Vacchi et al., 2016; Benjamin et al., 2017).

If we follow this hypothesis, the paraglacial incision pulse in the main rivers should

have started after 17 ka (i.e., corresponding to the onset of fast incision in connected rivers of Trend 1). Yet, the incision acceleration in "Trend 2" gorges appears to be delayed by more than 5 ka with respect to "Trend 1" ones. Although several authors have proposed that post-glacial incision may be delayed after deglaciation by several thousands of years (Valla et al., 2010; Jansen et al., 2011), this delay could also be controlled by the distance between the sampled gorge and the tributary confluence to the main stream, that the climatic knickpoint had to incise through while migrating upstream. Indeed, the Estéron gorge is located ~7km upstream from its junction with the Var River, while the Bévéra Gorge is located ~15 km upstream from its junction from the Roya River, and our data show that incision rate increases earlier in the Estéron Gorge (ca. 12 ka) than in the Bévéra Gorge (ca. 10 ka). Regarding the Pérouré Gorge, the data are too scarce to discuss further any possible propagation of incision between 10 and 15 ka (Figure 7A).

Several other factors can be invoked to explain this variation in the onset of fast incision from one river to another, such as sediment availability, water discharge and bedrock resistance. Besides, we do not find any indication of upstream migration of knickpoints along the tributary river profiles, but only static lithological knickpoints formed in the most resistant limestone strata. The latter will be discussed in more detail in the following section.

5.2.3. Lithological control on incision propagation

We proposed from Trends 1 and 2 that the location of the sampled gorges, with respect to LGM ice-covered extension (connected or indirectly-connected), controls the processes and rates at which the incision occurs. However, the gorges included in Trend 3 do not belong to a single domain regarding the glacier coverage. Indeed, the High Verdon Gorge was connected to glaciers, while Barles and Bendola gorges were indirectly connected. Those three gorges display very similar incision rates (0.15-0.28 mm/yr) to the Redebraus Gorge (0.21±0.03 mm/yr), although the latter is the only one that is totally disconnected from any glacial

influence. Therefore, it seems that these gorges have not been impacted by deglaciation and did not undergo any significant post-glacial incision.

We argue here that bedrock resistance plays a major role in the distribution and propagation of erosion in a fluvial system, as observed in previous studies (e.g. da Silva Guimarães et al., 2021). The notion of bedrock resistance here is relative to the lithology of one unit compared to another. In this study, we compare mainly the resistance of thick Tithonian limestone bars to known less resistant marl lithologies that are widespread in underlying and overlying strata. The Bès River example seems to illustrate this effect. Along this tributary, that is connected to the Bléone River, we sampled the Pérouré Gorge, just less than 2 km downstream of previously sampled Barles Gorge (Cardinal et al., 2021). From these two gorges, we can observe significant differences in incision rates. The Pérouré Gorge shows an overall higher incision rate (0.76±0.11 mm/yr), with an apparent increase at 4 ka (3.34±0.88 mm/yr), while the Barles Gorge displays a steady incision rate of 0.15±0.03 mm/yr. When looking at the Bès River long profile (Figure 2A), we see that the two gorges are located at both ends of a knickzone, in which we see three lithological knickpoints formed at each Tithonian limestone outcrop. This example could highlight the role of a strong bedrock lithology as a barrier partly impeding upstream incision propagation, as demonstrated by several studies (Crosby and Whipple, 2006, Jansen et al., 2010, Bishop and Goldrick, 2010). Considering this effect, we suggest that the upstream migration of a post-glacial incision wave is able to pass through the first knickpoint, but significantly decreases and even disappears as it migrates upstream through the knickzone towards Barles Gorge (Figure 8, bottom, T1)

The Roya catchment case could also reflect the control of lithology, in which we sampled two tributaries: the Bévéra and the Bendola. As in the Bévéra River, we would expect an acceleration of incision related to knickpoint propagation along the Bendola River, which would have occurred earlier as the Bendola Gorge is located within less than 1 km from its

junction with the Roya River. When looking at the longitudinal river profiles (Figure 2D), we see that the outlet of the Bendola River is located along an outcrop of Tithonian limestone, and slightly upstream of the lips of the knickpoint formed in this resistant lithology, whereas the Bendola outlet is located in a much less resistant lithology (Middle Jurassic marls). We thus propose that the Bendola River did not undergo any significant base level drop as a result of the paraglacial crisis in the Roya River, and therefore was not subject to any upstream knickpoint propagation, as opposed to the Bévéra River (Figure 8, bottom, T2).

Regarding the High Verdon Gorge case, it seems that the gorge did not undergo any post-glacial incision rate change, as opposed to the Vésubie or Courbaisse gorges. The Verdon longitudinal river profile (Figure 2B) presents a concave profile, especially upstream of the High Verdon Gorge. The lithology upstream of the Tithonian limestone in which the gorge is incised, is mainly composed of lower-resistance marls. The easily erodible lithology, in addition to the steady-state river profile could have dampened the impact of a paraglacial incision wave coming from the upstream glaciated area, located more than 50 km upstream. In addition to this effect, the position of the gorge more than 70 km upstream from the confluence with the Durance River could have prevented the High Verdon Gorge from undergoing any significant knickpoint propagation.

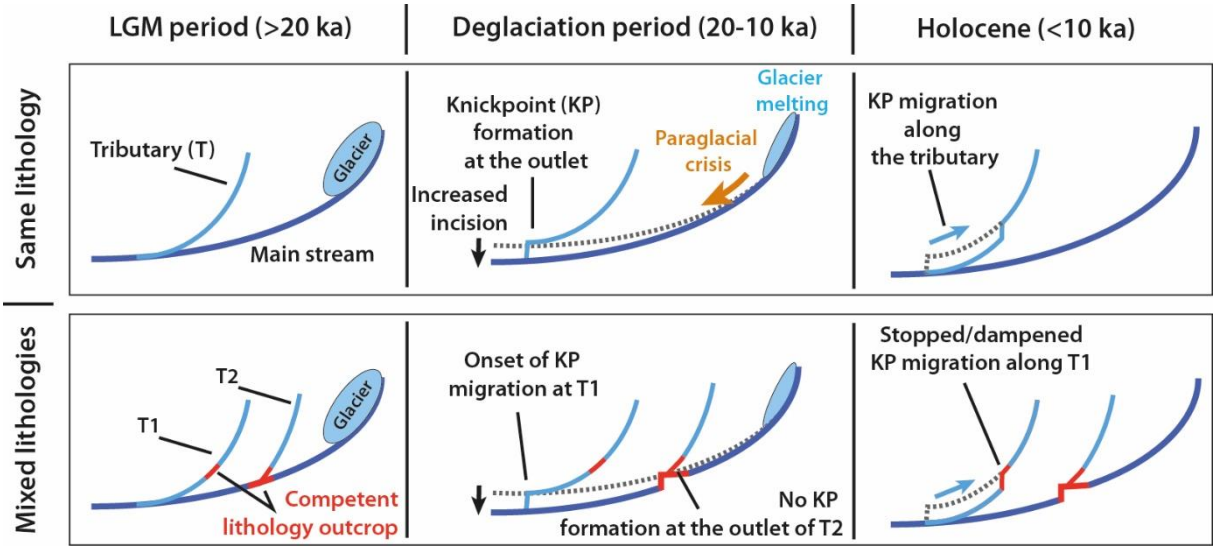

Figure 4-8 : Top: Theoretical sketch of tributary readjustment to a change of base level following paraglacial crisis in the main river with homogenous lithology. Bottom: Theoretical sketch of the impact of mixed lithologies (limestones/marls) on the incision propagation and tributary readjustment to a change of base level following paraglacial crisis in the main river.

5.2.4. Trend 3: steady-state

Trend 3, which includes data from Barles (Cardinal et al., 2021), High Verdon, Redebraus and Bendola (this study) gorges shows a slow and steady mean incision rate of ~0.25 mm/yr since maximum 80 ka. The main remaining question is: what drives these steady and lower incision rates displayed in Trend 3?

The climatic influence is shown through punctual and very efficient incision pulses, which can hinder any lower and longer-term signal. Therefore, to better understand such low incision rates we must integrate our data in a larger time window, where short-term climatic influence will be smoothed. Incision rates inferred from these isolated gorges seem comparable to previously-determined long-term erosion rates. Based on the CRE dating of alluvial terraces in the Buëch river (Figure 1C), Brocard et al. (2003) deduced a long-term (190 ka) incision rate of about 0.8 mm/yr. Based on bulk sediment cosmonuclides (^{10}Be) concentration, Mariotti et al. (2021) obtained catchment-average denudation rates ranging from 0.1 to 1.4 mm/yr since 75 ka in the Var River catchment (Figure 1C).

Under steady-state conditions, erosion rate is believed to match rock uplift rate (Royden and Perron, 2013). Long-term exhumation rates obtained from the external crystalline massifs

to the foreland are of the order of 0.3-1.4 mm/yr. In the Argentera ECM (Figure 1B), cooling rates estimated by low-temperature thermochronology (Apatite fission track and Apatite U-Th/He dating), are in agreement with exhumation rates of 0.8-1.4 mm/yr over the last 10 Ma (Bogdanoff et al., 2000; Bigot-Cormier et al., 2006; Sanchez et al., 2011). In the Frontal domain, Apatite (U-Th/He) dating on basin sediments had shown a reset induced by the Digne thrust sheet (Figure 1B) and returns exhumation rates of around 0.7 mm/yr since 5 Ma (Schwartz et al., 2017). East of the city of Nice, Bigot-Cormier et al. (2004) analysed seismic-reflection profiles to infer uplift rates of 0.3-0.5 mm/yr of the North Ligurian margin since 5 Ma. Regarding the present-day uplift, several studies using GPS data in the Alps (Serpelloni et al., 2013; Nocquet et al., 2016; Walpersdorf et al., 2018; Sternai et al., 2019; Piña-Valdés et al., 2022) evidence limited to slow vertical displacements of <0.5 mm/yr in the SW Alps.

Although, these values encompass different time scales, from long-term (10 Ma) to short-term (>100 a) and show a large variability, Trend 3 mean incision rates estimated at about of ~0.25 mm/yr in Trend 3 seem in agreement with those slow uplift rates. Therefore, our data could indicate that incision process within these disconnected (from glacier) or isolated river gorges is a response to a steady base-level drop induced by tectonically-driven rock uplift.

6. Conclusion

In conclusion, our ^{36}Cl CRE dating of incised bedrock gorges seems to highlight three different incision rate trends in the Southwestern Alps:

- Trend 1, in which connected gorges seem to have undergone an increase, directly after the LGM, followed by a decrease of incision. We propose that the variations in the recorded incision rates could firstly be related to an increase in the sediment yield and then to the depletion of sediment, commonly associated with the paraglacial period.
- Trend 2, with gorges affected by a small increase in incision rates after the deglaciation that could reflect the propagation of an erosion wave in tributaries of connected rivers.

- Trend 3, apparently unaffected by the last glacial-interglacial period, as suggested by the observed slow and steady incision rates (~0.25 mm/yr since maximum 80 ka). These values are similar to long-term erosion rates and in the range of the modern vertical GPS displacements.

As well as potentially highlighting the control of resistant lithology on incision propagation within river catchments, these observations, although based on a limited number of sites, provide insights for discussing the influence of different forcings (climate and tectonics) in the SW Alps. In locations significantly affected by late-Quaternary glaciers, the influence of climate is shown through the direct and indirect impact of deglaciation. There, the associated high gorge incision rates could hinder the lower and longer-term tectonic signal. Indeed, when out of the glacial influence, river incision rates are comparable to long-term (> 10 Ma) erosion rates. Therefore, our results and interpretations suggest that Late-Quaternary river incision in the Southwestern Alps is readjusting to both short-term climatic forcing and long-term tectonic forcing.

Acknowledgment

This study has been funded by the French Geological Survey (Bureau de Recherches Géologiques et Minières; BRGM) through the national program “Référentiel Géologique de France” (RGF-Alpes). This work has been supported by the French government, through the UCA-JEDI Investments in the Future project managed by the National Research Agency (ANR) with the reference number ANR-15-IDEX-01. The ^{36}Cl measurements were performed at the ASTER AMS national facility (CEREGE, Aix en Provence) which is supported by the INSU/CNRS, the ANR through the "Projets thématiques d’excellence" program for the "Equipements d’excellence" ASTER-CEREGE action and IRD. The authors thank Myette Guiomar and the Réserve Géologique de Haute Provence for their support during field work. This manuscript benefitted from constructive reviews from Fritz Schlunegger and an

anonymous reviewer who are thanked for their comments and suggestions.

References

Arnold, M., Merchel, S., Bourlès, D.L., Braucher, R., Benedetti, L., Finkel, R.C., Aumaître, G., Gottdang, A. and Klein, M., 2010. The French accelerator mass spectrometry facility ASTER: improved performance and developments. Nucl. Instrum. Methods Phys. Res., B 268, 1954–1959.

Bacon, S.N., McDonald, E.V., Caldwell, T.G. and Dalldorf, G.K., 2009. Timing and distribution of alluvial fan sedimentation in response to strengthening of late Holocene ENSO variability in the Sonoran Desert, southwestern Arizona, USA. Quaternary Res., 73, 425-438.

Ballantyne, C.K., 2002. A general model of paraglacial landscape response. The Holocene, 12, 3, 371-376.

Beck, C., Deville, E., Blanc, E., Philippe, Y., and Tardy, M., 1998. Horizontal shortening control of Middle Miocene marine siliciclastic accumulation (Upper Marine Molasse) in the southern termination of the Savoy Molasse Basin (northwestern Alps/southern Jura). Geol. Soc. Spec. Publ., 134, 263–278.

Benjamin, J., Rovere, A., Fontana, A., Furlani, S., Vacchi, M., Inglis, R. H., Galili, E., Antonioli, F., Sivan, D., Miko, S., Mourtzas, N., Felja, I., Meredith-Williams, M., Goodman-Tchernov, B., Kolaiti, E., Anzidei, M. and Gehrels, R., 2017. Late Quaternary sea-level changes and early human societies in the central and eastern Mediterranean Basin: An interdisciplinary review. Quat. Int., 449, 29-57.

Bierman, P. and Steig, E.J., 1996. Estimating rates of denudation using cosmogenic isotope abundances in sediment. Earth Surf. Process. Landf., 21, 2, 125–139.

Bigot-Cormier, F., Sage, F., Sosson, M., Déverchère, J., Ferrandini, M., Guennoc, P., Popoff, M. and Stéphan, J.-F., 2004. Déformations pliocènes de la marge nord-Ligure (France) : les conséquences d'un chevauchement crustal sud-alpin. Bull. Soc. géol. Fr., 175, 2, 197-211.

Bigot-Cormier, F., Braucher, R., Bourlès, D., Guglielmi, Y., Dubar, M. and Stéphan, J.-F., 2005. Chronological constraints on processes leading to large active landslides. Earth Planet. Sci. Lett., 235, 141-150.

Bilau, A., Rolland, Y., Schwartz, S., Godeau, N., Guihou, A., Deschamps, P., Brigaud, B., Noret, A., Dumont, T. and Gautheron, C., 2020. Extensional reactivation of the Penninic

Frontal Thrust 3 Ma ago as evidenced by U-Pb dating on calcite in fault zone cataclasite. Solid Earth, 12, 1, 237-251.

Bishop, P. and Goldrick, G., 2010. Lithology and the evolution of bedrock rivers in post-orogenic settings: Constraints from the high elevation passive continental margin of SE Australia. Geological Society, London, Special Publications, 346, 267-287.

Bogdanoff, S., Michard, A., Mansour, M. and Poupeau, G., 2000. Apatite fission track analysis in the Argentera massif: evidence of contrasting denudation rates in the External Crystalline Massifs of the Western Alps. Terra Nova, 12, 117-125.

Bonneau, L., Toucanne, S., Bayon, G., Jorry, S. J., Emmanuel, L. and Jacinto, R. S., 2017. Glacial erosion dynamics in a small mountainous watershed (Southern French Alps): A source-to-sink approach. Earth Planet. Sci. Lett., 458, 366-379.

Braucher, R., Merchel, S., Borgoman,o J. and Bourlès, D.L., 2011. Production of cosmogenic radionuclides at great depth : a multi element approach. Earth Planet. Sci. Lett., 309, 1-9.

Braucher, R., Keddadouche, K., Aumaître, G., Bourlès, D.L., Arnold, M., Pivot, S., Baroni, M., Scharf, A., Rugel, G. and Bard, E., 2018. Chlorine measurements at the 5 MV French AMS national facility ASTER: associated external uncertainties and comparability with the 6MV DREAMS facility. Nucl. Instrum. Methods Phys. Res., B 420, 40–45.

Brisset, E., Guiter, F., Miramont, C., Revel, M., Anthony, E.J., Belhon, C., Arnaud, F., Malet, E. and de Beaulieu, J.-L., 2015. Lateglacial/Holocene environmental changes in the Mediterranean Alps inferred from lacustrine sediments. Quaternary Sci. Rev., 110, 49-71.

Brocard, G.Y., van der Beek, P., Bourlès, D., Siame, L. and Mugnier, J.-L., 2003. Long-term fluvial incision rate and postglacial river relaxation time in the French Western Alps from ^{10}Be dating of alluvial terraces with assessment of inheritance, soil developpement and wind ablations effects. Earth Planet. Sci. Lett., 209, 197-214.

Brocard, G. and van der Beek, P., 2006. Influence of incision rate, rock strength, and bedload supply on bedrock river gradients and valley-flat widths: Field-based evidence and calibrations from western Alpine rivers (southeast France). Geol. Soc. Am. Bull., 398, 101-126.

Brocklehurst, S.H. and Whipple, K.X., 2002. Glacial erosion and relief production in the Esatern Sierra Nevada, California. Geomorphology, 42, 1-24.

Burbank, D.W., Leland, J., Fielding, E., Anderson, R.S., Brozovic, N., Reid, M.R., and Duncan, C., 1996. Bedrock incision, rock uplift and threshold hillslopes in the northwestern Himalayas. Nature, 379, 505-510.

Cardinal, T., Audin, L., Rolland, Y., Schwartz, S., Petit, C., Zerathe, S., Borgniet, L., Braucher, R., Nomade, J., Dumont, T., Guillou, V. and ASTER team, 2021. Interplay of fluvial incision and rockfalls in shaping periglacial mountain gorges. Geomorphology, 381, 107665.

Champagnac, J.D., Molnar, P., Andersion, R.S., Sue, C. and Delacou, B., 2007. Quaternary erosion-induced isostatic rebound in the western Alps. Geol. Soc. Am. Bull., 35, 3, 195-198.

Champagnac, J.-D., van der Beek, P., Diraison, G. and Dauphin, S., 2008. Flexural isostatic response of the Alps to increased Quaternary erosion recorded by foreland basin remnants, SE France. Terra Nova, 20, 213-220.

Church, M. and Ryder, J.M., 1972. Paraglacial sedimentation: A consideration of fluvial processes conditionned by glaciation. GSA Bulletin, 83, 3059-3072.

Clark, P.U., Dyke, A.S., Shakum, J.D., Carlson, A.E., Clark, J., Wohlfarth, B., Mitrovica, J.X., Hostetler, S.W. and McCabe, A.M., 2009. The Last Glacial Maximum. Science, 325, 710-714.

Crosby, B. T. and Whipple, K. X., 2006. Knickpoint initiation and distribution within fluvial networks: 236 waterfalls in the Waipaoa River, North Island, New Zealand. Geomorphology, 82, 16-38.

da Silva Guimarães, E., Delunel, R., Schlunegger, F., Akçar, N., Stutenbecker, L. and Christl, M., 2021. Cosmogenic and Geological Evidence for the Occurrence of a Ma-Long Feedback between Uplift and Denudation, Chur Region, Swiss Alps. Geosciences, 11, 339.

Darnault, R., Rolland, R., Rolland, Y., Bourlès, D., Revel, M., Sanchez, G. and Bouissou, S., 2012. Timing of the last deglaciation revealed by receding glaciers at the Alpine-scale: impact on mountain geomorphology. Quaternary Sci. Rev., 3, 127-142.

Davis, B.A.S., Brewer, S., Stevenson, A.C., Guiot, J. and Data Contributors, 2003. The temperature of Europe during the Holocene reconstructed from pollen data. Quaternary Sci. Rev., 22, 1701-1716.

DiBiase, R. and Whipple, K.X., 2011. The influence of erosion thresholds and runoff variability on the relationships among topography, climate, and erosion rate. J. Geophys. Res., 116, F04036.

England, P. and Molnar, P., 1990. Surface uplift, uplift of rocks, and exhumation of rocks. Geology, 18, 1173-1177.

Federici, P. R., Granger, D. E., Pappalardo, M., Ribolini, A., Spagnolo, M. and Cyr ,A. J., 2008. Exposure age dating and Equilibrium Line Altitude reconstruction of an Egesen moraine in the Maritime Alps, Italy. Boreas, 37, 245–253.

Federici, P. R., Granger, D. E., Ribolini, A., Spagnolo, M., Pappalardo, M. and Cyr, A. J., 2012. Last Glacial Maximum and the Gschnitz stadial in the Maritime Alps according to 10Be cosmogenic dating. Boreas, 41, 277–291.

Ferrier, K.L., Huppert, K. L. and Perron, J.T., 2013. Climatic control of bedrock river incision. Nature, 496, 206-209.

Fox, M., Leith, K., Bodin, T., Balco, G. and Shuster, D.L., 2015. Rate of fluvial incision in the Central Alps constrained throught joint inversion of detrital ^{10}Be and thermochronometric data. Earth Planet. Sci. Lett., 411, 27-36.

Gidon, M.,1997. Les chaînons subalpins au nord-est de Sisteron et l'histoire tectonique de la nappe de Digne. Géologie Alpine, 73, 23–57.

Glotzbach, C., van der Beek, P. A. and Spiegel, C., 2011. Episodic echumation and relief growth in the Mont Blanc massif, western Alps from numerical modelling of thermochronology. Earth Planet. Sci. Lett., 304, 417-430.

Godard, V., Hippolyte, J.-C., Cushing, E., Espurt, N., Fleury, J., Bellier, O., Ollivier, V. and the ASTER Team, 2020. Hillslope denudation and morphologic response to rock uplift gradient. Earth Surf. Dynam., 8, 221–243.

Haccard, Y., Beaudoin, B., Gigot, P. and Jorda, M., 1989. Carte géologique de France (1/50 000), feuille LA JAVIE (918). Orléans : Bureau de recherche géologiques et minières. Note explicative par Haccard, Y., Beaudoin, B., Gigot, P. et Jorda, M. (1989), 152 p.

Hack, J.T., 1960. Interpretation of erosional topography in humid temperature regions. Am. J. Sci., 258, A : 80-97.

Hallet, B., 1996. Glacial quarrying: a simple theorical model. Ann. Glaciol., 22, 1-8.

Heiri, O., Koinig, K.A., Spötl, C., Barrett, S., Brauer, A., Drescher-Schneider, R., Gaar, D., Ivy-Ochs, S., Kreshner, H., Luetscher, M., Moran, A., Nicolussi, K., Preusser, F., Schmidt, R., Schoeneich, P., Schw¨orer, C., Sprafke, T., Terhorst, B. and Tinner, W., 2014. Paleoclimate records 60–8 ka in the Austrian and Swiss Alps and their forelands. Quaternary Sci. Rev., 106, 186–205.

Herman, F., Seward, D., Valla, P.G., Carter, A., Kohn, B., Willet, S.D. and Ehlers, T.A., 2013. Worldwide acceleration of mountain erosion under a cooling climate. Nature, 504, 423-426.

Herman, F. and Champagnac, J.-D., 2016. Plio-Quaternaire incrase of erosion rates in mountain belts in response to climate change. Terra Nova, 28, 2-10.

Hinderer, M., 2001. Late Quaternary denudation in the Alp, valley and lake filling and modern river loads. Geodinamica Acta, 14, 231-263.

Holm, K., Bovis, M. and Jakob, M., 2004. The landslide repsonse of alpine basins to post-Little Ice Age glacial timing and retreat in southwestern British Columbia. Geomorphology, 57, 201-216.

Howard, A.D., Dietrich, W.E. and Seidl, A., 1994. Modelling fluvial erosion on regional to continental scales. J. Geophys. Res.: Solid Earth., 99, B7, 13,971-13,986.

Ivy-Ochs, S., Kerschner, H., Reuther, A., Preusser, F., Heine, K., Maisch, M., Kubik, P.W. and Schlüchter, C., 2008. Chronology of the last glacial cycle in the European Alps. J. Quaternary Sci., 23, 559-573.

Jansen ,J. D., Codilean, A. T., Bishop, P. and Hoey, T. B., 2010. Scale Dependence of Lithological Control on Topography: Bedrock Channel Geometry and Catchment Morphometry in Western Scotland. The Journal of Geology, 118, 3, 223-246.

Jansen, D. J., Fabel, D., Bishop, P., Xu, S., Schnabel, C. and Codilean, A. T., 2011. Does decreasing paraglacial sediment supply slow knickpoint retreat? Geology, 39, 6, 543-546.

Jourdon, A., Rolland, Y., Petit, C. and Bellahsen, N., 2014. Style of Alpine tectonic deformation in the Castellane fold-and-thrust belt (SW Alps, France): Insights from balanced cross-sections. Tectonophysics, 633, 143-155.

Julian, M., 1980. Les Alpes franco-italiennes, Etude Geomorphologique. Aix-Marseille Universitée.

Kirby, E. and Whipple, K.X., 2012. Expression of active tectonics in erosional landscapes. Journal of Structural Geology, 44, 54-75.

Korup, O. and Schlunegger, F., 2007. Bedrock landsliding, river incision, and transience of geomorphic hillslope-channel coupling: evidence from inner gorges in the Swiss Alps. J. Geophy. Res., 112, F03027.

Kuhlemann, J., Frisch, W., Székely, B., Dunkl, I. and Kázmér, M., 2002. Postcollisional sediment budget history of the Alps: Tectonic versus climatic control. Int. J. Earth Sci., 91, 818–837.

Lague, D., Hovius, N. and Davy, P., 2005. Discharge, discharge variability, and the bedrock channel profile. J. Geophys. Res., 110, F04006.

Lavé, J. and Avouac, J.P., 2001. Fluvial incision and tectonic uplift across the Himalayas of

central Nepal. J. Geophy. Res., 106, B11: 25 561-25 593.

Lebrouc, V., Schwartz, S., Baillet, L., Jongmans, D. and Gamond, J.F., 2013. Modeling permafrost extension in a rock slope since the Last Glacial Maximum: Application to the large Séchilienne landslide (French Alps). Geomorphology, 198, 198-200.

Lickorish, H. W. and Ford, M., 1998. Sequential restoration of the external Alpine Digne thrust system, SE France, constrained by kinematic data and synorogenic sediments. Geol. Soc. Spec. Publ., 134, 189–211.

Mair, D., Lechmann, A., Yesilyurt, S., Tikhomirov, D., Delunel, R., Vockenhuber, C., Akçar, N. and Schlunegger, F., 2019. Fast long-term denudation rate of steep alpine headwalls inferred from cosmogenic ^{36}Cl depth profiles. Scientific Reports, 9, 11023.

Mathey, M., Sue, C., Pagani, C., Baize, S., Walpersdorf, A., Bodin, T., Husson, L., Hannouz, E. and Potin, B., 2020. Present-day geodynamics of the Western Alps: new insights from earthquake mechanisms. Solid Earth, 12, 1661-1681.

Mariotti, A., Blard, P.-H., Charreau, J., Toucanne, S., Jorry, S.J., Molliex, S., Bourlès, D.L., Aumaître, G. and Keddadouche, K., 2021. Nonlinear forcing of climate on mountain denudation durings glaciations. Nat. Geosci., 14, 16-22.

Meigs, A., Krugh, W.C., Davis, K. and Bank, G., 2006. Ultra-rapid landscape response and sediment yield following glacial retreat, Icy Bay, soutehrn Alaska. Geomorphology, 78, 207-221.

Merchel, S., Bremser, W., Alfimov, V., Arnold, M., Aumaître, G., Benedetti, L., Bourlès, D.L., Caffee, M., Fifield, L.K., Finkel, R.C., Freeman, S. P. H. T., Martschini, M., Matsushi, Y., Rood, D.H., Sasa, K., Steier, P.,Takahashi, T.,Tamari, M., Tims, S.G., Tosaki ,Y., Wilcken, K.M. and Xu, S., 2011. Ultra-trace analysis of ^{36}Cl by accelerator mass spectrometry: an interlaboratory study , Anal. Bioanal. Chem., 400, 3125-3132.

Molnar, P. and England, P., 1990. Late Cenozoic uplift of mountain ranges and global change: chicken or egg? Nature, 346, 29-34.

Nocquet, J.-M., Sue, C., Walpersdorf, A., Tran, T., Lenôtre, N., Vernant, P., Cushing, M., Jouanne, F., Masson, F., Baize, S., Chéry, J. and van der Beek, P. A., 2016. Present-day uplift of the western Alps. Sci. Rep., 6, 28404.

Norton, K.P., Abbühl, L.M. and Schlunegger, F., 2010. Glacial conditioning as an erosional driving force in the Central Alps. Geology, 38, 7, 655-658.

Nouibat, A., Stehly, L., Paul, A., Schwartz, S., Bodin, T., Dumont, T., Rolland, Y., Brossier, R. and CIFALPS Group, 2022. Lithospheric transdimensional ambient-noise tomography

of W-Europe : implications for crustal-scale geometry of the W-Alps. Geophysical Journal International, 229, 862-879.

Ouimet, W.B., Whipple, K.X., Crosby, B.T., Johnson, J.P. and Schildgen, T.F., 2008. Epigenetic gorges in fluvial landscapes. Earth Surf. Proc. Land., 33, 1993-2009.

Pan, B., Burbank, D.W., Wang, Y., Wu, G., Li, J. and Guan, Q., 2003. A 900 k.y. Record of strath terrace formation during glacial-interglacial transitions in northwest China. Geology, 31, 957-960.

Pratt, B., Burbank, D.W., Heimsath, A. and Ojha, T., 2002. Impulsive alluviation during early Holocene strengthened monsoons, central Nepal Himalaya. Geology, 30, 10, 911-914.

Penck, W., 1924. Die morphologische analyse. Engelhorn's Nachfolger, Stuttgart, 283 p.

Petit, C., Goren, L., Rolland, Y., Bourlès, D., Braucher, R., Saillard, M. and Cassol, D., 2017. Recent, climate-driven river incision rate fluctuations in the Mercantour crystalline massif, southern French Alps. Quaternary Sci. Rev., 165, 73-87.

Petit, C., Rolland ,Y., Braucher, R., Bourlès, D., Guillou, V. and Petitperrin, V., 2019. River incision and migration deduced from ^{36}Cl cosmic-ray exposure durations: The Clue de la Cerise gorge in southern French Alps. Geomorphology, 330, 81-88.

Peti,t C., Salles, T., Godard, V., Rolland, Y. and Audin, L. River incision, ^{10}Be production and transport in a source-to-sink sediment system (Var catchment, SW Alps). EGUsphere [preprint].

Piña-Valdés, J., Socquet ,A., Beauval, C., Doin, M.-P., D'Agostino, N. and Shen, Z.-K., 2022. 3D GNSS velocity field sheds light on the deformation mechanisms in Europe: Effects of the vertical crustal motion on the distribution of seismicity. Journal of Geophysical Research: Solid Earth, 127, e2021JB023451.

Protin, M., Schimmelpfennig, I., Mugnier, J.-L., Ravanel, L., Le Roy, M., Deline, P., Favier, V., Buoncristiani, J.-F. and ASTER Team, 2019. Climcatic reconstruction for the Younger Dryas/Early Holocene transtition and the Little Age based on paleo-extents of Argentière glacier (French Alps). Quaternary Sci. Rev., 221, 105863.

Rea, B. R., Pellitero, R., Spagnolo, M., Hughes, P., Ivy-Ochs, S., Renssen, H., Riboloni, A., Bakke, J., Lukas, S. and Braithwaite, R. J., 2020. Atmospheric circulation over Europe during the Younger Dryas. Sci. Adv., 6.

Renssen, H., Seppä, H., Heiri, O., Roche, D.M., Goosse, H. and Fichefet, T., 2009. The spatial and temporal complexity of the Holocene Thermal Maximum. Nature Geoscience 2, 411-414.

Renssen, H., Seppä, H., Crosta, X., Goosse, H. and Roche, D.M., 2012. Global characterization of the Holocene Thermal Maximum. Quaternary Sci. Rev., , 48, 7-19.

Rolland, Y., Petit, C., Saillard, M., Braucher, R., Bourlès, D., Darnault, R., Cassol, D. and ASTER Team, 2017. Inner gorges incision history: A proxy for deglaciation ? Insights from Cosmic Ray Exposure dating (^{10}Be and ^{36}Cl) of river-polished surfaces (Tinée River, SW Alps, France). Earth Planet. Sci. Lett., 457, 271-281.

Rolland, Y., Darnault, R., Braucher, R., Bourlès, R., Petit, C., Bouissou, S. and ASTER Team, 2019. Deglaciation history at the Alpine-Mediterranean transition (Argentera-Mercantour, SW Alps) from ^{10}Be dating of moraines and glacially polished bedrock. Earth Surf. Process. Landsforms, 45, 2, 393-410.

Royden, L., and Perron, J.T., 2013. Solutions of the stream power equation and application to the evolution of river longitudinal profiles, J. Geophys. Res. Earth Surf., 118, 497–518.

Sadier, B., Delannoy, J.-J., Benedetti, L., Bourlès, D.L., Jaillet, S., Geneste, J.-M., Lebatard, A.-E. and Arnold, M., 2012. Further constraints on the Chauvet cave artwork elaboration. PNAS, 109, 8002-8006.

Saillard, M., Petit, C., Rolland, Y., Braucher, R., Bourlès, D. L., Zerathe, S., Revel, M. and Jourdon A., 2014. Late Quaternary incision rates in the Vésubie catchment area (Southern French Alps) from in situ-produced ^{36}CI cosmogenic nuclide dating: Tectonic and climatic implications. J. Geophy. Res.. Earth Surface, 119, 1121-1135.

Sanchez, G., Rolland ,Y., Corsini, M., Braucher, R., Bourlès, D., Arnold, M. and Aumaître, G., 2010. Relationships between tectonics, slope instability and climate change: Cosmic Ray exposure dating of active faults, landslides and glacial surfaces in the SW Alps. Geomorphology, 107, 1-2, 1-13.

Sanchez, G., Rolland, Y., Jolivet, M., Brichau, S., Corsini, M. and Carter, A., 2011. Exhumation controlled by transcurrent tectonics: the Argentera–Mercantour massif (SW Alps). Terra Nova, 23, 2, 116-126.

Savi, S., Norton, K.P., Picotti, V., Akçar, N., Delunel, R., Brardinoni, F., Kubik, P. and Schlunegger, F., 2014. Quantifying sediment at the end of the last glaciation: Dynamic reconstruction of an alpine debris-flow fan. GSA Bulletin, 126, 5-6, 773-790.

Schaller, M., Hovius, N., Willett, S.D., Ivy-Ochs, S., Synal, H.-A. and Chen, M.-C., 2005. Fluvial bedrock incision in the active mountain belt of Taiwan from in situ-produced cosmogenic nuclides. Earth Surf. Proc. Land., 30, 955-971.

Schimmelpfennig, I., Benedetti, L., Finkel, R., Pik, R., Blard, P.-H., Bourlès, D.L., Burnard, P.

and Williams, A., 2009. Source of in situ ^{36}Cl in basaltics rocks. Implication for calibration of production rates. Quat. Geochronol., 4, 441-461.

Schwartz, S., Gautheron, C., Audin, L., Dumont, T., Nomade, J., Barbarand, J., Pinna-Jamme, R. and van der Beek, P., 2017. Foreland exhumation controlled by crustal thickening in the Western Alps. Geology, 45, 2, 139-142.

Seidl, M.A. and Dietrich, W.E., 1992. The problem of channel erosion into bedrock. Catena Supp., 23, 101-124.

Serpelloni, E., Faccenna, C., Spada, G., Dong D. and Williams, S. D. P., 2013. Vertical GPS ground motion rates in the Euro-Mediterranean region: New evidence of velocity gradients at different spatial scales along the Nubia-Eurasia plate boundary. J. Geophys. Res.: Solid Earth, 118, 6003-6024.

Sklar, L. S. and Dietrich, W. E., 2001. Sediment and rock strength controls on river incision into bedrock. Geology, 29, 12, 1087-1090.

Sternai, P., Herman, F., Valla, P. G. and Champagnac, J.-D., 2013. Spatial and temporal variations of glacial erosion in the Rhône valley (Swiss Alps): Insights from numerical modeling. Earth Planet. Sci. Lett., 368, 119-131.

Sternai, P., Sue, C., Husson, L., Serpelloni, E., Becker, T.W., Willet, S.D., Faccenna, C., Giulio, A.D., Spada, G., Jolivet, L., Valla, P., Petit, C., Nocquet, J.-M., Walpersdorf, A. and Castelletort, S., 2019. Present-day uplift of the European Alps: Evaluating mechanisms and models of their relative contributions. Earth-Sci. Rev., 190, 589-604.

Stock, J.D., Montgomery, D.R., Collins, B.D., Dietrich, W.E. and Sklar, L., 2005. Field measurements of incision rates following bedrock exposure: implications for process controls on the long profiles of valleys cut by rivers and debris flows. GSA Bulletin, 117, 11-12, 174-194.

Stock, J.D. and Montgomery, D.R., 1999. Geologic constraints on debrock river incision using the stream power law. J. Geophys. Res., 104, B3, 4983-4993.

Stone, J.O., 2000. Air pressure and cosmogenic isotope production. J. Geophys. Res.: Solid Earth, 105, 23,753-23,759.

Sue, C. and Tricart, P., 1999. Late alpine brittle extension above the Frontal Pennine Thrust near Briançon, western Alps. Eclogae Geol. Helv., 92, 2, 171-181.

Sue, C., Delacou, B., Champagnac, J.-D., Allanic, C. and Burkhard, M., 2007. Aseismic deformation in the Alps: GPS vs. seismic strain quantification. Terra Nova, 1, 182-188.

Tucker, G.E. and Whipple, K.X., 2002. Topographic outcomes predicted by stream erosion

models: Sensitivity analysis and intermodel comparison. J. Geophy. Res., 107, B9, ETG 1-1-ETG 1-16.

Vacchi ,M., Marriner, N., Morhange, C., Spada, G., Fontana, A. and Alessio, R., 2016. Multiproxy assessment of Holocene relative sea-level changes in the western Mediterranean: sea-level variability and improvements in the definition of the isostatic signal. Earth-Sci. Rev, 155, 172-197.

Valla, P.G., van der Beek, P.A. and Carcaillet, J., 2010. Dating bedrock gorge incision in the French Western Alps (Ecrin-Pelvoux massif) using cosmogenic 10Be. Terra Nova, 22, 18-25.

Valla, P.G., Shuster, D.L. and van der Beek, P.A., 2011. Significant increase in relief of the European Alps during mid-Pleistocene glaciations. Nat. Geoscience, 4, 688–692.

Van den Berg, F., Schlunegger, F., Akçar, N. and Kubik, P., 2012. ^{10}Be-derived assessment of accelerated erosion in a glacially conditioned inner gorge, Entlebuch, Central Alps of Switzerland. Earth Surf. Process. Landforms, 37, 11, 1175-1188.

van der Beek, P. and Bourbon, P., 2008. A quantification of the glacial imprint on relief development in the French western Alps. Geomorphology, 97, 52-72.

van der Woerd, J., Tapponnier, P., Ryerson, F.J., Meriaux, A.-S., Meyer, B., Gaudemer, Y., Finkel, R.C., Caffee, M.W., Zhao, G. and Xu, Z., 2002. Uniform postglacial slip-rate along the central 600 km of the Kunlun Fault (Tibet), from ^{26}Al, ^{10}Be, and ^{14}C dating of riser offsets, and climatic origin of the regional morphology. Geophys. J. Int., 148, 356-388.

Walpersdorf, A., Pinget, L., Vernant, O., Sue, C., Deprez, A. and RENAG team, 2018. Does long-term GPS in the Western Alps finally confirm earthquake mechanisms? Tectonics, 37, 3721-3737.

Wanner, H., Beer, J., Bütikofer, J., Crowley, T.J., Cubash, U., Flückiger, J., Goosse, H., Grosjean, M., Joos, F., Kaplan, J.O., Küttel, M., Müller, S.A., Prentice, I.C., Solomina, O., Stocker, T.F., Tarasov, P., Wagner, M. and Widmann, M., 2008. Mid- to Late Holocene climate change: an overview. Quaternary Sci. Rev., 27, 1791-1828.

Wanner, H., Solomina, O., Grosjean, M., Ritz, S.P. and Markéta, J., 2011. Structure and origin of Holocene cold events. Quaternary Sci. Rev., 30, 3109-3123.

Wanner, H., Mercolli, L., Grosjean, M. and Ritz, S.P., 2015. Holocene climate variability and change: a data-based review. J. Geol. Soc. London, 172, 254-263.

Whipple, K.X. and Tucker, G.E., 1999. Dynamics of the stream-power river incision model: Implications for height limits of mountain ranges, landscape response timescales, and

research needs. J. Geophy. Res., 104, 17,661–17,674.

Whipple, K.X., Hancock, G.S. and Anderson, R.S., 2000. River incision into bedrock: Mechanics and relaive efficacy of plucking, abrasion, and cavitation. GSA Bulletin, 112, 3, 490-503.

Whipple, K.X., 2001. Fluvial landscape response time: how plausible is steady-state denudation? Am. J. Sci., 301, 313-325.

Whipple, K.X. and Tucker, G.E., 2002. Implications of sediment-flux-dependent river incision models for landscape evolution. J. Geophy. Res., 107, B2, ETG 3-1-ETG 3-20.

Willet, S.D., 1999. Orogeny and orography: the effects of erosion on the structure of mountain belts. J. Geophy. Res., 104, B12, 28 957-28 981.

Willet, S.D., Slingerland, R. and Hovius, N., 2002. Uplift, shortening, and steady-state topography in active mountain belts. Am. J. Sci., 301, 455-485.

Wobus, C., Whipple, K.X., Kirby, E., Snyder, N., Johnson, J., Spyropolou, K., Crosby, B. and Sheehan, D., 2006. Tectonics from topography: procedures, promise, and pitfalls. In: Willett, S.D., Hovius, N., Brandon, M.T., Fisher, D.M., (Eds.), Tectonics, Climate, and Landscape Evolution. Geological Society of America Special Paper, 398, 55-74.

Zerathe, S., Lebourg, T., Braucher, R. and Bourlès, D., 2014. Mid-Holocene cluster of larger-scale landslides revealed in the Southwestern Alps by ^{36}Cl dating. Insight on an Alpine-Scale landslide activity. Quaternary Sci. Rev., 90, 106-127.

Chapitre 5 : Re-evaluating the use of inner bedrock gorges as proxy for deglaciation and incision rate quantification

Résumé

Dans les zones précédemment englacées, le débat sur l'origine des gorges, dites "inner-gorges", n'est toujours pas résolu, et notamment concernant l'échelle de temps de leur formation et les processus impliqués (fluviaux vs glaciaires). En utilisant la méthode de datation CRE dans de telles gorges, Rolland et al. (2017) ont quantifié des taux d'incision dans la vallée de la Tinée (Alpes du Sud-Ouest). Pour apporter un nouveau regard sur ces questions, nous réexaminons ces données. Cela nous permet d'explorer les différents scénarios pouvant expliquer l'exposition des parois des gorges étudiées, pour enfin proposer une nouvelle interprétation sur la formation et l'évolution de ces gorges et des processus érosifs agissant dans les bassins versants alpins anciennement glaciaires. Nous proposons que les taux d'incision fluviale postglaciaire peuvent être surestimés, car il apparaît que la formation des gorges internes des Alpes est un processus à long terme qui se déroule sur plusieurs cycles interglaciaires-glaciaires.

Re-evaluating the use of inner bedrock gorges as proxy for deglaciation and incision rate quantification

Thibaut Cardinal[1], Yann Rolland[2-3], Carole Petit[1] and Laurence Audin[2]

[1] Université Côte d'Azur, CNRS, Observatoire de la Côte d'Azur, IRD, Géoazur, 250 rue Albert Einstein, Sophia Antipolis 06560 Valbonne, France cardinal@geoazur-unice.fr

[2] Université Grenoble Alpes, Université Savoie Mont Blanc, CNRS, IRD, Université Gustave Eiffel, ISTerre, 38000 Grenoble, France

[3] Université Savoie Mont Blanc, CNRS, Pôle Montagne, Edytem, F-73370 Le Bourget-du-Lac, France

Abstract

In previously glaciated areas, the debate on the origin of inner bedrock gorges is still inconclusive, and specifically regarding the time scale for their formation and the processes involved (fluvial vs. glacial). Using the CRE dating method in such inner gorges, Rolland et al. (2017) quantified incision rates in the Tinée valley (South-Western Alps). To bring a new perspective to these issues, we reanalysed those data. This allows us to explore several different possibilities that could explain the exposure history of the sampled gorges walls and thus to propose a new interpretation of the formation and evolution of these gorges and the erosive processes acting in previously glaciated alpine catchments. We propose that postglacial fluvial incision rates may be overestimated, as it appears that the formation of the internal gorges of the Alps is a long-term process that unfolds over several interglacial-glacial cycles.

1. Introduction

Over the repeated Quaternary climate changes, glacial advance and retreat have shaped the contemporary alpine landscape (Valla et al., 2011, 2012; Herman et al., 2013; Glotzbach et

al., 2013). Glaciated areas accumulate topographic disequilibrium during glaciations (Brocard and van der Beek, 2006), which might not be fully compensated during interglacials and may thus accumulate over several glacial periods (Salcher et al., 2014). Following the retreat of glaciers, previously glaciated valleys undergo accelerated erosion in an attempt to readjust from glacially-induced perturbations (Norton et al., 2010; Fox et al., 2015). This period of readjustment is called the "paraglacial" (Church and Ryder, 1972) and is characterized by enhanced fluvial incision and sediment yield (Ballantyne, 2002; Meigs et al., 2006). As glaciers and rivers are both setting the local base level of adjacent hillslopes, they have a great impact on valleys denudation and overall relief evolution (Willett, 1999). However, in addition to their mechanical erosive high efficiency, glaciers undergo repeated cycles of important thickness fluctuation related to climate variations. Burbank (2002) argue that hillslopes are more affected by this associated disequilibrium than fluctuation of river incision efficiency. Therefore, glaciers are thought to be a more effective agent of erosion than rivers. Nevertheless, Koppes and Montgomery (2009) argued that the erosive capacity of glaciers has been overestimated, so the efficiency of glacial vs fluvial erosion is still debated. To overcome this issue, the rate and chronology at which erosion acts, and its relationships with climate variations, should be better understood.

Extensive studies have been conducted in the Alps to date the Quaternary geomorphological markers of erosion, through dating methods such as Cosmic Ray Exposure (CRE), or luminescence and radiocarbon ages (e.g. Ivy-Ochs et al., 2008). Indeed, as glaciers advance on their valley bedrock and erode the latter by ablation and cavitation (e.g. Magrani et al., 2021), they subsequently leave markers of their former presence when retreating (Ivy-Ochs et al., 2006; Federici et al., 2012). Similarly, rivers leave trace of their former bed as they incise through the bedrock (Leland et al., 1998). As the Alpine topography have been profusely shaped by glaciers, many of these markers can be found and dated, thereby allowing to constrain the

temporal and spatial extension of Quaternary glaciations (Ivy-Ochs et al., 2008). These markers can be found and dated in the Argentera-Mercantour External Alpine Massif (Federici et al., 2016), but are scarcer in the Southwestern French side of the massif (Brisset et al., 2015). Glaciations and subsequent erosion have been heavily studied in the area, through a qualitative approach (Schweizer, 1968; Julian, 1980) and quantitatively with dating of: glacial polished surfaces (Sanchez et al., 2010; Darnault et al., 2012; Rolland et al., 2019), glacial lake sediment sequences (Brisset et al., 2015), detrital river sediments and marine turbidites (Bonneau et al., 2017; Mariotti et al., 2021) and hillslope destabilization (Bigot-Cormier et al., 2005. Sanchez et al., 2010; Bouissou et al., 2012).

Using CRE dating on fluvial bedrock gorges, Rolland et al. (2017) quantified incision rates in the Tinée Valley (SW French Alps), as it has been done for instance in the Himalayas (Pratt et al., 2002), Taiwan (Schaller at al., 2005) and in the nearby Vésubie Valley (Saillard et al., 2014). The gorges sampled by the authors are considered as inner-gorges, as they are located in areas that were previously covered by glaciers. However, the discussion about the origin of inner gorges still remains inconclusive. One possible origin is rapid incision pulses following glacial retreat (Meigs et al., 2006; Valla et al., 2010; Saillard et al., 2014; Rolland et al., 2017). Another hypothesis suggests that inner bedrock gorges may be the product of fluvial and sub-glacial erosion over the course of repeated glacial-interglacial cycles (Koppes and Montgommery, 2009; Dixon, 2011). This example thus contributes to the ongoing controversy on the efficiency of glacial vs fluvial erosion. Furthermore, the interpretation which aims at identifying the denudation process of the dated surface, and therefore the significance of CRE data, is not straightforward. Indeed, the exposure age of bedrock gorge walls can be rejuvenated or completely reset due to gravitational events (Valla et al., 2010; Cardinal et al., 2021) or lateral erosion during sediment filling excavation (Schaller et al., 2005; Ouimet et al., 2008) and therefore not be suitable for river incision rate quantification.

In the light of these issues and of new interpretations of regional incision rates (Cardinal et al., 2022), we re-examine the data presented by Rolland et al. (2017) and further explore the different scenarios that could have led to the exposure of the sampled gorges. This allows us to propose a new interpretation for the formation of inner-gorges and the erosive processes acting in previously glaciated Alpine catchments.

2. Context and State of the Art

2.1. Geomorphologic and geologic context

The Var catchment is located in the Southwestern Alps, on the French side of the Argentera-Mercantour Massif (AM; Figure 1A). The headwaters of the Var River and of two of its main tributaries (Tinée and Vésubie River) are located in the AM massif and therefore in the previously glaciated area during the Last Glacial Maximum (Figure 1B). The sharp topography of the massif can reach up to 3200 m.a.s.l. and still bears, at altitudes > ~2000 m, morphologies typical of glacial erosions. Glacial erosion created typical U-shape valleys, that transform into deeply V-shaped fluvially incised valleys. For instance, the Tinée Valley was occupied by a glacier which was connected to numerous tributary glaciers that carved glacial cirques and overhanging valleys (Figure 1C).

Uplifted and eroded since ~20 Ma (Lickorish & Ford, 1998; Sanchez et al., 2011), the AM crystalline massif is composed of metamorphic rocks, mainly gneisses and granites (Sanchez et al., 2010; Rolland et al., 2019; Figure 2). From the massif crests, the Tinée river flows towards the South and through the Mezosoic to Cenozoic sedimentary cover of the Nice and Castellane arcs (Petit et al., 2017), before joining the Var River to finish its course in the Mediterranean Sea, only ≈100 km from its headwater (Figure 2). Today, although still characterized by a V-shape, the Tinée Valley has its thalweg covered by alluvial sediments, which only reveal the bedrock in a few places.

The proximity of the high-elevation AM Massif with the Mediterranean Sea creates a favourable environment for deep incision and sharp relief formation (Brisset et al., 2015), through the effect of numerous erosion processes, from glacial, to fluvial and gravitational (Sanchez et al., 2010). This proximity from the Mediterranean Sea also influences greatly the regional climate (Federici et al., 2016). Indeed, the southern part of the AM Massif is particularly exposed to northwestern Mediterranean air masses, while being sheltered from perturbations originating in the North Atlantic (Federici et al., 2016; Brisset et al., 2015).

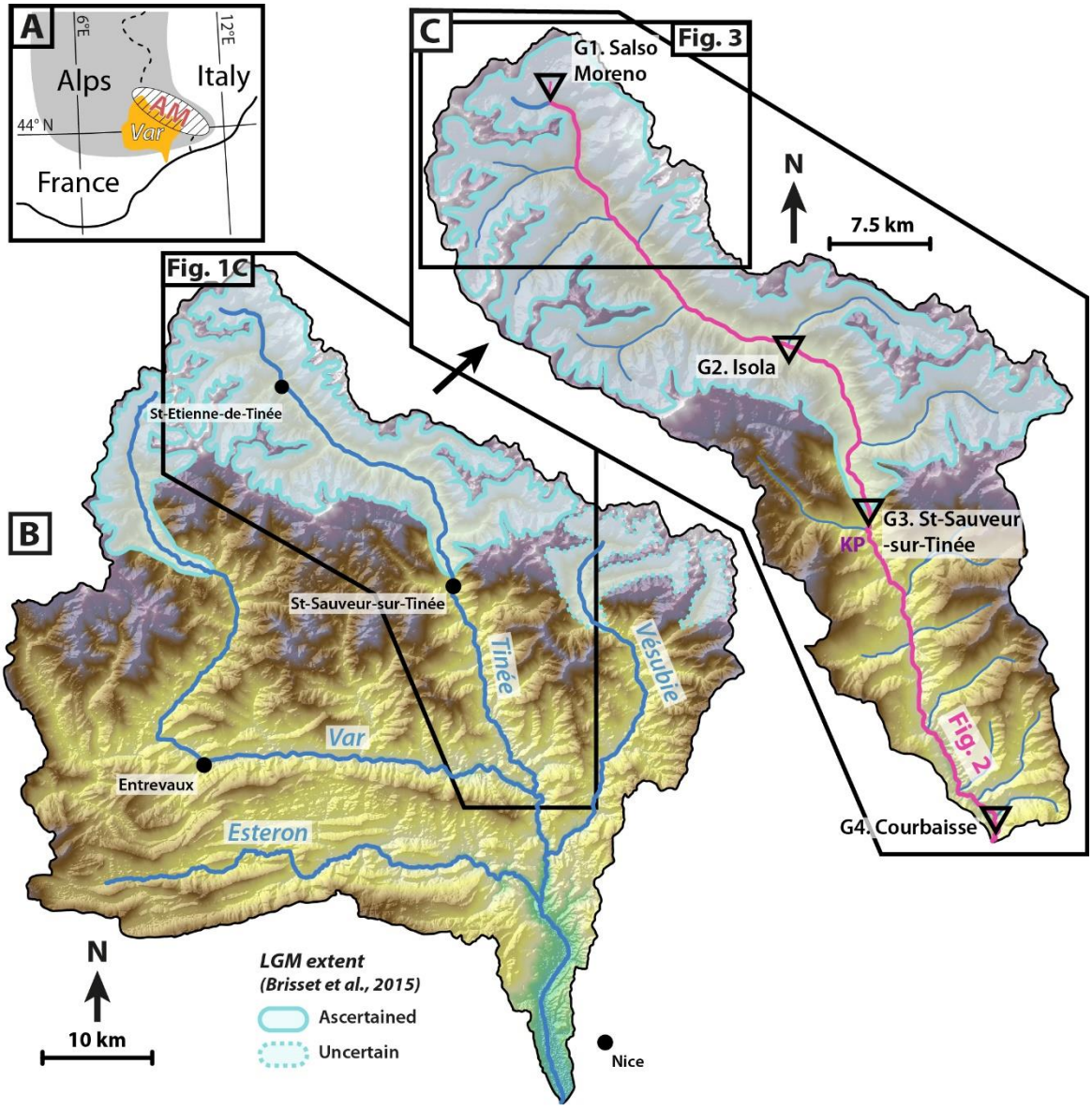

Figure 5-1 : A, Location of the Var catchment and the Argentera-Mercantour massif (AM) in the Southwestern Alps. B, Topographic map of the Var catchment and location of the Var river and its three main tributaries (Tinée, Vésubie and Esteron).

C, Topographic map of the Tinée catchment and location of the four sampled gorges by Rolland et al. (2017). The pink line is the location of the longitudinal river profile presented in Figure 2. It encompasses the main Tinée River up to the connexion with the river (Ravin de la Tour) which originate from Salso Moreno plateau (located on Figure 3). The light blue area shows the Last Glacial Maximum (LGM) glacier extent (modified from Brisset et al., 2015). KP: knickpoint, mentioned in Figure 2.

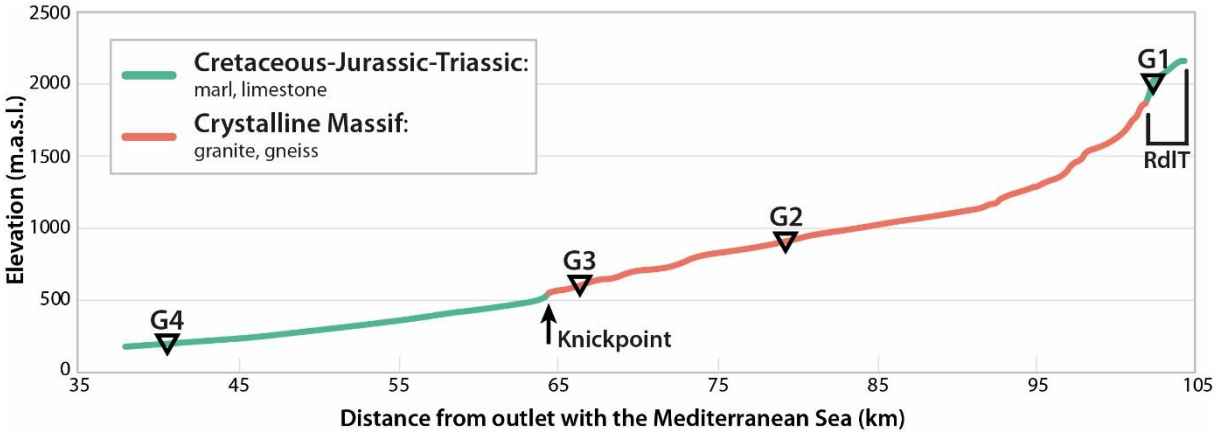

Figure 5-2 : Longitudinal profile and lithology of the Tinée River, up to the connexion with the river (Ravin de la Tour: RdlT) which originate from Salso Moreno plateau (located on Figure 3). The knickpoint (KP; Figure 1C) is located upstream of St-Sauveur-sur-Tinée.

2.2. Glaciation chronology in the Tinée Valley and its surrounding (Southwestern Alps)

The Last Glacial Maximum (LGM) correspond to the period when glaciers reached their maximum extent, at about 23–27 ka (Hughes and Gibbard 2015). With a heterogeneous extension throughout the Alps, The LGM is dated at 21.5 ka in the Southwestern Alps (Jorda et al., 2000). In this region, the glacier extended in the lower valley down to 600 m.a.s.l., with a thickness ranging from 600 to 1000m (Cossart et al., 2008). The LGM is followed by a period of glacier melting and retreat starting at 18-19ka, during which glaciers lost up to 80% of their volume (Ivy-Ochs et al., 2008). The deglaciation was not continuous. Indeed, numerous climatic events marked the deglaciation process during the Late-glacial period, from 18 to 11 ka (Ivy-Ochs et al. 2008). Even though the climatic conditions were gradually warming, the Late-glacial period is punctuated by several phases of glacial re-advances: The Gschnitz, Bühl, Clavadel/Sender, Daun and Egesen stadials, from the oldest to the youngest (Ivy-Ochs et al., 2006; 2008). The first four stadials occurred during the Oldest Dryas (between 18-17 to 14.7 ka), while the last (Egesen) happened during the Younger Dryas (12.9 to 11.6ka; Ivy-Ochs et

al., 2008; Heiri et al., 2014). A period of considerable warming, called the Bølling/Allerød, took place between the Oldest and the Younger Dryas. From 11.7 ka, the Alps enter in the Holocene (Ivy-Ochs et al., 2008; Heiri et al., 2014). This period of warmer and wetter climate (Wanner et al., 2011, 2015) also underwent period of minor glacier re-advance (Ivy-Ochs et al. 2006; Schimmelpfennig et al. 2012; Federici et al., 2016).

Three Late-Glacial stages have been dated in the Southwestern Alps. In the Italian side (NE) of the Argentera-Mercantour Massif (Figure 1A), Federici et al. (2016) dated preserved set of frontal moraines in the Gesso valley. The lowest moraine, at 750 m.a.s.l., permits to estimate the onset of the LGM deglaciation at 21–24 ka, and is followed by the deposition of two other moraines, located at ≈850 m.a.s.l. and 1800 m.a.s.l., which the authors linked to the Bühl and the Egesen stadials, respectively. However, glacier ice volume fluctuations and the chronology of glacial retreat/re-advances is not well constrained in the French side of Southwestern Alps. Markers of Quaternary glaciation, such as frontal moraines, are rare in the Tinée, Vésubie and Var low valleys. Indeed, the size, elevation and proximity to the Mediterranean Sea make the Var catchment a highly reactive catchment, where sediments are rapidly transported and flushed to the sea (Bonneau et al., 2017; Mariotti et al., 2021). The LGM glacier is believed to have advanced down to 40 km into the Tinée valley (500 m.a.s.l.), reaching St-Sauveur-sur-Tinée (Figure 1B), as speculated by Julian (1980) (Brisset et al., 2015, Petit et al., 2017). One sample of a polished surface located above St-Etienne-de-Tinée suggests that this portion of the Tinée main valley was deglaciated by 21.9±5.5 ka (Bigot-Cormier et al., 2005, recomputed by Sanchez et al., 2010; Figure 3).

Furthermore, glaciation markers, such as glacial polished surfaces, and long-term archives, such as lake sediments sequences, can be found in high-altitude cirques located in tributaries overhanging valleys. Several studies have been carried out in such cirques in the

upper Tinée Valley (Bigot Cormier et al., 2005; Sanchez et al., 2010; Darnault et al., 2012; Brisset et al., 2015; Rolland et al., 2019), which yield the following results (Figure 3) and interpretations:

(i) High elevation (2800 m.a.s.l, above Fer lake) polished surfaces suggest the onset of the LGM deglaciation at 18-33 ^{10}Be ka (Darnault et al., 2012 recomputed by Rolland et al., 2019).

(ii) deglaciation onset in the Salso Moreno Plateau, on the northern extremity of the Tinée catchment, has been dated at ≈15 ^{10}Be ka on a polished surface located at ≈2500 m.a.s.l. (Sanchez et al., 2010). These estimations are consistent with the exposure age of polished surfaces located at ≈2300 m.a.s.l. close to Vens upper Lake (14.7±1.0 ^{10}Be ka; Rolland et al., 2019), as well as with polished surfaces at 2700 m.a.s.l. above the Fer lake (13-15 ^{10}Be ka; Darnault et al., 2012 recomputed by Rolland et al., 2019). Dating of a polished surface close to the outlet (≈1400 m.a.s.l.) of Rabuons valley with the main Tinée valley suggests a deglaciation onset in the tributary valley at 14.2±2.0 ka (Bigot-Cormier et al., 2005, recomputed by Sanchez et al., 2010), which is similar as the age of the deglaciation in the upper part of the Rabuons valley (Rabuons Lake, ≈2500 m.a.s.l.; Darnault et al., 2012 recomputed by Rolland et al., 2019). These exposure ages suggest the occurrence of a second deglaciation phase between 15 and 13 ka which coincides with the Bølling/Allerød warming period, although the deglaciation age as low as 1400 m.a.s.l. in the Rabuons valley seems at odd with the other results. Lake sediment core analysis in the Vens lake by Brisset et al. (2015) shows consistent results, with markers of deglaciation of the cirque between 13.1 and 14 ^{14}C ka.

(iii) Young exposure age of polished surfaces in the Salso Moreno plateau (8.1±0.3 ^{10}Be ka; Sanchez et al., 2010), Fourchas lake (9.8±1.7 ^{10}Be ka; Rolland et al., 2019) and Fer lake (4.8±01- ^{10}Be ka; Darnault et al., 2012 recomputed by Rolland et al., 2019) are found at an

elevation of ≈2500 m.a.s.l. These ages coincide with a deglaciation period following the colder Younger Dryas stage. They also suggest the presence of small glaciers until ≈8 ka in high and confined areas (Darnault et al., 2012), certainly protected from melting by a rocky cover as illustrated at the Fourchas lake (Rolland et al., 2019).

Glacial unloading in in known to be followed by a period of hillslope debuttressing at the origin of landslides (Meigs, 1998; Cossard et al., 2008; Ballantyne et al., 2014). In the upper Tinée Valley, two well-studied landslides affect the NE hillslopes: the La Clapière landslide, located less than 1 km downstream Saint-Etienne-de-Tinée, and the Le Pra landslide, at the southwestern extremity of the Salso Moreno plateau (Figure 1B; 3). The onset of the gravitational destabilization of La Clapière landslide has been dated at 11-12 ka (Bigot-Cormier et al., 2005, recomputed by Sanchez et al., 2010). Bigot-Cormier et al. (2005) ascribes the nature of the destabilization to debuttressing following the deglaciation of the Tinée main Valley (21.9±5.3 ka; Bigot-Cormier et al., 2005, recomputed by Sanchez et al., 2010). Although Sanchez et al. (2010) attributes this event to a period of active seismicity in the AM Massif, the lag between the deglaciation and the onset of the destabilization (≈5ka, if we consider the lower bound of the uncertainty on the latter deglaciation age) is similar to those observed in other studies (Ballantyne et al., 2014: Schwartz et al., 2017). A second period of gravitational destabilization in the valley has been dated at 2.5-5ka, with the onset of Le Pra landslide (Sanchez et al., 2010). This period of destabilization could be related to Late Holocene warmer and wetter climatic conditions, during which water pressure could have built up in the hillslope until failure (Sanchez et al., 2010), as observed elsewhere in the region (Zerathe et al., 2014).

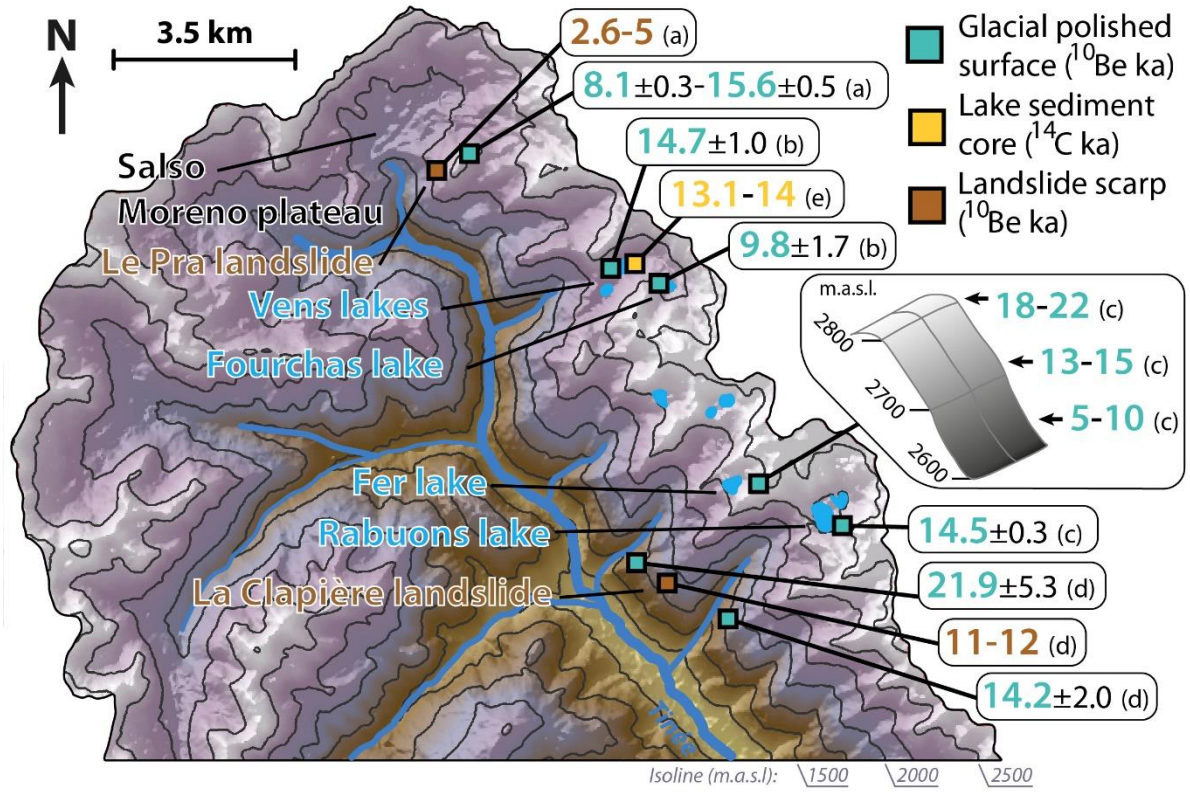

Figure 5-3 : Synthesis and location of the cosmogenic exposure ages (framed age with corresponding uncertainties or ages interval) obtained in the upper Tinée Valley by (a) Sanchez et al., 2010; (b) Rolland et al., 2019; (c) Darnault et al., 2012 recomputed by Rolland et al., 2019; (d) Bigot Cormier et al., 2005, recomputed by Sanchez et al., 2010 and (e) Brisset et al., 2015. Important features such as glacial lakes, plateaus and landslides are also named and located (text with white contour). Note that the sampling above Fer Lake by Darnault et al. (2012) have been done on a sub-vertical slope, and therefore represented here with a 3D sketch to be more comprehensible. The elevation difference between isolines is 250 m.

2.3. Incision rate estimation in Tinée gorges by Rolland et al. (2017)

Rolland et al. (2017) chose the deeply incised Tinée valley to quantify incision rates within gorges located along the Tinée River, and one of its tributary: Le Ravin de la Tour. From the high glacial plateau of Salso Moreno (≈2000 m.a.s.l.) to the outlet with the Var River (≈200 m.a.s.l.), four sites have been studied: (G1) Salso Moreno Gorge, (G2) Isola Gorge, (G3) St Sauveur Gorge and (G4) Courbaisse Gorge (Figure 1C). Sampled sites G1 to G3 were directly covered by LGM glacier, and G4 was not. In those areas, four vertical walls of heights ranging from 30 to 50 m above river bed, have been sampled for Cosmic Ray Exposure (CRE) dating. For a detailed presentation of the method, the reader is referred to a previous section (Chapter 2 of this thesis). In regard of the lithological heterogeneity along the Tinée Valley, rock samples of gneisses (G1-G3) and limestones (G4) have been collected for ^{10}Be and ^{36}Cl concentration

measurements, respectively. The reader is referred to the paper of Rolland et al. (2017) for further description of the sites and sampling strategy.

3. New analysis of CRE ages and results

The CRE age data obtained by Rolland et al. (2017) have been re-analysed following the methodology presented by Cardinal et al. (2022; Chapter 4). We used an adapted version of the code developed by Glotzbach et al. (2011) for CRE age analysis and incision rate quantification. The motivation behind this method is to provide an analysis framework that rely on robust statistic criteria in order to make the incision rate estimation as unbiased as possible. The code used split the CRE age data into 1, 2 or 3 successive time intervals in order to define line segments by weighted linear regression, and select the best-fitting scenario according to its R^2 value. From these linear regressions we can compute an exposure rate.

The CRE age vs. height plots are presented in Figure 4. From these plots we can make the following observations:

- Courbaisse Gorge (G4) data yield an exposure rate of 2.97±0.72 mm/yr, supported by a robust R^2 of 0.92;
- Salso Moreno (G1) data yield an exposure rate of 18.57±4.29 mm/yr from 0 to 1.5 ka, with a satisfying R^2 of 0.86;
- The rest of the results yield poorly constrained linear regression results, with R^2 between 0.69 to as low as 0.41. This can be explained either by uneven sampling or by large data scattering visible in some data sets.
- The most extreme example of data scattering is the one of St Sauveur, from 15 to 25 ka, where the associated linear regression is nearly vertical and yields an extreme exposure rate of 119.68±2277.36 mm/yr and a R^2 of 0. These values confirm the scattered characteristics of the data.

Furthermore, as mentioned by Rolland et al. (2017), we can observe clusters of similar ages but at different height. These clusters are at odds with the concept of the progressive exposure of the polished surface with incision, where we would expect a gradual decrease of ^{36}Cl concentration toward the bottom of the gorge wall. Conversely, these cluster seems to indicate that a large portion of the wall was exposed in one event. The visible CRE ages clusters are the following (Figure 4):

- Salso Moreno (G1): 0 to 1.5 ka;
- Isola (G2): 2.2-3.6 ka;
- St Sauveur (G3): 16.3-19.9 ka;
- Courbaisse (G4): 12.7-13.9 and 8.2-9.0 ka.

CRE ages from Courbaisse Gorge (G4) show ages with low temporal scattering that encompass a small fraction of the sampled walls (<10m high). These ages align well with one another and allow a good regression computation. The same is observed on G1 (Salso Moreno) data, but only from 1.5 to 0 ka, where the little uncertainty on CRE ages makes it easier to compute a satisfying linear regression. CRE data from G2 and G3 display larger cluster with very scattered ages and large uncertainties, making it difficult to compute a robust linear regression.

Most of these CRE ages clusters encompass high portion of the walls (>30 m high), and therefore suggest synchronous events of wall exposition, even thought the ages scattering makes it difficult to constrain the ages of these events, and even less a trustworthy exposure rate.

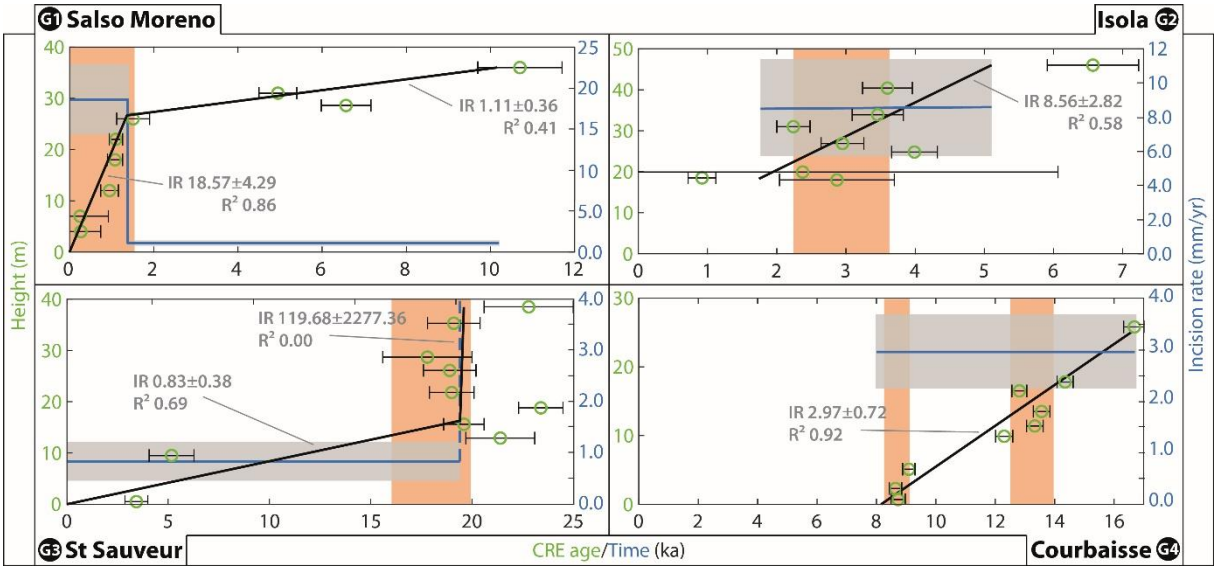

Figure 5-4 : Recomputed CRE age vs height (green circles) and corresponding regression (black line, with R² value); mean incision rate (blue line) throughout time, with uncertainty (grey envelope), plot of the (G1) Salso Moreno, (G2) Isola, (G3) St Sauveur and (G4) Courbaisse gorges sampled by Rolland et al. (2017). Cluster of ages identified by the authors are represented (orange rectangle). Incision rates (IR) and associated uncertainties are expressed in millimetres per year (mm/yr).

4. Interpretations

CRE data interpretation cannot only rely on statistical approach and requires detailed field observations of the sampled surfaces. However, results of the re-analysis of CRE dating (Rolland et al., 2017) from this robust statistical analysis alone raise some questions about the processes that led to the exposure of the sampled walls, and therefore the gorges origin. These questions will be explored through several scenarios and discussed in the following sections.

4.1. Paraglacial bedrock incision pulse scenario

The Courbaisse Gorge (G4) CRE ages suggest that nearly 30 m of walls got gradually exposed throughout a time period of 9 ka, starting at 17 ka and ending at 8 ka. The low scattering of the data and the high quality of the linear regression (R^2: 0.92) very likely reflect the action of progressive fluvial incision in agreement with the theoretical expectation that CRE concentration increase with height as the gorges walls are gradually exposed with the river entrenchment (Figure 5). The inferred incision rate from Courbaisse Gorge data is ≈3 mm/yr. This incision rate value is similar to the nearby Vésubie Gorge: 3.4 mm/yr between 15 and 9 ka

(Saillard et al., 2014, recomputed by Cardinal et al., 2022; Chapter 4 of this thesis). However, oppositely to the data from Vésubie River, which incision slows down from 3.4 to 1.4 mm/yr after 9ka, no incision rate variation is visible in the Courbaisse Gorge. The CRE ages align with each other in such a way that no variation is detectable. As discussed by the authors of these previous studies (Saillard et al., 2014; Rolland et al., 2017) and by Cardinal et al. (2022), the observed incision rate is probably the consequence of a paraglacial incision pulse (Church and Ryder, 1972) following the LGM deglaciation. Indeed, the enhanced fluvial processes, such as stream flow (Seidl and Dietrich, 1992; Tucker and Whipple, 2002) and sediment yield (Hinderer, 2001; Ballantyne, 2002; Meigs et al., 2006; Savi et al., 2014) could have led to a period of high fluvial incision in the Tinée River. For a more thorough discussion on the implication of paraglacial processes, the reader is referred to Chapter 4 of this thesis, section 5.3.

If we follow the same interpretation for the other gorges (G1 and G2), we obtain maximum incision rates ranging from 8 to 18 mm/yr (if we exclude the data from St Sauveur) and the observed CRE ages cluster could therefore indicate periods of rapid incision. From these results, a first observation can be made: these incision rates are a lot larger than the previously inferred incision rate from Courbaisse Gorge (3 mm/yr), even though they are located along the same river. However, gorges G1 to G3 are located in an area previously covered by glaciers and have therefore accumulated topographic disequilibrium during the glaciations (Brocard and van der Beek, 2006; Norton et al., 2010). It could be possible that post-glacial readjustment has not been reach in the upstream part compared to the downstream part and can therefore explain the variations in incision rate. The limit of the extent of the LGM glacier is marked by the presence of a knickpoint along the Tinée River longitudinal (Figure 2). Downstream of the knickpoint, the profile shows a much smoother and concave curve that suggest a steady state. Upstream, the profile is convex until 1200 m.a.s.l., where it becomes

concave as it gains elevation rapidly. However, and conversely to this hypothesis, the observed knickpoint most likely have a strictly lithological origin, as it marks the transition from limestone-marls to granite-gneiss rocks of the crystalline massif (Figure 2).

A second observation can be made: if the CRE age clusters represent punctual events of high incision rates, it seems that none of the gorge underwent these events at the same moment. Regarding the previously glacially-covered gorges (G1 to G3), we observe a delay from one gorge to the other suggesting that the more upstream a gorge is located, the later it underwent high incision. This observation can suggest that the progressive Tinée glacier retreat uncovered these inner gorges gradually and thereby put them under paraglacial processes influence one after the other. If this interpretation seems realistic from St Sauveur gorge, which incision onset is immediately following the LGM (19-20 ka), the incision onset of the two upper gorges, Isola and Salso Moreno, occurs much later, at 3-4 and 1.5-2 ka respectively. Considering that last traces of glaciers were dated at 14-15 ka in hanging valley upstream of Isola (Bigot-Cormier et al., 2005; Darnault et al., 2012; Rolland et al., 2019) and around 8 ka in Salso Moreno Plateau (Sanchez et al., 2010), this delay seems important and cannot be explain by this hypothesis. Another hypothesis to explain this delay would involve the progressive upward retreat of a knickpoint. However, it seems unrealistic that this knickpoint could have reach Salso Moreno only ~2ka after passing through Isola, located 24 km downstream, while it took it ~15 ka to retreat from St Sauveur to Isola, 13 km apart, directly after the LGM, at a period that should be the paraglacial peak of enhanced incision.

The scenario that the CRE ages from gorges G1 to G4 reflect incision seems a valid interpretation and is the one that Rolland et al. (2017) chose. Nevertheless, the timing of the incision onset and the magnitude and velocity at which the gorge walls seem to have been exposed, compared to local incision rate, make this scenario less likely for gorges G1 to G3.

Furthermore, CRE dating in gorge G2 and G3 fail to provide accurate results. Because of the scattered CRE ages and large associated uncertainties, the code used is not able to compute linear regressions that produce a satisfying R^2 (>0.8). Hence, it seems unlikely that the inferred exposure rates reflect fluvial incision. Therefore, with the aim to re-investigate Tinée CRE data, several other scenarios will be explored.

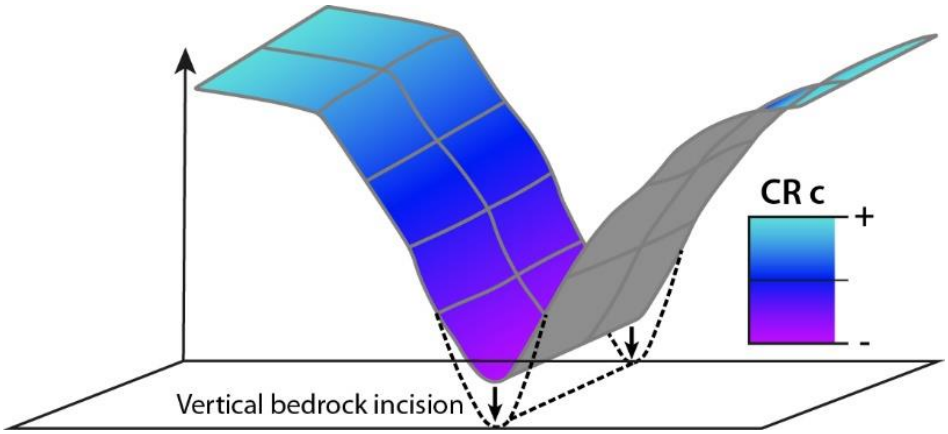

Figure 5-5 : Theoretical representation of progressive gorge wall exposure during ongoing vertical bedrock incision and expected Cosmogenic Radionuclide concentration (CR c).

4.2. Post-incision rejuvenation scenarios

As mentioned before, if the process responsible for the exposure of the sampled wall is fluvial incision, then, the CRE ages demonstrate the efficiency of incision to expose more than 30 m of bedrock in a very short amount of time. However, several other possibilities can explain such a rapid exposure. Indeed, once fluvial incision has dug the gorges and expose the walls to cosmic rays, other processes can modify the Cosmogenic Radionuclide (CR) concentration by removing part of the surface in which the CR began to accumulate following first exposure. Therefore, the apparent exposure age of a surface can be reset or rejuvenateed. If the process of rejuvenation only partially impacts the surface, then the new following CR production would add up to the one inherited from the period of first exposure.

Several processes or events could rejuvenate a gorge wall surface after its exposure by incision:

- The cover of an ice-cap can block exposure to cosmic rays, which would only resume once the glacier is retreated;
- Anthropic imprint.
- Gravitational destabilization removing a part the gorge wall;
- Lateral erosion during flood events;
- Lateral erosion during excavation of sediments filling the gorge.

While in the Tinée Valley case the two first scenario can be easily discarded by comparing glacier-retreat chronology and the timing of exposure events in the gorges and the un-humanly-disturbed facies of the gorges, the three others will be discussed in the following sections.

4.2.1. Scenario 1: gorge wall destabilization

Glacier retreat has been shown to be followed by a period of hillslope instabilities (Ballantyne et al., 2014). Indeed, glacial debuttressing and associated stress unloading are prone to trigger rock-slope failures (Cossart et al., 2018), which can take the form of landslides or rock-falls. Furthermore, glacier retreat, being associated with warmer climatic condition, can be combined with a period of permafrost degradation in periglacial slopes (e.g. Ravanel et al., 2010; Hilger et al., 2021).

Exposure events dated in G1 to G3 could be interpreted as massive slope destabilization in the gorges, following, more or less closely, the Tinée glacier retreat. Rather than one massive event that would impact the whole height of the wall, several rock fall of limited extension could have scarred the wall at multiple locations (Figure 6). The non-synchronicity of these numerous rock falls could explain the scattering of CRE ages visible in St Sauveur and Isola gorges (Figure 4). Furthermore, the resulting detached boulders can subsequently accumulate

of the foot of the slope and create a debris cover that shield the lower part of the gorge from cosmic rays and prevent CR accumulation, also delaying bedrock incision (Figure 6). After total removal of these blocks, the gorge wall would start to accumulate CR again, but their CR concentration would be much lower. This effect could explain the two very young ages at the foot of the St Sauveur Gorge (3-5 ka; Figure 4). The lack of data in the lowest part of Isola gorge does not allow us to corroborate this hypothesis.

If these rock falls are attributed to glacial debuttressing, then their occurrence should follow glacier retreat. Therefore, it is reasonable to expect a different onset of destabilization period for each gorges, and none in Courbaisse Gorge as it was not covered by glacier. Rock falls in St Sauveur seems to follow very closely glacier retreat (18-20 ka), which fits well with this hypothesis. However, rock falls seems to have occurred at 2.5-3.5 ka and 0-1.5 ka in Isola and Salso Moreno gorges, respectively. The timing does not fit with deglaciation chronology and exceeds the average ≈5 ka gap observed between glacier retreat and the onset of rock-slope failure in previously glaciated valleys (Ballantyne et al., 2014: Schwartz et al., 2017). However, Sanchez et al. (2010) proposed that a period of destabilization occurred on the Tinée Valley at 2.5-5 ka, related to a seismic active period. This latter estimation fits well with the possible occurrence of rock-falls in the upper Tinée gorges.

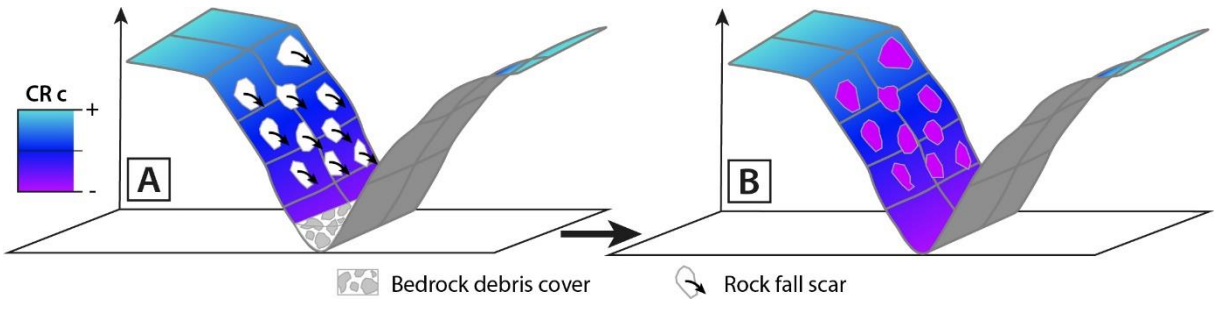

Figure 5-6 : Theoretical representation of (A) the occurrence of rock-falls post-incision and the formation of a bedrock debris cover and (B) impact of those rock-fall and associated CR concentration local rejuvenation along the gorge walls.

4.2.2. Scenario 2: Lateral erosion during the paraglacial crisis

The onset of a paraglacial erosion pulse follows closely the beginning of a deglaciation phase. Indeed, glacier melting and retreat uncover sediments that were accumulated in front or below the glacier during its advance and provides enhanced flow of meltwaters to remobilize it. The combination of higher discharge and sediment yield input in the fluvial system is thought to promote erosion (Ballatyne, 2002). Indeed, the sediment transported by the river will, by abrasion and plucking process, erode the bedrock (Stock et al., 2005; DiBiase and Whipple, 2011). However, if the sediment input is excessively profuse, it can cover the underlying riverbed from erosion and thereby impedes bedrock incision (Sklar et Dietrich, 2001). In the case of narrow gorges, the bedrock can be insulated from incision by a cover of the coarser sediment, while the walls can be exposed to lateral erosion by thinner suspended materials (Figure 7A). If the lateral erosion is efficient enough, the gorge walls CR concentrations will therefore decrease (Figure 7B).

This scenario can explain the punctual rejuvenation events in gorges G1 to G3. The presence of an alluvium coverage of the Tinée bedrock today could be a relic of the aforementioned bedrock alluvial coverage. The scattering visible in G2 and G3 data could then be the effect of uneven erosion along the walls. Indeed, unequal erosion of the gorge wallwould lead to unequal distribution of inherited CR concentration.

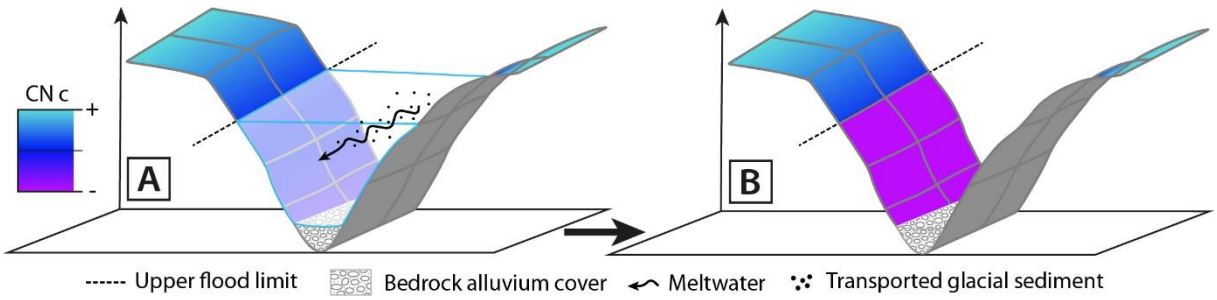

Figure 5-7 : Theoretical representation of (A) the filling a gorge by a flood of meltwater eroding the lateral wall but not the bedrock as it is protected by an alluvium cover and (B) the associated wall rejuvenation.

4.2.3. Scenario 3: lateral erosion by the excavation of sediment filling

A pulse of glacial or hillslope-derived sediments can cover the bedrock and temporarily insulate it from erosion, but in some extreme cases in which the input is so large that it overwhelmed the transport capacity of a river, it can partly or completely fill a gorge or a valley (Figure 8A; Ouimet et al., 2008; Ivy-Ochs et al., 2009). Once the sediment input is exhausted, the river quickly (<2 ky; Pratt et al., 2002) excavates the gorge by incising through the aggraded sediment and degrades the lateral gorge walls (Figure 8A; Pratt et al., 2002). The sediment infill shields bedrock from cosmic ray exposure, while lateral erosion rejuvenates the adjacent walls by removing a layer of rocks where CR were previously accumulated (Figure 8B; Pratt et al., 2002; Schaller et al., 2005; Ivy-Ochs et al., 2009). In this case, exposure ages reflect the onset of the re-incision, i.e. the moment when fluvial transport capacity outdo the sedimentary input. Paraglacial period is known to end once the sediment yield is depleted (Jansen et al., 2011). Thus, is it reasonable to think that the excavation of the sealed gorges would only begin once the paraglacial period is over. In the case of a glaciated valley, the sediment infill could originate from remobilized glacial sediment (Ballantine, 2002), debuttressing hillslopes (Ouimet et al., 2008; Ballantyne et al., 2014) or sedimentary filling of subglacial gorge during the glaciation advance (Montgommery and Korup, 2011). Schaller et al. (2005) tested this hypothesis and demonstrated that the excavation of sedimentary filling in gorge and related lateral wall erosion could yield surface exposure ages three times younger than the true age of the wall (i.e. the age corresponding to the gorge formation by fluvial incision) in the case of a 1m-thick layer removal. This scenario only differs from Scenario 2 (previous section), in that the sediment input is much larger and does not just cover the bedrock.

Applying this scenario to the St Sauveur Gorge suggests that the excavation took place right after the LGM. The source of the sediments might have been a frontal moraine, quickly excavated because not yet fed by upstream hillslope processes. The Isola Gorge sedimentary

filling possibly took much more time to be excavated, as it could have originated from a subglacial compacted sealing (Montgommery and Korup, 2011) and subsequently fed by the sedimentary input from the deglaciation of tributary hanging valleys and hillslope debuttressing. The scattering of CRE ages in these two gorges might be caused by uneven lateral erosion during the excavation, as some surfaces might have been protected by local alluvium coverage (Schaller et al., 2005). It seems from the CRE data and from field observations that the excavation of Salso Moreno Gorge is still ongoing, as the bedrock is not visible and the gorge bottom is filled with mixed coarse and thin sediments most probably originating from the remobilized moraine visible on the Salso Moreno Plateau upstream (Figure 9). This last observation provides a robust argument for this last scenario as the cause of the rapid exposure of the G1 to G3 gorges walls.

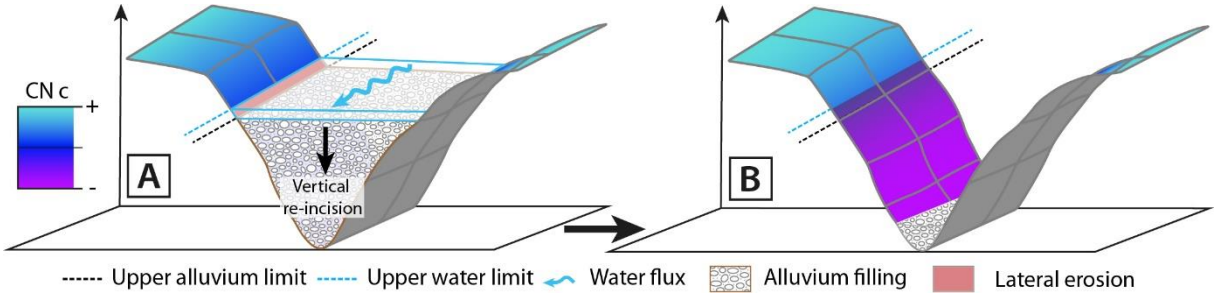

Figure 5-8 : Theoretical representation of (A) alluvium filling of a gorge and subsequent lateral erosion of the wall during river "re-incision" in an attempt to excavate the gorge, and (B) the associated wall rejuvenation.

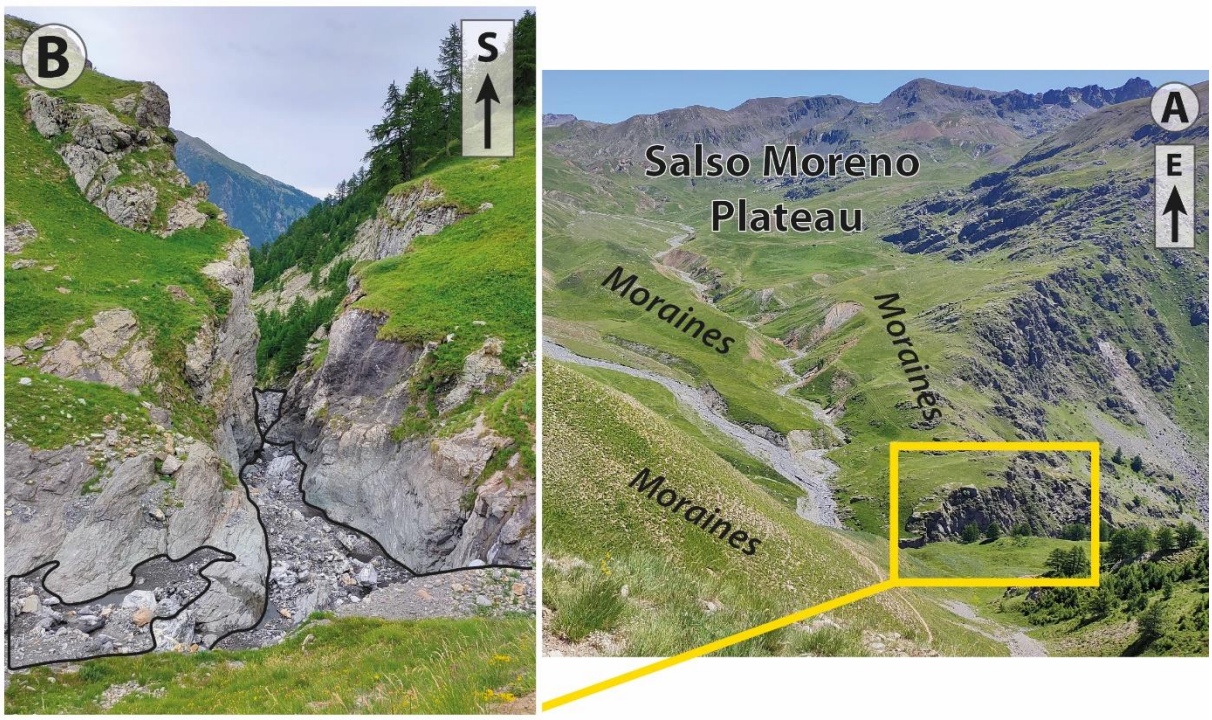

Figure 5-9 : Photography of (A) Salso Moreno Plateau and its remobilized moraine, and (B) Salso Moreno Gorge filled with sediment (outline in black).

5. Discussion

5.1. Which of these scenarios is the most probable?

After re-analyzing CRE data from the upper Tinée River (Rolland et al., 2017), we propose here that the dated exposure of the Salso Moreno (G1), Isola (G2 and St Sauveur (G3) are most likely not related to pure bedrock fluvial incision. We base this opinion on a statistical analysis and on the exploration of several alternative scenarios to explain the data and their significance. The challenge encountered in proposing an interpretation for these data is the necessity to find a scenario that can reasonably explain the scattering of the CRE ages and the rapid exposure of the walls. Rolland et al. (2017) attributed this exposure to very large incision rates, as it has been documented in other studies (e.g. 2–10 mm/yr in the Himalayas, Burbank et al., 1996; 4–17 mm/yr in Taiwan, Hartshorn et al., 2001; and locally 6.5-13 mm/yr in the French Alps, Valla et al., 2010). However, the CRE age distribution and the relatively bad quality of the upper Tinée gorges data, compared to other gorge where fluvial incision has been

clearly identified as the main process (Courbaisse Gorge in this study and others in Cardinal et al., 2022) suggest otherwise. The CRE data could therefore reflect an erosion process different than bedrock incision to explain the rapid exposure of the walls.

The first possibility explored (Scenario 1) is the occurrence of numerous rock-falls. However, as stated by Rolland et al. (2017), the authors carefully selected polished surfaces to sample. Rock-fall scars should have been easily recognizable from river polished surface, as granit-gneisses most likely do not undergo altering processes such as dissolution. Furthermore, the occurrence of a massive rock-fall affecting the full height of the wall is unlikely.

The second possibility (Scenario 2) evoke the occurrence of a flood-like event that would have filled the gorge and eroded laterally its wall through the mobilization of suspended sediment, while the bedrock remained protected by a cover of alluvium. However, a long lasting water column of more than 30 m high is required to erode the full height of the sampled gorges walls, which seems unrealistic. Furthermore, several studies have shown that the role of suspended sediment as an erosive tool is much weaker than bedload coarser sediment (Johnson et al., 2010; Cook et al., 2013).

The third possibility (Scenario 3) propose a rejuvenation of the gorge wall together with lateral erosion as the river cut through and excavate a sediment “plug” that fills the gorge, as previously observed elsewhere (Pratt et al., 2002; Schaller et al., 2005; Ivy-Ochs et al., 2009). The filling could be the consequence of a massive sedimentary input, characteristic of paraglacial period impact observed in the region (Saillard et al., 2014; Rolland et al., 2017; Cardinal et al., 2022) and/or landslide activity in the Tinée Valley (Bigot-Cormier et al., 2005; Sanchez et al., 2010), and would account for the presence of river polished surface along the gorge walls.

Rejuvenation depends on the thickness of surface rock removed during the erosion of the walls. The evoked erosion processes can affect the walls unevenly, leaving surfaces intact or very lightly eroded (Schaller et al., 2005), while other ones can suffer important denudation. The CR concentration on these sampled surfaces is the addition of the concentration since the second episode of exposure (post-incision) to the inherited concentration more or less rejuvenated, which could explain the CRE age scattering visible in the data.

Scenario 3 therefore seems the most probable, as it provides a reasonable explanation for: (i) the rapid rate of exposure, (ii) the CRE ages scattering, (iii) it fits well with the interpretation from other studies in the area regarding incision being controlled by paraglacial processes (Saillard et al., 2014; Cardinal et al., 2022), which in this case would provide the necessary sedimentary input, (iv) gravitational activity providing additional sediment (Bigot-Cormier et al., 2005; Sanchez et al., 2010). This scenario has been proposed in other studies to explain similar observations (Pratt et al., 2002; Schaller et al., 2005; Ivy-Ochs et al., 2009). However, it is possible that the aforementioned sedimentary gorge filling may the result of a combination of several events and processes. Indeed, the sediment load could originate from sub-glacial erosion and accumulate under the glacier. After glacier retreat, this filling would then be subjected to fluvial processes but also sustained by remobilized sediment from upstream, tributary valleys and hillslopes, thus delaying its excavation.

5.2. When are inner gorges formed?

All the above scenarios imply that CRE ages correspond to episode of rejuvenation, and therefore that the gorges were not dug during the interglacial following LGM, but that the gorge walls exposure was only rejuvenated during the last deglaciation. This hypothesis echoes with the ongoing debate regarding the origin of inner gorges.

Indeed, inner gorges are thought to be the product of fluvial incision during interglacial periods (Garwood, 1910; Brocard et al., 2003; Meigs et al., 2006). This hypothesis is supported by the idea that glacial erosion is much stronger than fluvial erosion, therefore that fluvial markers formed during interglacial period are erased during the glaciation (Hallet et al., 1996). This is a cycle in which fluvial markers are erased by glaciers and re-shaped between each glaciation, constantly lowering down the topography. If we follow this idea, then the formation of all the gorges visible in previously glaciated area of the Alps started after the LGM.

Montgommery and Korup (2011) have estimated that if the current relief of the Swiss Alps have been shaped solely during the last interglacial period, then an erosion rate between 8.5-18 mm/yr would be required to achieve it. The maximum incision rate (8.56-18.57 mm/yr) estimated in the upper Tinée Valley (if we consider the exposure of sampled gorge walls as relative to fluvial incision) falls exactly into this range of erosion rates and fits with these estimations. However, Montgommery and Korup (2011) considered this range of erosion rates as unrealistic over the course of a single interglacial period, but most importantly over the course of several interglacial, as glaciers would have to reset this fluvial topography during each glaciation. This would lead to catastrophic valley lowering corresponding to long-term denudation rate exceeding 10 mm/yr and resulting in the removal of more than 10 km of upper crust during the last 1 Myr, contradicting thermochronological and geological data (Montgommery and Korup, 2011 and references therein). Furthermore, Kaplan et al. (2009) argue that glacial erosion, by lowering high altitude topography prone to glaciers development, would impede the extension of those latter over repeated glacial cycle and inevitably limit the efficiency of glacial and paraglacial erosion. The hypothesis of a “self-defeating mechanism” (Kaplan et al., 2009; Magrani et al., 2021) thus suggest that high erosion rate cannot be sustained in the long-term.

In the case of the upper Tinée, the high incision rate values are also inconsistent with the long-term incision rate estimated at 0.8 mm/yr (Brocard et al., 2003) and with short-term incision rates constrained from gorges where the fluvial incision implication is well demonstrated (<3mm/yr; e.g. Courbaisse Gorge, Vésubie Gorges, Saillard et al., 2014; and others, Cardinal et al., 2022). Korup and Montgommery (2011) propose that inner gorges are carved within the course of several interglacials and are preserved from glacial erosion by a sedimentary "sealing" of the gorges. Inner gorges could also be carved during glaciation period by sub-glacial meltwater stream, as proposed by Tricart and Soons (1960), who also argued that sub-glacial incision is more efficient than post-glacial incision. Nevertheless, the upper Tinée data and our interpretations are in better agreement with the hypothesis that gorges are progressively incised throughout multiple interglacial periods, as it involves sedimentary filling of the gorges that needs to be excavated before bedrock fluvial incision can resume (Korup and Montgommery, 2011).

6. Conclusion

We took a new look on previously published CRE data by Rolland et al. (2017). The authors sampled three inner gorges in the upper Tinée catchment, which was glaciated during the LGM. They concluded that the exposure of the gorges walls was related to the fluvial incision and quantified high incision rates (8 to 18 mm/yr). Applying a new statistic method, we re-analysed their data. The results show poor quality regression lines, mainly because of the scattering of the CRE ages, which compelled us to question the nature of the events and processes that led to the exposure of the inner gorges walls. We explored different scenarios involving: (i) rock falls (Scenario 1), (ii) flood (Scenario 2) and (iii) transient sedimentary filling (Scenario 3). Taking into account the CRE data distribution, the valley history regarding glaciations and gravitational destabilization and what had been observed by previous studies in similar contexts, Scenario 3 (iii) appeared to be the most probable one. However, in the absence

of firm evidences of past aggradation and excavation to corroborate this hypothesis, such as leftovers of alluvium deposit above riverbed, our interpretation remains speculative. Nevertheless, we can observe present aggradation in the Salso Moreno Gorge and this scenario gives a decent explanation for the scattering in the CRE data and the oddly high exposure rate. Therefore, we propose that post-glacial fluvial incision rates can be over-estimated, as it seems that the formation of Alpine inner gorges is a long-term process that takes place within several interglacial-glacial cycles. Consequently, this interpretation implies that Alpine glaciers cannot fully erase fluvial markers, therefore diminishing the efficiency of glacial erosion as well.

Reference

Ballantyne, C.K., 2002. A general model of paraglacial landscape response. The Holocene, 12, 3, 371-376.

Ballantyne, C. L., Wilson, P., Gheorghiu, D. and Rodés, A., 2014. Enhanced rock-slope failure following ice-sheet deglaciation: timing and causes. Earth Surf. Process. Landforms, 39, 900–913.

Bigot-Cormier, F., Braucher, R., Bourlès, D., Guglielmi, Y., Dubar, M. and Stéphan, J.-F., 2005. Chronological constraints on processes leading to large active landslides. Earth Planet. Sci. Lett., 235, 141-150.

Bishop, P. and Goldrick, G., 2010. Lithology and the evolution of bedrock rivers in post-orogenic settings: Constraints from the high elevation passive continental margin of SE Australia. Geological Society, London, Special Publications, 346, 267-287.

Bonneau, L., Toucanne, S., Bayon, G., Jorry, S. J., Emmanuel, L. and Jacinto, R. S., 2017. Glacial erosion dynamics in a small mountainous watershed (Southern French Alps): A source-to-sink approach. Earth Planet. Sci. Lett., 458, 366-379.

Bouisson, S., Darnault, R., Chemenda, A. and Rolland, Y., 2012. Evolution of gravity-driven rock slope failure and associated fracturing: Geological analysis and numerical modelling. Tectonophysics, 526-529, 157-166.

Brisset, E., Guiter, F., Miramont, C., Revel, M., Anthony, E.J., Belhon, C., Arnaud, F., Malet, E. and de Beaulieu, J.-L., 2015. Lateglacial/Holocene environmental changes in the Mediterranean Alps inferred from lacustrine sediments. Quaternary Sci. Rev., 110, 49-71.

Brocard, G. and van der Beek, P., 2006. fluence of incision rate, rock strength, and bedload

supply on bedrock river gradients and valley-flat widths: Field-based evidence and calibrations from western Alpine rivers (southeast France). Geol. Soc. Am. Bull., 398, 101-126.

Burbank, D.W., Leland, J., Fielding, E., Anderson, R.S., Brozovic, N., Reid, M.R. and Duncan, C., 1996. Bedrock incision, rock uplift and threshold hillslopes in the northwestern Himalayas. Nature, 379, 505-510.

Burbank, D. W., 2002. Rates of erosion and their implications for exhumation. Mineralogical Magazine, 66, 1, 25-52.

Cardinal, T., Audin, L., Rolland, Y., Schwartz, S., Petit, C., Zerathe ,S., Borgniet, L., Braucher, R., Nomade, J., Dumont, T., Guillou, V. and ASTER team, 2021. Interplay of fluvial incision and rockfalls in shaping periglacial mountain gorges. Geomorphology, 381, 107665.

Cardinal, T., Rolland ,Y., Petit C., Audin, L., Schwartz, S., Valla, P. G., Zerathe, S., Braucher, R. and ASTER Team. Fluvial bedrock gorges as markers for Late-Quaternary tectonic and climatic forcing in the Southwestern Alps. Geomorphology, under review.

Church, M. and Ryder, J.M., 1972. Paraglacial sedimentation: A consideration of fluvial processes conditionned by glaciation. GSA Bulletin, 83, 3059-3072.

Cook, K. L., Turowski, J. M. and Hovius, N., 2013. A demonstration of the importance of bedload transport for fluvial bedrock erosion and knickpoint propagation. Earth Surf. Process. Landforms, 38, 683-695.

Cossart, E., Braucher, R., Fort, M., Bourlès, D.L. and Carcaillet, J., 2008. Slope instability in relation to glacial debuttressing in alpine areas (Upper Durance catchment, southeastern France): evidence from field data and 10Be cosmic ray exposure ages. Geomorphology, 95, 3-26.

Crosby, B. T. and Whipple, K. X., 2006. Knickpoint initiation and distribution within fluvial networks: 236 waterfalls in the Waipaoa River, North Island, New Zealand. Geomorphology, 82, 16-38.

Darnault, R., Rolland, R., Rolland, Y., Bourlès, D., Revel, M., Sanchez, G. and Bouissou, S., 2012. Timing of the last deglaciation revealed by receding glaciers at the Alpine-scale: impact on mountain geomorphology. Quaternary Sci. Rev., 3, 127-142.

DiBiase, R. and Whipple, K.X., 2011. The influence of erosion thresholds and runoff variability on the relationships among topography, climate, and erosion rate. J. Geophys. Res., 116, F04036.

Dixon, J. D., 2011. Deceptively old Alpine gorges. Nat. Geosci., 4, 8–9.

Federici, P. R., Ribolini, A. and Spagnolo, M., 2016. Glacial history of the Maritime Alps from the Last Glacial Maximum to the Little Ice Age, in Hughes P. D. and Woodward J. C., eds., Quaternary Glaciation in the Mediterranean Mountains. Geological Society, London, Special Publications, 433, 135-159.

Fox, M., Leith, K., Bodin, T., Balco, G. and Shuster, D.L., 2015. Rate of fluvial incision in the Central Alps constrained throught joint inversion of detrital 10Be and thermochronometric data. Earth Planet. Sci. Lett., 411, 27-36.

Garwood, E. J., 1910. Features of Alpine scenery due to glacial protection. Geographic. J., 36, 3, 310–39.

Glotzbach, C., van der Beek, P. A. and Spiegel, C., 2011. Episodic echumation and relief growth in the Mont Blanc massif, western Alps from numerical modelling of thermochronology. Earth Planet. Sci. Lett., 304, 417-430.

Glotzbach, C., van der Beek, P., Carcaillet, J. and Delunel, R., 2013. Deciphering the driving forces of erosion rates on millennial to million-year timescales in glacially impacted landscapes: An example from the Western Alps. J. Geophys. Res.: Earth Surface, 118, 1491-1515.

Hallet, B., Hunter, L. and Bogen, J., 1996. Rates of erosion and sediment evacuation by glaciers: A review of field data and their implications. Glob. Planet. Change 12, 213-235.

Hartshorn, K., Hovius, N., Slingerland, R., Dade, B. and Lin, J., 2001. Linking observations and physics of fluvial bedrock erosion in an active mountain belt, east central Taiwan. Eos (Transactions, American Geophysical Union), 82, F585.

Heiri, O., Koinig, K.A., Spötl, C., Barrett, S., Brauer, A., Drescher-Schneider, R., Gaar, D., Ivy-Ochs, S., Kreshner, H., Luetscher, M., Moran, A., Nicolussi, K., Preusser, F., Schmidt, R., Schoeneich, P., Schwörer, C., Sprafke, T., Terhorst, B. and Tinner, W., 2014. Paleoclimate records 60-8 ka in the Austrian and Swiss Alps and their forelands. Quaternary Sci. Rev., 106, 186-205.

Herman, F., Seward, D., Valla, P.G., Carter, A., Kohn, B., Willet, S.D. and Ehlers, T.A., 2013. Worldwide acceleration of mountain erosion under a cooling climate. Nature, 504, 423-426.

Hilger, P., Hermanns, R.L., Czekirda, J.,Myhra, K.S., Gosse, J.C. and Etzelmüller, B., 2021. Permafrost as a first order control on long-term rock-slope deformation in (Sub-) Arctic Norway. Quat. Sci. Rev. 251, 106718.

Hinderer, M., 2001. Late Quaternary denudation in the Alp, valley and lake filling and modern river loads. Geodinamica Acta, 14, 231-263.

Hughes, P. D. and Gibbard, P. L., 2015. A stratigraphical basis for the Last Glacial Maximum (LGM). Quaternary International, 383, 174–185.

Ivy-Ochs, S., Kerschner, H., Reuther, A., Maisch, M., Sailer, R., Schaefer, J., Kubik, P.W., Synal, H. and Schlüchter, C., 2006. The timing of glacier advances in the northern European Alps based on surface exposure dating with cosmogenic 10Be, 26Al, ^{36}Cl, and 21Ne, in Siame L. L., Bourlès D. L., and Brown E. T., eds., In Situ–Produced Cosmogenic Nuclides and Quantifi cation of Geological Processes: Geological Society of America Special Paper, 415, 43–60.

Ivy-Ochs, S., Kerschner, H., Reuther, A., Preusser, F., Heine, K., Maisch, M., Kubik, P.W. and Schlüchter, C., 2008. Chronology of the last glacial cycle in the European Alps. J. Quaternary Sci., 23, 559-573.

Ivy-Ochs, S., Poschinger, A. V., Synal, H-A. and Maisch, M., 2009. Surface exposure dating of the Flims landslide, Graubünden, Switzerland. Geomorphology, 103, 104-112.

Jansen, J. D., Codilean, A. T., Bishop, P. and Hoey, T. B., 2010. Scale Dependence of Lithological Control on Topography: Bedrock Channel Geometry and Catchment Morphometry in Western Scotland. The Journal of Geology, 118, 3, 223-246.

Jansen, J. D., Fabel, D., Bishop, P., Xu, S., Schnabel, C. and Codilean, A. T., 2011. Does decreasing paraglacial sediment supply slow knickpoint retreat? Geology, 39, 6, 543-546.

Johnson, J. P. L., Whipple, K. X. and Sklar, L. S., 2010. Contrasting bedrock incision rates from snowmelt and flash floods in the Henry Mountains, Utah. GSA Bulletin, 122, 1600-1615.

Jorda, M., Rosique, T. and Évin, J., 2000. Données nouvelles sur l'âge du dernier maximum glaciaire dans les Alpes méridionales françaises. Compte Rendu de l'Académie des Sciences Paris. Sciences de la Terre et des Planètes/Earth and Planetary Sciences 331, 187-193.

Julian, M., 1980. Les Alpes franco-italiennes, Etude Géomorphologique. Aix-Marseille Université.

Kaplan, M. R., Hein, A. S., Hubbard, A. and Lax, S. M., 2009. Can glacial erosion limit the extent of glaciation? Geomorphology, 103, 172-179.

Koppes, M. N. and Montgommery, D. R., 2009. The relative efficacy of fluvial and glacial erosion over modern to orogenic timescales. Nature Geosciences, 2, 644-647.

Leland, J., Reid, M. R., Burbank, D. W., Finkel, R. and Caffee, M., 1998. Incision and differential bedrock uplift along the Indus River near Nanga Parbat, Pakistan Himalaya, from ^{10}Be and ^{26}Al exposure age dating of bedrock straths. Earth Planet. Sci. Lett., 154, 93–107.

Lickorish, H. W. and Ford, M., 1998. Sequential restoration of the external Alpine Digne thrust system, SE France, constrained by kinematic data and synorogenic sediments. Geol. Soc. Spec. Publ., 134, 189–211.

Federici, P. R., Granger, D. E., Ribolini, A., Spagnolo, M., Pappalardo, M. and Cyr, A. J., 2012. Last Glacial Maximum and the Gschnitz stadial in the Maritime Alps according to ^{10}Be cosmogenic dating. Boreas, 41, 277–291.

Magrani, F., Valla, P. G. and Egholm, D., 2021. Modelling alpine glacier geometry and subglacial erosion patterns in response to contrasting climatic forcing. Earth Surf. Process. Landforms, 47, 4, 1-19.

Mariotti, A., Blard, P.-H., Charreau, J., Toucanne, S., Jorry, S.J., Molliex, S., Bourlès, D.L., Aumaître, G. and Keddadouche, K., 2021. Nonlinear forcing of climate on mountain denudation durings glaciations. Nat. Geosci., 14, 16-22.

Meigs, A., Krugh, W.C., Davis, K. and Bank, G., 2006. Ultra-rapid landscape response and sediment yield following glacial retreat, Icy Bay, soutehrn Alaska. Geomorphology, 78, 207-221.

Montgomery, D.R. and Korup, O., 2011. Preservation of inner gorges through repeated Alpine glaciations. Nat. Geosci., 4, 1, 62–67.

Norton, K.P., Abbühl, L.M. and Schlunegger, F., 2010. Glacial conditioning as an erosional driving force in the Central Alps. Geology, 38, 7, 655-658.

Ouimet, W.B., Whipple, K.X., Crosby, B.T., Johnson, J.P. and Schildgen, T.F., 2008. Epigenetic gorges in fluvial landscapes. Earth Surf. Proc. Land., 33, 1993-2009.

Petit, C., Rolland, Y., Braucher, R., Bourlès, D., Guillou, V. and Petitperrin, V., 2019. River incision and migration deduced from ^{36}Cl cosmic-ray exposure durations: The Clue de la Cerise gorge in southern French Alps. Geomorphology, 330, 81-88.

Pratt, B., Burbank, D.W., Heimsath, A. and Ojha, T., 2002. Impulsive alluviation during early Holocene strengthened monsoons, central Nepal Himalaya. Geology, 30, 10, 911-914.

Ravanel, L., Allignol, F., Deline, P., Gruber, S. and Ravello, M., 2010. Rockfalls in the Mont Blanc Massif in 2007 and 2008. Landslides, 7, 4, 493–501

Rolland, Y., Petit, C., Saillard, M., Braucher, R., Bourlès, D., Darnault, R., Cassol, D. and

ASTER Team, 2017. Inner gorges incision history: A proxy for deglaciation ? Insights from Cosmic Ray Exposure dating (^{10}Be and ^{36}Cl) of river-polished surfaces (Tinée River, SW Alps, France). Earth Planet. Sci. Lett., 457, 271-281.

Rolland, Y., Darnault, R., Braucher, R., Bourlès, R., Petit, C., Bouissou, S. and ASTER Team, 2019. Deglaciation history at the Alpine-Mediterranean transition (Argentera-Mercantour, SW Alps) from 10Be dating of moraines and glacially polished bedrock. Earth Surf. Process. Landsforms, 45, 2, 393-410.

Ruszkiczay-Rüdiger, Z., Kern, Z., Urdea, P., Madarász, B., Braucher, R. and ASTER Team, 2021. Limited glacial erosion during the last glaciation in mid-latitude cirques (Retezat Mts, Southern Carpathians, Romania). Geomorphology, 384, 107719

Saillard, M., Petit, C., Rolland, Y., Braucher, R., Bourlès, D. L., Zerathe, S., Revel, M. and Jourdon, A., 2014. Late Quaternary incision rates in the Vésubie catchment area (Southern French Alps) from in situ-produced ^{36}CI cosmogenic nuclide dating: Tectonic and climatic implications. J. Geophy. Res.. Earth Surface, 119, 1121-1135.

Salcher, B. C., Kober, F., Kissling, E. and Willet, S. D., 2014. Glacial impact on short-wavelength topography and long-lasting effects on the denudation of a deglaciated mountain range. Global and Planetary Change, 115, 59-70.

Sanchez, G., Rolland, Y., Jolivet, M., Brichau, S., Corsini, M. and Carter, A., 2011. Exhumation controlled by transcurrent tectonics: the Argentera–Mercantour massif (SW Alps). Terra Nova, 23, 2, 116-126.

Sanchez, G., Rolland, Y., Corsini, M., Braucher, R., Bourlès, D., Arnold, M. and Aumaître, G., 2010. Relationships between tectonics, slope instability and climate change: Cosmic Ray exposure dating of active faults, landslides and glacial surfaces in the SW Alps. Geomorphology, 107, 1-2, 1-13.

Savi, S., Norton, K.P., Picotti, V., Akçar, N., Delunel, R., Brardinoni, F., Kubik, P. and Schlunegger, F., 2014. Quantifying sediment at the end of the last glaciation: Dynamic reconstruction of an alpine debris-flow fan. GSA Bulletin, 126, 5-6, 773-790.

Schaller, M., Hovius, N., Willett, S.D., Ivy-Ochs, S., Synal, H.-A. and Chen, M.-C., 2005. Fluvial bedrock incision in the active mountain belt of Taiwan from in situ-produced cosmogenic nuclides. Earth Surf. Proc. Land., 30, 955-971.

Schimmelpfennig, I., Schaefer, J. M., Akçar, N., Ivy-Ochs, S., Finkel, R. C. and Schlüchter, C., 2012. Holocene glacier culminations in the Western Alps and their hemispheric relevance. Geology, 40, 891–894.

Schwartz, S., Zerathe, S., Jongmans, D., Baillet, L., Carcaillet, J., Audin, L., Dumont, T., Bourlès, D., Braucher, R. and Lebrouc, V., 2017. Cosmic ray exposure dating on the large landslide of Séchilienne (Western Alps): A synthesis to constrain slope evolution. Geomorphology, 278, 329-344.

Schweizer, G., 1968. Le tardiglaciaire et le niveau des neiges permanentes dans les hautes montagnes des Alpes-Maritimes. L'exemple du bassin supérieur de la Tinée. Méditerranée, 9, 23-40.

Seidl, M. A. and Dietrich, W. E., 1992. The problem of channel erosion into bedrock. Catena Supp., 23, 101-124.

Sklar, L. S. and Dietrich, W. E., 2001. Sediment and rock strength controls on river incision into bedrock. Geology, 29, 12, 1087-1090.

Stock, J.D., Montgomery, D.R., Collins, B.D., Dietrich, W.E. and Sklar, L., 2005. Field measurements of incision rates following bedrock exposure: implications for process controls on the long profiles of valleys cut by rivers and debris flows. GSA Bulletin, 117, 11-12, 174-194.

Tricart, J. and Soons, J. M., 1960. A subglacial gorge: La Gorge du Guil (Hautes-Alpes). J. Glaciol., 3, 646-651.

Tucker, G. E. and Whipple, K. X., 2002. Topographic outcomes predicted by stream erosion models: Sensitivity analysis and intermodel comparison. J. Geophy. Res., 107, B9, ETG 1-1-ETG 1-16.

Valla, P.G., van der Beek, P.A. and Carcaillet, J., 2010. Dating bedrock gorge incision in the French Western Alps (Ecrin-Pelvoux massif) using cosmogenic ^{10}Be. Terra Nova, 22, 18-25.

Valla, P.G., Shuster, D.L. and van der Beek, P.A., 2011. Significant increase in relief of the European Alps during mid-Pleistocene glaciations. Nat. Geoscience, 4, 688–692.

Wanner, H., Solomina, O., Grosjean, M., Ritz, S.P. and Markéta, J., 2011. Structure and origin of Holocene cold events. Quaternary Sci. Rev., 30, 3109-3123.

Wanner, H., Mercolli, L., Grosjean, M. and Ritz, S.P., 2015. Holocene climate variability and change: a data-based review. J. Geol. Soc. London, 172, 254-263.

Willet, S.D., 1999. Orogeny and orography: the effects of erosion on the structure of mountain belts. J. Geophy. Res., 104, B12, 28 957-28 981.

Zerathe, S., Lebourg, T., Braucher, R. and Bourlès, D., 2014. Mid-Holocene cluster of larger-scale landslides revealed in the Southwestern Alps by ^{36}Cl dating. Insight on an Alpine-

Scale landslide activity. Quaternary Sci. Rev., 90, 106-127.

Chapitre 6 : The interplay of geology, climate and tectonics on river incision: the example of the High Verdon Gorges, Southwestern French Alps

Résumé

La distinction entre les forçages court-terme et long-terme sur l'incision fluviale, ainsi que la compréhension de l'influence locale (lithologie et morphologie du chenal) et globale (structures tectoniques) dans la variation spatiale de l'efficacité de l'incision, sont des débats actuels. Pour apporter un nouvel éclairage sur ces questions, nous avons choisi d'étudier les Hautes Gorges du Verdon (HVG), situées dans l'avant-pays des Alpes du Sud-Ouest. Nous y avons échantillonné des surfaces polies pour la datation CRE ^{36}Cl, ce qui nous a permis de contraindre un taux d'incision long-terme allant de 0,06 à 0,2 mm/an entre 60 et 15 ka. Comparés aux taux de soulèvement et de dénudation régionaux, ces taux soulignent le rôle du soulèvement tectonique comme principal moteur de l'incision du Verdon au Quaternaire supérieur. Cette incision long-terme, extrapolée au reste des parois verticales de la gorge d'environ 300 m de haut, suggère que la formation des HVG a commencé il y a environ 1,5 à 2 Ma, bien que le réseau de drainage du bassin versant du Verdon ait pu se former plus tôt, lors de la crise de salinité messinienne.

The interplay of geology, climate and tectonics on river incision: the example of the High Verdon Gorges, Southwestern French Alps.

Cardinal, T.[1], Petit, C.[1], Rolland, Y.[2-3], Schwartz, S.[2], Valla, P.G.[2], Scalabrino, B.[1], Audin, L.[2], Bertauts, M.[2], Zerathe, S.[2], Thiéblemont, D.[4], Braucher R.[5] and ASTER Team[5]

[1] *Université Côte d'Azur, CNRS, Observatoire de la Côte d'Azur, IRD, Géoazur, 250 rue Albert Einstein, Sophia Antipolis 06560 Valbonne, France*

[2] *Université Grenoble Alpes, Université Savoie Mont Blanc, CNRS, IRD, Université Gustave Eiffel, ISTerre, 38000 Grenoble, France*

[3] *Université Savoie Mont Blanc, CNRS, Pôle Montagne, Edytem, F-73370 Le Bourget-du-Lac, France*

[4] *DGR/CGEO, BRGM, B.P. 6009, 45060 Orléans, Cedex, France*

[5]*Université Aix-Marseille, CNRS-IRD-Collège de France-INRAE, UM 34 CEREGE, Technopôle de l'Environnement Arbois-Méditerranée, BP80, 13545 Aix-en-Provence, France*

**ASTER Team: Georges Aumaître, Didier L. Bourlès†, Karim Keddadouche*

Abstract

Deciphering the impact of short-term or long-term forcing on fluvial incision, as well as understanding the influence of local (channel lithology and morphology) and global (tectonic motions) parameters in the spatial variation of incision efficiency, are ongoing geomorphological research fields. To shed new light on these issues, we chose to study the "Hautes Gorges du Verdon" (High Verdon Gorges or HVG), located in the foreland of the South-Western Alps. We collected 24 samples along three polished surfaces for Cosmic Ray Exposure (CRE) ^{36}Cl dating, which allowed us to constrain short-term incision rates ranging from 0.06 to 0.2 mm/yr between 60 and 15 ka. Compared to known regional uplift and denudation rates, incision rates obtained in the HVG suggest tectonic or isostatic uplift as the

main driver of Verdon River incision in the Late Quaternary. This comparison allows us to propose that the downcutting of the Verdon Gorges started approximatively 1.5 to 2 Ma ago, even if the drainage network of the Verdon catchment area could have been shaped earlier, during the Messinian salinity crisis.

1. Introduction

Rivers, through their erosive power, play a key role in adjusting the landscapes to multiple forcings such as tectonic uplift, sea-level fluctuations or climate variations (Whipple et al., 2004; Whipple & Tucker, 1999). Indeed, bedrock channels set the base level for adjacent hillslopes and thus control long-term relief evolution and denudation rates (e.g., Whipple et al., 2000). Rivers not only control mass wasting by undercutting hillslopes in mountainous areas (Howard et al., 1994), they also transport the resulting sediments towards depositional basins in mountain forelands (Guerit et al., 2016).

The rate at which river incision shapes landscapes is highly variable and is controlled by processes operating at different temporal and spatial scales (Daniels, 2008). These processes interact with each other, and the study of short-term ($<10^3$ yr) processes may allow to better understand their respective contributions together with longer-term forcings ($>10^4$ to 10^5 yr). For example, as climate variations control water discharge in rivers (Ely, 1997), understanding how punctual flood events influence bedrock incision rates can provide insights on the long-term landscape sensitivity to climate changes (10^3-10^4 yrs, Molnar; 2001; Hartshorn et al., 2002; Lague et al., 2005). Through the recurrence of short-term processes ($<10^3$ yr), rivers are irrevocably adjusting their incision rates to long-term tectonic uplift rates in order to achieve an ideal steady state in which vertical incision equals to rock uplift (Whipple & Tucker, 1999; Wobus et al., 2006). However, deciphering the dominant forcing if any (e.g., tectonic *vs.* climate) remains difficult (Herman et al., 2013).

The so-called “external” forcings control river erosion by providing the necessary tools for bedrock incision: water discharge and sediment availability. While the first provides the energy for sediment transport, the latter acts as a ‘mechanical tool’ for rivers to incise their bedrock (Sklar and Dietrich, 2006; Jansen et al., 2011) . However, several studiesshowed that an excessive amount of sediments will, to the contrary, prevent incision by overloading the river, raising the channel bed by aggradation and therefore temporarily shielding the bedrock (Sklar and Dietrich, 2001; Hartshorn et al., 2002). Furthermore, the efficiency of bedrock incision is controlled by intrinsic morphological and geological features(lithology, slope, with/depth ratio, local relief (Schumm, 1977). The degree of jointing and the weathering state of the bedrock also influence river incision rates (e.g., Whipple et al., 2000). These added elements together act as a “geological factor” that dictates the locus of erosion and its efficiency (Cowie et al., 2008; Hartshorn et al., 2002; Herman et al., 2013; Sklar and Dietrich, 2001).

In fold-and-thrust belts, the folding of sedimentary layers with a distinct resistance to erosion produces complex river network geometries with alternating strike-parallel and perpendicular stream sections defining a transverse drainage pattern (Oberlander, 1965; Stokes et al., 2008; Twidale, 2004). Beside these local heterogeneities, large-scale regional horizontal tectonic movements can be detected in the shape of the river network by systematic changes in flow directions resulting from the planar deformation of the river network with its substrate (Guerit et al., 2016). On the other hand, vertical tectonic motions of the bedrock together with along-channel variations in the rock resistance to erosion will affect both the river longitudinal profile and the shape of surrounding hillslopes. The complete understanding of interactions between such small- and large-scale parameters and incision processes over large spatial and temporal scales is not yet achieved (Jansen et al., 2011).

With the goal to shed some new light on the response of a river system to internal and external factors, we choose to study the High Verdon Gorge (HVG), located in the Southwestern Alps foreland (Figure 1A). The Verdon catchment presents the advantage of cross-cutting the whole Meso-Cenozoic sedimentary sequence of the southern subalpine fold-and-thrust belt, including highly resistant upper Jurassic limestones in which the HVG were carved. The Verdon River headwaters are located in an area previously covered by Quaternary glaciers (Brisset et al., 2015), while its outlet in the Durance river is near the junction between the Alpine deformation front and the Valensole foreland basin (Figure 1B). In this paper, we present new, and use some published (Cardinal et al., 2022), ^{36}Cl Cosmic Ray Exposure (CRE) datings of river-polished surfaces in the HVG and interpret them for the recent (Late Quaternary) period, and discuss a long-term (Pliocene to Quaternary) evolutionary scenario of the Verdon River in its Alpine and Mediterranean context.

2. Context

2.1. Structural context and drainage patterns of the Verdon River

The study area is located upstream of the foreland basin of the Southwestern European Alps (Figure 1A and B). The Castellane fold-and-thrust belt (also called the “Castellane Arc”) was first formed during the Pyrenean collisional phase (Cretaceous to Eocene) and underwent reactivation during the Oligocene due to the onset of Alpine collision and SW propagation of the Penninic front, which resulted in the development of an Oligocene foredeep filled with turbiditic sequences (Espurt et al., 2012; Jourdon et al., 2014). During the Miocene, compressional deformation propagated outwards and caused the uplift of the sedimentary wedge together with the flexure and filling of the Valensole molassic basin in the foreland (Figure 1B). This deformation phase ended with the underthrusting of Neogene molassic sequences below the Digne Nappe during Late Miocene times (Schwartz et al., 2017). The Valensole basin is filled with marine to continental conglomeratic sequences, and erosional

unconformities have been tentatively correlated to the Mio-Pliocene transition marked by the Messinian Salinity Crisis (Clauzon et al., 1996, 2011; Hippolyte et al., 2011). The last marine sequences found in the Valensole basin are dated as Late Tortonian and correspond to shallow water molasses (Ford et al., 1999; Ford and Lickorish, 2004). Gravel deposits mark the end of sedimentation in the Valensole basin, which upper surface has been dated around 1.8 to 2 Ma; however, towards the Alpine front, alluvial cones continue to prograde on the basin, ending with the Balene breccia formation dated at 0.7 to 1 Ma (Dubar, 1984; Dubar et al., 1998). The arrival of coarse, detritic deposits in the Valensole basin in the early Quaternary (ca. 2.4 Ma) is interpreted as reflecting active tectonics on the Castellane Arc and/or cooler climatic conditions (Dubar, 1984; Dubar et al., 1998)

With a length of 166.5 km and a catchment area of 2218 km², the Verdon River is the main tributary of the Durance River. The Verdon River and its catchment have their headwaters in the Helminthoid flysch nappes (~2500 m. a. s. l.) and run towards the south through the unmetamorphosed Mesozoic sedimentary cover of the Alpine foreland. Near the city of Castellane, the Verdon course takes a turn upon encountering the outer folds and thrusts of the Castellane Arc and consequently flows in a W-E direction, wandering around and cutting across the fold axes (Chardonnet, 1943; Jorda, 1975). From this point, the Verdon cuts its way through Jurassic limestones in which it dug one of the most impressive European gorge, the High Verdon Gorges (HVG, Figure 1A). Downstream, the Verdon River meets the Valensole Plateau and follows the Valensole conglomerate regular slope while repeatedly crossing some Jurassic limestone outcrops (Goguel, 1935), until it reaches its outlet in the Durance River (255 m.a.s.l., Figure 1B). The longitudinal profile of the Verdon River reflects well lithological variations encountered along the channel length. Indeed, significant convexity can be seen where the river has incised the massive Tithonian limestone and formed the HVG, whereas upstream and

downstream, the river profile, although modified by artificial dam lakes, is overall concave (Figures 1C and 2).

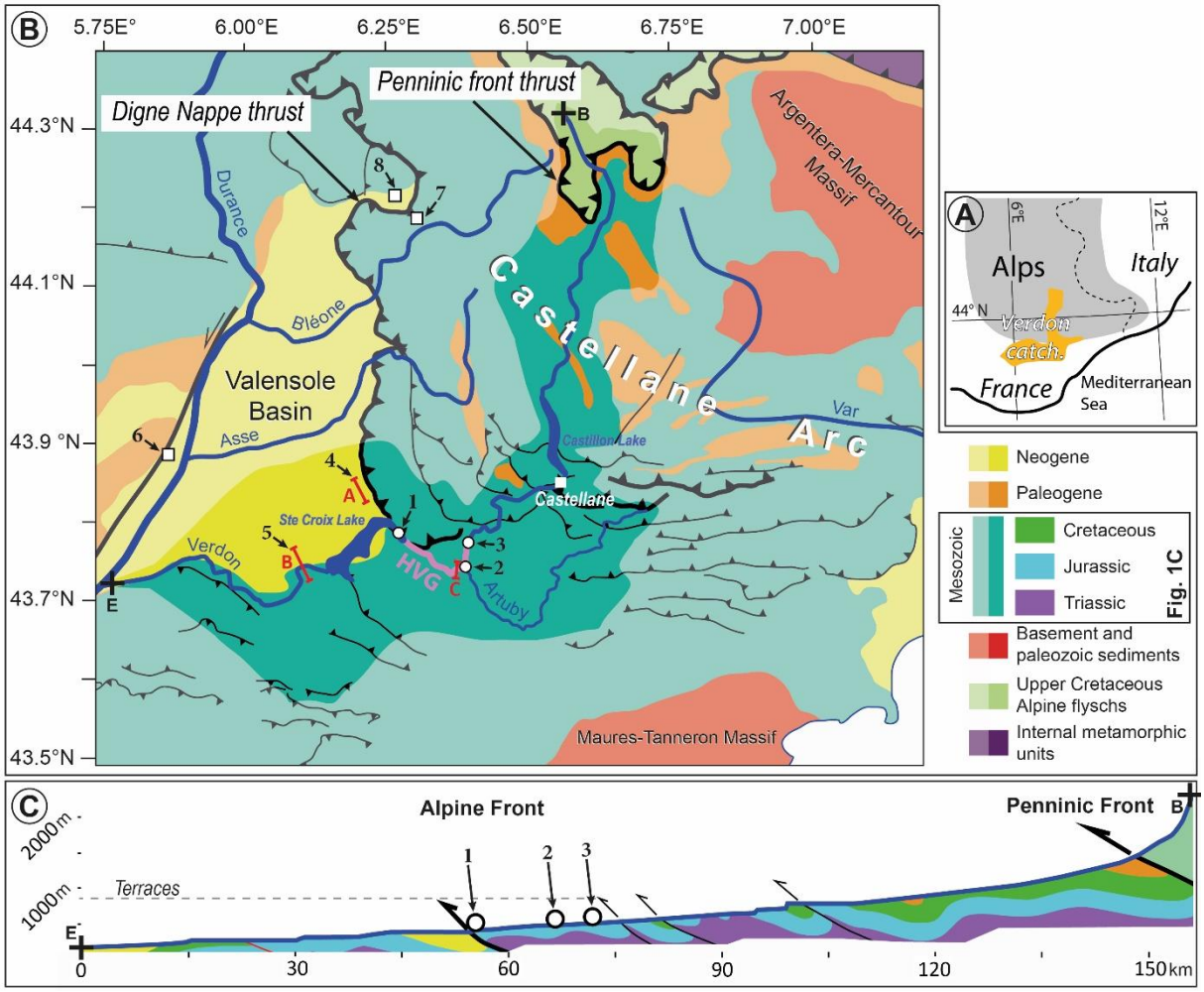

Figure 6-1 : A: Location of the Verdon Catchment in the Southwestern Alps. B: Simplified geological map of the study area. The Verdon catchment area is underlined by brighter colours, corresponding to the colours in the legend and on the cross-section. The High Verdon Gorge (HVG) are highlighted along the river in pink. C: Schematic geological cross-section along the Verdon River longitudinal profile. Black crosses indicate the beginning (B) and the end (E) of the river profile. Note that in the profile Cretaceous, Jurassic and Triassic periods are distinguished from the more general term "Mezosoic" used in the geological map B, as highlighted in the legend. The Black outlined circles 1 to 3 on the map and on the profile indicate the sampling sites. Thick red lines A, B, and C show the location of the topographic profiles shown on Figure 10. Locations numbered 4 to 8 are incision or uplift rates from literature which are discussed in Section 5.4

The origin of the Verdon River course is a matter of debate. Indeed, the upstream portion of the river trends roughly parallel to the N-S direction of tectonic structures (Goguel, 1935; Jorda, 1975). Further its middle part crosscuts sub-perpendicularly the fold axes affecting the Jurassic cover, while encompassing the upper part of the HVG and the southern boundary of the Castellane Arc (Chardonnet, 1943), from the city of Castellane to the junction between the

Verdon and Artuby rivers (Figure 1B). To explain these cross-cutting relationships, many authors agree on the hypothesis that the Verdon River course is, in the area, antecedent (Blanchard, 1915; Chardonnet, 1943; Goguel, 1935; Nicod, 2004). This hypothesis implies that the Verdon River was originally flowing on a rather low-relief peneplane and was then forced into incising the underlying Tithonian limestones during a Cenozoic tectonic uplift episode (Chardonnet, 1943).

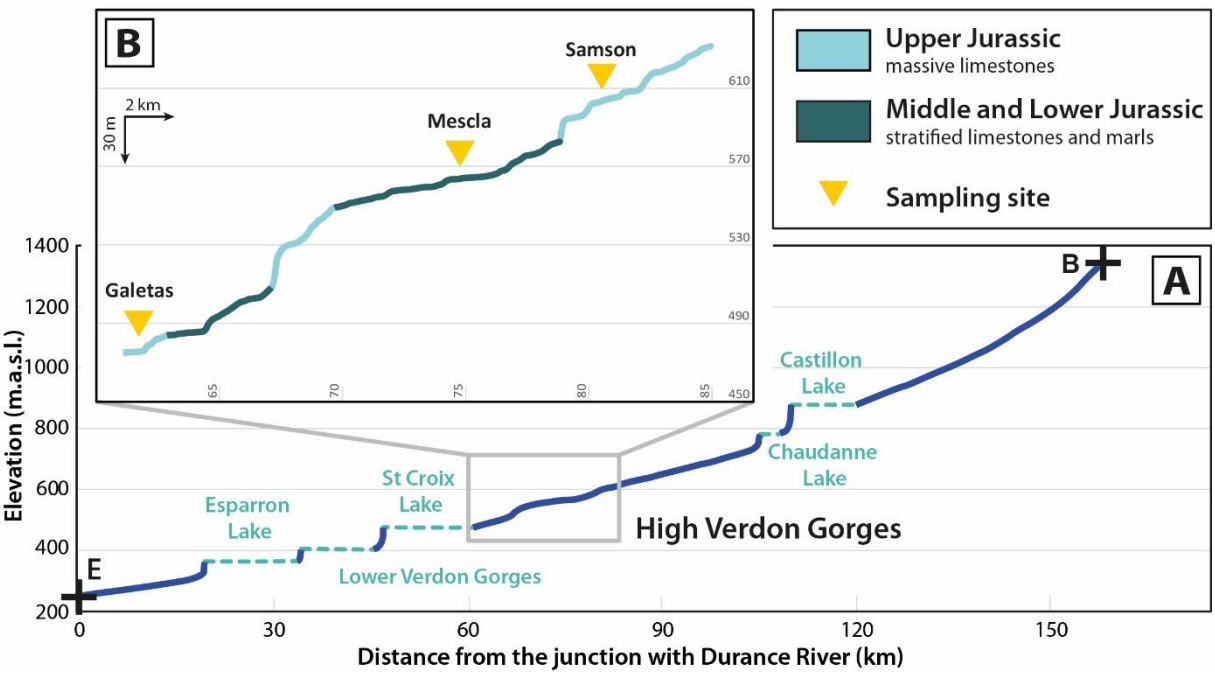

Figure 6-2 : A: Verdon River profile and location of the HVG and dam lakes. B: Longitudinal profile of the Verdon River along the HVG, lithology schematic outcrop and location of the sampled sites. Black crosses indicate the beginning (B) and the end (E) of the river profile (see location of these point in Figure 1B).

2.2. Catchment morphology

The overall "L shape" of the Verdon catchment suggests possible drainage captures (Blanchard, 1915) and/or a complex adaptation to a deformed terrain (Goguel, 1935). From a closer look, the Verdon catchment and long river profile (Figure 1) can be divided into three portions:

- The upper Verdon Valley, from the headwaters to downstream of Castellane town;
- The HVG, knickzone interrupting the overall concave profile (Figure 2A);

- The lower Verdon Valley, from the Sainte Croix Lake to its junction with the Durance River.

Regarding the upper section, the Verdon River catchment width decreases downstream as a result of massive captures from the Asse and Bléone rivers to the West and from the Var River to the East (Blanchard, 1915; Chardonnet, 1943; Jorda, 1975). These authors considered that the HVG constitutes a abnormally high local base level for the upper Verdon. The HVG forms a limestone (Tithonic) lithological knickpoint which likely mitigates the propagation of incision upstream, as observed in several studies (Crosby and Whipple, 2006, Jansen et al., 2010, Bishop and Goldrick, 2010, Cardinal et al., 2022). Therefore, undergoing slower incision, the upper Verdon main elevation remains high, which makes it vulnerable to capture by the more competitively erosive surrounding catchments.The high mean elevation also allowed extensive glacier coverage in the upper Verdon catchment. For comparison, the Würmian glaciers extent reached a length of 40 km along the Verdon River, against only 20 km along the Var River. The HVG therefore has a high impact on the morphological evolution of the upstream catchment. Between the Sainte Croix and Castillon lakes, the HVG course displays a complex pattern (Figure 1B). Downstream, the Verdon drainage area then considerably grows from the contribution of the Artuby River (from 962 km² to 1300 km²) and the incorporation of the Valensole Plateau drainage network.

2.3. High Verdon Gorges morphology

The 26 km-long HVG (Figure 3A) appears as a deep cut in the massive limestones of the Mesozoic sequence. The cohesive nature of the bedrock results in maintaining steep walls with mean height around 300 m (Figure 3B and C), which makes it one of the most impressive mountain gorges in western Europe. However, the limestones show different facies along the gorges, from the compact late Jurassic to early Cretaceous Tithonian bars with limited jointing, to middle-upper jurassic limestones and marls with a higher degree of bedding, fracturing and

weathering (Figure 2). The lithological variations are visible on the river profile in the HVG, where Tithonian limestone outcrops are highlighted by strong knickpoints (Figure 2B). Furthermore, the gorge transversal profile is alternatively wide and narrow (Figure 3A), in agreement with the successiveoutcropping of middle-upper Jurassic and Tithonian limestones, respectively (Martel, 1908), demonstrating the contrast in rock resistance along the gorges.

A combination of rock falls, fluvial and karstic erosive processes operates inside the gorges (Chardonnet, 1943; Martel, 1908; Nicod, 2004). The gorge walls are affected by rock falls, creating scree slopes overgrown by vegetation at the foot of weak lithology walls and large boulder accumulations in the riverbed overlooked by resistant lithology walls. Intense fluvial erosion is visible through the widespread presence of pot-holes and polished surface, sometimes preserved high up in the steep walls but especially along the riverbanks and within the boulder accumulation in the river bed (Figure 4). Locally, the development of karst network results in open cavities and large overhangs (called “baumes”; Figure 4). These cavities in turn guide the course of the river and focus the fluvial erosion. The karstic network is also intricated with the current riverbed. Indeed, a part of the river flow is incorporated into the subsurface karst system at “La Mescla” (Figure 3A, Blanchard, 1915; Fabre and Nicod, 1978).

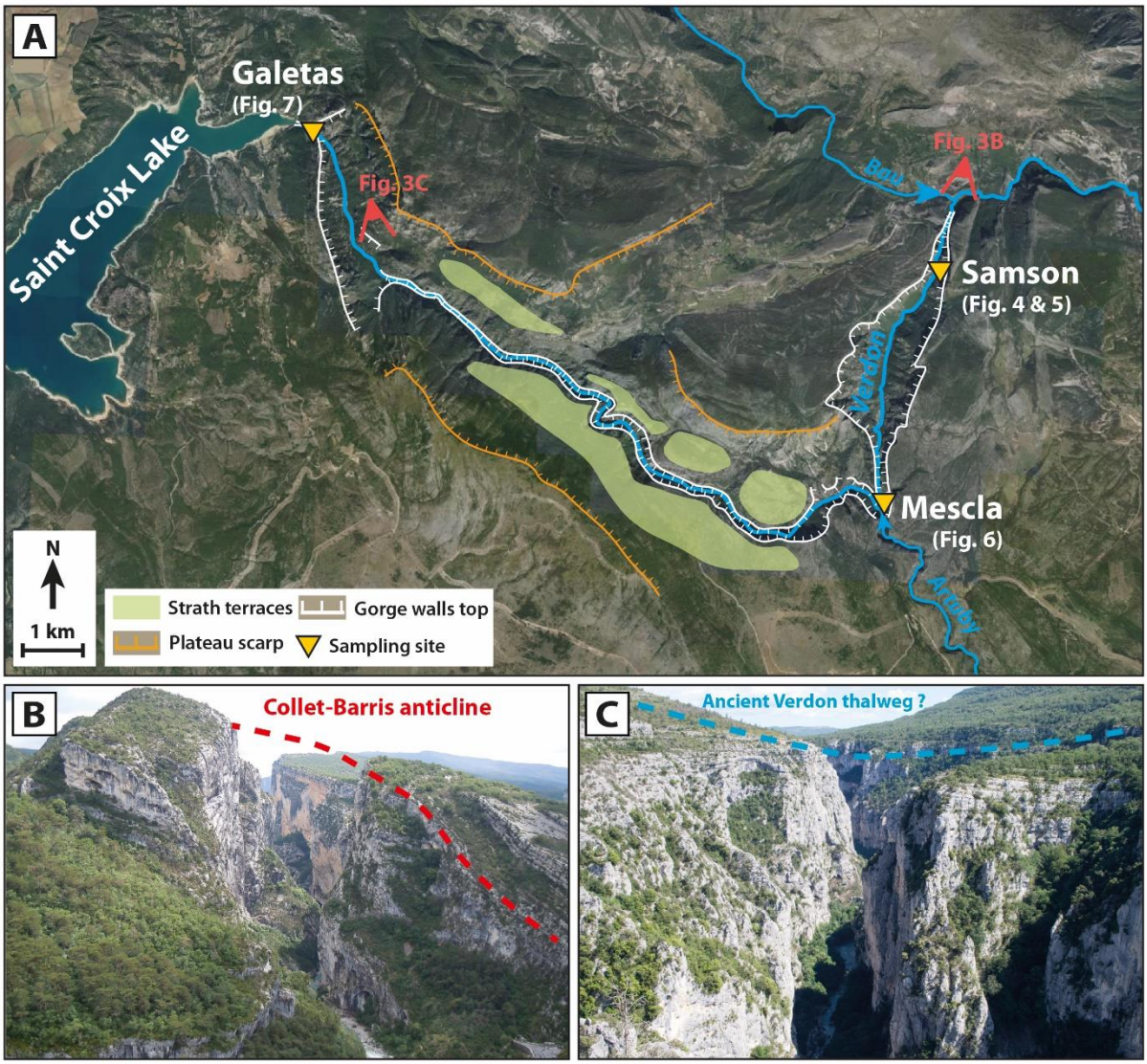

Figure 6-3 : A: Aerial image (IGN) of the HVG with the main topographic features and the location of the sampled sites and photos point of view (B and C). B: Samson Corridor and location of the Collet-Baris anticline. C: Location of the possible ancient Verdon thalweg position.

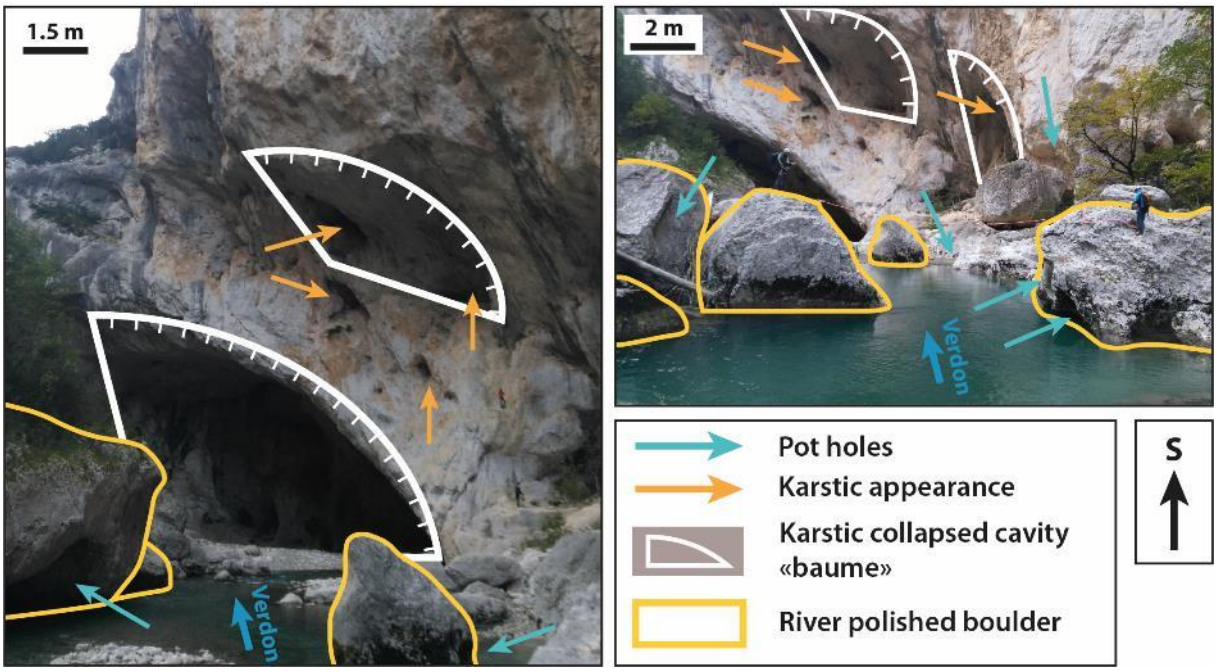

Figure 6-4 : Field pictures of the High Verdon Gorges (at the vicinity of the Samson sampling site) and highlight of the main geomorphological erosion features.

2.4. Incision of the High Verdon Gorges

The top of the HVG vertical walls are marked by a flat erosion surface (Figure 3A), possibly corresponding to a level of terraces as their slope does not match that of the limestone bedding (Chardonnet, 1943). Located between 800-850 m.a.s.l., the terraces level is visible along the downstream part of the HVG, after la Mescla (Martel, 1908). The terraces are not present in the upstream part of the HVG, but the numerous emergences of karstic network at the same altitude (800-850 m.a.s.l.) suggest that this paleo-level is continuous along the whole HVG (Chardonnet, 1943). These terraces underline an ancient and wider river channel (Figure 3C), which is different from the present steep and narrow HVG.

No geochronological constraint is available to precise the timing of incision and the formation of these terraces. However, some geological indices can help estimating the period at which the incision started. Indeed, continental deposits (conglomerates) from the Late Pleistocene, corresponding to the latest period of filling of the Valensole Basin, can be found at the same elevation as the terraces and karstic network, i.e., between 800-850 m.s.a.l. (Blanc, 1992; Chardonnet, 1943). The event responsible for the onset of the HVG formation is believed to be the massive sea-level drop related to the Messinian

Salinity Crisis (Blanc, 1992; Nicod, 2004), as it was proposed in surrounding areas (Clauzon et al., 2011; Hippolyte et al., 2011). However, some authors suggest that the formation of the HVG is not older than the Pliocene (Chardonnet, 1943). From the elevation of the karstic network in the Lower Verdon Gorges (downstream of the St Croix Lake), Blanc (1992) estimated an incision rate of 0.34-0.33 mm/yr since the Pliocene-Quaternary boundary. However, no available data allows constraining incision rates for the recent Quaternary period.

3. Methods

3.1. Sampling strategy

In order to bring new insights on the incision history of the HVG, three sites were selected and sampled for dating with the Cosmic Ray Exposure (CRE) method.

Considering the size of the HVG, it seemed more adequate to sample several sites along the gorges rather than one single wall as done previously in neighbouring areas (Valla et al., 2010; Saillard et al., 2014; Rolland et al., 2017; Petit et al., 2019; Cardinal et al., 2021; 2022). The main challenges in the HVG was the narrowness of the gorges and the along-strike lithological variations. Indeed, the portions of the gorges made of the most massive (Tithonian) limestones, in which well-preserved river polished surfaces can be expected, are also the narrowest ones, limiting exposure to cosmic rays due to strong topographic shielding. Conversely, well-exposed surfaces were found in portions of the gorges where the stratified limestones bedrock is very fractured and was most likely impacted by post-incision erosion process (mainly rock-falls). A compromise between gorge-wall preservation and reasonable topographic shielding resulted in the selection of three areas along the HVG (Figures 3, and 5 to 7) located in:

- The downstream part of the Samson Corridor, at the upstream entrance of the gorge;
- La Mescla, in the middle part of the gorges, at the junction with the Artuby River;
- The Galetas bridge, at the gorges outlet.

While being very narrow but well-preserved, the Samson corridor opens up in his downstream part to a wide section of the gorge (Figure 3A), corresponding to a lithological change from massive to stratified limestone (Figure 2B). Sub-vertical polished surfaces showing good preservation with the presence of pot-holes were sampled (Figure 5).

La Mescla, is characterized by a deep meander at the junction with the Artuby River (Figure 3). Fluvial incision focused on the south flank by the tight curve of the meander has opened up this portion of the gorges and created a much wider space than in the direct surroundings, resulting in a more optimal exposure to cosmic rays. Although this portion of the gorges is characterized by thin and heavily fractured limestone beds, some river-polished features are visible in the thickest strata (Figure 6A, B, C). Two strikingly different polished surfaces were sampled (Figure 6). Section 1 (Green area, Figure 6A; D) is directly facing the entrance of the meander, while the second one is located slightly downstream, at the centre of the meander (yellow area, Figure 6A, D). The first section shows an overhanging profile, with pot-holes in the lower part and underwater erosion pools at the foot of the wall (Figure 6B, C, E), while the second section shows a smoother, nearly flat profile in its lower part (Figure 6A, F). The site is also characterized by considerable sediment aggradation, creating a pebble cordon growing towards the Artuby River junction (Figure 6D).

At the Galetas bridge, we were confronted with the limit of accessibility, both from above, because of the height the gorge walls, and below, because of the river depth. Therefore, instead of a vertical profile along a single wall, we choose to sample a longitudinal profile by sampling three polished surfaces at 8-10 m above the modern riverbed along the massive Tithonian beds that form the outlet of the HVG (Figure 7). The samples were collected with a hammer and chisel and their height above the river bed was measured with a tape mesure.

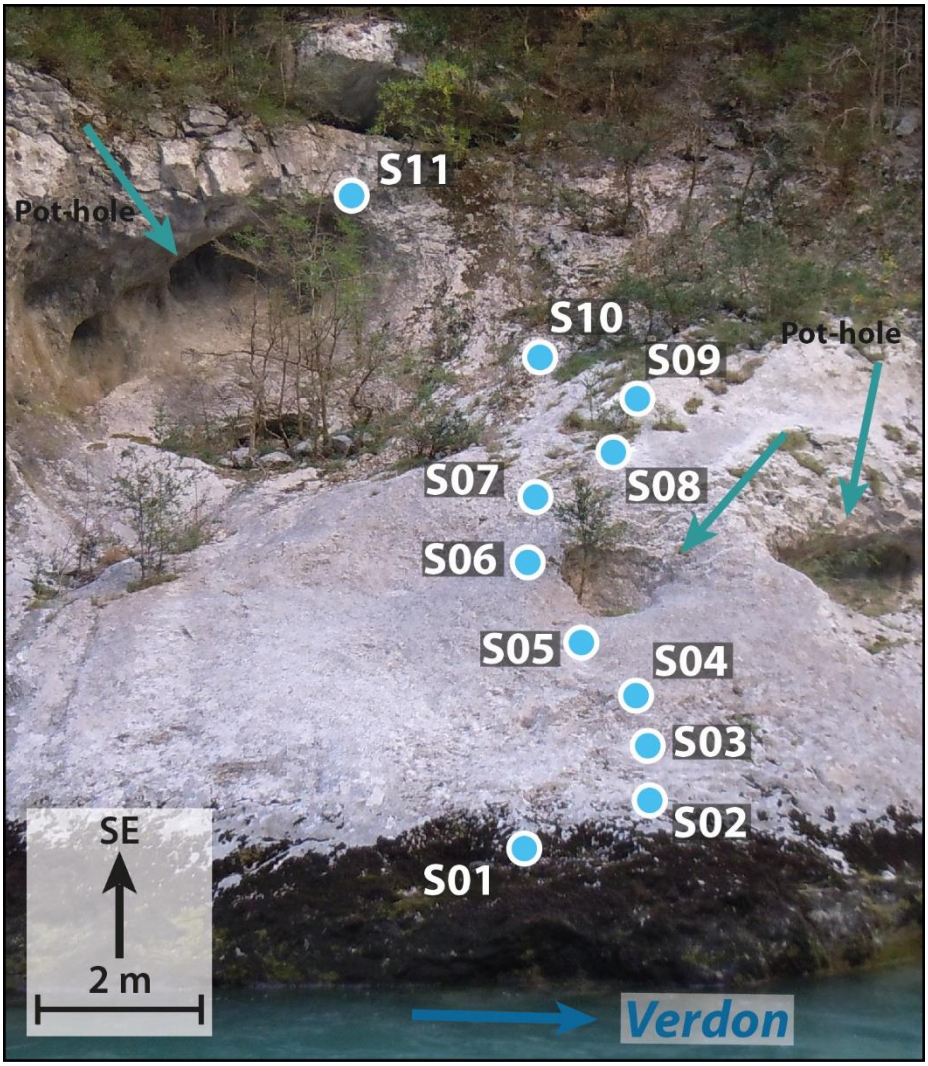

Figure 6-5 : Field pictures of river-polished surface sampled in the Samson Corridor and sample location. Note the presence of pot-holes attesting of the surface preservation since its exposure by incision.

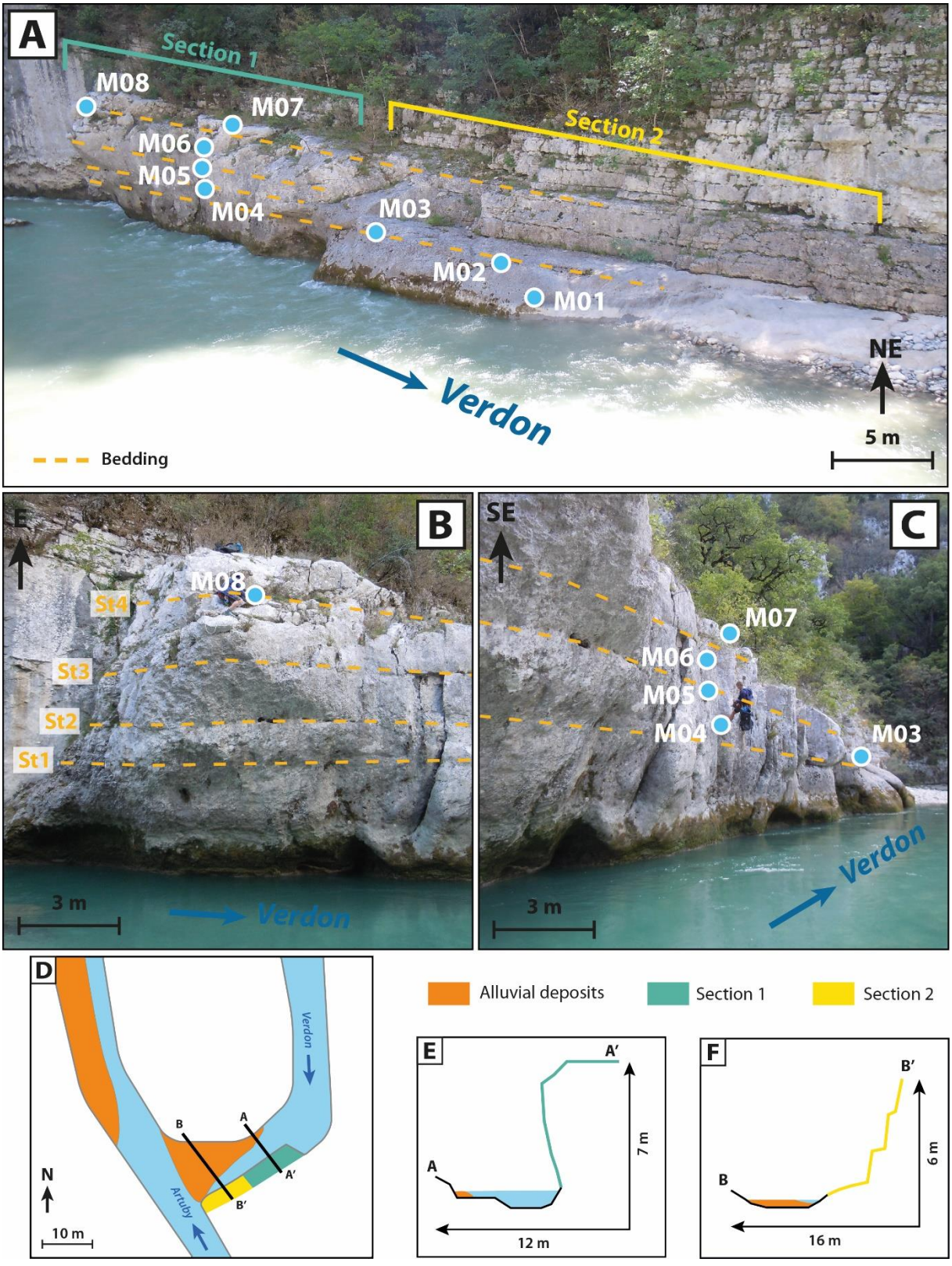

Figure 6-6 : A: Field pictures of river-polished surfaces sampled at La Mescla with sample location. Bedding (yellow dashed line) is gently dipping southwards (5°). B and C: Details on section 1 with overhanging walls. D. Sketch map of the La Mescla site; E and F: Schematic topographic cross-sections of sections 1 and 2.

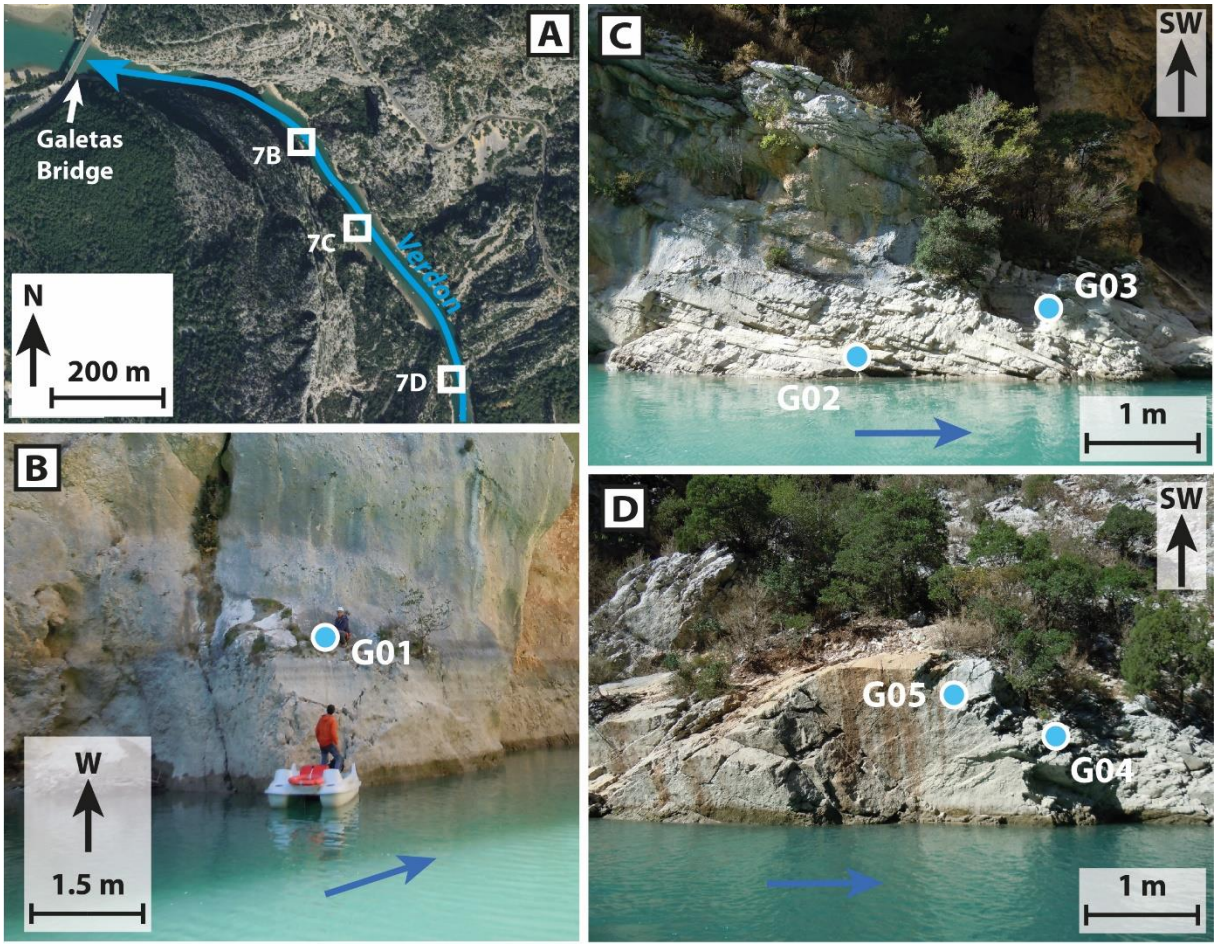

Figure 6-7 : A: Aerial image (IGN) of Galetas area and location of the three sampled river-polished surfaces. B, C and D: Details of the three sampled river-polished surfaces and sample location. Blue arrows show the river flow direction.

3.2. ^{36}Cl CRE dating

^{36}Cl concentrations in collected limestone samples were quantified in order to estimate Cosmic Ray Exposure (CRE) ages and unravel the exposure history of the steep (almost vertical) bedrock gorge walls that were theoretically gradually exposed through river incision (Schaller et al., 2005; Ouimet et al., 2008). ^{36}Cl concentrations were determined by accelerator mass spectrometry (AMS) measurements performed on ASTER, the French national AMS facility (CEREGE, Aix-en-Provence) (Arnold et al., 2010). A sea-level and high-latitude ^{36}Cl production rate for calcium spallation of 42.2±3.4 atoms ^{36}Cl g^{-1} a^{-1} (Schimmelpfennig et al., 2009, Braucher et al., 2011) was used and scaled following Stone (2000) and corrected for topographic shielding (TS), constrained from field measurement data and using the online tool

CRONUS-Earth from Balco et al. (2008). For more details on the dating method and the analytical protocol, the reader is referred to several previous studies (Zerathe et al., 2014; Cardinal et al., 2021; 2022). All exposure ages are indicated according to before present (BP) nomenclature.

3.3. Incision rate computation

The numerical code developed by Glotzbach et al. (2011), originally designed for thermochronology age-elevation relationships, was used to determine temporal variations in incision rates from the CRE data. The code defines the regression segments that best fit the CRE ages data and the associated uncertainties with elevation distribution. As in Glotzbach et al. (2011), a Monte Carlo approach was used to randomly divide the data into 1, 2 or 3 successive time intervals in order to define regression segments by weighted linear regression, and to select the best-fitting ones according to their R^2 value. The following criteria were applied: no negative incision rate is allowed; regression segments constrained by less than 3 data points are rejected; the intersection between two curve segments must correspond to the intersection between the two sets of data that were used to calculate them.

4. Results and local interpretations

The sample characteristics are reported in Table 1. CRE ages determined from the ^{36}Cl concentrations are reported in the CRE age vs. height plots (Figure 8). The term "riverbed" used here refers to the bedrock, which corresponds to the bottom of the river channels. It was measured only in a few locations. The actual geometry of the river thalweg is therefore poorly constrained.

Sample	Height above river bed (m)	Samp. thick. (cm)	TS factor	Spallation scaling	^{35}Cl (ppm)	Ca (%)	Atoms ^{36}Cl (at/g)	Atoms ^{36}Cl ± (at/g)	CRE age (ka)
Samson (lat: 43.7842°; long: 6.3936°; mean elevation: 606 m.a.s.l.)									
S01	2	1	0.16	1.67	37.3	40.7	83944	6349	15.9±1.2
S02	2,4	1	0.16	1.67	29.9	40.7	89670	8452	17.2±1.6
S03	3,3	1	0.16	1.67	32.5	40.8	91776	5730	17.5±1.1
S04	3,7	1	0.16	1.67	35.0	40.7	118596	7068	22.7±1.4
S05	4,6	1	0.16	1.67	31.5	40.6	136006	8988	26.4±1.7
S06	5,8	2.5	0.16	1.67	32.0	41.7	188287	9862	36.0±1.9
S07	6,8	1	0.16	1.67	28.1	40.8	187869	9775	36.9±1.9
S08	7,1	1	0.16	1.67	28.6	40.8	205363	13024	40.4±2.6
S09	7,7	1.5	0.16	1.67	23.4	40.7	205909	11192	40.9±2.2
S10*	8	1.5	0.16	1.67	33.1	40.6	190457	16417	37.3±3.2
S11*	11	1	0.16	1.67	24.5	40.4	110890	8575	21.6±1.7
La Mescla (lat: 43.7399°; long: 6.3794°; mean elevation: 564 m.a.s.l.)									
M01	1.1	1	0.39	1.61	43.1	40.5	388057	38470	32.5±3.2
M02	2.0	1	0.39	1.61	47.3	40.5	568763	36811	48.2±3.1
M03	2.8	1	0.39	1.61	33.5	40.6	677155	29949	59.0±2.6
M04	3.9	1	0.39	1.61	36.5	40.5	386654	34273	32.6±2.9
M05*	4.7	3	0.39	1.61	37.8	41.1	184681	13407	15.0±1.1
M06*	5.6	2.5	0.39	1.61	43.7	41.1	198667	26792	16.1±2.2
M07	6.3	2	0.39	1.61	43.0	40.7	669682	32058	57.4±2.7
M08	6.2	1.5	0.39	1.61	49.3	40.6	651036	29465	55.4±2.5
Galetas (lat: 43.7972°; long: 6.2576°; mean elevation: 475 m.a.s.l.)									
G01	10	1	0.20	1.49	16.2	40.5	288596	13927	53.2±2.6
G02	8.0	1	0.54	1.50	26.9	40.5	423770	18845	28.0±1.2
G03*	10	1	0.54	1.50	19.5	40.6	308352	15745	20.3±1.0
G04	8.9	1	0.67	1.49	48.6	40.5	356756	18990	18.3±1.0
G05	9.0	2.5	0.67	1.49	49.4	41.1	596356	29548	31.6±1.6

Tableau 6-1 : ^{36}Cl CRE sample characteristics and geochronological results. Sample field information, topographic shielding (TS) factor of the sampled surfaces, samples thickness (Samp. thick.), natural chlorine contents, calcium, cosmogenic ^{36}Cl contents in the limestone samples, resulting ^{36}Cl CRE ages are indicated. Samples with an asterisk correspond to CRE ages identified as outliers and discarded for incision rate computation.

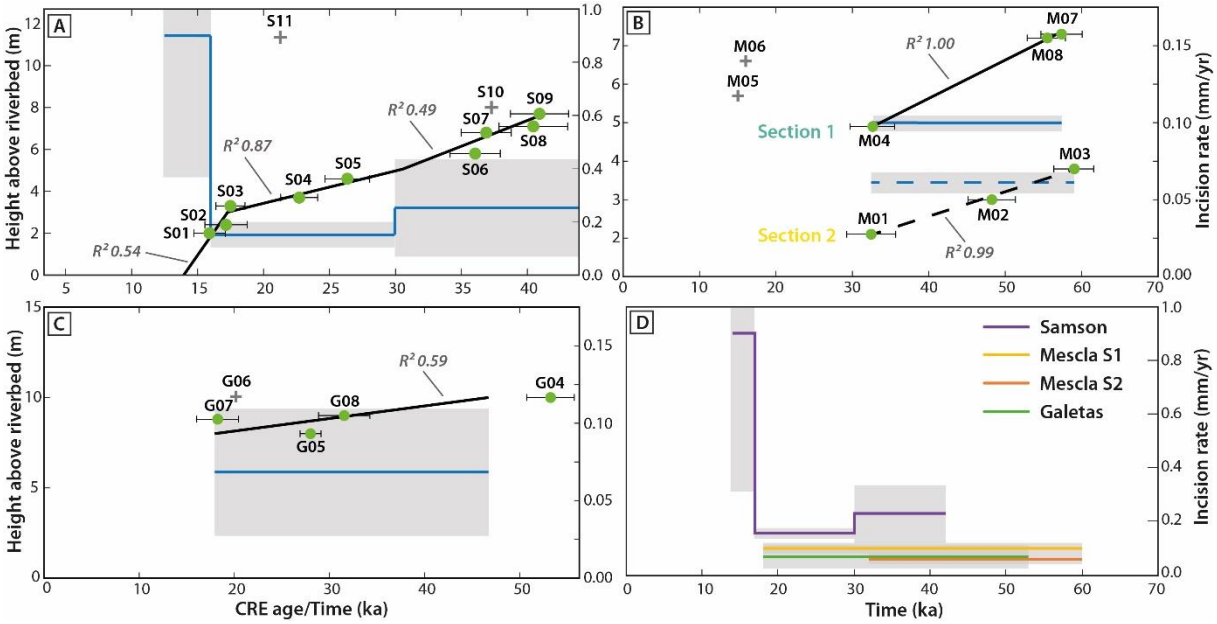

Figure 6-8 : CRE age vs. height (left y-axis) plot and associated incision rates (right y-axis) of (A) Samson, (B) La Mescla with Section 1 (continuous line) and Section 2 (dashed line), and (C) Galetas. Black lines correspond to linear regressions, blue lines correspond to the incision rates inferred from those regressions and corresponding uncertainties (light grey rectangles). D. Inferred incision rates variations over time for the studied sites, and corresponding uncertainties.

4.1. Samson

A total of 11 samples were collected along a 12 m-high polished surface in the Samson Corridor, which gave CRE ages ranging from 15 to 45 ka. These data were already presented by Cardinal et al. (2022), where the authors made a conservative choice to consider only one regression line for deriving incision rates. As in the present study, to constrain more precisely the timing of incision in the HVG, the code was allowed to use three regression lines in order to obtain incision rate variations. Apart from two samples (samples S10 and S11) that clearly demonstrate the occurrence of rock-falls (as seen in Cardinal et al., 2021), the rest of the data shows a consistent history of progressive incision with three incision rate trends:

- 0.25±0.17 mm/yr from 45 to 30 ka
- 0.18±0.03 mm/yr from 30 to 16 ka
- 0.90±0.53 mm/yr from 16 to 15 ka

Considering the large uncertainties associated with the calculated incision rates, and relatively similar estimates, it can be concluded that the first two periods are difficult to

distinguish from each other and that incision in the Samson area underwent only one major incision rate change after ca. 16 ka. The lack of CRE data does not allow us to constrain an incision rate for the remaining 2 m of the surface, corresponding to the last 15 ka (Figure 8A).

4.2. La Mescla

Eight samples were collected along the two sections described above, and gave CRE ages ranging from 60 to 15 ka for Section 1 and 60 to 30 ka for Section 2. Both sections are located along the concave banks of the meander. The data collected from La Mescla indicate a much more contrasted incision history, which seems in agreement with the complex morphology of the site. Indeed, as described above, the sampled site can be seen as two distinct sections: an upstream part with an overhanging high wall, and a downstream part with a nearly flat surface. The top of each section corresponds to the top of a limestone bed: St04 for the highest portion and St01 for the lowest portion (Figure 6A). Three observations can be made:

- Samples collected at the top of each of the two sections (03 : section 1; 07 and 08, section 2) show similar exposure ages (55-60 ka), despite different heights above river bed (2.8m for sample 03 and 6.2-6.3m for samples 08 and 07);
- Samples 01 and 04, collected 2 m below the highest samples of their respective portion but at different heights above river bed (1.1 m for sample 01, 3.3 m for sample 04), have a similar exposure age (32 ka);
- Intermediate samples 05 and 06 (height above river bed: 4.7 m for sample 05 and 5.6 m for sample 06) both have a very similar age of 15-16 ka, much younger than the rest of the data, despite being located in an intermediate position relative to the river bed.

To understand these contrasted CRE ages, the evolution of this specific portion of the HVG must be reconstructed. The samples 08, 07 and 03, although located at different heights above the present river bed, have similar exposure ages and could therefore represent a paleo-riverbed

with a steeper slope than the present one (Figure 9A). The CRE age of samples 01 and 04 could then represent a second paleo-riverbed at ca. 30 ka, 2 m below the first one, but with a similar slope (Figure 9B). The CRE ages would therefore indicate that between 60 and 30 ka, incision occurred at a rate of 0.06-0.1mm/yr.

However, Section 1 of La Mescla site seems to have undergone a more focused and intense incision, since the above mentioned tilted paleo-riverbed seems to have been flattened to match the modern riverbed. Indeed, Section 1 is directly facing the upper part of the meander, while Section 2 is located more deeply in the inside of the meander curve (Figure 6D). Hence, the upstream portion is more exposed to the direct impact of the river flow, while the downstream portion may be shielded from the shear strength and turbulence of the flow, as most of it is absorbed in the upstream section of the meander. Such a focused lateral erosion could have destabilized the bedrock wall by undercutting its foot, creating an overhanging cliff. Indeed, Samples 05 and 06 show similar young exposure ages of ~16 ka, which can be interpreted as rock falls. Indeed, althought probably smoothed by dissolution, the shallow cavity scarred by a vertical fracture, in which samples 05 and 06 are located, could be indicative of a rock fall (Figure 6C) and therefore could explain the much younger CRE age of those samples compared to the surrounding ones. The CRE data agree with an acceleration of incision at the same time for the Samson area (Figure 8A), suggesting a period of enhanced incision occurring around 16 ka (age of the possible rock falls). Such an incision wave could have flattened, very locally and by a combinaision of vertical incision and lateral erosion, the riverbed by erasing what could have been a small lithological knickpoint at La Mescla that did not propagate upstream, as observed in other studies (Johnson et al., 2010 and references therein).

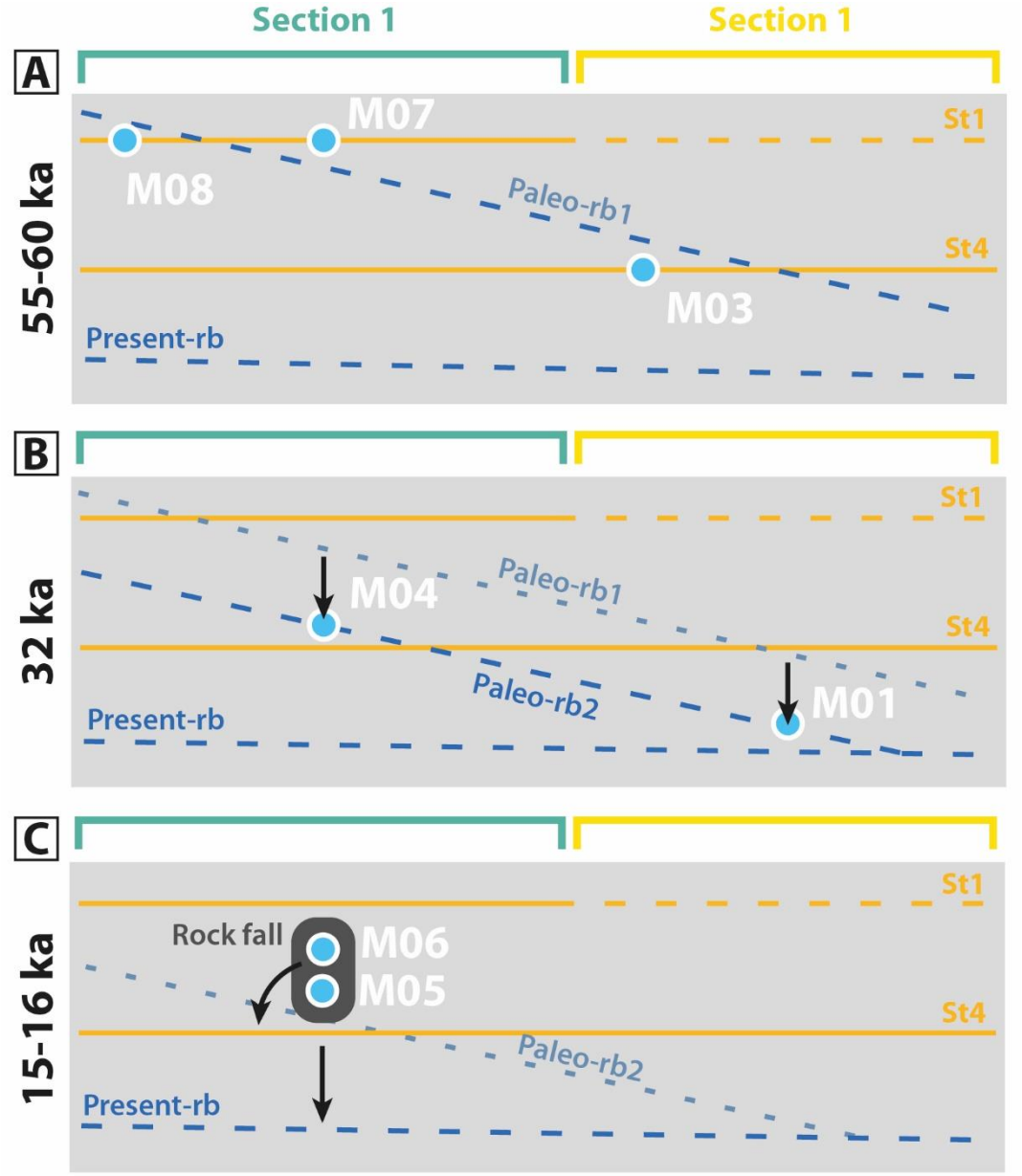

Figure 6-9 : Sketch (not to scale) of the proposed evolution and incision history of the La Mescla sampled site at (A) 55-60 ka, (B) 32 ka and (C) 15-16 ka. Paleo-rb: proposed slope of paleo-riverbed; Present-rb: estimated present riverbed slope; St : limestone strata. The term "riverbed" used here refers to the bedrock, which corresponds to the channel bottom.

4.3. Galetas

A total of 5 samples was collected along three river polished surfaces at the outlet of the HVG. The CRE ages range between 55 and 15 ka. The compilation of these data suggest a low and yet poorly constrained incision rate of 0.07±0.04 mm/yr between the 15-55 ka period.

5. Discussion

5.1. Short-term incision

The code was allowed to calculate incision rates with relatively few points, permitting to highlight rapid variations in incision rates. The disadvantage of this approach is that these incision rates are not always well constrained from the CRE data. This strategy allows us to infer an acceleration of incision from 0.2 to 0.9 mm/yr between 17 and 15 ka in the Samson area (Figure 8C), but with too few points to really constrain it. At the same period, a sequence of rock falls in the La Mescla site can be inferred, suggesting a period of increased downcutting at that time. Following the regional interpretation proposed by Cardinal et al. (2022), several rivers connected to the Last Glacial Maximum (LGM) glaciation in the SW French Alps underwent a period of enhanced fluvial incision following the main glacier retreats (19-17 and 14 ka; Rolland et al., 2019). From these results, it seems that the Verdon River may have undergone the same evolution, but since only three ages younger than 20 ka are obtained in the entire dataset, it remains difficult to infer any detailed post-glacial history of the HVG with confidence.

5.2. Long-term incision

Our results yield two ranges of slow but steady incision rates for the HVG: 0.06-0.07 mm/yr in the downstream parts of the HVG (Galetas and La Mesla Section 2), a roughly similar value of 0.1 mm/yr in the area of focused incision (La Mescla Section 1) between 60 and 15 ka (Figure 8C), and a larger value around 0.2 mm/yr on average in the upstream part (Samson) of the HVG.

Based on these estimates and on data obtained on the HVG by CRE dating, the following questions can be subsequently explored: (1) What is the onset time of HVG formation? (2)

What is the main driver for the long-term incision? (3) What is the respective contribution of glacial/interglacial phases in lowering or enhancing these long-term incision rates?

5.2.1. What is the onset time of HVG formation?

From the CRE data, the long-term Verdon River incision rates can be bracketed between 0.06 and 0.2 mm/yr on scales up to several 10's of ka (neglecting the brief, less constrained, 0.9 mm/yr incision rate ~at 15 ka obtained in the Samson corridor). These incision rates are lower than those inferred by Brocard et al. (2003) in the neighboring Buech river (0.8 mm/yr over the last 190 ka). If these results are extrapolated from the bottom of the gorge to the first level of terraces, up to 300 m above the present riverbed near La Mescla (Figure 10), computed first-order ages estimates range between 1.5 and 5 Ma, which would thus represent the onset of the main incision period that dug the HVG up to 300 m.

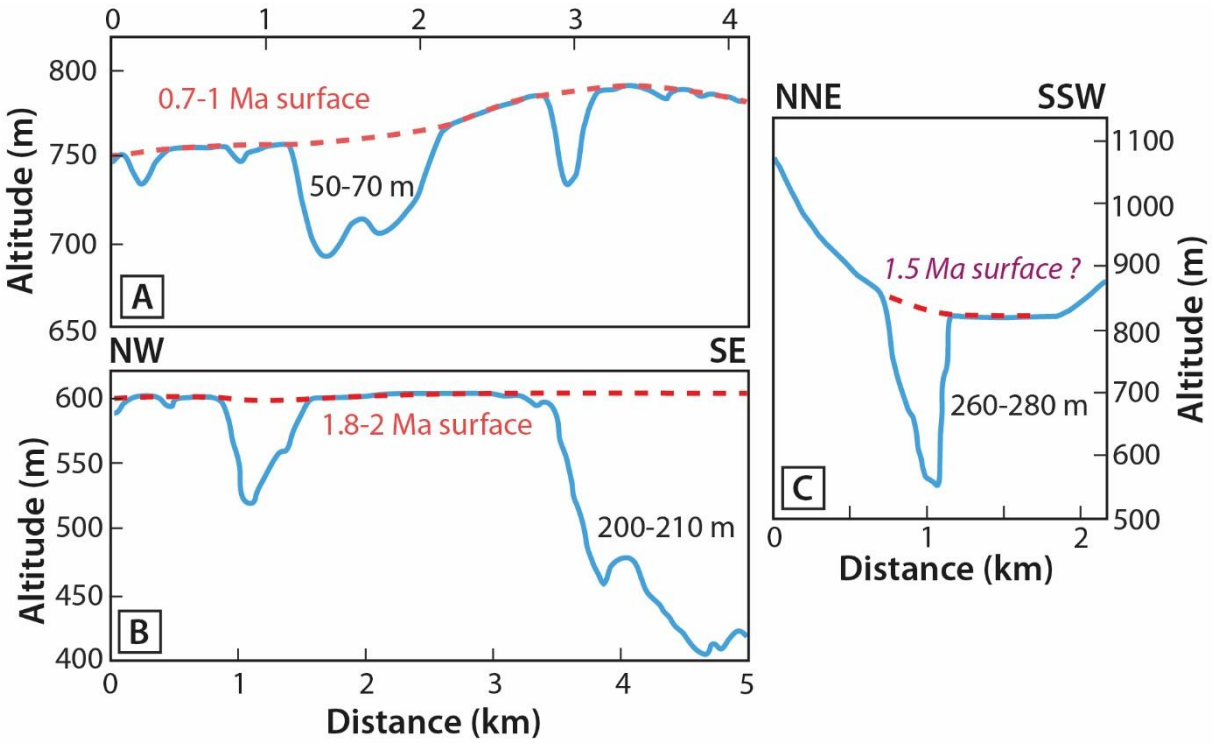

Figure 6-10 : Topographic profiles drawn from the IGN DEM with corresponding surface abandonment ages. A: across the Valensole Plateau near Moustier Sainte Marie; after Dubar et al. (1998), B: along the lower Verdon channel; after Dubar et al. (1998) and C: in the HVG near the La Mescla site (this study). See profiles location on figure 1B. Note that the vertical and horizontal scales are different between each panel.

The last deposits of the Valensole basin are dated around 1.8 to 2 Ma (Dubar, 1984; Dubar et al., 1998; Hippolyte et al., 2011), except for local clastic deposits of the Balene breccia formation, which are dated around 0.7 to 1 Ma (Dubar et al., 1978, 1998). This continental formation is presently incised by tributaries of the Verdon River. The upstream position of this formation suggests that downcutting of the lower Verdon River can have started before 1 Ma (Dubar et al., 1998). In that case, the maximum height of the HVG (~300m) would correspond to a long-term incision rate of 0.3 mm/yr, which is higher but of the same order of magnitude than short-term rates deduced from CRE data.

The end of sediment deposition in the Valensole basin is ascribed to Early Quaternary climate cooling, and was supposed to correspond to the onset of river network entrenchment in the Valensole plateau and its surroundings (Dubar, 1984). While global cooling started in the late Pliocene for the Northern hemisphere (Suc and Zagwijn, 1983; Haug et al., 2005), evidence for increased incision and valley downcutting in the Alps seem to have occurred later, around 0.9-1 Ma (Muttoni et al., 2003; Valla et al., 2011), hence around the mid-Pleistocene transition between the glacial/interglacial cycles periodicity of 40-ka to 100-ka (Lisiecki, 2010). Therefore, the onset of the Valensole basin deposits incision can be bracketed between 1 and 2 Ma, which is consistent with the younger age estimate (ca. 1.5 Ma) of gorge entranchement and the higher bound of incision rates (~0.2 mm/yr) estimated from our CRE datings and extrapolation along the HVG.

5.2.2. What is the main driver for the long-term incision?

The present total incision of the Balene breccia formation, located in the Valensole Basin, is of 50 to 70 m, leading to a mean incision rate of 0.07 to 0.1 mm/yr over the last 0.7-1 Ma. Between the Valensole abandonment surface dated at 1.8 to 2 Ma and the Verdon thalweg around the Sainte Croix Lake, it can be estimated that the Verdon River has incised about 220

m, which gives a mean incision rate of 0.1 mm/yr since that time. This estimate is consistent with the above mentioned estimation obtained from the Balene breccia formation (Table 2). From morphological analysis and CRE dating of the Durance terraces, Siame et al. (2004) inferred a similar incision rate for the Durance River on its eastern side, with rates of 0.1 mm/yr since 2 Ma. The value of 0.1 mm/yr can therefore ve assumed to constitute a good estimate for the long-term (i.e., since 1.8 to 2 Ma) average incision rate of rivers in the Valensole plateau. Such an incision rate is possibly driven by large-scale isostatic and/or tectonic uplift (Champagnac et al., 2008), although local tectonic structures might have also played a role (Hippolyte and Dumont, 2000; Siame et al., 2004).

Time interval (ka)	**Uncertainty (ka)**	**Height (m)**	**Uncertainty (m)**	**Observation**	**Site name**	**Site number**	**Reference**
20	1	1.4	0.5	Incision	Galetas	1	This study
30	5	2	0.5	Incision	Mescla	2	This study
50	5	10	0.5	Incision	Samson	3	This study
850	150	60	10	Incision	Balene breccia	4	Dubar, 1984 and this study
1900	100	200	10	Incision	Valensole surface	5	Dubar, 1998 and this study
2000	100	200	50	Uplift	East Durance	6	Siame et al., 2011
1450	100	290	10	Incision	Samson	3_{ext}	This study (extrapolated)
3000	400	345	5	Uplift	Digne nappe	7	Hippolyte et al., 2011
3000	400	645	5	Uplift	Digne nappe	7_{corr}	Hippolyte et al., 2011 (corrected)
6000	500	3500	500	Denudation	Velodrome	8	Schwartz et al., 2017

Tableau 6-2 : Synthesis of incision and uplift measurements estimates in the study area. Site numbers and location refer to figure 11.

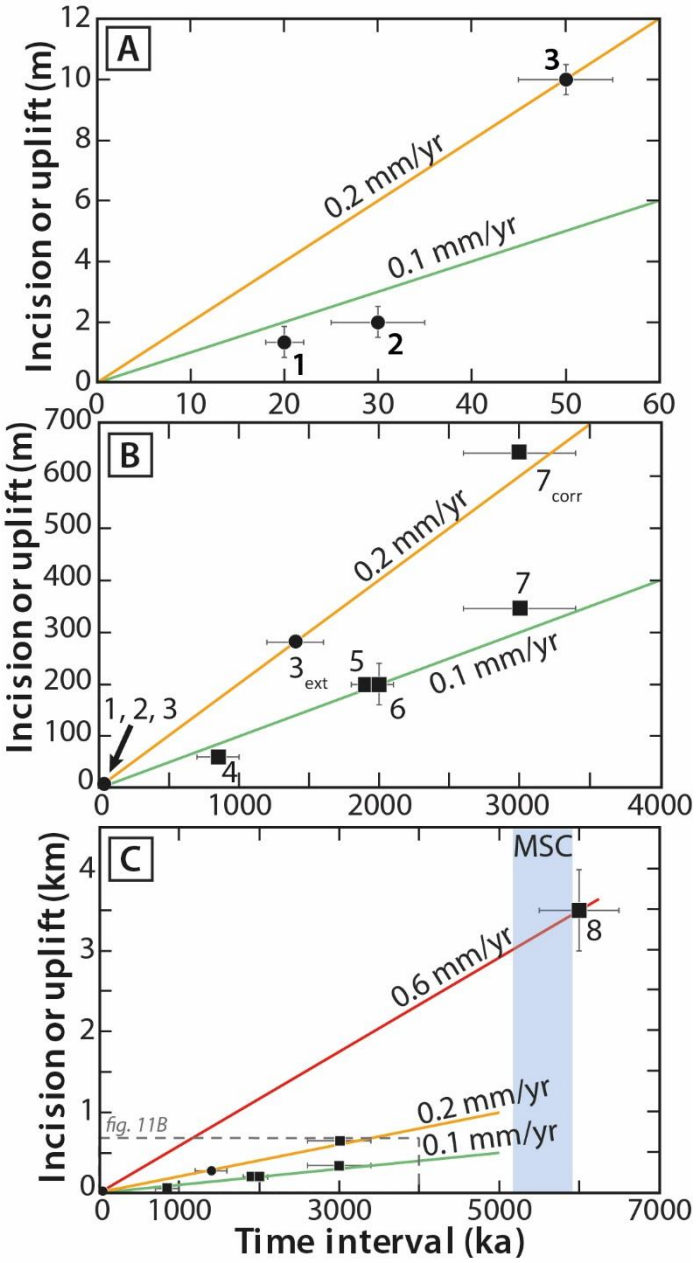

Figure 6-11 : Compilation of incision and uplift rates at different time scales. A: Incision rates in the HVG from CRE dating (this study) over 20 to 50 ka. B: Same data as on A with additional incision or uplift rate estimates from the literature (sites 4, 5, 6 and 7). Point 3_{ext} corresponds to the extrapolation of the recent 0.2 mm/yr incision rate (site 3) to the actual gorge height measured in the Verdon canyon. Points 7_{corr} corresponds to the uplift of the Digne nappe in the Esquichiere canyon relative to the Valensole basin (Hippolyte et al., 2011, point 7), to which is added an uplift of 0.1 mm/yr of the Valensole basin relative to the base level, in order to allow comparison with the other points. C. Same as B (B corresponds to the grey-dashed rectangle on the bottom left) with long-term AFT/AHe exhumation rate estimates from Schwartz et al. (2017) interpreted as uplift estimates. The Messinian Salinity Crisis (MSC) period is indicated (transparent blue rectangle). See Table 2 for details.

This mean incision rate of 0.1 mm/yr is roughly consistent with the higher range of incision rates inferred for the medium part of the HVG: "La Mescla" site and, considering its large uncertainties, and the Galetas site in the lower part of the HVG. It is also consistent with contemporary average denudation rates ranging between 0.04 and 0.12 mm/yr computed from

topographic analysis and ^{10}Be CRE data on the Valensole Plateau hillslopes (Godard et al., 2020). Incision rates in the Samson corridor (0.2 mm/yr) is twice as high, as in neighbouring catchments for the recent period covering the last ca. 40 ka (ranging from 0.15 and 0.28 mm/yr; Cardinal et al., 2022). This can be ascribed either to differential tectonic motions (with respect to the lower Verdon Gorges and Valensole plateau) or to delayed incision of a steep, disequilibrium river profile that might have accumulated between several glacial cycles (Rolland et al., 2017). The tectonic hypothesis argues for the role of Pliocene to Quaternary faults, accommodating Plio-Quaternary shortening along the Digne-Castellane arcs (e.g., Sanchez et al., 2010; Bauve et al., 2014). These structures could locally consist of EW trending blind thrusts and folds responsible for the measured incision rates in the Samson corridor. For instance, in the Samson corridor, the Verdon River cuts across a topographic dome corresponding to an anticline axis cored by lower Jurassic limestones (the Collet-Barris anticline), instead of flowing in the neighbouring, lower-altitude syncline to the west (Figure 1C and 3B). This can be interpreted as an antecedence assisted by the network of N-S and E-W faults (Nicod, 2004) and suggests a possible, very slow differential uplift between the Mesozoic sedimentary cover units of the Castellane arc and the Valensole basin of 0.1 mm/yr since the incision onset of the HVG. This value is consistent with previously obtained estimates of differential uplift rates on Quaternary canyons in the Digne nappe, although the age of the canyons are only indirectly constrained (Hippolyte et al., 2011). The contractional deformation is still ongoing, as shown by the seismicity observed south of the Castellane area (Le Pichon et al., 2010; Larroque et al., 2021 for a synthesis).

To the Northwest of the HVG, thermochronology data from Miocene sediments underthrusted below the Digne nappe yielded long-term exhumation rates of about 0.5 to 0.6 mm/yr since ca. 6 Ma (Figure 11C; Schwartz et al., 2017). These higher values are possibly due to the activity of a crustal-scale, “thick-skin”, thrust located below the Barles half-window

(Nouibat et al., 2022; Schwartz et al., 2017). Here, NNW-SSE to NW-SE trending thrust wedges (Esclangon and Tanaron horse structures) have accommodated N70°E-trending compressional deformation and are responsible for the Plio-Quaternary uplift of Barles area (Hippolyte et al., 2012). In addition, based on balanced and restored cross-sections through southwestern Subalpine and Central Provencal zones, Balansa et al. (2022) suggested that the relative northeastward migration of buried basement highs contributed to the observed Pliocene-Quaternary contractional deformation and upflit of the central and northern extremity of the Valensole area. It is likely that this contractional deformation continued to migrate to the NNE until reaching the Barles half-window. The above mentioned local exhumation rates are consistent with the preservation of late Pliocene to early Quaternary canyons in the Digne nappe, as denudation can have been more focused and more intense in the Barles half-window than in the surrounding area, where the nappe is preserved and well visible today. Moreover, the late stage denudation history since 1-2 Ma is too recent and too shallow to be precisely recorded by AFT or AHe data.

Considering all these values together, and assuming that recent (<60 ka) incision rates in the HVG can be extrapolated to the overall Quaternary period, it can be proposed that: i) there is a very slow (0.1 mm/yr) uplift of the whole region since the last 1.5 to 2 Ma, encompassing the Valensole basin and the Digne Nappe – Castellane Arc units, which is possibly the result of late Alpine tectonics or isostatic uplift (eg. Champagnac et al., 2008); ii) there might be an additional, although very slow, thin-skin deformation (0.1 mm/yr of uplift) of the sedimentary cover of the Castellane Arc relative to the Valensole basin; iii) the situation is different in the Barles half-window, where higher rock exhumation rates occurred in the Late Miocene (ca. 6 Ma) in response to the activity of a crustal-scale thrust (recognized on crustal-scale geophysical images; Nouibat et al., 2022) and/or northeastward migration of a basement high (Schwartz et al., 2017; Balansa et al., 2022; Nouibat et al., 2022). Whether this activity

was constant during the last 6 Ma, or was initially very fast and progressively slowed down to reach the observed uplift/incision rates for the last 1.5-2 Ma further south is difficult to quantitatively assess. Vertical GPS motions in the study area are poorly constrained, with present-day uplift rates of 0.41±0.58 mm/yr at the nearest station at Moustier-Saint-Marie (Sternai et al., 2019), so it is impossible to compare our long-term uplift estimates values with modern and almost instantaneous uplift rates from geodesy (e.g., Piña-Valdés et al., 2022).

5.3. What is the respective contribution of glacial/interglacial phases in lowering or enhancing incision?

In this framework, and comparing our results with long-term incision rates estimated in the Valensole Plateau and in the Verdon Gorges, the higher (up to 0.9 mm/yr at 15-16 ka, Figure 8A) incision rates obtained in the Samson corridor can be tentatively ascribed to its upstream position in the HVG. The Samson corridor is located at the boundary between two erosion regimes during the late-Quaternary period. Incision is mainly controlled by the influence of glaciation in the high Verdon Valley, while the lower Verdon Valley is only under a fluvial incision regime. Therefore, the higher incision rates estimated over a short period (~0.9 mm/yr from 16 to 14 ka) could be the result of a paraglacial crisis in the Verdon River posterior to the LGM. The same timing of enhanced incision is observed in neighbouring catchments following post-LGM deglaciation (Cardinal et al., 2022). Furthermore, increased incision after 16 ka could have triggered rock falls in the La Mescla site of the HVG (section 4.2). However, it is also possible that rockfall might solely be related to freezing and thawing effects, as observed by Cardinal et al. (2021) in a similar periglacial gorge setting. Therefore, the enhanced incision in the higher part of HVG could result from an increased interaction with the High Verdon Valley, where glacial incision has been efficient. The effect of enhanced incision following glaciers melting could have been hindered and buffered in the rest of the gorges, due to the resistance of the Tithonian limestones to such influences.

6. Conclusions

We sampled three 10 m-high river-polished walls within the High Verdon Gorge, in order to apply the Cosmic Ray Exposure dating approach and derive incision rates. These data are used to discuss the gorge origin and both short-term and long-term dynamics. Each site shows local complexities related to the intricate course of the Verdon River and, except for the upstream boundary of the HVG (Samson corridor), no significant variations in incision rates with time are evidenced. It remains therefore difficult to relate the HVG downcutting to the post-LGM paraglacial incision crisis, as it is more likely the case in other rivers also connected to the LGM glacial extent in the region (e.g. Cardinal et al., 2022). The relatively steady incision rates (0.06-0.2 mm/yr) obtained from our CRE data cover a time window between 60 and 15 ka and are comparable to long-term regional uplift, exhumation and denudation rate estimates. This leads us to propose that tectonic and/or isostatic uplift are the main drivers for the Late Quaternary incision of the Verdon River. Finally, this long-term incision, when extrapolated to the rest of the vertical 300 m-high gorge walls and to other estimated incision heights from the Valensole basin, is consistent with a Mid- to Early Quaternary (~1.5 to 2 Ma) onset of incision for the HVG. This age estimate could reasonably fit with the beginning of Alpine glaciations: although the general pattern of the river network was probably already present in Late Miocene times, intense downcutting responsible for the initial entrenchment of the Verdon River can be ascribed to the Quaternary climate cooling.

Acknowledgments

This study has been funded by the French Geological Survey (Bureau de Recherches Géologiques et Minières; BRGM) through the national program “Référentiel Géologique de France” (RGF-Alpes). This work has also been supported by the French government, through the UCA-JEDI Investments in the Future project managed by the National Research Agency (ANR) with the reference number ANR-15-IDEX-01. The ^{36}Cl measurements were performed

at the ASTER AMS national facility (CEREGE, Aix en Provence) which is supported by the INSU/CNRS, the ANR through the "Projets thématiques d'excellence" program for the "Equipements d'excellence" ASTER-CEREGE action and IRD. This manuscript benefitted from constructive reviews by two anonymous reviewers and efficient editorial handling by O. Fabbri.

References

Arnold, M., Merchel, S., Bourlès, D.L., Braucher, R., Benedetti, L., Finkel, R.C., Aumaître, G., Gottdang, A. and Klein, M., 2010. The French accelerator mass spectrometry facility ASTER: improved performance and developments. Nucl. Instrum. Methods Phys. Res., B 268, 1954–1959.

Balansa, J., Espurt, N., Hippolyte, J.-C., Philip, J., and Caritg, S. (2022). Structural evolution of the surimposed Provençal and Subalpine fold-thrust belts (SE France). Earth-Science Reviews, 227, 103972.

Balco, G., Stone, J.O., Lifton, N.A., and Dunai T.J. (2008). A complete ans easily accessible means of calculating surface exposure ages or erosion rates from ^{10}Be and ^{26}Al measurements. Quaternary Geochonology, 3, 174-195.

Bauve, V., Plateaux, R., Rolland, Y., Sanchez, G., Bethoux, N., Delouis, B., and Darnault, R., 2014. Long-lasting transcurrent tectonics in SW Alps evidenced by Neogene to present-day stress fields. Tectonophysics, 621, 85-100.

Bishop, P., and Goldrick, G., 2010. Lithology and the evolution of bedrock rivers in post-orogenic settings: Constraints from the high elevation passive continental margin of SE Australia. Geological Society, London, Special Publications, 346, 267-287.

Blanc, J.-J. (1992). Signification géodynamique des réseaux karstiques étagés du canyon de Baudinard (moyennes gorges du Verdon). Karstologia, 20(1), 37–48.

Blanchard, R. (1915). L'hydrographie du bassin supérieur du Verdon. Revue de Géographie Alpine, 3(1), 57–67.

Braucher, R., Merchel, S., Borgomano, J. and Bourlès, D.L., 2011. Production of cosmogenic radionuclides at great depth : a multi element approach. Earth Planet. Sci. Lett., 309, 1-9.

Brisset, E., Guiter, F., Miramont, C., Revel, M., Anthony, E. J., Delhon, C., et al. (2015). Lateglacial/Holocene environmental changes in the Mediterranean Alps inferred from lacustrine sediments. Quaternary Science Reviews, 110, 49–71.

Cardinal, T., Audin, L., Rolland, Y., Schwartz, S., Petit, C., Zerathe, S., ... and Aster Team, 2021. Interplay of fluvial incision and rockfalls in shaping periglacial mountain gorges. Geomorphology, 381, 107665.

Cardinal, T., Petit, C., Rolland, Y., Audin, L., Schwartz, S., Valla, P. G., et al., 2022. Fluvial bedrock gorges as markers for Late-Quaternary tectonic and climatic forcing in the Southwestern Alps. Geomorphology, 418, 108476.

Champagnac, J.-D., van der Beek, P., Diraison, G., & Dauphin, S., 2008. Flexural isostatic response of the Alps to increased Quaternary erosion recorded by foreland basin remnants, SE France. Terra Nova, 20(3), 213–220.

Chardonnet, J. (1943). Le relief du Grand Cañon du Verdon. Bulletin de l'Association de Géographes Français, 20(157), 87–97.

Clauzon, G., Suc, J.-P., Gautier, F., Berger, A., & Loutre, M.-F. (1996). Alternate interpretation of the Messinian salinity crisis: controversy resolved? Geology, 24(4), 363–366.

Clauzon, G., Fleury, T.-J., Bellier, O., Molliex, S., Mocochain, L., & Aguilar, J.-P. (2011). Morphostructural evolution of the Luberon since the Miocene (SE France). Bulletin de la Société Géologique de France, 182(2), 95–110.

Cowie, P. A., Whittaker, A. C., Attal, M., Roberts, G., Tucker, G. E., & Ganas, A. (2008). New constraints on sediment-flux–dependent river incision: Implications for extracting tectonic signals from river profiles. Geology, 36(7), 535–538.

Crosby B. T. and Whipple K. X., 2006. Knickpoint initiation and distribution within fluvial networks: 236 waterfalls in the Waipaoa River, North Island, New Zealand. Geomorphology, 82, 16-38.

Daniels, J.M. (2008). Distinguishing allogenic from autogenic causes of bed elevation change in late Quaternary alluvial stratigraphic records. Geomorphology, 101, 159-171.

Dubar, M. (1984). Chronologie et signification des dépôts continentaux du Néogène supérieur du bassin de Riez-Valensole (Alpes-de-Haute-Provence, France). Bulletin de la Société Géologique de France, 7(5), 971–978.

Dubar, M., Aguilar, J.-P., Chaline, J., Michaux, J., and Semah, F. (1998). Données chronologiques (mammifères et magnétostratigraphie) sur les dépôts plio-pleistocènes au toit du bassin de Valensole ; implications morphodynamiques. Géologie de la France, (1), 57–68.

Dubar, M., Guerin, C., and Heintz, E. (1978). Les nouveaux gisements villafranchiens du ravin de Cornillet (Moustiers Sainte-Marie, Alpes de Haute Provence, France) et leur contexte

géologique. Geobios, 11(3), 367–381.

Ely, L.L., 1997. Response of extreme floods in the southwestern United States to climatic variations in the late Holocene. Geomorphology, 19, 175-201.

Espurt, N., Hippolyte, J.-C., Saillard, M., & Bellier, O. (2012). Geometry and kinematic evolution of a long-living foreland structure inferred from field data and cross section balancing, the Sainte-Victoire System, Provence, France. Tectonics, 31(4).

Fabre, G., & Nicod, J. (1978). Niveaux de base actuels dans les principaux canyons du Languedoc oriental et des Plans de provence. International Journal of Speleology, 10(3), 5.

Ford, M., Lickorish, W. H., & Kusznir, N. J. (1999). Tertiary foreland sedimentation in the Southern Subalpine Chains, SE France: a geodynamic appraisal. Basin Research, 11(4), 315–336.

Ford, M., & Lickorish, W. H. (2004). Foreland basin evolution around the western Alpine Arc. Geological Society, London, Special Publications, 221(1), 39–63.

Glotzbach, C., van der Beek, P. A., & Spiegel, C. (2011). Episodic exhumation and relief growth in the Mont Blanc massif, Western Alps from numerical modelling of thermochronology data. Earth and Planetary Science Letters, 304(3–4), 417–430.

Godard, V., Hippolyte, J.-C., Cushing, E., Espurt, N., Fleury, J., Bellier, O., et al. (2020). Hillslope denudation and morphologic response to a rock uplift gradient. Earth Surface Dynamics, 8(2), 221–243.

Goguel, J. (1935). La formation du réseau hydrographique du Verdon. In Annales de Géographie (Vol. 44, pp. 492–495).

Guerit, L., Dominguez, S., Malavieille, J., & Castelltort, S. (2016). Deformation of an experimental drainage network in oblique collision. Tectonophysics, 693, 210–222.

Hartshorn, K., Hovius, N., Dade, W. B., & Slingerland, R. L. (2002). Climate-Driven Bedrock Incision in an Active Mountain Belt. Science, 297(5589), 2036–2038.

Haug, G.H., Ganopolski, A., Sigman, D.N., Rosell-Mele, A., Swann, G.E.A., Tiedemann, R., et al. (2005). North Pacific seasonality and the glaciation of North America 2.7 million years ago. Nature, 433, 821-825.

Herman, F., Seward, D., Valla, P. G., Carter, A., Kohn, B., Willett, S. D., & Ehlers, T. A. (2013). Worldwide acceleration of mountain erosion under a cooling climate. Nature, 504(7480), 423–426.

Hippolyte, J.-C., & Dumont, T. (2000). Identification of Quaternary thrusts, folds and faults in

a low seismicity area: examples in the Southern Alps (France). Terra Nova, 12(4), 156–162.

Hippolyte, J.-C., Clauzon, G., & Suc, J.-P. (2011). Messinian-Zanclean canyons in the Digne nappe (southwestern Alps): tectonic implications. Bulletin de La Société Géologique de France, 182(2), 111–132.

Howard, A. D., Dietrich, W. E., & Seidl, M. A. (1994). Modeling fluvial erosion on regional to continental scales. Journal of Geophysical Research: Solid Earth, 99(B7), 13971–13986.

Jansen, J. D., Fabel, D., Bishop, P., Xu, S., Schnabel, C., & Codilean, A. T. (2011). Does decreasing paraglacial sediment supply slow knickpoint retreat? Geology, 39(6), 543–546.

Johnson, J.P.L., Whipple, K.X., Sklar, L.S., and Hanks, T.C. (2009), Transport slopes, sediment cover and bedrock channel incision in the Henry Mountains, Utah. Journal of Geophysical Research, 114, F02014.

Johnson, J. P. L., Whipple, K. X., & Sklar, L. S. (2010). Contrasting bedrock incision rates from snowmelt and flash floods in the Henry Mountains, Utah. GSA Bulletin, 122(9–10), 1600–1615.

Jorda, M. (1975). Les montagnes du Haut Verdon, Etude géomorphologique. Méditerranée, 20(1), 37–58.

Jourdon, A., Rolland, Y., Petit, C., & Bellahsen, N. (2014). Style of Alpine tectonic deformation in the Castellane fold-and-thrust belt (SW Alps, France): Insights from balanced cross-sections. Tectonophysics, 633, 143–155.

Lague, D., Hovius, N., and Davy, P. (2005). Discharge, discharge variability, and the bedrock channel profile. Journal of Geophysical Research: Earth Surface, 110(F4).

Larroque, C., Baise, S., Albaric, J., Jomard, H., et al. (2021). Seismotectonic of southeast France : from Jura mountains to Corsica. Comptes Rendus Géosciences, 353, S1, 105-151.

Le Pichon, X., Rangin, C., Hamon, Y., Loget, N., Lin, J.Y., Andreani, L. and Flotte, N. (2010). Geodynamics of the France Southeast Basin. Bull. Soc. Géol. Fr., 6, 477-501.

Lisiecki, L.E. (2010). Links between eccentricity forcing and the 100,000-year glacial cycle. Nature Geoscience, 3, 349-352.

Martel, E.-A. (1908). Le profil en long du Grand Cañon du Verdon. In Annales de Géographie (Vol. 17, pp. 395–403).

Molnar P. (2007). Climate change, flooding in arid environnements, and erosion rate. Geology, 29, 1071-1074

Muttoni, G., Carcano, C., Garzanti, E., Ghielmi, M., Piccin, A., Pini, R., et al. (2003). Onset of

major Pleistocene glaciations in the Alps. Geology, 31(11), 989–992. https://doi.org/10.1130/G19445.1

Nicod, J. (2004). Présentation du bloc-diagramme : Grand Canyon du Verdon. Méditerranée, 102(1), 17–24.

Nouibat, A., Stehly, L., Paul, A., Schwartz, S., Bodin, T., Dumont, T., et al. (2022). Lithospheric transdimensional ambient-noise tomography of W-Europe: implications for crustal-scale geometry of the W-Alps. Geophysical Journal International, 229, 2, 862–879.

Oberlander, T. M. (1965). The Zagros streams: a new interpretation of transverse drainage in an orogenic zone. Syracuse Geographical Series, 1.

Petit C., Rolland Y., Braucher R., Bourlès D., Guillou V. et Petitperrin V., 2019. River incision and migration deduced from ^{36}Cl cosmic-ray exposure durations: The Clue de la Cerise gorge in southern French Alps. Geomorphology, 330, 81-88.

Piña-Valdés J., Socquet A., Beauval C., Doin M.-P., D'Agostino N. and Shen Z.-K., 2022. 3D GNSS velocity field sheds light on the deformation mechanisms in Europe: Effects of the vertical crustal motion on the distribution of seismicity. Journal of Geophysical Research: Solid Earth, 127, e2021JB023451.

Rolland, Y, Petit, C., Saillard, M., Braucher, R., Bourlès, D., Darnault, R., et al. (2017). Inner gorges incision history: A proxy for deglaciation? Insights from Cosmic Ray Exposure dating (^{10}Be and ^{36}Cl) of river-polished surfaces (Tinée River, SW Alps, France). Earth and Planetary Science Letters, 457, 271–281.

Rolland, Y., Darnault, R., Braucher, R., Bourlès, D., Petit, C., Bouissou, S., & ASTER Team. (2020). Deglaciation history at the Alpine-Mediterranean transition (Argentera-Mercantour, SW Alps) from ^{10}Be dating of moraines and glacially polished bedrock. Earth Surface Processes and Landforms, 45(2), 393-410.

Rolland, Y., Bilau, A., Cardinal, T., Nouibat, A., Bienveignant, D., Boschetti, L., et al. (2022). Bridging the Gap between Long–Term Orogenic Evolution (> 10 Ma Scale) and Geomorphological Processes That Shape the Western Alps: Insights from Combined Dating Approaches. Geosciences, 12(11), 393.

Saillard M., Petit C., Rolland Y., Braucher R., Bourlès D. L., Zerathe S., Revel M. and Jourdon A., 2014. Late Quaternary incision rates in the Vésubie catchment area (Southern French Alps) from in situ-produced ^{36}CI cosmogenic nuclide dating: Tectonic and climatic implications. J. Geophy. Res.. Earth Surface, 119, 1121-1135.

Sanchez, G., Rolland, Y., Schreiber, D., Giannerini, G., Corsini, M., & Lardeaux, J. M. (2010).

The active fault system of SW Alps. Journal of Geodynamics, 49(5), 296-302.

Schimmelpfennig I., Benedetti L., Finkel R., Pik R., Blard P.-H., Bourlès D.L., Burnard P. et Williams A., 2009. Source of in situ ^{36}Cl in basaltics rocks. Implication for calibration of production rates. Quat. Geochronol., 4, 441-461.

Schumm, 1977. The fluvial system - S. A. Schumm, New York, Wiley, 1977

Schwartz, S., Gautheron, C., Audin, L., Dumont, T., Nomade, J., Barbarand, J., et al. (2017). Foreland exhumation controlled by crustal thickening in the Western Alps. Geology, 45(2), 139–142.

Siame, L., Bellier, O., Braucher, R., Sébrier, M., Cushing, M., Bourlès, D., et al. (2004). Local erosion rates versus active tectonics: Cosmic ray exposure modelling in Provence (south-east France). Earth and Planetary Science Letters, 220(3–4), 345–364.

Sklar, L. S., & Dietrich, W. E. (2001). Sediment and rock strength controls on river incision into bedrock. Geology, 29(12), 1087–1090.

Sklar L. S. and Dietrich W. E. (2006). The role of sediment in controlling steady-state bedrock channel slope: Implications of the saltation–abrasion incision model. Geomorphology, 82, 58-83.

Sternai, P., Sue, C., Husson, L., Serpelloni, E., Becker, T. W., Willett, S. D., et al. (2019). Present-day uplift of the European Alps: Evaluating mechanisms and models of their relative contributions. Earth-Science Reviews, 190, 589–604.

Stokes, M., Mather, A. E., Belfoul, A., & Farik, F. (2008). Active and passive tectonic controls for transverse drainage and river gorge development in a collisional mountain belt (Dades Gorges, High Atlas Mountains, Morocco). Geomorphology, 102(1), 2–20.

Stone J.O., 2000. Air pressure and cosmogenic isotope production. J. Geophys. Res.: Solid Earth, 105, 23,753-23,759.

Suc, J.-P., & Zagwijn, W. H. (1983). Plio-Pleistocene correlations between the northwestern Mediterranean region and northwestern Europe according to recent biostratigraphic and palaeoclimatic data. Boreas, 12(3), 153–166.

Thomas, F., Rizza, M., Bellier, O., Billant, J., Dussouillez, P., Fleury, J., et al. (2021). Assessing post-Pliocene deformation in a context of slow tectonic deformation: Insights from paleoseismology, remote sensing and shallow geophysics in Provence, France. Natural Hazards, 105(2), 1453–1490.

Turowski, J. M., Hovius, N., Wilson, A., and Horng, M.-J. (2008). Hydraulic geometry, river sediment and the definition of bedrock channels. Geomorphology, 99(1), 26–38.

Twidale, C. R. (2004). River patterns and their meaning. Earth-Science Reviews, 67(3–4), 159–218.

Valla P.G., van der Beek P.A. and Carcaillet J., 2010. Dating bedrock gorge incision in the French Western Alps (Ecrin-Pelvoux massif) using cosmogenic 10Be. Terra Nova, 22, 18-25.

Valla, P. G., Shuster, D. L., and van der Beek, P. A. (2011). Significant increase in relief of the European Alps during mid-Pleistocene glaciations. Nature Geoscience, 4 (10), 688–692.

Whipple, K. X. (2004). Bedrock rivers and the geomorphology of active orogens. Annual Review of Earth and Planetary Sciences, 32(1), 151–185.

Whipple, K. X., and Tucker, G. E. (1999). Dynamics of the stream-power river incision model: Implications for height limits of mountain ranges, landscape response timescales, and research needs. Journal of Geophysical Research: Solid Earth, 104 (B8), 17661–17674.

Whipple, K. X., Hancock, G. S., & Anderson, R. S. (2000). River incision into bedrock: Mechanics and relative efficacy of plucking, abrasion, and cavitation. GSA Bulletin, 112(3), 490–503.

Wobus, C., Whipple, K. X., Kirby, E., Snyder, N., Johnson, J., Spyropolou, K., et al. (2006). Tectonics from topography: Procedures, promise, and pitfalls. Special Papers-Geological Society of America, 398, 55.

Zerathe, S., Lebourg, T., Braucher, R. & Bourlès, D., 2014. Mid-Holocene cluster of larger-scale landslides revealed in the Southwestern Alps by ^{36}Cl dating. Insight on an Alpine-Scale landslide activity. Quaternary Sci. Rev., 90, 106-127.

Chapitre 7 : Conclusions

1. Rappel des objectifs de la thèse

Les objectifs de cette thèse étaient les suivants :

- Utilisation de taux d'incision comme proxy pour la chronologie des périodes de déglaciation et pour la quantification de taux de soulèvement ;
- Détermination des vitesses et du moteur de l'incision dans les Alpes du Sud-Ouest depuis le LGM.

Et à travers ces objectifs principaux, j'ai tenté de :

- Mettre à l'épreuve l'application de la méthode de quantification de taux d'incision par l'utilisation des nucléides cosmogéniques dans des gorges ;
- Améliorer la connaissance du processus d'incision et de formation des gorges.

2. Synthèse des résultats et interprétations

2.1. Dans quelle mesure l'application de la datation par les nucléides cosmogéniques permet de quantifier des taux d'incision ?

L'interprétation de données d'âge d'exposition d'une surface par la quantification de la concentration en nucléides cosmogéniques in-situ présente une variable inconnue : quel processus est à l'origine de l'exposition datée ? Afin de quantifier des taux d'incision dans le substrat rocheux à l'aide de cette méthode, les surfaces érodées doivent avoir été exposées suite à l'action érosive de la rivière entrainant l'abaissement vertical progressif de son lit. Cependant, d'autres processus et évènements peuvent affectées la surface a posteriori, et donc influencer la concentration de nucléides cosmogéniques.

Dans la première étude utilisant la méthode des nucléides cosmogéniques dans une gorge, Schaller et al. (2005) invoque une « ré-incision » par érosion latérale lors du déblaiement d'un remplissage sédimentaire de la gorge. Montgommery et Korup (2011) évoque la couverture

ponctuelle d'un glacier pour faire masque aux rayons cosmiques. Dans ce cas, on peut facilement imaginer qu'une gorge formée avant la glaciation voit sa concentration des nucléides cosmogénique stagner ou même diminuer si le temps de couverture est plus long que la période de désintégration atomique des nucléides considérés. De plus, l'incision sous-glaciaire peut éroder et découvrir des surfaces hors d'atteinte des rayons cosmiques, retardant le début de la production de nucléides. Le chapitre 3 discute de l'occurrence de chutes de blocs pour expliquer les « anomalies » dans la répartition des âges selon leur hauteur, si l'on considère une exposition progressive de la paroi exclusivement via de l'incision verticale. Le chapitre 5 propose une nouvelle interprétation de l'exposition des parois de trois gorges, localisées le long d'une même vallée, basée sur l'aspect de la distribution âge/hauteur. Ici l'apparition de nombreux âges similaires mais localisés à des hauteurs différentes suggèrent un épisode brusque d'exposition, qui est attribué au déblaiement rapide d'un remplissage sédimentaire et à l'érosion latérale associée plutôt qu'à de l'incision purement fluviatile. Or, pour déterminer des taux d'incision, les surfaces doivent strictement avoir été épargnées de toutes formes de fortes érosions post-incision (Ouimet et al., 2008).

Dans ces trois études, l'élément qui a amené à regarder les données sous un autre angle et reconsidérer le processus à l'origine de l'exposition datée est l'aspect de la distribution âge/hauteur. En effet, comment expliquer des âges plus jeunes positionnés sur la paroi au-dessus d'âges plus vieux ? Cette distribution ne correspond pas à l'évolution théorique de l'exposition de la paroi dans le cas d'une incision verticale et appelle donc à l'invocation d'autres processus et événements. Il n'est pas aisé de voir les marques de ces événements lors de l'échantillonnage. Les arêtes saillantes d'une niche d'arrachement peuvent être arrondies par la météorisation. Des dépôts alluviaux haut perchés sont des marqueurs de remplissage sédimentaire, mais ce genre de dépôt est difficilement possible le long de parois verticales. De plus, l'échantillonnage se faisant sur corde le long des parois de gorge plus ou moins étroites,

il n'est pas toujours possible pour le grimpeur, qui échantillonne, comme pour le piéton, qui mesure la hauteur des échantillons à l'aide d'un laser, d'avoir assez de recul pour identifier ce genre de marques.

D'autres phénomènes, non-observés ici, peuvent également influencer la production de nucléides cosmogéniques dans une gorge. L'occurrence de crues peut éroder latéralement le pied de la paroi, délimitant ainsi une « zone active » où la concentration de nucléides cosmogéniques est fréquemment dégradée. Les chutes de blocs affectant la paroi verticale peuvent entrainer l'accumulation de blocs rocheux au pied de la paroi, créant ainsi un masque limitant l'exposition aux rayons cosmiques.

La quantification de taux d'incision à partir de la datation de l'exposition des parois d'une gorge doit donc être considéré avec précaution et une attention toute particulière doit être prêtée aux âges « anormalement » jeunes (par rapport aux autres âges voisins), explicable par l'évocation d'autres processus érosifs.

2.2. Quels paramètres locaux contrôlent l'incision des gorges et affectent leur évolution ?

Le chapitre 4 illustre le rôle de la lithologie comme un facteur limitant la transmission de l'incision d'un cours d'eau principal à son affluent avec le cas du bassin versant de la Roya. Dans ce chapitre également, une knickzone constituée de forts knickpoints lithologiques formant des gorges le long du Bès est présentée comme une zone tampon, qui limite la propagation de l'incision vers l'amont de la rivière. Dans le Chapitre 6, le tracé du Verdon, et notamment la présence d'un méandre très serré, est mentionné comme étant un facteur limitant dans la propagation de l'incision de l'amont vers l'aval. En effet, le méandre semble être un piège à particule, réduisant donc l'alimentation en sédiment, outil de l'incision, vers l'aval.

Concernant l'évolution des gorges, le chapitre 3 montre que les parois, une fois exposées par l'incision, sont soumises à des chutes de blocs. Le cas de la Clue de Barles montre que, sur le long terme, le profil latéral d'une gorge s'élargit et peut prendre une forme en V tout en s'incisant verticalement, comme le ferait le profil d'une vallée à mesure que son thalweg s'enfonce par incision. La seule différence entre les deux est donc la compétence de la roche dans laquelle la rivière incise, retardant le processus d'élargissement dans le cas d'une gorge. Le Chapitre 5 propose que les gorges peuvent se remplir de sédiments qui, pour être évacués, entrainent une érosion latérale des parois, élargissant donc encore l'entaille créée au préalable par la rivière.

2.3. Quel est le moteur de l'incision dans les Alpes du Sud après le Dernier Maximum Glaciaire ?

L'étude régionale présentée dans le chapitre 4 a montré que, selon la localisation des gorges par rapport aux dernières glaciations du LGM, les variations climatiques tout comme le soulèvement tectonique contrôlent l'incision. Dans les zones significativement affectées par les glaciers du Würm, l'influence du climat est démontrée par l'impact des déglaciations. Dans ces zones, les taux d'incision élevés d'incision pourraient masquer le signal tectonique long-terme plus faible. En effet, en dehors de l'influence glaciaire, les taux d'incision des rivières sont comparables aux taux d'érosion long-terme (> 10 Ma) et au vitesse de soulèvement. Par conséquent, nos résultats et nos interprétations suggèrent que l'incision fluviale du Quaternaire supérieur dans les Alpes du Sud-Ouest réajuste la topographie à la fois au forçage climatique court-terme et au forçage tectonique long-terme.

Quel est le forçage dominant ?

L'impact des variations climatiques à travers les cycles glaciaire-interglaciaire semble être dominant. De précédentes études ont quantifié des taux d'incision post-LGM dans les Alpes de

l'Ouest montrant des valeurs entre 2 et 18 mm/an que les auteurs associent à l'impact des déglaciations post-LGM (Valla et al., 2010 ; Van den Berg et al., 2012 ; Saillard et al., 2014 ; Rolland et al., 2017). Ces valeurs élevées représentent des pulses d'incision court-terme qui n'expliquent cependant pas la formation totale des gorges mais seulement les parties basses. De plus, le Chapitre 5 propose que les taux les plus extrêmes concernant les hauteurs de parois les plus élevées (les 3 gorges de la Haute Tinée, Rolland et al., 2017), ne représentent pas le processus d'incision de ces gorges mais le rajeunissement de leurs parois par d'autres processus érosifs.

Bien que ces résultats réduisent l'implication court-terme de la déglaciation post-LGM, ils ne contredisent pas l'hypothèse que les variations climatiques soient le moteur dominant de l'incision. En effet, les gorges peuvent se former au cours de plusieurs cycles glaciaire-interglaciaire (Montgommery et Korup, 2011). En revanche, cette hypothèse suppose que l'action érosive des glaciers durant les périodes de glaciation n'est pas suffisante pour effacer les marqueurs d'érosion formés durant les périodes interglaciaires. Le débat concernant l'efficacité de l'érosion fluviatile contre celle des glaciers reste ouvert, mais nous proposons dans cette étude des hypothèses qui vont dans le sens de l'idée que l'efficacité des deux processus peut être surestimée (Koppes and Montgommery, 2009).

Les résultats de cette thèse montrent en revanche que hors de l'atteinte des glaciers, les taux d'incision sont faibles, stables et s'étendent sur des périodes de temps (>30 ka) plus longues que celles obtenues par la datation des autres gorges dans la région. Après comparaison avec des taux locaux de soulèvement et de dénudation, ces taux d'incision sont attribués à la réponse des cours d'eau au soulèvement tectonique.

3. Conclusions

A la fin de cette thèse, ce travail a permis de proposer les conclusions suivantes :

- La quantification et l'interprétation de l'incision par la méthode des nucléides cosmogéniques dans les gorges peut fournir des résultats convaincants mais requiert tout de même la considération d'autres processus pour expliquer les éventuelles anomalies.
- La lithologie contrôle la propagation de l'incision dans un bassin versant, et notamment sa propagation dans les affluents en réponse à une accélération de l'incision dans le cours d'eau principal.
- Les gorges semblent être le produit de plusieurs cycles glaciaire-interglaciaire.
- Les taux d'incision provenant de gorges dans les Alpes du Sud-Ouest se rangent en trois catégories : (a) 3-1 mm/yr, (b) 0,5-1 mm/yr, (c) ~0,25 mm/yr, selon la localisation de ces gorges par rapport à la glaciation du LGM.
- Les gorges directement connectées aux glaciers enregistrent une accélération de l'incision pendant la période de déglaciation (14-19 ka) alors que les gorges indirectement connectées (affluents) enregistrent une accélération de l'incision plus tardive (10-12 ka).
- Les gorges totalement déconnectées de l'influence ou de l'extension des glaciers enregistrent des taux d'incision constants et faibles (~0,25 mm/yr) pouvant être une réponse à un soulèvement tectonique régional.

4. Perspectives

4.1. Echantillonnage et datation de terrasses alluviales

Durant les missions de terrain effectuées dans cette thèse à la recherche de marqueurs d'incision, des niveaux de terrasses alluviales ont été identifiés le long du Var, en aval d'Entrevaux (Figure 1) et en amont de l'embouchure avec la mer Méditerranée (Figure 2). Un niveau de terrasses préservé par un glissement de terrain est également visible le long du Bès, en amont de la Clue de Barles (Figure 3).

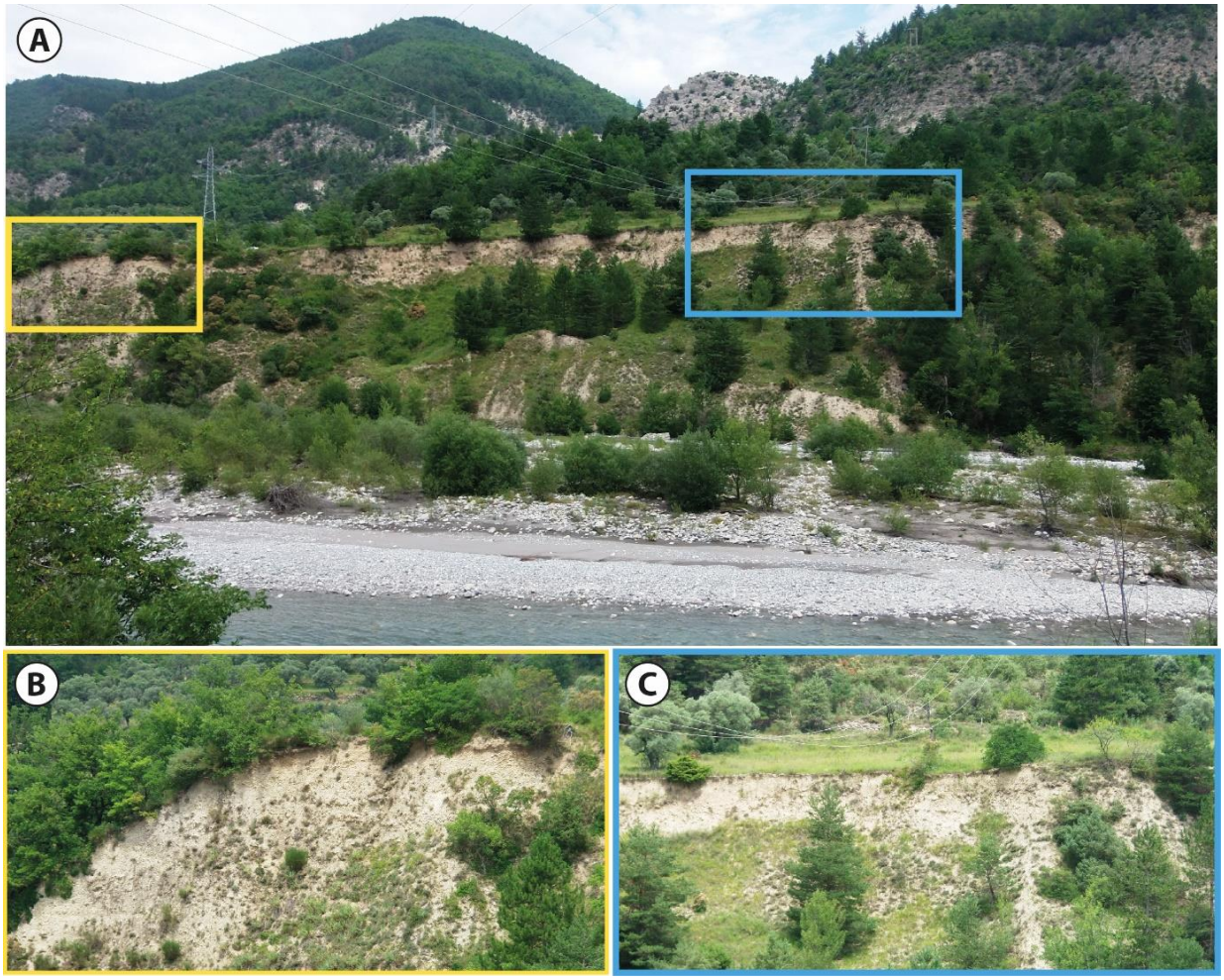

Figure 7-1 : A, Terrasse alluviale le long du Var en aval d'Entrevaux. B et C, zoom sur les zone encadrées jaune et bleue, respectivement.

La détermination de la concentration en ^{10}Be et ^{26}Al dans des galets riches en quartz à la surface de la terrasse permet de dater l'abandon de la terrasse, si l'on considère que l'âge d'abandon de la terrasse est contemporain de l'âge du dépôt de la couche la plus élevée de la terrasse (Carcaillet et al., 2009). Ensuite, connaissant la position de la terrasse par rapport au lit actuel de la rivière et l'âge d'abandon de cette terrasse qui est considéré comme le début de l'épisode d'incision, on peut estimer une vitesse moyenne d'incision. Cette vitesse n'est cependant qu'une moyenne, car elle ne prend pas en compte les variations de vitesse d'incision dans le temps.

Figure 7-2 : A, marqueurs de la présence d'une terrasse alluviale, proche de Saint-Laurent-du-Var à l'embouchure du Var. B, zoom sur la zone encadrée en rouge.

Figure 7-3 : Niveau de terrasse alluviale reposant sur un substrat de Terres Noires et recouvert d'une couche d'avalanche de débris, le long du Bès en amont de la Clue de Barles.

4.2. Morphométrie

La comparaison de taux d'incision provenant de différents bassins versants n'est pas simple, car l'incision est fortement influencée par la morphologie du cours d'eau et du bassin versant. De plus, nous avons obtenu dans cette étude des taux d'incision de différentes gorges, qui doivent être considérées comme un point unique dans leur bassin versant respectif et doivent donc être considérées avec précaution comme représentatives de l'incision en cours à l'échelle du bassin versant. Dans un effort de normalisation des données, il semble donc important de prendre en compte certaines caractéristiques locales (échelle de la gorge) et plus globales (échelle du bassin versant), qui sont différentes d'un bassin versant à l'autre. Afin de contextualiser chaque gorge dans son bassin versant respectif, et donc d'obtenir une compréhension approfondie du processus d'incision à l'échelle du bassin versant à partir de la datation CRE des gorges, l'utilisation de la Stream Power Law (SPL) s'avèrerait être un bon complément à nos datations.

La SPL est un des modèles les plus utilisés dans la modélisation de l'incision fluviatile (Lague, 2014). La SPL s'exprime comme suit (Whipple et Tucker, 1999) :

$$E = KA^m S^n$$

où E est le taux d'érosion (LT^{-1}), K est le coefficient d'érodabilité ($T^{-1}L^{(1-2m)}$), A est l'aire drainée (L^2), $S = -\partial z/\partial x$ est la pente locale (L/L) et *n* et *m* sont des constantes. Le coefficient d'érodabilité K englobe l'influence de la lithologie, du climat, et donc du taux de précipitation, et des processus de transport des sédiments, tandis que l'aire drainée A englobe le débit (Wobus et al., 2006). Les termes A et S sont élevés à l'exposant *m* et *n*, respectivement. *m* est le rapport de *m/n*, qui décrit la concavité du profil de rivière, tandis que *n* représente la pente globale du profil d'une rivière.

Alors que l'aire de drainage et la pente du chenal peuvent être obtenues à partir d'un MNT, les paramètres inconnus K, m/n et *n* sont souvent fixés sur la base des résultats provenant

de la littérature. Ces présomptions peuvent conduire à une estimation inexacte des processus érosifs agissant sur les zones étudiées (Harel et al., 2016 ; Gailleton et al., 2021). En effet, il est souvent supposé que $0,4<m/n<0,6$ (Kirby et Whipple, 2012) et $n=1$, si l'on considère que l'incision est proportionnelle à la puissance du cours d'eau (Whipple et Tucker, 1999).

Afin de contraindre le paramètre m/n, la méthode de l'approche intégrale présentée par Perron et Royden (2013) est couramment utilisée. Cette méthode, contrairement à la méthode pente/aire drainée (Wobus et al., 2006), utilise l'altitude au lieu de la pente et peut donc contourner l'erreur liée aux données topographiques bruitées, et une intégrale spatiale de la surface de drainage appelée χ, pour créer un profil de rivière transformé. La courbe résultante de z en fonction de χ est appelée Chi-Plot (Perron et Royden, 2013). Parce que le Plot n'utilise pas l'aire drainée (comprise dans le calcul de χ tout de même), il devient possible de comparer les profils de rivière indépendamment de leur échelle spatiale. Ce dernier est donc utile pour comparer plusieurs rivières localisées dans différents bassins versant avec le même niveau de base, et comme dans notre étude et mettre en avant les éventuels facteurs qui perturbent leur profil en long, comme des variations de soulèvement ou d'érodabilité (K).

Un profil lisse et concave suggère un état d'équilibre de la rivière qui a réajusté son profil à d'éventuels forçages (Wobus et al., 2006). Toutes variations de concavité ou de pente le long d'un profil de rivière peut être le résultat de variations spatiales et temporelles du taux de soulèvement, de variations temporelles des conditions climatiques ou de variations spatiales de la résistance du substrat rocheux (Kirby et Whipple, 2001 ; Wobus et al., 2006).

Dans le cas de bassins versants présentant la même lithologie, toutes variations du K pourraient potentiellement souligner des disparités de conditions climatiques. Cependant, le terme K est très peu contraint (Stock and Montgomery, 1999) et dépend d'un grand nombre de paramètres qu'il faut déterminer indépendamment ou choisir d'après la littérature. Sa comparaison d'un bassin versant à l'autre est hasardeuse et demande de faire des suppositions

sur les processus d'érosion et caractéristiques locales des bassins versants et systèmes hydriques étudiés.

Références

Alfimov, V. and Ivy-Ochs, S., 2009. How well do we understand production of ^{36}Cl in limestone and dolomite ? Quaternary Geochronology, 4, 462-474.

Arnold, M., Merchel, S., Bourlès, D.L., Braucher, R., Benedetti, L., Finkel, R.C., Aumaître, G., Gottdang, A. and Klein M., 2010. The French accelerator mass spectrometry facility ASTER: improved performance and developments. Nucl. Instrum. Methods Phys. Res., B 268, 1954-1959.

Bacon, S.N., McDonald, E.V., Caldwell, T.G. and Dalldorf, G.K., 2009. Timing and distribution of alluvial fan sedimentation in response to strengthening of late Holocene ENSO variability in the Sonoran Desert, southwestern Arizona, USA. Quaternary Research, 73, 425-438.

Balco, G., Stone, J.O., Lifton, N.A. and Dunai, T.J., 1996. A complete and easily accesible means of caltulating surfaces exposure ages or erosion rates from 10Be and 26Al measurements. Quaternary Geochronology, 3, 174-195.

Ballantyne, C.K., 2002. A general model of paraglacial landscape response. The Holocene, 12, 3, 371-376.

Ballantyne, C. L., Wilson, P., Gheorghiu, D. and Rodés, A., 2014. Enhanced rock-slope failure following ice-sheet deglaciation: timing and causes. Earth Surf. Process. Landforms, 39, 900–913.

Bloom, A.L., 1998. Geomorphology. A systemic analysis of Late Cenozoic Landforms, 3rd ed., Prentice Hall, Upper Saddle River, New Jersey, 482 p

Bierman, P. and Steig, E.J., 1996. Estimating rates of denudation using cosmogenic isotope abundances in sediment. Earth Surf. Process. Landf., 21, 125–139.

Bilau, A., Rolland, Y., Schwartz, S., Godeau, N., Guihou, A., Deschamps, P., Brigaud, B., Noret, A., Dumont, T., Gautheron, C., 2020. Extensional reactivation of the Penninic Frontal Thrust 3 Ma ago as evidenced by U-Pb dating on calcite in fault zone cataclasite. Solid Earth, 12, 237–251.

Bigot-Cormier, F., Sosson, M., Poupeau, G., Stéphan, J.-F. and Labrin, E., 2006. The denudation history of the Argentera Alpine External Crystalline Massif (Western Alps, France-Italy): an overview from the analysis of fission tracks in apatites and zircons. Geodin. Acta, 19, 455–473.

Bishop, P., Hoey, T.B., Jansen, D. and Artza, I.L., 2005. Knickpoint recession rate and

catchement area: the case of uplifted rivers in Eastern Scotland. Earth Surface Processes and Landforms, 30, 767-778.

Bogdanoff, S., Michard, A., Mansour, M. and Poupeau, G., 2000. Apatite fission track analysis in the Argentera massif: evidence of contrasting denudation rates in the External Crystalline Massifs of the Western Alps. Terra Nova, 12, 117–125

Bonneau, L., Jorry, S. J., Toucanne, S., Silva Jacinto, R. and Emmanuel, L., 2014. Millennial-Scale Response of a Western Mediterranean River to Late Quaternary Climate Changes: A View from the Deep Sea, J. Geol., 122, 687–703.

Bonneau, L., Toucanne, S., Bayon, G., Jorry, S.J., Emmanuel, L. and Jacinto, R.S., 2017. Glacial erosion dynamics in a small mountainous watershed (Southern French Alps): a source-to-sink approach. Earth Planet. Sci. Lett. 458, 366–379.

Burbank, D. W., 2002. Rates of erosion and their implications for exhumation. Mineralogical Magazine, 66, 1, 25-52.

Braucher, R., Castillo, P.D., Siame, L., Hidy, A.J. and Bourlès, D.L., 2009. Determination of both exposure time and denudation rate from an in situ-produced 10Be depth profile : a mathematical proof of uniqueness. Model sensitivity and applications to natural cases. Quaternary Geochronology, 4, 1, 56-67.

Braucher, R., Merchel, S., Borgomano, J. and Bourlès, D.L., 2011. Production of cosmogenic radionuclides at great depth: a multi element approach. Earth and Planetary Science Letters, 309, 1-9.

Braucher, R., Keddadouche, K., Aumaître, G., Bourlès, D.L., Arnold, M., Pivot, S., Baroni, M., Scharf, A., Rugel, G. and Bard, E., 2018. Chlorine measurements at the 5 MV French AMS national facility ASTER: associated external uncertainties and comparability with the 6MV DREAMS facility. Nucl. Instrum. Methods Phys. Res., B 420, 40–45.

Brisset, E., Guiter, F., Miramont, C., Revel, M., Anthony, E.J., Belhon, C., Arnaud, F., Malet, E. and de Beaulieu, J.-L., 2015. Lateglacial/Holocene environmental changes in the Mediterranean Alps inferred from lacustrine sediments. Quaternary Sci. Rev., 110, 49-71.

Brocart, G.Y., 2003. Origine, variabilité spatio-temporelle et signature morphologique de l'incision fluviatile sans les Alpes dauphinoises (SE France). Géologie Alpine Mémoire H.S., 43, 167 p.

Brocart, G.Y., van der Beek, P., Bourlès, D., Siame, L. and Mugnier, J.-L., 2003. Long-term fluvial incision rate and postglacial river relaxation time in the French Western Alps from ^{10}Be dating of alluvial terraces with assessment of inheritance, soil developpement and

wind ablations effects. Earth and Planetary Sciences Letters, 209, 197-214.

Bucha, V., 1970. Influence of Earth's magnetic field on radio-carbon dating. In : Radiocarbon Variations and Absolute Chronology, I.U. Olsson (Eds.) John Wiley, New York, 501-511.

Burbank, D.W., Leland, J., Fielding, E., Anderson, R.S., Brozovic, N., Reid, M.R., and Duncan, C., 1996. Bedrock incision, rock uplift and threshold hillslopes in the northwestern Himalayas. Nature, 379, 505-510.

Carcaillet, J., Mugnier, J.L., Koçi, R. and Jouanne, F., 2009. Uplift and active tectonics of southern Albania inferred from incision of alluvial terraces. Quaternary Research, 71, 3: 465-476.

Champagnac, J.D., Molnar, P., Andersion, R.S., Sue, C. and Delacou, B., 2007. Quaternary erosion-induced isostatic rebound in the western Alps. Geological Society of America, 35, 195-198.

Chapron, E., 1999. Contrôle climatique et tectonique de la sédimentation lacustre de l'avant pays alpin (lac du Bourget) durant le quaternaire récent. Géologie Alpine Mémoire H.S., 68, 258 p.

Clark, P.U., Dyke, A.S., Shakum, J.D., Carlson, A.E., Clark, J., Wohlfarth, B., Mitrovica, J. X., Hostetler, S.W. and McCabe, A.M., 2009. The last Glacial Maximum. Science, 325, 710–714.

Clauzon, G., 1979. Le canyon messinien de la Durance (Provence, France) : une preuve paléogéographique du bassin profond de dessication. Palaeogeography, Palaeoclimatology, Palaeoecology, 29, 15-40.

Clauzon, G., 1982. Le canyon messinien du Rhône : une preuve décisive du ''dessicated deep-basin model'' [Hsü, Cita et Ryan, 1973]. Bulletin de la Société Géologique de France, 24, 597-610.

Clauzon, G., 1996. Limites de séquences et évolution géodynamique. Geomorphology, 1, 3-22

Codilean, A.T., 2006. Calculation of the cosmogenic nuclide production topographic shielding sclaning factor for large areas using DEMs. Earth Surface Processes and Landforms, 31, 6, 785-794.

Cossart, E., Braucher, R., Fort, M., Bourlès, D.L. and Carcaillet, J., 2008. Slope instability in relation to glacial debuttressing in alpine areas (Upper Durance catchment, southeastern France): evidence from field data and 10Be cosmic ray exposure ages. Geomorphology, 95, 3-26.

Cyr, A.J., Granger, D.E., Olivetti, V. and Molin, P., 2010. Quantifying rock uplift rates using

channel steepness and cosmogenic nuclide-determined erosion rates: Examples from northern and southern Italy. Lithosphere, 2-3, 188-198.

Daniels, J.M., 2008. Distinguishing allogenic from autogenic causes of bed elevation change in late Quaternary alluvial stratigraphic records. Geomorphology, 101, 159-171.

Darnault, R., Rolland, R., Rolland, Y., Bourl`es, D., Revel, M., Sanchez, G. and Bouissou, S., 2012. Timing of the last deglaciation revealed by receding glaciers at the Alpine-scale: impact on mountain geomorphology. Quaternary Sci. Rev., 3, 127–142.

Davis, B.A.S., Brewer, S., Stevenson, A.C., Guiot, J., Contributors, Data, 2003. The temperature of Europe during the Holocene reconstructed from pollen data. Quaternary Sci. Rev. 22, 1701–1716.

Desilets, D. and Zreda, M., 2003. Spatial and temporal distribution of secondary cosmicray nucleon intensities and applications to in situ cosmogenic dating. Earth and Planetary Science Letters, 206, 21-42.

Dunai, T., 2000. Scaling factors for production rates of in situ produced cosmogenic nuclides: A critical reevaluation. Earth and Planetary Science Letters, 176, 157-169.

Dunne, F., Elmore, D. and Muzikar, P., 1999. Scaling factors for the rates of production of cosmogenic nuclides for geometric shielding and attenuation at depth on sloped surfaces. Geomorphology, 27, 3-11.

England, P. and Molnar, P., 1990. Surface uplift, uplift of rocks, and exhumation of rocks. Geology, 18, 1173-1177.

Federici, P. R., Ribolini, A. and Spagnolo, M., 2016. Glacial history of the Maritime Alps from the Last Glacial Maximum to the Little Ice Age, in Hughes, P.D. and Woodward, J.C., eds., Quaternary Glaciation in the Mediterranean Mountains. Geological Society, London, Special Publications, 433, 135-159.

Ford, M., Duchêne, S., Gasquet, D., and Vanderhaeghe, O., 2006, Two-phase orogenic convergence in the external and internal SW Alps. J. Geol. Soc. London, 163, 815–826.

Fox, M., Leith, K., Bodin, T., Balco, G. and Shuster, D.L., 2015. Rate of fluvial incision in the Central Alps constrained throught joint inversion of detrital ^{10}Be and thermochronometric data. Earth Planet. Sci. Lett., 411, 27-36.

Gailleton, B., Mudd, S.M., Clubb, F.J., Grieve, S.W.D. and Hurst M.D., 2021. Impact of Changing Concavity Indices on Channel Steepness and Divide Migration Metrics. Journal of Geophysical Research: Earth Surface, 126, e2020JF006060.

Gautier, F., Clauzon, G., Suc, J.P., Cravatte, J. and Violanti, D., 1994. Age et durée de la crise

de salinité messinienne. C.R. de l'Académie des Sciences de Paris, IIa, 318, 1103-1109.

Gardner, T.W., 1983. Experiment study of knickpoint and longitudinal profile evolution in cohesive, homogeneous material. Geological Society of America Bulletin, 94, 664-672.

Genuite, K., Delannoy, J.-J., Bahain, J.-J., Gresse, M., Jaillet, S., Philippe, A., Pons-Branchu, E., Revil, A. and Voinchet P., 2021. Dating the landscape evolution around the Chauvet-Pont d'Arc cave. Scientific Reports, 11, 8944.

Gidon, M.,1997. Les chaînons subalpins au nord-est de Sisteron et l'histoire tectonique de la nappe de Digne. Géologie Alpine, 73, 23–57.

Glotzbach, C., van der Beek, P. A. and Spiegel, C., 2011. Episodic echumation and relief growth in the Mont Blanc massif, western Alps from numerical modelling of thermochronology. Earth Planet. Sci. Lett., 304, 417-430.

Godard, V., Ollivier, V., Bellier, O., Miramont, C., Shabanian, E., Fleury, J., Benedetti, L., Guillou, V. and ASTER Team, 2016. Weathering-limited hillslope evolution in carbonate landscapes. Earth and Planetary Science Letters, 446, 10-20.

Gosse, J. and Phillips, F., 2001. Terrestrial in situ cosmogenic nuclides: Theory and application. Quaternary Science Reviews, 20, 1475-1560.

Granger, D. and Muzikar, P. 2001. Dating sediment burial with in situ produced cosmogenic nuclides: theory, techniques, and limitations. Earth and Planetary Science Letters, 188, 269-281.

Granger, D. and Riebe, C., 2007. Cosmogenic Nuclides in Weathering and Erosion. In : Drever J., (ed.), Treatise on Geochemestry and Ground Water, Weathering, and Soils. Elsevier.

Gudmundsson, G.H., 1994. An order of magnitude estimate of the current uplift rates in Switzerland caused by the Würn alpine deglaciation. Eclogae Geologicae Helvetiae, 87, 545-557.

Guerit, L., Barrier, L., Jolivet, M., Fu, B. and Métivier, F., 2016. Denudation intensity and control in the Chinese Tian Shan: new constraints from mass balance on catchment-alluvial fan systems. Earth Surf. Process. Landforms, 41, 1088-1106.

Hack, J.T., 1960. Interpretation of erosional topography in humid temperature regions. American Journal of Sciences, 258, 80-97.

Harel, M.-A. Mudd, S.M. and Attal M., 2016. Global analysis of the streampower lawparameters based on worldwide 10Be denudation rates. Geomorphology, 268, 184-196.

Hartshorn, K., Hovius, N., Dade, W.B. and Slingerland, R.L., 2002, Climate-driven bedrock

incision in an active mountain belt. Science, 297, 2036-2038.

Hay, W.W., 1998. Detrital sediment fluxes from contients to oceans. Chemical Geology, 145, 287-323.

Hayakawa, Y. and Matsukura, Y., 2003. Recession rates of waterfalls in Boso peninsula, Japan, and a predictive equation. Earth Surface Processes and Landforms, 28, 675-684.

Heiri, O., Koinig, K.A., Spötl, C., Barrett, S., Brauer, A., Drescher-Schneider, R., Gaar, D., Ivy-Ochs, S., Kreshner, H., Luetscher, M., Moran, A., Nicolussi, K., Preusser, F., Schmidt, R., Schoeneich, P., Schw¨orer, C., Sprafke, T., Terhorst, B. and Tinner, W., 2014. Paleoclimate records 60–8 ka in the Austrian and Swiss Alps and their forelands. Quaternary Sci. Rev., 106, 186–205.

Herman, F., Seward, D., Valla, P.G., Carter, A., Kohn, B., Willett, S.D. and Ehlers, T.A., 2013. Worldwide acceleration of mountain erosion under a cooling climate. Nature, 504, 423–426.

Hinderer, M., 2001. Late Quaternary denudation in the Alp, valley and lake filling and modern river loads. Geodin. Acta, 14, 231–263

Hovius, N., 2000. Macroscale process systems of mountain belt erosion. In: Geomorphology and global tectonics, Summerfield M.A., ed., Wilet and Sons Ltd, 77-105.

Ivy-Ochs, S., Kerschner, H., Reuther, A., Maisch, M., Sailer, R., Schaefer, J., Kubik, P.W., Synal, H. and Schlüchter, C., 2006. The timing of glacier advances in the northern European Alps based on surface exposure dating with cosmogenic 10Be, 26Al, ^{36}Cl, and 21Ne, in Siame, L. L., Bourlès, D. L., and Brown, E. T., eds., In Situ–Produced Cosmogenic Nuclides and Quantifi cation of Geological Processes: Geological Society of America Special Paper, 415, 43–60.

Ivy-Ochs, S., Kerschner, H., Reuther, A., Preusser, F., Heine, K., Maisch, M., Kubik, P.W. and Schlüchter, C., 2008. Chronology of the last glacial cycle in the European Alps. J. Quaternary Sci., 23, 559-573.

Jaboyedoff, M., Oppikofer, T., Abella, A., Derron, M. H., Loye, A., Metzger, R. and Pedrazzini, A., 2010. Use of LIDAR in landslide investigations: a review. Natural Hazards, 61, 1, 5-28.

Jansen, J.D., Codilean, A.T., Bishop, P. and Hoey, T.B., 2010. Scale Dependence of Lithological Control on Topography: Bedrock Channel Geometry and Catchment Morphometry in Western Scotland. The Journal of Geology, 118, 223–246.

Jansen, D.J., Fabel, D., Bishop, P., Xu, S., Schnabel, C. and Codilean, A.T., 2011. Does

decreasing paraglacial sediment supply slow knickpoint retreat? Geology, 39, 543–546.

Johnson, J.P. and Whipple, K.X., 2007. Feedbacks between erosion and sediment transport in experimental bedrock channels: earth surface processes and landforms. Earth Surface Processes and Landforms, 32, 1048-1062.

Jones, R.S., Whitehouse, P.L., Bentley, M.J., Small, D. and Dalton, A.S., 2019. Impact of glacial isostatic adjustement on cosmogenic surface-exposure dating. Quaternary Science Reviews, 212, 206-212.

Jorda, M., Rosique, T. and Évin, J., 2000. Données nouvelles sur l'âge du dernier maximum glaciaire dans les Alpes méridionales françaises. Compte Rendu de l'Académie des Sciences Paris. Sciences de la Terre et des Planètes/Earth and Planetary Sciences, 331, 187-193.

Jourdon, A., Rolland, Y., Petit, C. and Bellahsen, N., 2014. Style of Alpine tectonic deformation in the Castellane fold-and-thrust belt (SW Alps, France): Insights from balanced cross-sections. Tectonophysics, 633, 143-155.

Kirby, E., and Whipple, K.X, 2001. Quantifying differential rock-uplift rates via stream profile analysis: Geology, 29, 5, p. 415-418.

Kirby, E. and Whipple, K.X., 2012. Expression of active tectonics in erosional landscapes. Journal of Structural Geology, 44, 54-75.

Koppes, M. N. and Montgommery, D. R., 2009. The relative efficacy of fluvial and glacial erosion over modern to orogenic timescales. Nature Geosciences, 2, 644-647.

Krijgsman, W., Hilgen, F.J., Raffi, I., Sierro, F.J. and Wilson, D.S., 1999. Chronology, causes and progression of the Messinian salinity crisis. Nature, 400, 652-655.

Lal, D., 1988. In situ-produced cosmogenic isotopes in terrestrial rocks. Annual Review of Earth and Planetary Sciences, 16, 355–388.

Lal, D., 1991. Cosmic ray labeling of erosion surfaces: in situ nuclide production rates and erosion models. Earth and Planetary Science Letters, 104, 424-439.

Lague, D., Hovius, N. and Davy, P., 2005. Discharge, discharge variability, and the bedrock channel profile. J. Geophys. Res., 110, F04006.

Lague, D., 2014. The stream power river incision model: evidence, theory and beyond. Earth Surf. Process. Landforms 39, 38–61.

Lavé, J. and Avouac, J.P., 2001. Fluvial incision and tectonic uplift across the Himalayas of central Nepal. Journal of Geophysical Research, 106, 25 561-25 593.

Leland J., Reid M.R., Burbank D.W., Finkel R. and Caffee M., 1998. Incision and differential

bedrock uplift along the Indus River near Nanga Parbat, Pakistan Himalaya, from 10Be and 26Al exposure age dating of bedrock straths. Earth and Planetary Science Letters, 154, 93-107.

Li, Y.-K., 2013. Determining topographic shielding from digital elevation models for cosmogenic nuclide analysis : a GIS approach and field validation. Journal of Mountain Science, 10, 3, 355-362.

Lickorish, H. W. and Ford, M., 1998. Sequential restoration of the external Alpine Digne thrust system, SE France, constrained by kinematic data and synorogenic sediments. Geol. Soc. Spec. Publ., 134, 189–211.

Loget, N. and van den Driessche, J., 2009. Wave train model for knickpoint migration. Geomorphology, 106, 3-4, 376-382.

Lourens, L.J., Hilgen, F.J., Laskar, J., Shackleton, N.K. and Wilson, D., 2004. The neogene period. In: Gradstein F., Ogg J., Smith A., Eds., A geological time scale. Cambridge University Press, Cambridge, UK, 409-440.

Mariotti, A., Blard, P.-H., Charreau, J., Toucanne, S., Jorry, S.J., Molliex, S., Bourlès, D. L., Aumaître, G. and Keddadouche, K., 2021. Nonlinear forcing of climate on mountain denudation durings glaciations. Nat. Geosci., 14, 16–22.

Marrero, S.M., Phillips, F.M., Cafee, M.W. and Gosse, J.C., 2016. CRONUS-Earth cosmogenic ^{36}Cl calibration. Quaternary Geochronology, 31, 199-219.

Mathey, M., Sue, C., Pagani, C., Baize, S., Walpersdorf, A., Bodin, T., Husson, L., Hannouz, E. and Potin, B., 2020. Present-day geodynamics of the Western Alps: new insights from earthquake mechanisms. Solid Earth, 12, 1661–1681.

Meigs, A., Krugh, W.C., Davis, K. and Bank, G., 2006. Ultra-rapid landscape response and sediment yield following glacial retreat, Icy Bay, soutehrn Alaska. Geomorphology, 78, 207-221.

Merchel, S., Bremser, W., Alfimov, V., Arnold, M., Aumaître, G., Benedetti, L., Bourlès, D.L., Caffee, M., Fifield, L.K., Finkel, R.C., Freeman, S. P. H. T., Martschini, M., Matsushi, Y., Rood, D.H., Sasa, K., Steier, P.,Takahashi, T.,Tamari, M., Tims, S.G., Tosaki ,Y., Wilcken, K.M. and Xu, S., 2011. Ultra-trace analysis of ^{36}Cl by accelerator mass spectrometry: an interlaboratory study , Anal. Bioanal. Chem., 400, 3125-3132.

Merritts, D.J., Vincent, K.R. and Wohl, E.E., 1994. Long river profiles, tectonism, and eustasy: A guide to interpretting fluvial terraces. Journal of Geophysical Research, 99, 14 031-14 050.

Molnar, P., and England, P., 1990. Late Cenozoic uplift of mountain ranges and global climate change: Chicken or egg ? Nature, 346, 29-34.

Montgomery, D.R., 1994. Valley incision and the uplift of mountain peaks. Journal of Geophysical Research, 99, 13913-13921.

Montgomery, D.R. and Brandon, M.T., 2002. Topographic controls on erosion rates in tectonically active mountain ranges. Earth and Planetary Science Letters, 201, 481-489.

Montgomery, D.R. and Korup, O., 2011. Preservation of inner gorges through repeated Alpine glaciations. Nat. Geosci., 4, 1, 62–67.

Mudd, S.M., Harel, M.-A., Hurst, M.D., Grieve, S.W.D. and Marrero S.M., 2016. The CAIRN method : automated, reproductible calculation of catchment-average denudation rates from cosmogenic nuclide concentrations. Earth Surface Dynamics, 4, 655-674.

Nishiizumi, K., Finkel, R.C., Klein, J. and Khol, C.P., 1996. Cosmogenic production of ^{7}Be and ^{10}Be in water targets. Journal of Geophysical Research, 101, 10, 22 225-22 232.

Nocquet, J.-M. and Calais, E., 2004. Geodetic measurements of crustal deformation in the western Mediterranean and Europe. Pure Appl. Geophys., 161, 3, 661-681.

Nocquet, J.-M., Sue, C., Walpersdorf, A., Tran, T., Lenôtre, N., Vernant, P., Cushing, M., Jouanne, F., Masson, F., Baize, S., Chéry, J. and van der Beek, P.A., 2016. Present-day uplift of the western Alps. Sci. Rep. 6, 28404.

Norton, K.P. and Vanacker, V., 2009. Effects of terrain smoothing on topographic shielding correction factors for cosmogenic nuclide-derived estimates of basin-averaged denudation rates. Earth Surface Processes and Landforms, 34, 145-154.

Norton, K.P., Abbühl, L.M. and Schlunegger, F., 2010. Glacial conditioning as an erosional driving force in the Central Alps. Geology, 38, 7, 655-658.

Ouimet, W.B., Whipple, K.X., Crosby ,B.T., Johnson, J.P. and Schildgen, T.F., 2008. Epigenetic gorges in fluvial landscapes. Earth Surf. Proc. Land., 33, 1993-2009.

Pan, B., Burbank, D.W., Wang, Y., Wu, G., Li, J. and Guan, Q., 2003. A 900 k.y. Record of strath terrace formation during glacial-interglacial transitions in northwest China. Geology, 31, 957-960.

Peltier, W. and Fairbanks, R., 2006. Global glacial ice volume and Last Glacial Maximum duration from an extended Barbados sea level record. Quaternary Science Reviews, 25, 3 322-3 337.

Perron, J.T. and Royden, L., 2013. An integral approach to bedrock river profile analysis. Earth Surface Processes and Landforms, 38, 570-576.

Petit, C., Rolland, Y., Braucher, R., Bourlès, D., Guillou, V. and Petitperrin, V., 2019. River incision and migration deduced from ^{36}Cl cosmic-ray exposure durations: The Clue de la Cerise gorge in southern French Alps. Geomorphology, 330, 81-88.

Phillips, J.D. and Lutz, J.D., 2008. Profile convexities in bedrock and alluvial streams. Geomorphology, 102: 554-566.

Pina-Valdés, J., Socquet, A., Beauval, C., Doin, M.-P., D'Agostino, N. and Shen, Z.-K., 2022. 3D GNSS velocity field sheds light on the deformation mechanisms in Europe: effects of the vertical crustal motion on the distribution of seismicity. J. Geophys. Res. Solid Earth 127, e2021JB023451.

Potgieter, M.S., 2013. Solar modulation of cosmic rays. Living Reviews in Solar Physics, 10, 3, 66 p

Pratt, B., Burbank, D.W., Heimsath, A. and Ojha, T., 2002. Impulsive alluviation during early Holocene strengthened monsoons, central Nepal Himalaya. Geology, 30, 10, 911-914.

Rolland, Y., Petit, C., Saillard, M., Braucher, R., Bourlès, D., Darnault, R., Cassol, D. and ASTER, Team, 2017. Inner gorges incision history: A proxy for deglaciation ? Insights from Cosmic Ray Exposure dating (^{10}Be and ^{36}Cl) of river-polished surfaces (Tinée River, SW Alps, France). Earth Planet. Sci. Lett., 457, 271-281.

Rolland, Y., Darnault, R., Braucher, R., Bourlès, D., Petit, C., Bouissou, S. and Aster team, 2020. Deglaciation history at the Alpine-Mediterranean transition (Argentera-Mercantour, SW Alps) from ^{10}Be dating of moraines and glacially polished bedrock. Earth Surface Processes and Landforms, 45, 2, 393-410.

Renssen, H., Seppä, H., Heiri, O., Roche, D.M., Goosse, H. and Fichefet, T., 2009. The spatial and temporal complexity of the Holocene Thermal Maximum. Nat. Geosci., 2, 411–414.

Renssen, H., Seppä, H., Crosta, X., Goosse, H. and Roche, D.M., 2012. Global characterization of the Holocene thermal maximum. Quaternary Sci. Rev., 48, 7–19.

Sadier, B., Delannoy, J.-J., Benedetti, L., Bourlès, D.L., Jaillet, S., Geneste, J.-M., Lebatard, A.-E. and Arnold, M., 2012. Further constraints on the Chauvet cave artwork elaboration. Proceedings of the National Academy of Sciences of the United States of America, 109, 8002-8006.

Saillard, M., Petit, C., Rolland, Y., Braucher, R., Bourlès, D. L., Zerathe, S., Revel, M. and Jourdon, A., 2014. Late Quaternary incision rates in the Vésubie catchment area (Southern French Alps) from in situ-produced ^{36}CI cosmogenic nuclide dating: Tectonic and climatic implications. J. Geophy. Res.. Earth Surface, 119, 1121-1135.

Salcher, B. C., Kober, F., Kissling, E. and Willet, S. D., 2014. Glacial impact on short-wavelength topography and long-lasting effects on the denudation of a deglaciated mountain range. Global and Planetary Change, 115, 59-70.

Sanchez, G., Rolland, Y., Corsini, M., Braucher, R., Bourl`es, D., Arnold, M., Aumaître, G., 2010. Relationships between tectonics, slope instability and climate change: Cosmic Ray exposure dating of active faults, landslides and glacial surfaces in the SW Alps. Geomorphology, 107, 1–13.

Schaller, M., Hovius, N., Willett, S.D., Ivy-Ochs, S., Synal, H.-A. and Chen, M.-C., 2005. Fluvial bedrock incision in the active mountain belt of Taiwan from in situ-produced cosmogenic nuclides. Earth Surf. Proc. Land., 30, 955-971.

Schildgen T., Dethier D.P., Bierman P. and Caffee M., 2002. 26Al and 10Be dating of late pleistocene and holocene fill terraces: a record of fluvial deposition and incision, Colorado front range. Earth Surface Processes and Landforms, 27, 773-787.

Schimmelpfennig, I., Benedetti, L., Finkel, R., Pik, R., Blard, P.-H., Bourlès, D.L., Burnard, P. and Williams, A., 2009. Source of in situ ^{36}Cl in basaltics rocks. Implication for calibration of production rates. Quaternary Geochronology, 4, 441-461.

Schlunegger, F. and Norton, K. P., 2013. Water versus ice: The competing roles of modern climate and Pleistocene glacial erosion in the Central Alps of Switzerland. Tectonophysics, 602, 370-381.

Schwartz, S., Gautheron, C., Audin, L., Dumont, T., Nomade, J., Barbarand, J., Pinna-Jamme, R. and van der Beek P., 2017. Foreland exhumation controlled by crustal thickening in the Western Alps. Geological Society of America, 45, 2, 139-142.

Seidl, M.A., Finkel, R.C., Caffee, M.W., Hudson, B.G. and Dietrich, W.E., 1997. Cosmogenic isotope analysis applied to river longitudinal profile evolution: Problems and interpretations. Earth Surface Processes and Landforms, 22, 195-209.

Serpelloni, E., Faccenna, C., Spada, G., Dong, D. and Williams, S.D.P., 2013. Vertical GPS ground motion rates in the Euro-Mediterranean region: New evidence of velocity gradients at different spatial scales along the Nubia-Eurasia plate boundary. J. Geophys. Res.: Solid. Earth, 118, 6003–6024.

Sklar, L. S. and Dietrich, W. E., 2001. Sediment and rock strength controls on river incision into bedrock. Geology, 29, 12, 1087-1090.

Small, E. and Anderson, R., 1995. Geomorphically driven late cenozoic rock uplift in the Sierra Nevada, California. Science, 270, 277-280.

Sternai, P., Herman, F., Valla P. G. and Champagnac, J-P., 2013. Spatial and temporal variations of glacial erosion in the Rhône valley (Swiss Alps): Insights from numerical modeling. Earth and Planetary Science Letters, 368, 119-131.

Sternai, P., Sue, C., Husson, L., Serpelloni, E., Becker, T.W., Willet, S.D., Faccenna, C., Giulio, A.D., Spada, G., Jolivet, L., Valla, P., Petit, C., Nocquet, J.-M., Walpersdorf, A. and Castelletort, S., 2019. Present-day uplift of the European Alps : Evaluating mechanisms and models of their relative contributions. Earth Science Reviews, 190, 589-604.

Stone, J.O., 2000. Air pressure and cosmogenic isotope production. Journal of Geophysical Research: Solid Earth, 105, 23753-23759.

Sue, C., Delacou, B., Champagnac, J.-D., Allanic, C. and Burkhard, M., 2007. Aseismic deformation in the Alps: GPS vs. seismic strain quantification. Terra Nova, 1, 182-188.

Thomas, F., Godard, V., Bellier, O., Shabanian, E., Ollivier, V., Benedetti, L., Rizza, M., Espurt, N., Guillou, V., Hollender, F., Molliex, S. and ASTER Team, 2017. Morphological controls on the dynamics of carbonate landscapes under a mediterranean climate. Terra Nova, 29, 3, 173-182.

Turowski, J.M., Lague, D. and Hovius, N., 2007. Cover effect in bedrock abrasion: a new derivation and its implications for the modeling of bedrock channel morphology. Journal of Geophysical Research-Earth Surface, 112, F04006.

Valla, P.G., van der Beek, P.A. and Carcaillet, J., 2010. Dating bedrock gorge incision in the French Western Alps (Ecrin-Pelvoux massif) using cosmogenic 10Be. Terra Nova, 22, 18-25.

Valla, P.G., Shuster, D.L. and van der Beek, P.A., 2011. Significant increase in relief of the European Alps during mid-Pleistocene glaciations. Nature Geoscience, 4, 688–692.

Van den Berg, F., Schlunegger F., Akçar N. and Kubik P., 2012. ^{10}Be-derived assessment of accelerated erosion in a glacially conditioned inner gorge, Entlebuch, Central Alps of Switzerland. Earth Surf. Process. Landforms, 37, 11, 1175-1188.

Van der Woerd, J., Tapponnier, P., Ryerson, F.J., Meriaux, A.-S., Meyer, B., Gaudemer, Y., Finkel, R.C., Caffee, M.W., Zhao, G. and Xu, Z., 2002. Uniform postglacial slip-rate along the central 600 km of the Kunlun Fault (Tibet), from 26Al, 10Be, and 14C dating of riser offsets, and climatic origin of the regional morphology. Geophysical Journal International, 148, 356-388.

Vernant, P., Hivert, F., Chery, J., Steer, P., Cattin, R. and Rigo, A., 2013. Erosion-induced isostatic rebound triggers extension in low convergent mountain ranges. Geology, 41, 4,

467-470.

Walcott, R., 1973. Structure of the Earth from glacio-isostatic rebound. Annual Review of Planetary and Science Letters, 1, 15–37.

Walker, M.J.C., 2005. Quaternary Dating Methods. John Wiley & Sons Ltd (Ed.), Chichester, England, 306 p.

Walpersdorf, A., Pinget, L., Vernant, O., Sue, C., Deprez, A. and RENAG team, 2018. Does long-term GPS in the Western Alps finally confirm earthquake mechanisms? Tectonics, 37, 3721–3737.

Wanner, H., Beer, J., Bütikofer, J., Crowley, T.J., Cubash, U., Flückiger, J., Goosse, H., Grosjean, M., Joos, F., Kaplan, J.O., Küttel, M., Müller, S.A., Prentice, I.C., Solomina, O., Stocker, T.F., Tarasov, P., Wagner, M. and Widmann, M., 2008. Mid- to late Holocene climate change: an overview. Quat. Sci. Rev., 27, 1791–1828.

Wanner, H., Solomina, O., Grosjean, M., Ritz, S.P. and Markéta, J., 2011. Structure and origin of Holocene cold events. Quat. Sci. Rev., 30, 3109–3123.

Weissel, J.K. and Seidl, M.A., 1998. Inland propagation of erosional escarpments and river profile evolution across the southeast Australian passive continental margin. In: Rivers over Rock: Fluvial Processes in Bedrock Channels. Tinkler K.J. et Wohl E.E., eds., American Geophysical Union, Washington DC. Geophysical Monograph, 107, 189-206.

Whipple, K.X., and G.E. Tucker G.E., 1999. Dynamics of the stream-power river incision model: Implications for height limits of mountain ranges, landscape response timescales, and research needs, J. Geophys. Res., 104, 17,661-17,674.

Whipple, K.X., 2001. Fluvial landscape response time: how plausible is steady-state denudation? American Journal of Science, 301, 313-325.

Whittaker, A.C., Attal, M. and Allen, P.A., 2010. Characterising the origin, nature and fate of sediment exported from catchments perturbed by active tectonics. Basin Research, 22, 809-828.

Willet, S.D., 1999. Orogeny and orography: the effects of erosion on the structure of mountain belts. Journal of Geophysical Research, 104, 28957-28981.

Willet, S.D., Slingerland, R. and Hovius, N., 2002. Uplift, shortening, and steady-state topography in active mountain belts. American Journal of Sciences, 301, 455-485.

Willet, S.D. and Brandon, M.T., 2002. On steady states in mountain belts. Geology, 30, 175-178.

Wobus, C., Whipple, K.X., Kirby ,E., Snyder, N., Johnson, J., Spyropolou, K., Crosby, B. and

Sheehan, D., 2006. Tectonics from topography: Procedures, Promise, and pitfalls. in Willett, S.D., Hovius, N., Brandon, M.T., and Fisher, D., eds., Tectonics, Climate, and Landscape Evolution: Geological Society of America Special Paper 398, 55-74.

Tables des figures

Chapitre 1 :

Chapitre 2 :

Chapitre 3 :

Chapitre 4 :

Chapitre 5 :

Chapitre 6 :

Chapitre 7 :

Table des tableaux :

Chapitre 2 :

Chapitre 3 :

Chapitre 4 :

Chapitre 6 :

Annexes

Annexe 1 : La méthode de photogrammétrie par « *Structure-from-Motion* » (SfM)

La méthode de photogrammétrie par SfM permet des reconstructions 3D à partir de données 2D (Legel, 2011 ; Pierrot-Deseilligny et Clery, 2011 ; Brunier et al., 2016). Cette méthode permet de créer des modèles 3D de haute résolution à partir desquels il est possible de produire des MNS (Modèle Numérique de Surface) et des orthophotographies (Legel, 2011 ; Remondino et al., 2014 ; Brunier et al., 2016). Les avantages de la SfM qui attirent les chercheurs sont son accessibilité et son faible coût, comparé à d'autres méthodes de modélisation 3D comme le LiDAR (*Light Detection And Ranging* ; Rothmund et al., 2013).

La méthode SfM repose sur l'analyse d'une série de photographies prises avec des angles de vues différents et se recouvrant (Szeliski, 2010 ; Fonstad et al., 2013 ; Lucieer et al., 2013). La photogrammétrie est surtout connue pour le traitement de photographies aériennes nadirales mais le renouveau de cette méthode a fait se développer d'autres approches : terrestres ou encore aéroportés par ULM ou drones (Photo 1 ; Rothmund et al., 2013 ; Colomina et Molina, 2014 ; Lingua et al., 2017 ; Sanz-Ablanedo et al., 2018 ; Chudley et al., in press). Ces nouvelles approches obliques permettent de cartographier des objets peu, voir in-, visibles, sur des photographies nadirales plus classiques. De plus, le drone permet de se rapprocher des objets perchés en altitude et d'atteindre des zones inaccessibles (Gerke, 2009). La qualité et la précision du modèle crée grâce à la méthode SfM dépend de plusieurs variables (Remondino et al., 2014 ; Medjkane et al., 2018 ; Sanz-Ablanedo et al., 2018) : la distance entre l'appareil de prise de vue et l'objet étudié, la taille de l'objet, l'aspect de l'objet (texture, brillance, présence de masques), la couverture de la série de photographie, le recouvrement entre les photographies, la qualité des photographies (réglages de l'appareil, conditions d'acquisition, ombres).

Protocole méthodologique

Les traitements de photogrammétrie ont été effectués sur le logiciel Metashape (Agisoft LLC, St. Petersburg, Russia). Le protocole méthodologique utilisé dans cette étude est le suivant :

- **Alignement des images et identification des points homologues** : un algorithme de type *Scale Invariant Feature Transform* (SIFT ; Lowe, 1999, 2004) compare des pixels entre les photos pour tester des correspondances. Si les points ont une signature radiométrique identique, ils sont considérés comme homologues et forment un premier nuage de points clairsemé (Lingua et al., 2009 ; Fonstad et al., 2013). L'identification de ces points permet d'aligner les photographies et d'estimer la position et les paramètres de l'appareil. Ces paramètres sont internes (focale, déformation de la lentille) et externes (localisation du centre de projection, orientation de la photo) (Robertson et Cipolla, 2009 ; Lingua et al., 2017).

- **Géoréférencement des points** : à l'aide de points de contrôle (GCP : *Ground Control Points*) aux coordonnées géographiques connues, le modèle est mis à l'échelle, orienté et projeté dans un système de coordonnées terrestre (Snavely et al., 2008 ; Girod et al., 2018). La localisation des GCP enregistrés est ensuite définie et vérifiée manuellement sur chaque photographie (Brunier et al., 2016).

- **Optimisation de l'alignement** : le procédé a pour but d'affiner la géométrie du nuage de points homologues. En effet, grâce aux informations 3D des GCP, les points sont repositionnés et les photos sont ré-alignées afin de réduire les erreurs de déformations (Vazquez-Tarrio, 2017 ; Sanz-Ablanedo et al., 2018).

- **Nuage dense** : la densification du nuage clairsemé se fait grâce à un algorithme de type MVS (*Multiview Stereopsis* ; Snavely et al. 2006 ; Furukawa et Ponce, 2010). De nouveaux points sont interpolés en se basant sur les informations contenues dans les photographies et leurs paramètres. Pour la suite des traitements, un MNS raster est créé à partir du nuage dense.

Détermination d'une valeur d'écrantage topographique à partir de méthode numérique

Afin d'affiner les données de terrain, mais aussi de les vérifier ou de les obtenir quand la mesure sur site a été impossible, les modèles 3D créés sont analysés. L'outil utilisé permettant de déterminer plus précisément l'écrantage grâce à la 3D est une adaptation de l'algorithme de Codilean (2006) en une boite à outil Arcgis, développée par Li (2013).

L'algorithme identifie, pour un azimut ($\emptyset_S$) et un angle d'élévation donné (θ_S) donné, toutes les cellules du MNS qui sont « à l'ombre ». L'algorithme répète graduellement l'opération pour une gamme d'azimut allant de 0 à 360° et une gamme d'angle d'élévation allant de 0 à 90° (Codilean, 2006). Le choix de l'intervalle entre les azimuts et angles d'élévation va conditionner la précision du résultat, mais aussi le temps de calcul. Ici, les intervalles d'azimut et d'élévation utilisés sont de 5° et 2° respectivement. Cette combinaison permet d'obtenir des résultats satisfaisant en zone montagneuse (Li, 2003), tout en tirant parti de la résolution du MNS utilisé (0,5 m). Un raster est créé à la fin du traitement, pour lequel chaque cellule se voit attribuer un facteur d'écrantage. Ensuite, il est possible d'extraire cette valeur pour chaque surface échantillonnée, d'après leurs coordonnées x,y et z.

Photo : Drone utilisé pour les prises d’images